REACTIVE CONTAMINANT TRANSPORT MODELING USING ANALYTIC ELEMENT FLOW SOLUTIONS

by

James R. Craig
September 21, 2004

A dissertation submitted to the
Faculty of the Graduate School of
The State University of New York at Buffalo
in partial fulfillment of the requirements for the
degree of

Doctor of Philosophy

Department of Civil, Structural, and Environmental Engineering

Acknowledgements

I could not have performed any of this work without the companionship and support of my fiancé Dawn. She helped me deal with many nights of dissertation-induced insomnia and sacrificed many Sundays, evenings, and even a few Saturdays to the cause, doing everything she could to ensure that when I got home I could forget all about the stress, even when she had plenty of her own.

Alan has repeatedly lent me his insight, remarkable editing skills, and about half his library (which I will eventually return). He gave me free reign over my work, allowing me to direct my curiosity wherever it roamed (and it roamed into quite a few time-consuming side projects and dead ends). More importantly, he has been the quintessential mentor: teaching me not just about contaminant transport and numerical methods, but about the procedures and politics of academic life, for which I am grateful. Plus he taught me a few chords.

Igor has been my sounding board for ideas and the ultimate Starbucks^{TM} brainstorming companion. He has been my window into the analytic element method, being both a patient instructor (when I didn't understand his answer) and an enjoyable intellectual sparring partner (when I didn't like his answer). Whether I was listening or debating, I was always learning, and more often than not, learning that he was right. He has also taught me more about nickel metal hydride batteries than I could ever wish to know.

Thanks to my officemates Shawn, Mary, James, and Karl for not being upset when I zoned out in the middle of a conversation and generally just being good people to be around. I enjoyed learning with you.

Thanks to Raghu Suribhatla who derived the expression for the elliptical element discharge derivative in appendix C, within hours of me asking for it.

Thanks to Starbucks^{TM} for keeping me awake.

I would also like to thank my patient committee members, Matt Becker, John Van Benschoten, and Doug Flewelling. Your willingness to abide exhaustively long proposals and act as a reality check is duly appreciated.

Finally, I would like to acknowledge the NCGIA and the National Science Foundation, who graciously funded my graduate education through IGERT award DGE-987066.

Contents

List of Figures

List of Tables

List of Symbols

- $A^{(e)}$ ..... Area of finite element e [L^2]
- a_n ..... Coefficient of polynomial series or basis function [-]
- B ..... Aquifer base elevation [L]
- B'_x, B'_y ..... Slope of aquifer base in x-direction, y-direction [L]
- c ..... Aqueous concentration [ML^{-3}]
- c_b^+ ..... Aqueous concentration of vertical influx to bottom of aquifer [ML^{-3}] > 0
- c_s^+ ..... Aqueous concentration associated with source term [ML^{-3}]
- c_t^+ ..... Aqueous concentration of vertical influx to top of aquifer [ML^{-3}] > 0
- c_j ..... Aqueous concentration of species j [ML^{-3}]
- c_j ..... Vertically-averaged aqueous concentration of species j [ML^{-3}]
- C ..... Vertically-averaged aqueous concentration [ML^{-3}]
- C_j ..... Vertically-averaged aqueous concentration of species j [ML^{-3}]
- $\hat{C}$ ..... Approximate finite element solution to vertically-averaged concentration [ML^{-3}]
- $\hat{C}_i$ ..... Vertically-averaged concentration at finite element node i [ML^{-3}]
- $C_{i,j}^n$ ..... Vertically-averaged concentration of finite difference cell ij at time n [ML^{-3}]
- Cr ..... Courant number or grid/mesh Courant number [-]
- d_n ..... Chebyshev polynomial coefficients [-]

- $\mathbf{D}$ ..... Dispersion tensor [$\mathrm{L^2T^{-1}}$]
- D_{xx}, D_{yy} ..... Dispersion coefficients [$\mathrm{L^2T^{-1}}$]
- D_{xy}, D_{yx} ..... Dispersion coefficients (cross-terms) [$\mathrm{L^2T^{-1}}$]
- $D_{xx(i+1/2,j)}$ ..... Face-averaged dispersion coefficients [$\mathrm{L^2T^{-1}}$]
- D^* ..... Species-specific diffusion coefficient [$\mathrm{L^2T^{-1}}$]
- $F(\mathbf{x}, \mathrm{t})$ ..... Forcing function
- G_x, G_y .....x- and y-components of the discharge derivative function [$\mathrm{LT^{-1}}$]
- H ..... Confined aquifer thickness [L]
- h ..... Saturated thickness [L]
- $h_{(i,j)}$ ..... Cell-averaged saturated thickness of finite difference cell ij [L]
- $h_{(i\pm1/2,j)}$, $h_{(i,j\pm1/2)}$ ..... Face-averaged saturated thicknesses of finite difference cell ij [L]
- i ..... $\sqrt{-1}$ [-]
- k ..... Hydraulic conductivity [$\mathrm{LT^{-1}}$]
- $\mathbf{K}$ ..... Anisotropic hydraulic conductivity tensor [$\mathrm{LT^{-1}}$]
- $K_{i/ref}$ ..... Selectivity coefficient w.r.t. reference cation [-]
- L ..... Length of element side or face/transect; Representative length scale [L]
- $L^{(e)}$ ..... Finite element effective length parameter [L]
- $L^{(s)}$ ..... Length of finite element side s [L]
- $\pounds$ ..... A generic differential operator [-]
- M^n ..... Total system mass at time n [M]
- M_{ij}^n ..... Mass in finite difference cell ij at time n [M]
- NC ..... Number of finite difference cells on grid [-]

- NE ..... Number of finite elements [-]
- NN ..... Number of finite element nodes [-]
- NS ..... Number of finite element sides [-]
- NR ..... Number of reactions [-]
- N_{AS} ..... Number of multiquadric area sink basis function points [-]
- N_{cat} ..... Number of cations [-]
- N_E ..... Number of analytic elements [-]
- N ..... Net vertical outflux (leakage) [LT^{-1}]
- N_t^- ..... Volumetric loss of water per unit area through the top of the aquifer [LT^{-1}] > 0
- N_b^- ... Volumetric loss of water per unit area through the bottom of the aquifer [LT^{-1}] > 0
- N_t^+ ..... Volumetric gain of water per unit area through the top of the aquifer [LT^{-1}] > 0
- N_b^+ ... Volumetric gain of water per unit area through the bottom of the aquifer [LT^{-1}] > 0
- N_i ..... Finite element basis function of node i [-]
- $N_i^{(e)}$ ..... Finite element basis function of node i in element e[-]
- N_{ave} ..... Average leakage within a multiquadric area-sink [LT^{-1}]
- N_{cat} ..... Number of cations participating in exchange reaction [-]
- $\mathbf{n}$ ..... Vector normal to boundary [L]
- Pe ..... Peclet number or grid/mesh Peclet number [-]
- $\mathbf{Q}$ ..... Integrated discharge in vector form [$\mathrm{L}^2\mathrm{T}^{-1}$]
- Q_{cx} ..... Cation exchange capacity of soil [meq/g]
- Q_X ..... Flux per unit length of line element [$\mathrm{L}^2\mathrm{T}^{-1}$]
- Q_x, Q_y ..... Vertically integrated discharge in x-direction, y-direction [$\mathrm{L}^2\mathrm{T}^{-1}$]

- $Q_{x(i\pm1/2,j)}$, $Q_{y(i,j\pm1/2)}$ Face-averaged integrated normal discharge in x-direction, y-direction [L^2T^{-1}]
- $Q_{x(i,j\pm1/2)}$, $Q_{y(i\pm1/2,j)}$ .....Face-averaged integrated tangential discharge in x-direction, y-direction [L^2T^{-1}]
- Q_t .....Vertically-integrated tangential discharge [L^2T^{-1}]
- Q_η ..... Vertically-integrated normal discharge [L^2T^{-1}]
- Q^+ .....Volumetric source flux of water (entering aquifer) [L^3T^{-1}]
- Q^- .....Volumetric sink flux of water (leaving aquifer) [L^3T^{-1}]
- $Q^+|_{i,j}$ .....Volumetric source flux of water to cell ij (entering aquifer) [L^3T^{-1}]
- $Q^-|_{i,j}$ ..... Volumetric sink flux of water (leaving aquifer) from cell ij [L^3T^{-1}]
- Q^{net} ..... Net flux from an analytic element or analytic element segment [L^3T^{-1}]
- q .....Sink/source term [LT^{-1}]
- $q_s(x,y)$ .....Distributed "dry" source of mass per unit area [$MT^{-1}L^{-2}$]
- q^{net} ..... Net flux through 3D finite difference cell face [L^3T^{-1}]
- q_x, q_y, q_z ..... Specific discharge components [LT^{-1}]
- $\vec{q}$ .....Specific discharge vector (q_x,q_y,q_z) [LT^{-1}]
- R .....Radius of circle [L]
- $R(\mathbf{x},\mathrm{t})$ .....Finite element residual term
- $R^{(e)}$ ..... Finite element nodal residual due to the influence of element e [$ML^{-3}T^{-1}$]
- R_f .....Retardation Factor [-]
- R_{kj} k^{th} .....rate of solute production of species j [M/T]
- S .....Vertically-averaged sorbed concentration [M/M]
- S_j .....Vertically-averaged sorbed concentration of species j [M/M]

- S_s ..... Specific storage coefficient [-]
- T_n ..... Chebyshev polynomial of order n [-]
- t ..... Time [T]
- v ..... Vertically-averaged seepage velocity [LT^{-1}]
- v_j ..... Valence of the j^{th} species [-]
- v_x, v_y, v_z ..... Vertically-averaged seepage velocity in x-, y-, and vertical direction [LT^{-1}]
- $v_{x(i\pm1/2,j)}$, $v_{y(i,j\pm1/2)}$ ..... Face-averaged normal seepage velocity in x-, y-direction [LT^{-1}]
- $v_{x(i,j\pm1/2)}$, $v_{y(i\pm1/2,j)}$ .... Face-averaged tangential seepage velocity in x-, y-direction [LT^{-1}]
- v_x^*, v_y^* ..... Effective velocity in x-direction, y-direction [LT^{-1}]
- v' ..... Corrected seepage velocity [LT^{-1}]
- v_t ..... Tangential seepage velocity [LT^{-1}]
- W ..... Complex discharge [$\mathrm{L}^2\mathrm{T}^{-1}$]
- $w(\mathbf{x}, \mathrm{t})$ ..... Finite element weighting function [-]
- $w_i^{(e)}$ ..... Finite element upstream weighting function for node i in element e [-]
- X ..... local analytic element coordinate [L]
- $\mathbf{x}$ ..... Position vector (x,y,z') [L]
- Y ..... local analytic element coordinate [L]
- z ..... Complex location in global coordinates [L]
- z' ..... Vertical coordinate (as measured from aquifer base) [L]
- z_1 ..... Complex location of line element endpoint in global coordinates [L]
- z_2 ..... Complex location of line element endpoint in global coordinates [L]
- Z ..... Complex location in local analytic element coordinates [L]

- α ..... Upstream weighting factor [-]
- α_l ..... Longitudinal dispersivity [L]
- α_t ..... Transverse dispersivity [L]
- $\hat{\alpha}_i$ ..... Upstream weighting values for triangular finite element [-]
- $\hat{\alpha}$ ... Upwind weighting parameter for streamline-upwind Petrov-Galerkin formulation [$1/L$]
- β ..... Curl [LT^{-1}]
- γ_m ..... Monovalent cation activity coefficient [-]
- γ_d ..... Divalent cation activity coefficient [-]
- Δ ..... Triangular zone of integration [L^2]
- Δ' ..... Triangular zone of integration in curved coordinates[L^2]
- ΔL ..... Representative mesh or grid spacing [L]
- ΔM_x^n ..... Change in system mass over time step n due to process x [M]
- Δt ..... time step [T]
- Δx ..... Cell dimensions/grid spacing in x-direction [L]
- Δx_i ..... Cell dimensions/grid spacing of column i in x-direction [L]
- Δy ..... Cell dimensions/grid spacing in y-dir [L]
- Δy_j ..... Cell dimensions/grid spacing of row j in y-direction [L]
- $\Delta z'$ ..... Cell dimensions/grid spacing in vertical direction [L]
- ε_{MB} ..... Dimensionless global mass balance error [-]
- ε_{NxM} ..... Dimensionless global mass distribution error calculated on N x M grid [-]
- μ ..... Ionic strength [mol L^{-1}]
- μ_a ..... Anionic component of ionic strength [mol L^{-1}]

- ν ..... elliptical element local coordinate [L]
- Γ ..... System boundary or mesh boundary [-]
- $\Omega(z)$ ..... Complex discharge potential [L^3T^{-1}]
- Ω ..... Model domain [-]
- ω ..... Temporal weighting factor [-]
- ω_k ..... Gaussian weights for integration [-]
- Φ ..... Discharge potential [L^3T^{-1}]
- Ψ ..... Stream function [L^3T^{-1}]
- ρ_b ..... Bulk dry density of porous media [ML^{-1}]
- Υ_x, Υ_y Relative influence of x-, y-direction changes in saturated thickness and porosity [$1/L$]
- ϕ ..... Hydraulic head [L]
- τ ..... elliptical element local coordinate [L]
- $\hat{\tau}^{(e)}$. Element stabilization parameter for streamline-upwind Petrov-Galerkin formulation [-]
- θ ..... Porosity [-]
- θ'_x, θ'_y, θ'_z ..... Spatial gradient in porosity (x-direction, y-direction, vertical direction) [-]
- $\theta_{(i,j)}$ ..... Cell-averaged porosity of finite difference cell ij [L]
- $\theta_{(i\pm1/2,j)}$, $\theta_{(i,j\pm1/2)}$ ..... Face-averaged porosities of finite difference cell ij [L]
- ξ_i ..... Local triangular finite element coordinate for node i [L]
- ζ ..... Boolean: 1 if unconfined, 0 if confined [-]

Abstract

A new approach to modeling reactive contaminant transport in groundwater is developed and evaluated. The approach is unique in that it uses a grid- or mesh-independent representation of model input parameters, including continuous velocities, dispersion coefficients, and saturated thickness values obtained directly from analytic element groundwater flow solutions.

The approach is realized within a suite of revised finite element, finite difference, and characteristic methods that are designed to improve the accuracy and reduce the computational costs of complex reactive vertically-averaged transport simulations in surficial aquifers. These methods are implemented in a fully object-oriented parallel-friendly software framework, benchmarked against existing analytic and numerical solutions, tested against traditional discrete methods, and applied to a set of difficult field-scale test problems.

It was found that the majority of the methods benefited from continuous representation, and that the use of the analytic element method can facilitate the development of computationally efficient multi-scale reactive transport models.

Importantly, this work represents the first thorough implementation of a linkage between reactive contaminant transport models and the analytic element method for modeling groundwater flow, and the first detailed analysis of such a linkage.

Chapter 1

Introduction

1.1 Motivation

Numerical models of contaminant transport function as descriptive and predictive tools to support important policy decisions regarding the regulation and remediation of contamination in aquifers. The usefulness of these models depends upon their ability to provide highly accurate information about the location and concentration of contaminants within the subsurface. With the increased application of subsurface fate and transport models, researchers are finding that accurate models of contaminant transport must increasingly include complex chemistry. For example, a dissolved contaminant species can interact with the soil, its non-aqueous liquid phase, biological organisms, and with other aqueous species in a kinetic, non-linear fashion at varying temporal scales. Complicating the matter, the advective and dispersive transport of dissolved contaminant is often influenced by flow processes occurring at geographic scales much larger than the reactive zone of interest. To effectively simulate reactive transport in large systems, complex regional scale models of groundwater quality are becoming increasingly desirable (NRC 2000).

Given the increasing complexity of the chemical reactions considered by modelers and the increasing sizes of model domains, it is necessary to find ways to alleviate the computational burden associated with complex reactive transport models. There are multiple ways to approach this problem:

- Rely upon the increasing power of computational hardware,
- Increase the computational efficiency of current numerical reactive transport simulators, or

- Reduce the size (i.e., scope) of the numerical transport problem

This third approach is the tactic taken in this dissertation. The size of the transport problem, determined by the spatial scale and complexity of the problem domain, may be reduced in several ways. For example, the model may be *conceptually* simplified by reducing the number of interacting chemical species, reducing the complexity of the reactions, or reducing the spatial extent of the simulation domain. However, the assumptions required for such simplifications are often not applicable. An alternative is to reduce or remove the numerical constraints associated with the scale, complexity, and resolution of the model. Such constraints increase the computational cost of simulation by requiring a certain minimum amount of calculation be performed. With most physics-based simulation models (and particularly contaminant transport models) the most inhibitive computational constraints are those associated with spatial and temporal discretization. By reducing or removing such constraints, the computations needed to obtain some desired output are also reduced.

Traditionally, fate and transport models are solved by discretizing the domain into cells (for finite difference models) or elements (in finite element models). The governing equations are solved for each cell or element node in the grid or mesh. First, the groundwater flow problem is discretized and solved to obtain the hydraulic head and velocity distribution in the aquifer. The transport model is then solved to obtain the distribution of solute mass in the aquifer over time, using discrete velocities from the flow model. For transient flow, the flow model must be updated during the transport solution process. Most commonly, the same grid is used for both transport and flow modeling, potentially incurring unnecessary computational costs in one or both processes. While flow models require higher resolution near high pressure gradients, transport models often require higher resolution near large concentration gradients and/or highly reactive zones. The locations of such regions are often incongruent. This is a fundamental drawback of the use of a grid-based discrete flow model as a basis for transport simulation, as it unnecessarily adds more (computationally demanding) constraints on the grid or mesh geometry of the transport problem. Superfluous degrees of freedom (either finite element nodes or finite difference cells) are included to solve the flow problem accurately. The transport simulator uses these nodes because they are present, not because they are necessary for accurate solution.

In addition to the contradictory needs of flow and transport models, there are other discretization constraints placed upon conventional transport models. One of these is the requirement that

adjacent areas on the grid or mesh have similar resolutions. These "adjacency constraints" make it difficult to simulate transport at multiple spatial scales. This is particularly problematic for modeling of remediation systems (e.g., reactive barriers, bioremediation), where the scale of hydrodynamic transport and the scale of chemical reaction can be significantly different. It is desirable to have fine spatial resolution in reactive zones, which exhibit large concentration gradients and/or high variation in species concentrations. Away from these reactive zones, it is desirable to use coarse discretization, to minimize the computational cost. Adjacency constraints require fine resolution of the grid or mesh even away from the areas where it is needed, placing higher computational demands upon an already complicated model. Thus, models are typically either large in extent at a low resolution or small in extent with high resolution. This resolution is typically constrained by the smallest feature in the model.

Despite some of these inevitable drawbacks, the most common practice at this time is to simulate contaminant transport using models discretized for both flow and transport and limited to a small range of grid or mesh resolution within a given model. The public domain finite difference program MODFLOW (McDonald and Harbaugh 1988) is the most popular method for flow simulation, and the finite difference program MT3DMS (Zheng and Wang 1999) is the prevalent choice for transport simulation. While other models are available and used in practice, the large majority are dependent upon the constructs and assumptions of discrete finite difference (FD) or finite element (FE) models for transport *and flow* simulation. Such limitations make it difficult to remove or reduce the dependence of reactive transport simulation upon "the grid". Recently, researchers have attempted to resolve or remove the problems listed above via the use of multi-grid techniques (e.g., (Leake and Claar 1999; Quarteroni and Valli 1999)) or meshless methods (Belytschko et al. 1996; Šarler 2002). This dissertation instead develops and evaluates an alternative approach to reducing grid constraints via the intelligent use of analytic flow solutions.

An alternative to finite difference or finite element modeling, the analytic element method (AEM) solves the groundwater flow problem without the use of a grid, and with greatly reduced limitations upon model spatial extent. AEM produces continuous velocity and hydraulic head fields and is essentially scale-independent, with the ability to model hydrogeologic features at small and large scales simultaneously. These characteristics are promising for developing reactive transport models that are less constrained by the flow model and more amenable to multi-scale modeling. To investigate these potential benefits, the primary goal of this dissertation is to develop and

implement a general framework for coupling transport models to analytic element flow solutions. The investigation is limited to 2-dimensional (vertically-averaged) transport using steady-state 2-dimensional flow solutions.

There are multiple potential benefits to an AEM-based contaminant transport model:

- The use of AEM flow solutions allows the transport grid or mesh to be developed with only minimal regard for how the flow system was conceptualized and discretized. The transport grid discretization process can be designed specifically to accommodate resolution of the aqueous and/or sorbed concentration field. The result is that the computational cost of transport models that use AEM are limited only by relevant hydrodynamic transport and chemical considerations: the artifacts of flow discretization are no longer a constraint.

- The continuous solutions from AEM models allow for more accurate handling of certain terms of the governing equation, particularly in finite element methods and Eulerian-Lagrangian methods. Such incremental improvements may be an insufficient reason to choose one model over another. However, removal of additional sources of error improves the quality of a given model.

- Problems attributed to the multi-scale nature of many groundwater remediation scenarios may be reduced by the ability of AEM to concurrently model local and regional scale flow. The resultant high-resolution scale-independent flow solution may be used for creative multi-scale modeling of transport phenomena. With proper handling, the smallest flow feature in the model (e.g., a thin barrier or fracture) no longer has to dictate the local resolution of the transport grid or mesh.

- Existing and future analytic element models may be coupled to reactive contaminant transport models. Since the two have never been linked, this option has not been available to practitioners, and the use of AEM has been generally limited to water resources (rather than water quality) investigations (e.g., capture zone delineation)

Not all of these benefits will be analyzed within this dissertation, but rather the necessary groundwork is laid for further investigation.

Coupling transport models to the analytic element method is a step towards removing the constraints of a grid- or mesh- based representation (and the computational cost associated with

this representation) from the practice of contaminant transport modeling. It is also a necessary step in expanding the applicability of the analytic element method.

1.2 Overview of Research

The objective of the research contained in this dissertation is to develop and evaluate a new, flexible, approach for solving two-dimensional reactive contaminant transport problems in saturated groundwater systems. The new method has multiple unique features:

1. The approach uses the analytic element method (AEM), rather than traditional finite difference or finite element flow solutions, as the input to simulations of hydrodynamic (advective and dispersive) transport of solute. The primary contribution of this dissertation is the detailed development of approaches and algorithms that make use of AEM flow solutions for transport both possible and beneficial.

2. In the new method, most parameters used for transport (velocity, saturated thicknesses, porosity, dispersion coefficients) are represented as smooth (field-based) or piecewise continuous (vector-based) functions of position, rather than as cell-averaged (grid-based) and/or grid-interpolated parameters. Only the aqueous and sorbed concentration fields are represented as fully discretized/interpolated parameters on a grid or mesh. Concentration-dependent parameters, such as local retardation factors, the equilibrium immobile concentration field, and local reaction coefficients benefit from semi-continuous representation. A significant effort has been made to maintain the integrity of this continuous parameterization.

3. The new approach uses updated formulations for simulating vertically-averaged advective transport in surficial aquifers. These revised methods are more accurate for vertically-averaged simulations than commonly used existing implementations. The approach also uses revised finite element and finite difference methods for simulation of both dispersive and advective/dispersive transport that minimize loss of information in translating from a non-discrete to a discrete representation of flow parameters. With regards to finite difference and finite element transport modeling, this intelligent translation is (1) often required for adequate results and (2) more accurate than using discrete flow models for lower levels of grid or mesh resolution.

4. The approach is supported by a parallel-friendly object-oriented software representation of flow, transport, and reaction processes that facilitates simulation of spatially non-uniform transport and reactive phenomena (e.g., different numerical methods in different geographic locations; different chemical reactions in different spatial zones). This representation simplifies the allocation of computer resources where necessary. The fully object-oriented software also simplifies the future addition of new reactions, transport methods, discretization schemes, and analytic elements.

The four primary features listed above each contribute to the efficiency and accuracy of the new method. The use of AEM (contribution 1) alleviates many of the problems associated with velocity interpolation and limitations on model extent in more traditional approaches (e.g., the "weak well" problem discussed in (Konikow et al. 1996)). Likewise, the continuous representation of independent model parameters previously linked to "the grid" (contribution 2) removes errors due to discretization of the flow system and other transport parameters. Both advances reduce the grid-dependence of the simulated system, allowing for the development of a flexible and generic formulation of transport algorithms that may facilitate simulations of complex reactive phenomena.

The analysis required for development of accurate vertically-averaged transport modeling in mixed confined and unconfined systems (contribution 3) improves the ability to model surficial aquifers in a robust fashion, and provides the opportunity to couple the two-dimensional analytic element method to transport simulators in the most conceptually consistent manner.

Last, the object-oriented representation of transport and reactive processes (contribution 4) provides flexibility and efficiency, (e.g., by removing time-consuming global calculation of only locally important reactive phenomena). The primary benefit is that unnecessary calculations are removed, thereby allowing each simulation to be optimized for speed of computation. The combination of this efficient allocation of computer resources and reduction of grid constraints/interpolation effects facilitates the more rapid solution of difficult problems. In addition, the object-oriented framework encourages the development of new algorithms and the easy incorporation of new methods.

The new techniques and algorithms needed to construct an AEM-based transport simulator are rigorously developed in chapter 3. To evaluate these new methods and their implementation, a set of tests have been developed. The objectives of these tests are to (1) evaluate the ability of the AEM-based approach to accurately solve the applicable governing equations using novel methods, (2) evaluate the accuracy of some of these methods, (3) compare the effectiveness of

various options for coupling AEM and transport simulation, and (4) demonstrate the ability of the new approach to simulate difficult multi-scale reactive contaminant transport systems. The first of these objectives is addressed by benchmarking the contaminant transport software against existing analytic and numerical solutions for vertically-averaged 2-D transport (section 4.1). The second and third objectives are addressed in a set of tests that compare the new methods to existing approaches and to alternative methods. The last objective is met by development of two test cases: (a) simulation of diffusion-dominated transport through a low conductivity barrier (section 4.3) and (b) mixed large and small scale 2-D reactive transport through a permeable reactive barrier in a regional scale flow field (section 4.4). Adequate solutions to these two difficult problems have been previously unavailable due to factors listed above.

Within this dissertation, the developments and simulations have been primarily limited to 2-D, steady-state models. However, many of the concepts and algorithms can be extended to 3-D, and to some extent, transient flow. Such extensions are discussed briefly, but are beyond the scope of this dissertation.

1.3 Outline of Contents

This dissertation is structured as follows.

Chapter 2 (Background) contains background information about modeling of steady-state saturated groundwater flow and contaminant transport, with particular attention paid to flow and transport modeling of 2-dimensional vertically-averaged surficial aquifer systems. This literature review surveys many of the different methods used for transport modeling, and discusses the impact of system discretization upon the stability, accuracy, and computational cost of a given model. The section stresses the differences between the analytic element method representation and discrete (finite difference/finite element) representation of the flow field and its impact upon the practice of contaminant transport modeling. A considerable amount of attention is paid to the deleterious effects of flow system discretization upon solute transport, including errors due to interpolation and averaging. Various approaches for modeling simultaneous transport processes, including reaction and sorption, are also discussed, focusing upon those techniques that reduce the overall grid-dependence of the transport model. Section 2.2 extends some of the discussion in the literature review, with a more detailed explanation of the mathematics behind the analytic element method,

Eulerian-Lagrangian transport algorithms, vertically-averaged transport, discretization constraints, and the basics of finite element and finite difference methods for transport simulation.

Chapter 3 (Methods) contains details about the implementation of the new approach, including a section on the structure of the object oriented software (section 3.1), discussion of a generic mass balance accounting procedure (section 3.2), required derivations for use of continuous parameters in finite difference and random walk methods (sections 3.3.2, 3.4, and 3.5), and implementation of a comprehensive graded parameter finite element method designed to simulate small scale features embedded in a larger model without overdiscretization (3.6; 3.7). Following this is a brief discussion of the object-oriented implementation of complex reaction processes (section 3.8).

Chapter 4 (Numerical Testing) contains the results of models run with both the revised methods and existing formulations. Section 4.1 contains the results of benchmark tests of the software against existing analytic and numerical solutions. Sections 4.2 and 4.3 contain results from tests used to analyze the benefits of using the analytic element flow solution with various transport algorithms. Section 4.4 contains the results of a more complicated test case with complex reactive chemistry.

Chapter 5 (Discussion) relates the significance of this dissertation research, the contributions to the state of the science, and future research that may grow from this initial use of the analytic element method as a basis for reactive contaminant transport solutions.

Chapter 6 (Summary) briefly summarizes the research and results contained within this dissertation.

Chapter 2

Background

Most numerical methods for modeling of groundwater flow and solute transport rely heavily upon the fixed grid representation associated with finite difference and finite element solution techniques. As a consequence, all existing methods for transport simulation are also strongly limited by the scale of the modeled physical domain. The following section reviews key aspects of the history and limitations of grid-based solute transport solution techniques and the flow models upon which they are based. The first part of the chapter (subsection 2.1) is a literature review that qualitatively discusses past advances in modeling contaminant transport. The second subsection (2.2) introduces the mathematical underpinnings of the analytic element method, two-dimensional vertically-averaged contaminant transport, finite element (FE) methods, finite difference (FD) methods, and the constraints linked to discretization of flow and transport models.

2.1 Literature Review

2.1.1 Groundwater Flow Modeling

A necessary component of a solute transport simulator is a groundwater flow model. The flow velocity has a strong influence upon contaminant fate because the travel of solutes in moving water (advection) is usually the dominant mode of solute transport. Hydrodynamic dispersion, another modeled transport mechanism, is also influenced by the magnitude and direction of groundwater flow. Analytical methods for solute transport simulation often rely upon simplified (e.g., uniform) flow fields. However, deterministic numerical methods for transport simulation regularly use more complex flow fields obtained using FD or FE methods (Wang and Anderson 1982; Huyakorn and

Pinder 1983; Istok 1989; McDonald and Harbaugh 1988). These methods often solve a variation of the governing equation for saturated groundwater flow, which is based on fluid mass continuity and Darcy's law:

$$\nabla \cdot (\mathbf{K} \nabla \phi) = S_s \frac{\partial \phi}{\partial t} + q \tag{2.1}$$

where $\mathbf{K}$ is the anisotropic hydraulic conductivity tensor, ϕ is the hydraulic head, q is a sink/source term, and S_s is the specific storage of the porous media.

FD and FE methods always produce a discretized solution to Equation 2.1 comprised of a set of nodal or cell-averaged values for hydraulic head and groundwater fluxes. Because of the discrete solution, many velocity interpolation techniques have been developed to mimic continuous, smooth behavior using discrete values of the velocity at nodes or cell faces (Yeh 1981; Pollock 1988; Goode 1990; Cordes and Kinzelbach 1992; Durlofsky 1994; Zheng 1994; Pokrajac and Lazic 2002). Alternative methods for obtaining the flow solution, such as the analytic element method (AEM) (Strack 1989; Haitjema 1995; Fitts 2002) or classical boundary element methods (BEMs) (Liggett and Liu 1983; Bruch 1991) are also available. These methods supply velocity and hydraulic head distributions as continuous functions of position, without the need for interpolation. Until recently, methods such as AEM and BEMs have been infrequently used as a basis for contaminant transport simulations, and have never been used as the basis for a chemically complex transport model. The following two sections review relevant information about flow modeling with both discrete methods and the analytic element method. The boundary element method is not considered here, as the focus of this dissertation is on the use of the analytic element method.

2.1.1-A Finite Difference/Finite Element Methods for Groundwater Flow

Finite difference (FD) and finite element (FE) methods are used in many scientific and engineering fields to solve for the behavior of complex systems governed by sets of partial differential equations. The general approach for both methods is to first discretize the domain of interest into elements (for FE methods) or cells (for FD methods). Cells are representative volumes over which both the independent and dependent variables are averaged. Elements are defined as the volume in between nodes of a finite element mesh. Once the system is discretized, the differential equation may be approximated as algebraic formulae at each node or cell center and solved using matrix algebra techniques. The result of such simulations is a single value of the dependent variable (in the case

of groundwater flow, hydraulic head) for each node or cell in the domain. Both finite element and finite difference methods, therefore, sacrifice a continuous solution for computational simplicity. In most situations, this sacrifice is small with respect to the advantages of the methods, especially with groundwater flow models, which solve a relatively smooth and well-behaved differential equation. However, flow systems dominated by high contrasts in hydraulic conductivity or relatively small features such as wells or engineered barriers are prone to difficulties associated with discretization. There exist a number of references that discuss the application of finite difference methods and finite element methods to flow models (Wang and Anderson 1982; McDonald and Harbaugh 1988; Istok 1989; Zheng and Bennett 2002).

The accuracy of both FD and FE methods depends upon the number and relative spacing of nodes or cells. Therefore, the geographic extent of a model is constrained by the number of equations that may be stored on a computer. In addition, numerical constraints upon the proximity of nodes and cells for an accurate solution require a higher density of nodes or cells near locations of higher complexity (i.e., a pumping well). These numerical constraints limit the spatial extent and/or complexity of the domain. While there are numerical techniques that assist in relaxing these constraints using mixed-resolution "multi-grid" models (Leake and Claar 1999; Székely 1999; Mehl and Hill 2002), FD/FE simulations are always limited at some level by either the size or complexity of the domain. These methods always produce a non-continuous set of point values for hydraulic head and discharge.

Finite difference and finite element methods continue to be the most used methods for solving groundwater flow problems, as indicated by the success of such software packages as MODFLOW (McDonald and Harbaugh 1988) and FEFLOW (Diersch 1998b). In addition, MODFLOW acts as the groundwater flow program of choice for input into FD-based contaminant transport models such as MT3DMS (Zheng and Wang 1999) and MOC3D (Konikow et al. 1996).

2.1.1-B The Analytic Element Method

The analytic element method is an alternative method for modeling groundwater movement (solving equation 2.1) based upon the principles of potential theory. It is independent of a grid or mesh. Earlier advances of potential theory as applied to groundwater simulation were developed in the 19th century by Dupuit (1863) and Forcheimer (1886), who independently proposed the application of potential theory to 2-dimensional steady-state groundwater flow by neglecting the variation of

hydraulic head in the vertical direction. This application of potential flow theory was limited to confined flow and solutions were thus developed in terms of hydraulic head. Later advances by Girinski (1946) allowed for application of potential theory and complex analysis to both confined and unconfined flow by introducing the concept of the discharge potential. Polubarinova-Kochina (1952), Verrujit (1970), and Hálek and Švec (1979) outlined many developments in this earlier application of potential theory, primarily based upon conformal mapping. One of the principal concepts behind these flow solutions was superposition. Superposition allows groundwater flow to be modeled by the summation of functions, each of which represents the influence of a single hydrogeologic feature. In earlier application of these methods, the solutions were limited to the superposition of a few simple features, such as a set of wells or a single circular lake in uniform flow. This method of combining individual continuous solutions to local groundwater flow phenomena is quite different from the FD/FE paradigm, which solves the entire problem on a discretized grid. Many of these early superimposed solutions, in addition to using a distinctively different conceptual method, were exact solutions to a mathematical problem.

The analytic element method (AEM), which is based upon these previous innovations, was developed primarily by O.D.L. Strack and is thoroughly described by Strack (1989) and summarized by Haitjema (1995). Much like its predecessors, AEM relies heavily upon the concept of superposition of local solutions to the governing equations of steady-state groundwater flow. With AEM, however, the superposition of these functions ("elements") no longer required the exact mathematical solution demanded by earlier applications of potential theory. Instead, the elements, such as rivers or inhomogeneities in hydraulic conductivity, met hydrogeologic constraints along their boundaries by solving for adjustable coefficients within the functional form of general analytic solutions. These "analytic elements" allowed for a more complex and arbitrary geometry than their predecessors. In addition, because the implementation did not require exact solutions, AEM could apply earlier developments in potential theory to domains with hundreds or thousands of hydrogeologic features. Applications and advances of the method may be found in Strack (1981a), Strack (1981b), Strack and Haitjema (1981a), Strack and Haitjema (1981b), and Fitts (1985). These papers highlight some of the earliest applications of AEM to two-layer systems with and without spatially varying hydraulic conductivity. The papers also presented the capability of analytic elements to accurately depict groundwater flow on a scale that was impossible to model using traditional finite difference or finite element models.

While multiple 3-dimensional solutions have been developed (Haitjema 1985; Haitjema 1987; Janković 1997), the most common applications of the method continue to be comprised of 2-dimensional steady-state solutions. The current state of AEM, mostly dealing with these 2D applications, was summarized by Strack (1999). These newer advances include more flexible and accurate high-order elements (Janković and Barnes 1999a; Janković and Barnes 1999b), methods for computational speedup known as Superblocks (Strack et al. 1999; Craig et al. 2004), and more versatile analytic elements for modeling recharge and leakage in 2-dimensional aquifers (Strack and Janković 1999). The transport model within this dissertation is based upon this most current, high-order implementation. A detailed summary and analysis of high-order elements is outlined by Janković (1997). These collective advances have made it possible to model regional-scale confined/unconfined systems with high precision.

There have been very few attempts to couple contaminant transport models to flow solutions obtained from the analytic element method. The only existing linkage of AEM to a advective-dispersive transport model, WinTran (Rumbaugh 1993; Scientific Software Group 2003), uses a very simple implementation of the analytic element method and non-robust discretization of the flow solution as input to a simple finite element transport algorithm. For the most part, transport simulations based upon AEM have been limited to the task of tracing particles through the flow domain (Strack 1984; Strack 1989; Haitjema 1995), rather than attempting to solve the more difficult problem of dispersive and reactive groundwater transport. Currently, the simulation of transport phenomena using AEM flow solutions continues to be limited (both in research and in practice) to the identification of contaminant travel times and basic random walk simulations. An exception to this trend is the application of non-reactive particle tracking through massive heterogeneous 3-dimensional domains to investigate the process of hydrodynamic dispersion by large-scale advective mixing (e.g., Fiori et al. (2003) and Janković et al. (2003)).

2.1.2 Contaminant Transport Modeling

Deterministic modeling of contaminant transport has been the primary technique for assessing and predicting the impact of contaminants in the subsurface. This success is due to the adaptability and relative simplicity of discrete numerical methods. Research in numerical reactive contaminant transport modeling is intense, both in the broad scope of study, and in the large quantity of information published each year. A thorough review of the entire field is not within the scope of

this literature review. Instead, an overview of the methods and conceptual models applicable to vertically-averaged reactive transport in 2-dimensional domains is presented.

The transport modeling review is divided into 3 parts. First, relevant advective/dispersive transport modeling techniques are reviewed. Second, common methods for incorporating sorption and chemical transformations of modeled solutes are discussed. The operator-splitting technique is emphasized, focusing on the mathematical decoupling of transport and reaction. The final sections discuss the effects of discretization upon accuracy and efficiency of transport simulation. The focus of this literature review emphasizes the potential advantages and limitations of coupling transport methods with continuous flow solutions such as those provided by the analytic element method.

The governing equation for transport of a miscible solute in saturated groundwater systems is the advective-dispersive-reactive (ADR) equation (e.g., Bear (1979)):

$$\theta \frac{\partial c_j}{\partial t} = -\nabla(\vec{q} c_j) + \nabla \left(\mathbf{D} \theta \cdot \nabla \mathrm{c_j} \right) + \sum_{k=0}^{NR} R_{kj} - \rho_b \frac{\partial S_j}{\partial t} \tag{2.2}$$

where c_j [M/L^3] and S_j [M/M] are the aqueous and sorbed concentration of species j, $\vec{q}$ [L/T] is the three-dimensional discharge vector, $\mathbf{D}$ [L^2/T] is the dispersion coefficient tensor, which includes the effects of hydrodynamic dispersion and molecular diffusion, R_{kj} [M/T] is the rate of solute production in reaction k of NR different reactions, ρ_b is the bulk density of the solid [M/L^3], and θ is the porosity. The velocities, dispersion coefficients, and the system geometry (for unconfined systems) are typically obtained from discrete solutions to the flow equation.

There are three general classes of methods for solving the advective and dispersive transport terms of the ADR. Eulerian methods (e.g., finite difference, finite element, flux-limiting schemes, and finite volume methods) solve all the terms of equation 2.2 on a fixed spatial grid. Because of the extensive use of finite difference models in computational modeling, these were among the first published numerical models of solute transport (Huyakorn and Pinder 1983; Wang and Anderson 1982).

The second category of transport methods, Lagrangian methods, represents transport on a moving frame of reference by directly moving parcels of solute mass along pathlines. This category includes the random walk (Prickett et al. 1981) and Finite Cell methods (Sun 1999). The combined use of Lagrangian methods for advection (the first term on the right hand side of equation 2.2) and Eulerian methods for dispersion and/or reaction are referred to as Eulerian-Lagrangian (EL)

methods (e.g., the method of characteristics, Konikow and Bredehoeft (1978)).

An alternative to traditional Eulerian, Lagrangian, or EL methods is the deterministic streamline method, which was developed primarily in the petroleum engineering field (Thiele 1994; Batycky 1997). The method uses streamlines (the paths of particle trajectories in a steady-state flow field) as the primary frame of reference. A transformed 1-dimensional version of equation 2.2 is solved along each streamline.

Because of the prevalence of grid-based flow and transport models, independent model parameters (such as conductivity and porosity), and derived parameters (such as saturated thickness, dispersion coefficients, and some reaction parameters), have been limited to a grid- or mesh-based representation. Parameter values are most often averaged over a cell or element, with cells and elements (for independent parameters), or nodes (for derived parameters) being assigned a specific value of the variable. Some finite element formulations additionally allow for linear or quadratic variation in parameters within elements (Istok 1989). However, both derived and independent parameters typically conform to the geometry of the finite difference grid or finite element mesh, and evaluated using some form of interpolation. While there have been attempts to distort the grid to conform to the flow geometry and parameter distribution (e.g., Cirpka and Kitanidis (2000)), the parameters themselves have never been fully decoupled from the grid.

2.1.2-A Methods for Solving Transport Problems

The following subsection discusses the various approaches for solving the advection dispersion equation (ADE) given by equation 2.2. The need for more than one transport simulation method is ascribed to the lack of a single approach that is accurate and computationally efficient for all problem types. Common errors incurred during the numerical simulation process include:

- Oscillation - The solution of advection-dominated transport problems is often complicated by the occurrence of "oscillation" of the solution near the advancing front of a plume. This oscillation is exhibited as sinusoidal concentration distributions, often leading to (unrealistic) negative concentrations. This is a symptom of having too large of a grid resolution.

- Numerical Dispersion - Some numerical methods may lead to artificial spreading of the plume. This error is often intentional, as higher degrees of dispersion reduce or remove the aforementioned oscillation of the solution. This spreading is an artifact of discretization and may be

reduced by using finer resolution grid or mesh.

- Global Mass Balance Errors - Many methods for contaminant transport simulations are non-conservative. Such non-conservative schemes are subject to non-physical (and unintentional) loss or gain of mass. The degree of mass balance error is generally dependent upon the degree of variation in the flow solution (i.e., highly heterogeneous domains will exhibit higher mass balance errors than homogeneous domains).

- Local Mass Balance Errors - Local mass balance errors occur when non-physical loss of mass occurs at the sub-grid or sub-mesh level, even though the total mass in the system is conserved. In this case, the mass influx to a sub-region is not equal to the outflux from the same region.

While all methods perform relatively well for dispersion-dominated transport, alternative methods have been developed to avoid oscillation or numerical dispersion. Unfortunately, many of these methods can be either non-conservative, computationally inefficient, or require assumptions not applicable to the problem at hand (e.g., no transverse dispersion). Some numerical methods, not discussed here, are also subject to stability problems, where not even a poor numerical solution can be obtained unless the system has been sufficiently discretized.

Eulerian Methods

Eulerian methods for solving contaminant transport models rely upon the same premises as that of finite difference or finite element simulation of groundwater flow. Because of the extensive use of finite difference and finite element models for flow modeling, these were among the first numerical models of contaminant transport (Wang and Anderson 1982). At a set of fixed grid points in the model domain, numerical approximations of the governing equations (the advection-dispersion-reaction equation for each species) are developed. These approximations applied to each node to yield a set of algebraic equations (one per species per node), which may then be solved using matrix solution methods for each time step. While such problems have been well characterized mathematically, the behavior of the governing equation varies in space and time and can exhibit stability and accuracy problems, especially when coupled with complex chemical and hydrodynamic initial and boundary conditions. In addition, though robust when implemented for dispersion-dominated problems, finite difference and finite element methods exhibit "numerical dispersion" for advection-dominated problems (problems with high velocities and low dispersion)(e.g., Zheng and

Bennett (2002)). Such problems are typically overcome by strict adherence to rules governing cell size and time step duration (Peaceman 1977; Huyakorn and Pinder 1983; Zheng and Bennett 2002). The result is that sufficiently complex problems solved in a globally implicit Eulerian framework (which solves all parts of the governing equation simultaneously) may require both prohibitively small time-step durations *and* fine spatial resolution of chemically and/or hydraulically complex regions. Global Eulerian methods, limited by computer memory, become intractable once the accuracy and stability constraints require an excessive number of cells or nodes or an excessively small time step. A discussion of these constraints and their impact upon the computational costs of transport problems is given in section 2.2.5.

Most of the current research into purely Eulerian methods addresses software/hardware implementation (e.g., parallel processing) and/or incorporation of new types of reaction phenomena. Much of the improvements to the numerical methods themselves occurred in the 1990s, including Total Variation Diminishing (TVD) schemes (Datta-Gupta et al. 1991) and the Flux-Corrected transport (FCT) methods (Leonard 1988; Hills et al. 1994). Both TVD and FCT schemes reduce oscillatory behavior in highly advective Eulerian domains. A newer Eulerian technique, the Finite Analytic Method (Li and Wei 1998; Lowry and Li. 2002), relax some of the cell size constraints of classical Eulerian models, but are mathematically complex, like many of the revisions to the pure Eulerian approach, and can presently only simulate steady-state transport.

While Eulerian methods may seem ill-suited for connection to analytic flow solutions, it is important to note that there has been a significant degree of research into streamline-oriented grid modification (Cirpka et al. 1999b; Cirpka et al. 1999a) and incorporation of stream functions into fully Eulerian schemes (Frind and Matanga 1985). Both of these techniques embrace the benefits inherent in analytic flow models: a spatial discretization structure referenced to the transport patterns rather than the arbitrary geometry of a rectangular grid. It is likely that the most robust combination of Eulerian transport methods and AEM would replicate this approach, as the analytic element method is intrinsically non-rectilinear (i.e., AEM models do not generally conform to the orthogonal geometry of a rectangular grid). In addition, discrete Eulerian approaches for transport require a precise water balance from the flow solution to properly allocate solute mass. In certain formulations, this precise water balance is also required to maintain a mass balance on the contaminant. The analytic element method provides exact (water balance-maintaining) solutions to the flow problem, and is therefore well-suited for removing any errors linked to inadequacy of

the water balance in Eulerian methods.

Lagrangian Methods

Lagrangian methods represent an alternative method approach to solving contaminant transport problems where the frame of reference is not fixed in space. In the Lagrangian approach, the solute concentrations are not associated with fixed points or volumes, but with moving parcels of water associated with a mass of contaminant. Pure Lagrangian methods include the random walk method (Prickett et al. 1981) and the finite cell method (Sun 1999). These methods are inherently less grid-limited than traditional Eulerian methods (a grid is typically only needed to visualize the distribution of mass) and do not exhibit numerical dispersion or oscillation when simulating advection-dominated problems. However, the Lagrangian methods are typically restricted by their ability to accurately represent the concentration field and dispersion without a prohibitively large number of particles/parcels.

The random walk method, first implemented for contaminant transport modeling by Ahlstrom et al. (1977) and Prickett et al. (1981), represents the transport of contaminant as the movement of thousands of discrete particles, each associated with some initial mass. These particles are advected based upon the flow solution (by traditional particle tracking), then randomly displaced (according to a normal probability distribution). This normal probability distribution is used to simulate two similar phenomena: (1) the diffusion of contaminant based upon gradients in concentration and (2) the randomness of the pathway each particle follows (assuming this randomness is not reflected by the flow model itself). These calculations (advection, then dispersion) are repeated for each particle and time step. In order to establish concentration profiles, the particles are placed on a grid. Volume averaging is then used to calculate concentration by identifying the number of particles in each grid cell, and averaging the particle mass over the volume of the cells. Concentrations obtained in this manner are used for visualization of the plume and, in some cases, to perform reaction calculations. This series of calculations is designed to replicate the continuous change of the contaminant in the subsurface over short time steps. The random walk method has been been the subject of extensive analysis (Valocchi and Quinodez 1989; LaBolle et al. 1996; Hathorn 1996); in particular, there are multiple publications addressing the application and implementation of the random walk method to represent macrodispersion in aquifers (Uffink 1985; Kinzelbach 1988; Kinzelbach and Uffink 1991; Zheng and Bennett 2002). A primary conclusion of nearly all of these studies is that a

very large number of particles is necessary to sufficiently resolve the detail of a contaminant plume (dependent upon the application). Some attempts have been made to develop dynamic particle allocation schemes to ameliorate this problem (Schafer-Perini and Wilson 1991). However, the secondary problem of *local* mass conservation (LaBolle et al. 1996) is more difficult to overcome, and increases as higher degrees of dispersion are introduced.

Lagrangian methods are intrinsically grid-independent. However, the Lagrangian methods now available typically use a grid-based velocity field, and thus require interpolation of nodal velocity values linked to the fixed frame of reference (the grid) rather than the moving frame of reference (the particle). The grid-independent merger of analytic flow solutions and the random walk method could be very fruitful; continuous velocities could better simulate particle trajectories. In fact, an AEM-based implementation has been successfully used by Janković et al. (2003) to simulate advective-diffusive transport in highly heterogenous aquifers. However, implementation using an analytic flow solution does not remove the limitations of purely Lagrangian methods: local mass conservation problems near sinks, sources, and boundaries and the need for a large number of particles are still problematic.

Eulerian-Lagrangian methods

Pure Lagrangian methods continue to advance incrementally (e.g., with the development of the Finite cell method (Sun 1999)), but most recent developments in transport modeling favor the combination of Eulerian methods (better for dispersive transport) and Lagrangian methods (better for advective transport). These mixed approaches are designated Eulerian-Lagrangian (EL) methods. Different implementations of EL methods were studied extensively in the 80s and 90s (see Ewing and Wang (2001) for an exhaustive summary). The approaches include those derived directly from "characteristic" methods and those based upon the Localized Adjoint Method (LAM).

The prototypical EL method, the traditional method of characteristics (MOC) (Konikow and Bredehoeft 1978; Zheng 1993) operates on a fixed spatial grid. For every time step, a prescribed number of particles are placed in each cell. Each particle is assigned the concentration associated with that cell (rather than the mass used in random walk methods). These particles are then tracked forward in time using particle-tracking algorithms and new cell concentrations are calculated based on the average concentration associated with the particles within a cell at the end of the time step. Variations on this theme, including the backward and modified method of characteristics (BMOC;

MMOC) (Cheng et al. 1984; Baptista 1987) and the hybrid method of characteristics (Zheng 1990; Zheng and Bennett 2002), were developed to ameliorate the computational burden of traditional MOC and/or more effectively simulate dispersion-dominated systems. The BMOC tracks one particle backwards from each grid cell center over the time step. The new cell concentration is equal to the space-weighted old concentration at the backtracked particle location. The MMOC also relies upon backtracking of particle paths, but with multiple characteristics per cell. Both the BMOC and MMOC tends to behave well in highly advective domains, but introduce some numerical dispersion at the sharp front of a plume if low-order concentration interpolation is used (Healy and Russell 1989). The hybrid method of characteristics (HMOC) (Zheng 1990) combines the computational advantages of MMOC and the dispersive robustness of traditional MOC by dynamically choosing which method to use depending upon the local behavior of the system. At sharp advective fronts, traditional MOC is used; elsewhere, MMOC is used. While characteristic methods are far less computationally demanding than pure Lagrangian methods, they do not conserve mass (Tompson and Dougherty 1988), because of the inaccuracies from concentration interpolation and the incomplete treatment of boundary conditions (Celia et al. 1990).

The characteristic-based approach remains one of the most commonly used transport simulation techniques, predominantly due to its ease of implementation and its availability in the most popular transport program, MT3DMS (Zheng and Wang 1999). Another category of EL methods is that of Eulerian-Lagrangian localized adjoint methods (ELLAMs), introduced by Celia et al. (1990). Though characteristic methods (such as MOC) can be considered a specific variation of ELLAMs, the standard implementation is generally quite different, using features of optimal spatial methods (OSMs), which are Eulerian methods with upstream weighting schemes. ELLAMs provide the desirable advantage of global mass conservation and comprehensive treatment of boundary conditions (neither of which apply to classical characteristic methods). The ELLAM continues to advance at a steady pace (Healy and Russell 1993; Healy and Russell 1998; Bellin et al. 1994; Binning and Celia 2002). ELLAMs have been applied to multi-dimensional domains with simple reaction.

All of these Eulerian-Lagrangian methods, much like their Lagrangian predecessors, are constrained by the large number of particles needed to accurately characterize the concentration field (Yeh et al. 1992; Zheng and Bennett 2002). However, the flexibility provided by the merger of the two solution methods allows for robust solution of a wide variety of contaminant transport problems using a single approach. The robustness of the EL methods, combined with their Lagrangian

representation of advection, suggest beneficial integration with analytic flow solutions.

2.1.2-B Modeling Chemical Transformation

Chemical reactions are widespread in the subsurface, ranging from simple decay processes to bio-geochemical interactions between multiple chemical species and bacteria. For this reason, many transport models have incorporated algorithms for modeling complex reactions in conjunction with hydrodynamic transport.

Modeling Aqueous Chemical Reactions

It is often assumed that transformation of and interactions between chemical species or components may be described by a finite set of mathematical formulae derived from thermodynamic and kinetic considerations (i.e., rate laws and mass balance relationships) (Yeh and Tripathi 1989; Steefel and MacQuarrie 1996; Parkhurst and Appelo 1999). Different types of reaction (e.g., aqueous complexation, acid/base, redox, sequential decay, etc.) are expressed in terms of different thermodynamic relationships between species or components (Rubin 1983). The speed of the reaction dictates whether the reaction is represented by algebraic equations or ordinary differential equations. Equilibrium processes, where the reaction is fast relative to the transport process, may generally be expressed in terms of a set of algebraic equations. Kinetic reactions, however, must be represented by ordinary differential equations. Depending upon the specific reaction behavior, these equations may be either linear or non-linear functions of the local aqueous and sorbed concentrations. General-purpose reaction solvers, such as PHREEQC (Parkhurst and Appelo 1999) require a set of robust solvers that can handle the specific mathematical behavior of a wide variety of kinetic and equilibrium reaction types.

Regardless of the particular functional form of the chemical reactions, the coupling of reaction phenomena and transport is most often handled in one of two ways. In the first method, dubbed the “one-step”, “globally implicit” or “fully-coupled” method (Steefel and MacQuarrie 1996), the reactions are explicitly included within the governing equations (coupled partial and ordinary differential equations) and the interaction of chemical species or components are simulated through solution of fully coupled advection dispersion reaction equations. This method is used exclusively within fully Eulerian transport models. However, this technique incurs even more constraints upon temporal and spatial discretization than the methods for modeling hydrodynamic transport, and

usually requires extensive iteration within each time step. This is because geochemical reactions proceed at different rates of speed, introducing stiff behavior into the system of equations.

To remove the inhibitive constraints of the globally implicit formulation, operator-splitting (a.k.a., the "sequential approach" or "two-step" approach) may be used. Operator-splitting is a numerical technique whereby the transport processes of advection, dispersion, reaction, and sorption, which in reality occur simultaneously, are represented as a sequence of distinct events (Valocchi and Malmstead 1992). In the technique of operator-splitting with respect to reaction, the contaminant is transported by the mechanisms of advection and dispersion for a short period, assuming no reaction during this time step. Then the reaction transformation is simulated using the local concentrations over the same time duration, simulating a process that in reality occurs concurrently. An alternative method of operator-splitting is to represent advection alone as a distinct operation and treat reaction and dispersion as a simultaneous process (e.g., within MT3DMS). There is one primary assumption underlying the applicability of any operator-splitting method. If the time step is sufficiently small, the local concentrations are similar at the beginning and end of the contaminant movement, and the reactions would proceed in the same manner with either initial condition. Because it is used so often, the accuracy and applicability of operator-splitting has been studied extensively by those within the groundwater modeling community (Valocchi and Malmstead 1992; Miller and Rabideau 1993; Kaluarachchi and Morshed 1995; Steefel and MacQuarrie 1996; Barry et al. 1996; Barry et al. 1996; Barry et al. 2000).

When implemented in an operator-splitting framework, complex reactions are often solved as local "batch-reactor" problems, typically solved using a generic batch reaction solver (e.g., PHREEQC (Parkhurst and Appelo 1999)). In such problems, concentrations of chemical species are averaged over a volume (often the same volume associated with the finite difference grid) and transformation is simulated over a single time step, ignoring location as a variable. If the reactions are at equilibrium, the result is a single set of algebraic equations that need only be solved once for the time step. If all of the reactions are kinetic in nature, the solution procedure may be much more involved, requiring the solution of a set of mixed ordinary differential and algebraic equations that use the concentrations at the beginning of the time step as initial conditions. This kinetic behavior may affect the applicability of the operator-splitting procedure (Steefel and MacQuarrie 1996). Regardless of the specific type of reaction problem, operator-splitting enables computational decoupling of hydrodynamic and reactive phenomena, which allows bigger and more chemically complex

problems to be solved with fewer constraints upon spatial and temporal discretization.

In addition to those issues discussed above, there may be other difficulties encountered when modeling reactive transport. Restrictions on allowable time step duration and the potential non-linearity of multi-species reactions often impede the development of extremely complex reactive transport models: the computational cost of the reaction simulation simply becomes too cumbersome. This problem may be exacerbated by simulating reactions uniformly across the domain, regardless of their site-specific relevance to the application. In addition, while the hydrodynamic behavior of the system is usually unaffected by chemical transformations, certain reactions (e.g., precipitation of solids, growth of microbial mass) can decrease the conductivity/permeability of the media. Also, the oscillatory behavior of some methods for simulating contaminant transport may create negative concentrations, which often induce instabilities in the algorithms used to simulate reactive phenomena. Special treatment is required to handle each of these phenomena.

For further information regarding the development of numerical models for chemical reactions, the reader is referred to Parkhurst and Appelo (1999) and Bethke (1996). Yeh and Tripathi (1989) and Steefel and MacQuarrie (1996) have compiled thorough reviews that discuss the coupling of geochemical and hydrodynamic transport models.

Modeling Sorption

Sorption processes, like reaction processes, have a significant effect on the transport of contaminant in the subsurface (Weber et al.). Sorption is defined as the transfer of chemical species or components from the (mobile) aqueous phase to the (immobile) surface of the porous media. The general effect of sorption is to slow the progress of the contaminant as it reacts with the immobile aquifer material. Conceptual models of sorption range from simple equilibrium between sorbed and aqueous phases to rate-limited kinetic processes. While multiple conceptual models are used to represent the interaction of sorbed and aqueous species, the inclusion of sorption phenomena in a model leads to an additional term in the ADRE. This additional term may be expressed in explicit form within the transport solution (e.g., in fully Eulerian methods), by the use of operator-splitting (Kirkner and Reeves 1988), or by the use of a "retardation factor".

If the sorption phenomenon in a given model is non-competitive equilibrium sorption (i.e., sorbed and aqueous concentrations are always at equilibrium and this equilibrium relationship is independent of the concentrations of other species), the sorption phenomenon may be simulated

using what is dubbed the "retardation factor" approach. Writing out the simplest form of the single-species 1D advective dispersion equation with sorption,

$$\frac{\partial c}{\partial t} = -\frac{q}{\theta}\frac{\partial c}{\partial x} + D\frac{\partial^2 c}{\partial x^2} - \rho_b \frac{\partial c}{\partial S}\frac{\partial S}{\partial t} \tag{2.3}$$

The equation may be rewritten as follows:

$$R_f \frac{\partial c}{\partial t} = -\frac{q}{\theta}\frac{\partial c}{\partial x} + D\frac{\partial^2 c}{\partial x^2} \text{where} \quad R_f = 1 + \rho_b \frac{\partial c}{\partial S} \tag{2.4}$$

This is the basic form of the ADR with an apparent reduction in velocity ($v' = v/R_f$) and in dispersion ($D' = D/R_f$). This apparent reduction is a function of the sorbed concentration (S), the aqueous concentration, c, the porosity, θ, and the bulk density of the porous media, ρ_b. Once a relationship between the sorbed and aqueous concentrations has been identified, the inclusion of sorption phenomena into contaminant transport modeling may be handled by a simple reduction in the velocity and hydrodynamic dispersion coefficients (Zheng and Bennett 2002). The reduction factor (retardation coefficient) may be (1) constant (for a linear isotherm) or (2) a function of the sorbed and aqueous concentrations. There are numerical difficulties associated with non-linear sorbed/aqueous relationships (Zheng and Bennett 2002), but the retardation factor is the most common approach for representing sorption in transport simulations, especially in Eulerian-Lagrangian schemes (e.g., (Konikow et al. 1996)). Sorption is difficult to simulate with the retardation factor approach if the sorption process is either kinetic or competitive. In those cases, the local retardation factor is often a complicated non-linear function of local species concentrations and time.

An alternative means of representing sorption phenomena is via inclusion of sorption into the conventional mass balance scheme as an additional reaction term with an additional set of chemical components (that of the sorbed species). This option is preferred to the retardation factor approach for modeling kinetic or competitive sorption.

2.1.3 Discretization of Transport Parameters

Velocity Discretization

One of the primary benefits of the analytic element method is the production of highly accurate continuous velocity fields as output. This benefit has been touted by the users and developers

of AEM, but no research within the analytic element community has pointedly addressed the significance of the continuous velocity fields in groundwater modeling. However, a great amount of literature has been devoted to improvement and analysis of velocity interpolation techniques in the finite difference / finite element literature, mostly in the context of particle tracking (Yeh 1981; Pollock 1988; Goode 1990; Cordes and Kinzelbach 1992; Durlofsky 1994; Zheng 1994; Pokrajac and Lazic 2002). Many of the results of this research can be extrapolated to AEM, which may be conceptualized as providing a flow solution with infinitely fine grid or mesh resolution. For analytical solutions, the velocity is known explicitly at any point in the domain. However, in finite difference and finite element models, the velocity is known only at a set of discrete points. Therefore, velocity interpolation techniques have been developed to mimic continuous, smooth behavior using discrete values of the velocity at nodes. With a similar rationale, modified flow solution methods have been developed that represent the velocity in a more exact sense without additional cells or finite elements (e.g., Frind and Matanga (1985); Mosé et al. (1994)).

A common use of velocity information in transport modeling is to advect ("track") particles (either backward or forward) by integrating the velocity along the particle's path. Tracking is used in both Eulerian-Lagrangian and pure Lagrangian methods to represent advection of contaminant in the subsurface. Additional uses of velocity information include determination of discharge between finite difference cells, calculation of hydrodynamic dispersion coefficients, and calculation of the residual expression in finite element methods. The coarseness of velocity field discretization, in conjunction with the interpolation method used and the accuracy of the integration algorithm, drastically affect the outcomes of particle tracking or other uses of velocity information (Mosé et al. 1994).

Initially, particle tracking was performed using traditional integration methods (e.g., Runge-Kutta methods) based upon a velocity field represented using simple linear or bilinear interpolation between discrete nodal values (i.e., Prickett et al. (1981)). However, simple interpolation methods cause discontinuities in velocity or the velocity gradient, particularly in complicated flow domains. In addition, simple interpolation overlooks the local influence of certain features in the flow field, such as wells (Yeh 1981). Though bilinear interpolation (the most common technique) is in agreement with the general assumptions of the finite difference method (Goode 1990), there are still inherent errors associated with its use. Therefore, many adaptations of bilinear and linear velocity interpolation techniques have been developed. Pollock (1988) developed an oft-used semi-analytical

method that provides semi-analytic pathlines within each individual finite difference block, circumventing the need for Runge-Kutta methods. Cordes and Kinzelbach (1992) adapted Pollock's method for finite element geometries. Other, more complicated, schemes have been developed to reduce the "mesh error", or error due to spatial interpolation (Zhang et al. 1994; Cheng et al. 1984; Bensabat et al. 2000; Pokrajac and Lazic 2002). Some of these are higher order interpolation schemes (i.e., the cubic interpolation of Zhang et al. (1994)) and, while they create a smoother representation of Darcian velocity, do not maintain the water balance (Zheng and Bennett 2002).

In addition to new interpolation schemes, tracking techniques have been adapted to counter specific problems caused by the discrete representation of velocity fields. Goode (Goode 1990) developed a technique that preserved the discontinuity in the normal component of flow at transmissivity boundaries. Zheng (1994) presented techniques for handling velocity interpolation near "weak wells" (wells that pull water into less than 4 sides of a finite difference cell). In the same paper, Zheng also provided a means to repair velocity errors due to discontinuous discretization in the vertical direction.

While many of these papers cited the inaccuracies of particle tracking techniques, most of them did not examine, in detail, how this affects contaminant transport models that use particle tracking (either pure Lagrangian or Eulerian-Lagrangian (EL) methods). However, Oliveira and Baptista (1998) directly addressed the effects of poor tracking procedures in EL methods by both formal analysis and numerical experiments. Oliveira and Baptista concluded that poor tracking could cause both negative and positive numerical dispersion and significant mass balance errors. Their conclusion, citing multiple sources of incurred transport errors, was that the effect of tracking errors upon the accuracy and stability of Eulerian-Lagrangian methods is "severe". The primary problem mentioned is that inaccurate tracking of characteristic lines and non-conservative flow fields leads to incorrect positioning of the feet of characteristic lines, thus causing local mass balance errors. Similar results were obtained by Ruan and McLaughlin (1999), who investigated the effects of using various high-order velocity interpolation (and concentration interpolation) schemes for contaminant transport simulation. These high-order schemes are designed to compensate for a discrete representation of velocity.

The non-continuous representation of discharge and head in FD flow models introduces some other disadvantages. For example, finite difference models have to resort to complex algorithms for velocity refinement near "weak" sources and sinks (Zheng 1994; Charbeneau and Street 1979; Sun

et al. 1994). Such refinement schemes are required to adequately define capture zones and capture particles. Without these schemes, particles that should be captured pass through the grid cell.

With the analytic element method, the act of interpolation is unnecessary, as the velocities are continuous functions of space. Additionally, the continuous velocity representation in AEM bypasses the need for algorithms to handle "weak wells" or incongruous spatial discretization (i.e., for moving front algorithms), which are fully symptomatic of the flow grid representation. The only decision to be made is the integration method used for particle tracking. Strack (Strack 1989) presents a simple constant time step Euler method for use in analytic flow fields. However, research (i.e., Goode (1990)) suggests that higher order adaptive Runge-Kutta methods are preferable and provide more accuracy for minimal additional computational expense. Other alternatives for tracking within analytic flow domains are based upon the stream function (e.g., Frind and Matanga (1985); Strack (1989)). These methods can be used for verification of the accuracy of Runge-Kutta techniques, but are generally more time consuming and are not applicable to divergent flow fields.

Property Field Discretization

Discretization of the property fields (e.g., porosity), is typically overlooked as a source of error. This information is usually not known at a spatial scale sufficient to warrant precise representation. The conceptual model of porous media property distributions is therefore modified so that it easily conforms to the model; i.e., it is therefore represented discretely. However, there are some scenarios in which local perturbations in the porosity or sorption coefficients at a scale less than the desired mesh resolution may be desired, or cases where the gradient in a property has a notable impact on the solution. Because continuous representation of transport parameters is uncommon, there is no published error analysis of its effects upon transport simulation. However, the study of continuous non-homogeneous materials in material engineering has shown that modeling continuous parameter fields in a discrete, cell- or element-averaged manner reduces the accuracy of numerical solutions (Santare and Lambros 2000).

Researchers in groundwater modeling have directly investigated the effects of parameter discretization in flow models (not transport models) and its effects upon the simulation of highly heterogeneous media at varying scales. The process of "upscaling" is of great importance for groundwater modelers in understanding the behavior of groundwater systems at small and large scales simultaneously (Farmer 2002). Investigators in this field have compared the effects of solving

the same governing equations with random parameter fields at various levels of resolution (Farmer et al. 2003; Chen et al. 2003). It was found that the act of reducing the resolution of the parameter field (in these cases, hydraulic conductivity) induced significant differences (i.e., errors) in model results (expressed in terms of head). Similar errors will be incurred in transport simulations that use lower resolution representations of velocity and dispersion coefficients, except that errors in transport simulations will accumulate over time.

2.2 Mathematical Background

The following section provides the mathematical background for the methods developed in chapter 3.

2.2.1 The Analytic Element Method

For steady-state irrotational two-dimensional flow with piecewise constant aquifer properties, the governing equation for groundwater flow (equation 2.1) may be written as the Poisson equation in terms of a discharge potential, $\Phi[L^3/T]$ (Strack 1989):

$$\nabla^2 \Phi = N \tag{2.5}$$

where N $[\mathrm{LT}^{-1}]$ is the vertical flux of water out of the aquifer.

The 2-D analytic element method (Strack 1989; Haitjema 1995) expresses the steady-state flow solution to equation 2.5 in terms of the complex potential, $\Omega[L^3/T]$:

$$\Omega(z) = \Phi(z) + i\Psi(z) \tag{2.6}$$

where $\Psi[L^3/T]$ is the stream function (undefined when $N \neq 0$), and $z = x + iy$ is a location in the complex plane. Discharge potential is related to piezometric head, $\phi[L]$, by the following relationships for confined and unconfined flow, reliant upon the Dupuit-Forcheimer assumption:

$$\Phi = \begin{cases} \frac{1}{2}k\phi^2 & \text{if } \phi < H \\ kH\phi - \frac{1}{2}kH^2 & \text{if } \phi > H \end{cases} \tag{2.7}$$

where H $[L]$ is the layer thickness and k $[L/T]$ is the hydraulic conductivity.

The AEM is based upon superposition: Ω and W at any location z are expressed as the sum of complex potentials or discharge functions due to a set of distinct hydrologic features (elements). The vertically-integrated discharge in the domain is directly related to the complex potential by the following relationship:

$$W = Q_x - iQ_y = -\frac{\partial \Omega}{\partial z} \tag{2.8}$$

where W is termed the discharge function, and Q_x and $Q_y[L^2/T]$ are the vertically-integrated

discharge components, given by:

$$Q_x = \int_0^h q_x dz' \qquad Q_y = \int_0^h q_y dz' \tag{2.9}$$

where $h[L]$ is the saturated thickness of the domain, q_x and $q_y[L^3/T]$ are components of the specific discharge vector, and z' is the vertical coordinate measured from the aquifer base. The discharge function is evaluated via superposition of element discharge functions in the same manner as the complex potential. Thorough discussions and surveys of the mathematical principles behind the analytic element method may be found elsewhere (Strack 1989; Haitjema 1995; Janković 1997; Fitts 2002; Strack 2003).

The vertically-averaged horizontal velocity components v_x and v_y, essential for transport simulation, are related to Q_x and Q_y by:

$$v_x = \frac{Q_x}{h\theta} \qquad v_y = \frac{Q_y}{h\theta} \tag{2.10}$$

where the porosity, θ, may be any continuous function of space (e.g., analytic, radial basis function, piecewise continuous, etc.) and the saturated thickness, h, is a function of the hydraulic head and thickness. The functional form of the porosity has no effect upon the flow solution.

While it is adequate for the flow solution to express the leakage/recharge outflux N in its aggregate form, the magnitude of each component must be specified for transport modeling. The following convention is used:

$$N = N_t^- + N_b^- - N_t^+ - N_b^+ \tag{2.11}$$

where N_t^- [LT^{-1}] is the volumetric loss of water per unit area through the top of the aquifer, N_b^- [LT^{-1}] is the loss of water through the bottom of the aquifer, N_t^+ [LT^{-1}] is the gain of water through the top of the aquifer, and N_b^+ [LT^{-1}] is the gain of water through the bottom of the aquifer. All values are positive.

Due to the analytic element representation, the velocity, saturated thickness, recharge/leakage terms, and porosity may all be expressed as continuous functions of x-y coordinates. This allows for highly accurate particle tracking though continuous domains and continuous representation of species-specific dispersion coefficients, which are dependent upon velocities. It is important to note that the steady-state flow assumption often used in AEM is not necessarily a limiting factor in

solute transport modeling. Contaminant transport problems often involve long time scales where the short-term transients are often unimportant (Frind and Matanga 1985).

2.2.2 Vertically-Averaged Transport

For the approach presented in this dissertation, the applicable governing equation is the vertically-averaged advective-dispersive transport equation with sorption and reaction. The traditional three-dimensional advection-dispersion equation with retardation for a single solute may be expressed as (adapted from Bear (1972)):

$$R_f \frac{\partial c}{\partial t} = -\frac{1}{\theta}\nabla(\vec{q}c) + \frac{1}{\theta}\nabla\left(\mathbf{D}\theta \cdot \nabla c\right) \tag{2.12}$$

where c is the concentration of the solute at a point in space, R_f is the retardation factor, and $\mathbf{D}$ is the three-dimensional dispersion tensor. Assuming no variation of concentration or flux in the vertical direction ($\partial c/\partial z = 0$; $\partial q/\partial z = 0$), this equation may be integrated in the vertical direction to obtain a vertically-averaged formulation (adapted from Bentley and Pinder (1992), Gray (1982), and Yeh (2000)):

$$\begin{aligned} h\theta R_f \frac{\partial C}{\partial t} = &- \frac{\partial Q_x C}{\partial x} - \frac{\partial Q_y C}{\partial y} \\ &+ \frac{\partial}{\partial x}\left(h\theta D_{xx}\frac{\partial C}{\partial x}\right) + \frac{\partial}{\partial x}\left(h\theta D_{xy}\frac{\partial C}{\partial y}\right) \\ &+ \frac{\partial}{\partial y}\left(h\theta D_{yx}\frac{\partial C}{\partial x}\right) + \frac{\partial}{\partial y}\left(h\theta D_{yy}\frac{\partial C}{\partial y}\right) \\ &+ N_t^+ c_t^+ + N_b^+ c_b^+ - N_t^- C - N_b^- C \end{aligned} \tag{2.13}$$

Where c_t^+ and c_b^+ are the concentrations of water entering the system through the top and bottom of the aquifer, respectively. This revised formulation only has two spatial dimensions, and the dependent variable is the vertically-averaged concentration, C, defined as the aqueous concentration averaged over the saturated thickness of the aquifer:

$$C(x,y) = \frac{1}{h}\int_0^h c(x,y,z')dz' \tag{2.14}$$

Where z' [L] is the vertical coordinate measured from the base of the aquifer. If the advective terms ($\partial Q_x C/\partial x$, $\partial Q_y C/\partial y$) of equation 2.13 are expanded using the chain rule, a first-order term

is obtained:

$$-\frac{\partial Q_x C}{\partial x} - \frac{\partial Q_y C}{\partial x} = -Q_x \frac{\partial C}{\partial x} - Q_y \frac{\partial C}{\partial x} - \left(\frac{\partial Q_x}{\partial x} + \frac{\partial Q_y}{\partial y} - N_t^- - N_b^- \right) C \tag{2.15}$$

From a mass balance on water in the system, the rightmost term reduces to $-(N_t^+ + N_b^+)C$, and the governing equation may be rewritten as:

$$\begin{aligned} h\theta R_f \frac{\partial C}{\partial t} = & - Q_x \frac{\partial C}{\partial x} - Q_y \frac{\partial C}{\partial y} \\ & + \frac{\partial}{\partial x}\left(h\theta D_{xx} \frac{\partial C}{\partial x} \right) + \frac{\partial}{\partial x}\left(h\theta D_{xy} \frac{\partial C}{\partial y} \right) \\ & + \frac{\partial}{\partial y}\left(h\theta D_{yx} \frac{\partial C}{\partial x} \right) + \frac{\partial}{\partial y}\left(h\theta D_{yy} \frac{\partial C}{\partial y} \right) \\ & + N_t^+ \left(c_t^+ - C \right) + N_b^+ \left(c_b^+ - C \right) \end{aligned} \tag{2.16}$$

where N_t^+ and N_b^+ [LT^{-1}] are the influxes of fluid from the top and bottom of the domain, respectively (both are components of the net vertical flux, N), and c_t^+ and c_b^+ are the concentrations of solute in this recharged water. Additional source and sink terms (often considered boundary conditions for this governing equation) may also be included in this formulation. This form of the governing equation is valid for both discrete and continuous parameterization.

Equations 2.13 and 2.16 have been labeled the "divergence form" and the "convective form" of the solute transport equation, respectively (Diersch 1998a; Gresho and Sani 1998). They are distinguished by the inclusion or exclusion of the flow mass balance equation and, if the flow equation is met exactly, are identical. However, the convective form is more susceptible to errors introduced by improper spatial and temporal discretization of the flow system (Saaltink et al. 2004; Gresho and Sani 1998), and may not preserve mass balance if the level of discretization is insufficicent.

While there has been some research into the vertically-averaged transport formulation (Gray 1982; Bentley and Pinder 1992; Yeh 2000), robust implementations of this approach have been overlooked with the advent of three-dimensional models. However, regional scale transport models may benefit from a two-dimensional representation with reduced computational and data constraints. Also, single-layer three-dimensional contaminant transport models are commonly used in practice. Such "truncated-dimension" models may not adequately account for the implied vertical averaging, especially in unconfined aquifer systems. Finally, two-dimensional analytic element models are

commonly used for regional flow modeling. To effectively model transport using these existing flow solutions, an accurate and robust vertically-averaged formulation is needed.

2.2.3 The Finite Difference Method

The basic finite difference method for solving partial differential equations operates by discretizing the problem domain using a rectangular grid. The unknown variable $C(\mathbf{x})$ (where $\mathbf{x}$ is the position vector) is assumed to be well approximated by its average value over the grid cell, C_{ij} (where i and j denote the column and row, respectively, of the grid cell). Once the unknown variable is expressed in this discrete fashion, the spatial and temporal derivatives may be written in terms of discrete algebraic finite difference approximations. Such approximations are obtained from a truncated and rearranged Taylor series expansion. A Taylor series expansion expresses any continuous function $C(\mathbf{x})$ at one location ($\mathbf{x}$) by its value and that of its derivatives at another location ($\mathbf{a}$). In one dimension, the Taylor series may be written as

$$C(x) = C(a) + \left.\frac{\partial C}{\partial x}\right|_a (x-a) + \left.\frac{\partial^2 C}{\partial x^2}\right|_a \frac{(x-a)^2}{2!} + \left.\frac{\partial^3 C}{\partial x^3}\right|_a \frac{(x-a)^3}{3!} + ... \tag{2.17}$$

By rearranging this expression, an approximation of the first derivative at a is available based on the values of C at x and at a

$$\left.\frac{\partial C}{\partial x}\right|_a = \frac{C(x)-C(a)}{x-a} - \left[\left.\frac{\partial^2 C}{\partial x^2}\right|_a \frac{(x-a)}{2!} + \left.\frac{\partial^3 C}{\partial x^3}\right|_a \frac{(x-a)^2}{3!} + ...\right] \tag{2.18}$$

The term in the square brackets is the error associated with truncation of the Taylor series. In the finite difference method, this low order approximation is expressed in terms of the average or representative values over the grid cell, C_{ij}, and the distance between grid cell centers, Δx and Δy, instead of the value $(x-a)$. Expressing the truncation error as E, a simple finite difference approximation of the first derivative of C may be written as

$$\left.\frac{\partial C}{\partial x}\right|_{ij} \approx \frac{C_{i-1,j} - C_{ij}}{\Delta x} - E(\Delta x) \tag{2.19}$$

By varying both the number of terms retained in the Taylor series and the choices for how x and a are defined, both low and high order finite difference approximations may be written for spatial and temporal derivatives. These finite difference approximations are written in terms of discrete

quantities (the unknown values of C_{ij}, $C_{i+1,j-1}$, etc.) and are algebraic in form. By expressing a partial differential equation (PDE) in terms of its constituent finite difference approximations, an algebraic equation may be used as an approximation of the PDE at each grid cell. The resultant system of equations may be solved using standard linear matrix algebra algorithms (e.g., Gauss elimination), resulting in an adequate approximation of the solution for the actual partial differential equation. The accuracy of these methods is generally linked to the truncation error term, E, which is a function of the spatial grid resolution (Δx and Δy) and, for transient PDEs, the temporal resolution (Δt).

2.2.4 The Finite Element Method

Finite element solutions consider a differential equation of the form:

$$\pounds(C(\mathbf{x},\mathrm{t})) - \mathrm{F}(\mathbf{x},\mathrm{t}) = 0 \tag{2.20}$$

where $\pounds$ is a differential operator in space, $\mathbf{x}$, and time, t, C is the field variable (vertically-averaged concentration in this case), and F is a known "forcing" function, which often includes the influence of boundary conditions. Finite element methods define an approximate solution, $\hat{C}$ of the form:

$$\hat{C}(\mathbf{x},\mathrm{t}) = \sum_{\mathrm{i}=0}^{\mathrm{NN}} \mathrm{N_i}(\mathbf{x},\mathrm{t})\hat{\mathrm{C}}_\mathrm{i} \tag{2.21}$$

where N_i are interpolation functions (also referred to as basis or "shape" functions), $\hat{C}_i$ are the unknown values of the concentration field at the nodes of the FE mesh, and NN is the number of nodes in the FE mesh. When the approximate solution is substituted into (2.20), the differential equation is no longer satisfied exactly, and creates a residual, $R(\mathbf{x},\mathrm{t})$:

$$\pounds(\hat{C}(\mathbf{x},\mathrm{t})) - \mathrm{F}(\mathbf{x},\mathrm{t}) = \mathrm{R}(\mathbf{x},\mathrm{t}) \neq 0 \tag{2.22}$$

In the method of weighted residuals, the residuals at the nodes of the problem domain, Ω, are set to zero:

$$\int_\Omega w(\mathbf{x},\mathrm{t}) \left[\pounds(\hat{\mathrm{C}}(\mathbf{x},\mathrm{t})) - \mathrm{F}(\mathbf{x},\mathrm{t})\right] \mathrm{d}\Omega = 0 \tag{2.23}$$

where $w(\mathbf{x}, \mathrm{t})$ is the weighting function, which assigns weights to each residual. To evaluate this equation, we must specify the mathematical form of the approximate solution, $\hat{C}(\mathbf{x}, \mathrm{t})$ and the weighting function. In the finite element Galerkin method, the functional forms for $N(\mathbf{x}, \mathrm{t})$ and $w(\mathbf{x}, \mathrm{t})$ are the same. Within this dissertation, the upstream-weighted Petrov-Galerkin method is also considered, where the weighting function is not equal to the shape function for terms involving advection. Only low-order linear triangle basis functions are considered (see appendix D). However, much of the analysis contained herein is equally valid for other basis function types (i.e., quadrilateral, hermite, etc.).

Finite element methods, well-explained by Huyakorn and Pinder (1983) and thoroughly analyzed for advection-dispersion simulations by Gresho and Sani (1998), are able to minimize the computational demand of the preceding problem by discretizing the domain into "finite elements". The nodal weighting functions and basis functions are defined as only being non-zero within elements adjacent to the node they are associated with. This simplifies the problem considerably, and still provides much flexibility in the geometry of the problem. However, requirements of this revised method demand intelligent discretization of the system and require extensive bookkeeping and complicated algorithms for computing the integrals in the residual term. The accuracy of FE methods depends upon (1) the malleability of the approximate solution (the mesh resolution, order of the basis functions, etc.) and (2) the accuracy of the residual integration.

2.2.5 Discretization Constraints: Peclet and Courant Numbers

As briefly discussed previously in this chapter, both finite difference and finite element methods for transport simulation are limited by constraints upon spatial and temporal discretization. There are four primary constraint types considered here: two (Peclet and Courant constraints) are associated with the solution of general advection dispersion equations. These constraints, required for accurate and stable solution of the solute transport equations, are best expressed in terms of grid- or mesh-based dimensionless variables, as discussed below. The second two constraints, labeled here the "adjacency" constraints and the "row-column" constraints, are associated with discrete solution of any partial differential equation (though the row-column constraint is a limitation only of finite difference methods).

The Peclet number, Pe indicates the relative influence of advective transport to dispersive transport, and is given as (Peaceman 1977):

$$Pe = \frac{vL}{D} \tag{2.24}$$

Where v is the velocity, D is the dispersion coefficient, and L is a representative length scale. For simulation models, the "grid Peclet" or "mesh Peclet" number is defined with the length scale set equal to the local representative grid or mesh spacing. Within this dissertation, the representative length scales, ΔL, for any rectangular grid cell or triangular finite element are given as:

$$\Delta L = \begin{cases} \min(\Delta x_i, \Delta y_j) & \text{for FD grid cell } i,j \\ \sqrt{2A^{(e)}} & \text{for FE element } e \end{cases} \tag{2.25}$$

Where $A^{(e)}$ is the area of finite element e and Δx_i and Δy_j are the grid spacings of finite difference cell ij. Dispersion is considered to dominate when the Peclet number is much less than one, and advection is considered to dominate when it is much greater than one. For simulation of both advection and dispersion, the unconditionally stable Crank-Nicholson implementation of the finite difference method requires that grid Peclet numbers be less than 2 to avoid oscillation of the solution (Huyakorn and Pinder 1983). The equivalent Crank-Nicholson implementation of the finite element method requires mesh Peclet numbers less than 10 (Huyakorn and Pinder 1983), though other sources recommend Peclet numbers less than 4 (Voss 1984). Note that finite element methods have less stringent requirements on the node density to avoid oscillations, and therefore reduced constraints on the total number of degrees of freedom in the model. In order to meet the Peclet constraints, grid/mesh resolution usually must be the same order or smaller as the hydrodynamic dispersivity. Thus, highly dispersive systems can have fewer degrees of freedom and still avoid oscillation of the solution.

Another dimensionless number, the Courant number, is used to determine the appropriate temporal discretization required for *non-reactive* transport (individual reactions often require shorter time steps for accurate and stable simulation). The Courant number, Cr, is defined as (Peaceman 1977):

$$Cr = \frac{v\Delta t}{\Delta L} \tag{2.26}$$

The Courant number is an indicator of the speed of advection relative to the mesh. If $Cr << 1$,

then a parcel of solute within the grid cell will likely have stayed inside of the grid cell during the duration of the time step. If $Cr >> 1$, then the parcel will have entered and exited many grid cells or finite elements before the end of the time step. Without dispersion or diffusion, fully Eulerian approaches for solving any advection phenomenon are unstable when the Courant number is greater than one. This requirement, based upon the inability of discrete numerical methods to transfer information at a speed greater than $\Delta x/\Delta t$, is called the Courant-Friedrichs-Lewy (or CFL) stability criterion (Hoffman 1992). With dispersion (either numerical or intentional), this requirement is relaxed. Implicit or Crank-Nicholson approximations to the temporal derivative will provide unconditionally stable, but conditionally accurate solutions to the governing equations. Therefore, a maximum Courant number of one is still suggested for most even mildly complex simulations (Huyakorn and Pinder 1983). In addition, certain reaction formulations require Courant numbers that are even smaller than required for non-reactive transport simulations. When equilibrium or kinetic sorption is handled using operator-splitting, Courant numbers as low as 0.01 may be required to adequately characterize the interaction between mobile and immobile phases. While the Courant constraint is generally considered a means of determining the temporal discretization (Δt), it can also be considered as an inverse constraint upon spatial discretization (i.e., shrinking Δl can lead to a computationally inhibitive Δt).

As can be seen from the above constraints, the spatial and temporal discretization process is highly dependent upon the flow-based parameters (v; D) that fuel the governing equation for reactive solute transport. However, there are additional requirements of grid or mesh discretization needed for accuracy. The adjacency constraint, a property of both finite difference and finite element methods, requires that adjacent grid cells or elements be of similar size. For finite elements, this requirement stems from the improved behavior of condensed element geometry (e.g., an equilateral triangle) over long, thin elements (Knupp 2000; Shewchuk 2002). To ensure that each element is roughly equilateral, adjacent elements must be of similar size. For finite difference methods, truncation error is higher for grids that have nonuniform spacing. The degree of error is proportional to the change in spacing (as well as the size of the spacing). A general rule-of-thumb (as reported by Zheng and Bennett (2002)) is to increase grid spacing by no more than a factor of 1.5 or 2.

A final constraint, specific to the finite difference method, is the "row-column" constraint. Because the standard finite difference method operates upon a rectangular grid, the grid spacing must be uniform for each row and column. Therefore, even though fine discretization may only be

required at a single point, the small grid spacing is propagated across the entire gridded domain. Multigrid techniques (e.g., that of Leake and Claar (1999)) have been developed specifically to deal with this wholly geometric constraint.

In addition to the constraints above, it is desirable to have higher discretization in areas with high concentration gradients, in order to sufficiently resolve the complexity of the plume. However, such a discretization constraint is dependent upon the results of the transport model, and thus often cannot be determined until the simulation process has begun.

Chapter 3

Methods

The following section discusses in detail the software, algorithms, and new methods developed for this dissertation. The first of these developments is the software architecture upon which most of the research rests, the object-oriented flow and transport libraries developed specifically for this dissertation. The benefits of object-orientation are introduced and the structure of the libraries is presented and explained in section 3.1. A general calculation for estimating mass balance is presented in section 3.2. This is followed by an in-depth explanation of revisions applied to existing contaminant transport algorithms to effectively use AEM flow solutions and better account for continuous parameterization. Section 3.3 discusses the development of techniques for solving finite difference models of contaminant transport using translated AEM fluxes. Section 3.4 discusses the development and implementation of a new "effective parameter" method for modeling vertically-averaged transport using continuous representations of parameters. Section 3.6 and 3.7 discuss the development of a graded-parameter finite element method for use with analytic flow solutions. Many of these developments are primarily algorithmic in nature; but their implementation resulted in multiple fundamental observations about modeling with continuous parameters. Most importantly, this work represents the first fundamental analysis of the requirements and revisions required to use AEM flow solutions as a basis for transport simulation.

Much of section 3.3.2 was published in the proceedings of the Computational Methods in Water Resources 2004 International Conference (Craig and Rabideau 2004).

3.1 Object-Orientation

3.1.1 Motivation

Many of the computer models in the environmental sciences are "legacy" models, a term commonly used to describe computer programs written in Fortran in the mid-seventies and updated by major rewrites. The process of maintaining and modifying such codes can be intimidating, as many of these codes are written in a style that does not allow for simple revision. The acceptance of object-orientated programming (Booch 1994) has been a slow process for the scientific community due to the steep learning curve, the persistence of legacy code, and the once slower speed of many object-oriented programming languages. However, object-oriented programming has design benefits that enhance the understandability and modifiability of scientific code, potentially leading to a higher rate of development of environmental simulation algorithms.

To accommodate revision and addition, and to insure the extendibility of the code developed for this dissertation, object-oriented implementations of both the groundwater flow model (BLUEBIRD) and the contaminant transport models (CARDINAL) have been developed in C++. A thorough discussion of the object-oriented implementation of BLUEBIRD is given by Craig (Craig 2002), included in the digital appendix. Many of the object-oriented constructs, such as inheritance and encapsulation of data within object structures, are directly applicable to the inherently object-oriented nature of the analytic element method. Similarly, various transport simulation schemes use many of the same constructs and conceptual models (i.e., pathlines, grids, meshes) in their solution. These models benefit from an object-oriented implementation by the re-use of these data structures and a common conceptual model. Additionally, an object-oriented implementation allows for unification of multiple methods (i.e., analytic solutions along streamlines working in tandem with fully Eulerian numerical schemes). In an object-oriented framework, a library of methods, reaction schema, and solution techniques may be easily revised and supplemented.

3.1.2 Flow Modeling Library: Bluebird

The BLUEBIRD library contains a suite of classes and algorithms for modeling two-dimensional flow with the analytic element method. Details about the library are provided in the BLUEBIRD Developers manual (Craig 2002), included in the digital appendix. The general organization and functionality is discussed here. A basic working knowledge of the concepts of inheritance, data

encapsulation, instantiation, and communication in object-oriented programs is assumed. Readers is referred to Booch (Booch 1994) for an introductory discussion of these concepts.

The analytic element method, by its very nature, lends itself to an object framework based upon elements as the atomic classes. Elements each have their own geometric data (coordinates, shape), mathematical data (coefficients), and functionality (harmonic functions associated with the element). Individual elements may have very similar functional form but often different boundary conditions, suggesting the usefulness of inheritance relationships. The very nature of analytic elements seems to suggest the structure of the code.

Individual element structure and functionality are the primary sources of complexity in any software implementation of the analytic element method. For this reason, the focus of an OO implementation of the method is a robust classification of these elements, their similarities, and their dissimilarities. To effectively classify analytic elements into an object-oriented structure, a general description of the definition and requirements of an individual element is needed. An analytic element may be generically defined as having:

- Coordinates/dimensions that fully describe its location, shape, and orientation.
- An associated functional form/type including coefficients that, when associated with the appropriate function, describe the influence of the element in a domain
- A corresponding real-life entity/hydrogeologic feature, with a name and associated boundary conditions

Independently from the rest of the system, any one of these elements should be capable of providing:

- Geometric data about its borders
- Its contribution to the potential, complex discharge, divergence, curl, and other dependent variables

To be useful in a software implementation, an element data structure requires (1) access to particular information and (2) certain internal functionality. These requirements include:

- Access to information about the potential, complex discharge, and aquifer properties (e.g., conductivity) at its boundaries. This information may only be obtained by evaluating the influence of all other elements.

- The ability to solve for its own coefficients, given the latter information.
- The ability to update its "owners" (layers, groups of elements organized for calculation purposes (e.g., the nested superblocks of Craig et al. (2004)) or aggregate elements), either explicitly or when requested

Not all analytic elements have the same geometry, or the same coefficient structure, or same functional form. However, for an iterative solution method, any element without given coefficients has the same "need" to know the values of potential, complex discharge, and aquifer system properties (e.g., conductivity, base elevation, aquifer thickness) along its boundaries. To facilitate this communication, each element has been provided with explicit access to the two-dimensional "layer" in which it belongs. This layer class, CLayer, and its abstraction, CLayerABC, act both as suppliers of this information and as containers for collections of elements or information about aquifer properties. Additionally, all elements may have a name and (perhaps) a number of "subelements" contained within it, as deemed appropriate by Strack and Barnes (Strack and Barnes 2001). Data structures corresponding to these basic, universal needs are included in the master, or Level 1 class, CAnalyticElem. Functionality at this level is purely virtual (an instance of CAnalyticElem has no functional power: simply data). Subclasses (which inherit this more abstract data and functionality from their "parent" class) are required to "flesh out" the implementation of fully functional analytic elements. Figure 3.1 shows the subclass levels for the analytic element inheritance scheme as implemented in BLUEBIRD. The complete implementation of this scheme (the hierarchy of all analytic element subclasses) is shown in figure 3.2.

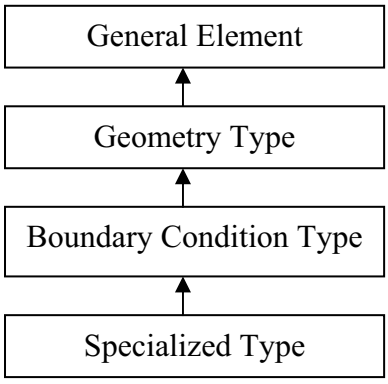

Figure 3.1: Multiple levels of inheritance subclasses for the master analytic element abstraction CAnalyticElem

Subclasses of CAnalyticElem are designed to be as general as possible without requiring excessive inheritance beneath them. The groupings should be able to represent as many different types of elements without being restricted by overburden of data within each element (for example, a polygonal element shouldn't have the burden of holding an empty "radius" variable). Therefore, the design of BLUEBIRD was such that the geometry and functional form were all encapsulated at the level directly beneath the master class (Level 2). This minimizes overhead, because the harmonic functions associated with the elements are evaluated at only one level of inheritance. At the same time, it maximizes generality, allowing head-specified linesinks and inhomogeneities (which have similar functional form but different boundary conditions) to be represented by the same class. Most of the virtual CAnalyticElem functions (for Φ, W, γ, β) are defined at this level. A given instance of a level 2 subclass (e.g., CStringElem in fig. 3.2) is also not fully functional, as it is still missing the ability to solve itself; it has no boundary conditions associated with it.

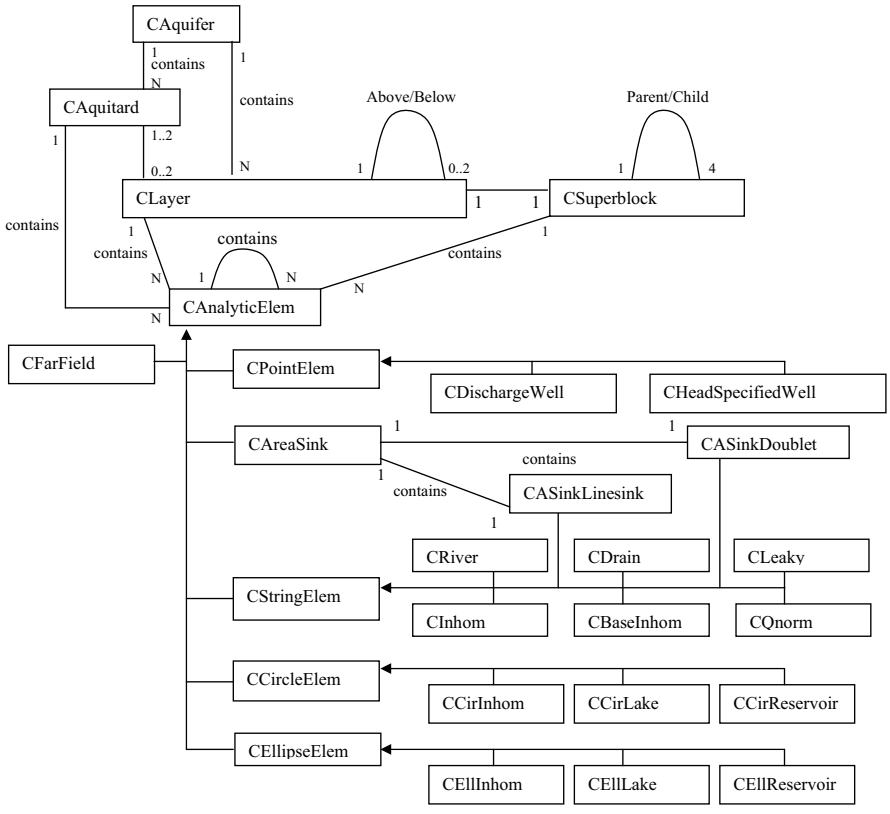

Figure 3.2: BLUEBIRD library class organization. Class inheritance is depicted by arrows, and 1:1, 1:N, and N:N container relationships are also depicted. The primary class, CAnalyticElem is the master class for all analytic elements.

At the bottom (3rd) level of inheritance, the specific boundary condition type is the subdivision

criteria. Each instance of these third-level classes (e.g., CRiver) represents an element in its most complete configuration, with specific boundary conditions (defined at level 3), geometry (defined at level 2), and functional form (also defined at level 2). In addition, it has the generic data and functionality rendered to it via the level 1 CAnalyticElem parent class. The only virtual subroutine redefined at the 3rd level is the algorithm for "self-solution". All of the other CAnalyticElem functionality is located one level up within the Geometric/Functional subclasses.

In addition, a 4th level of inheritance may be envisioned (i.e., for special elements that meet different variations of the same boundary conditions, such as a resistance lake).

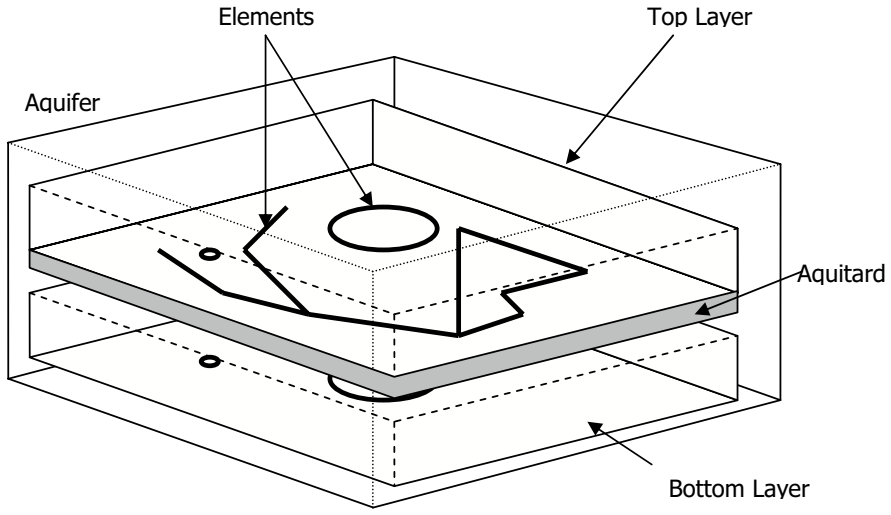

Figure 3.3: The abstraction of an analytic element model. Elements are contained by layers or aquitards, which in turn are contained by the aquifer.

A complete model configuration is shown in figure 3.3. A generic set of analytic elements CAnalyticElem are contained within a layer. This layer, in turn, is contained within a multi-layer aquifer (CAquifer), as are aquitards (CAquitard). The general solution process (shown in detail in figures 3.5 and 3.6) proceeds via solution of the aquifer, which requires iterative solution of its contained layers. These layers, in turn, are solved in an iterative element-by-element fashion (as discussed by Janković and Barnes (Janković and Barnes 1999a)). Individual analytic elements have internal functionality that allows them to calculate their own coefficients based upon their known boundary conditions and the current system conditions, as provided by their access to the CLayer abstract base class, CLayerABC. In addition, abstract OO classes for nested superblock structures (Craig et al. 2004) have been implemented. These structures may be superimposed upon groups

of elements within a single layer to reduce the per-iteration cost the iterative solution process. The awareness of all of these classes to each other is shown in figure 3.4.

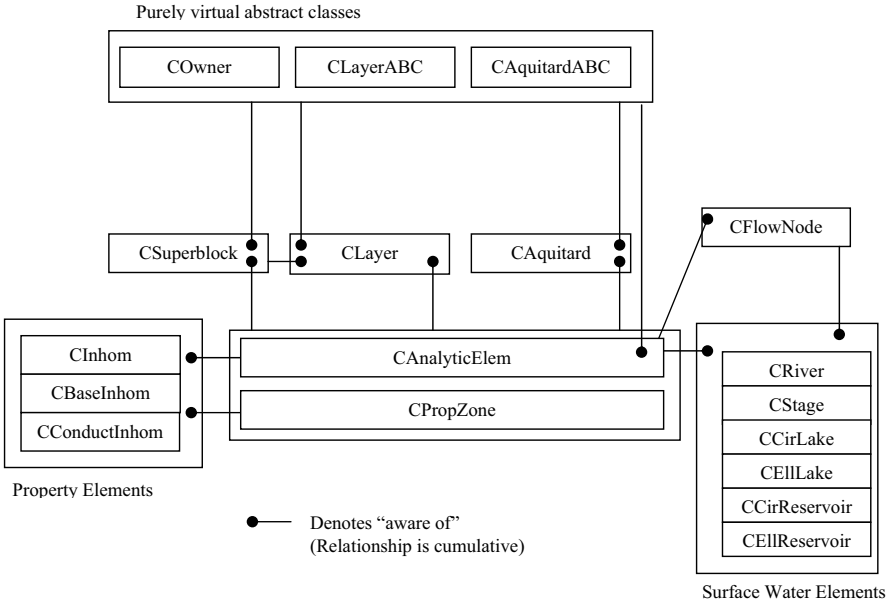

Figure 3.4: BLUEBIRD library class awareness. Analytic elements are only aware of the most abstract form of the layer that they are in, through which they may request information such as the potential from other elements or the hydraulic conductivity.

The process of developing, solving, and analyzing the results from an analytic element model heavily depends upon not only the configuration of the analytic element class hierarchy and functionality, but requires certain auxiliary classes and driver routines. The reader is referred to the BLUEBIRD developer manual (Craig 2002) for detailed information about these classes.

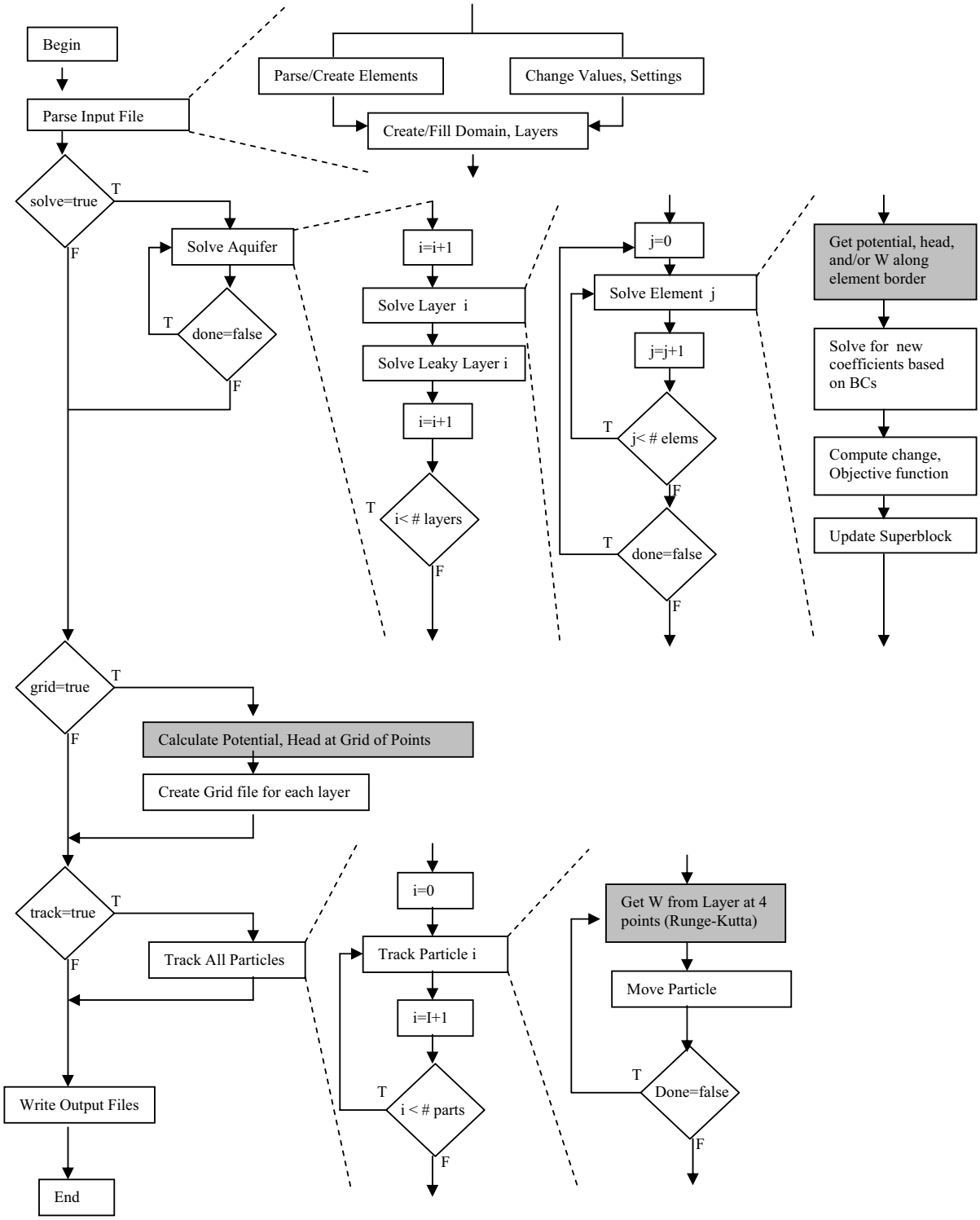

Figure 3.5: Flow chart of generic BLUEBIRD iterative solution algorithm. The potential evaluation function is depicted in Fig. 3.6

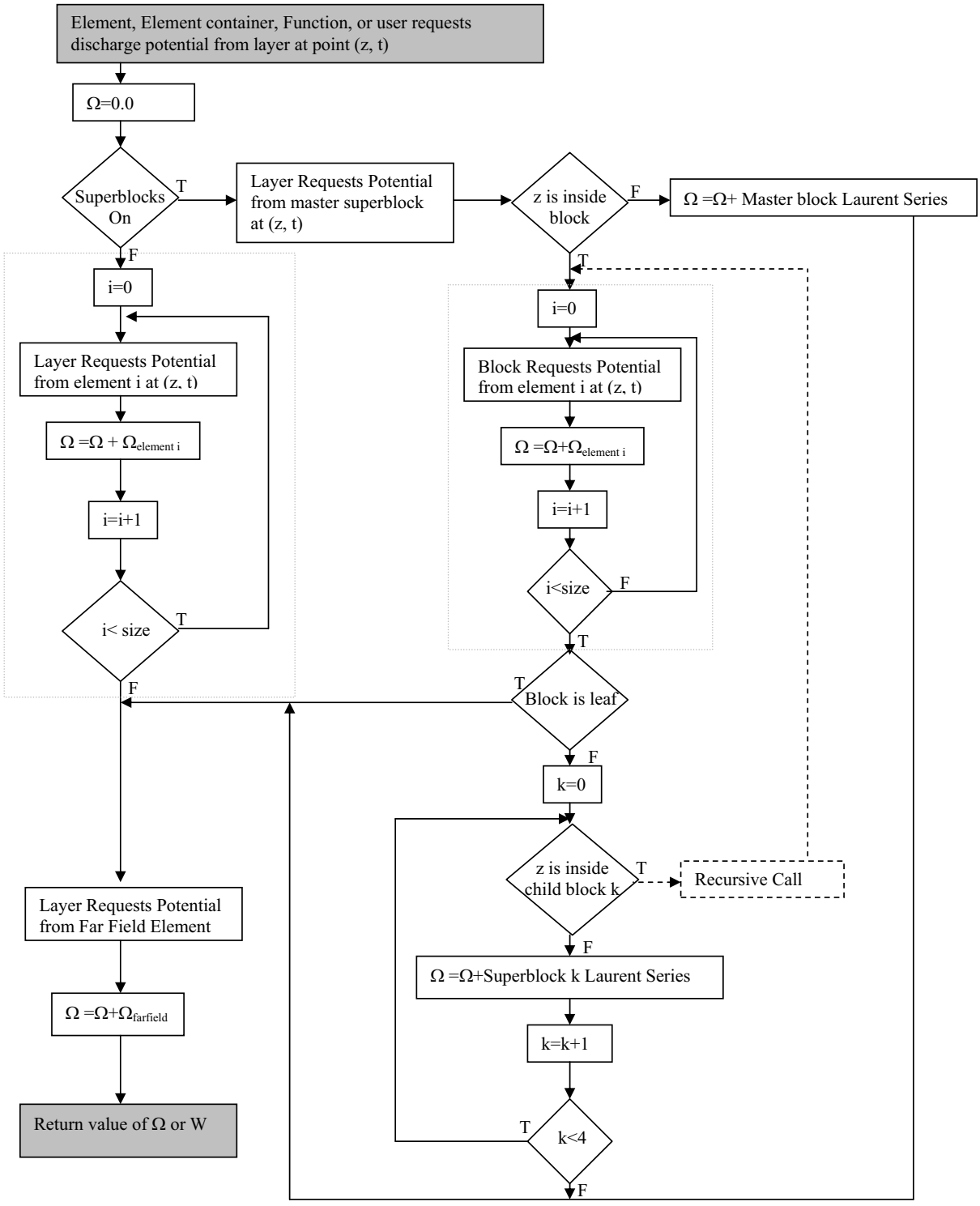

Figure 3.6: Flow chart of discharge potential evaluation in the BLUEBIRD library

3.1.3 Transport Modeling Library: Cardinal

The object-oriented CARDINAL library contains a suite of classes and algorithms for modeling two- and three-dimensional reactive contaminant transport using a wide variety of transport algorithms and a fully abstract representation of the aquifer. It has been designed specifically for use in conjunction with BLUEBIRD.

The structure of CARDINAL is designed for maximal modifiability: additional algorithms for hydrodynamic and reactive transport may be added with minimal modification of the original code. The primary means of ensuring this modifiability is the use of operator-splitting algorithms. The processes of advection, dispersion, and reaction, which in reality occur simultaneously, may be simulated sequentially over a given time step (note that this does not preclude the addition of schemes that model both simultaneously). Operator-splitting allows algorithms for hydrodynamic (advective and dispersive) transport algorithms to be developed independently from chemical reaction modules. This approach does not preclude the development of globally implicit algorithms for solving reaction and transport simultaneously. Rather, the current implementation embraces the independence of the two processes. In addition, the CARDINAL library is not reliant upon any particular grid or mesh formulation. Finite element, finite difference, or finite volume mesh discretization are all equally viable.

The two primary OO classes used as a basis for contaminant transport are the "transport scheme" (CTransportScheme) and the "reaction scheme" (CReactionScheme). An instance of the transport scheme may take a spatial distribution of concentrations at the start of a given time step of interest and returns the updated spatial distribution of concentrations at the end of the time step, after advection and dispersion have been simulated. Likewise, the reaction scheme takes a set of aqueous and immobile concentrations (not associated with any particular spatial location) and returns the updated concentrations at the end of the time step.

In addition to the primary classes that simulate the transport and reaction of contaminants, the CARDINAL library contains a suite of other classes for transport simulation. Included in this auxiliary group are a generic isotherm class (CIsotherm), a generic particle class (CParticle), and generic source/sink classes (CAreaSource, CPointSourceSink, CLinearSourceSink). New isotherm types or source conditions may be added with minimal effort. All of the information regarding the entire simulation domain (including sink/source geometry, grid/mesh information, transport schemes, and reaction schemes) are stored in a "driver" class, CChemDomain. CChemDomain is analogous to the

CAquifer class in the BLUEBIRD library, in that it may be viewed as a "container" class that holds information about the entire system.

The class organization diagram for CARDINAL is shown in figure 3.7. Note that the interaction between classes is significantly more complicated than the BLUEBIRD library, which is primarily comprised of different subclasses of analytic elements. The predominant classes of the transport library, however, are the transport and reaction schemes. New transport schemes and new reactions may be added with minimal modification of the library.

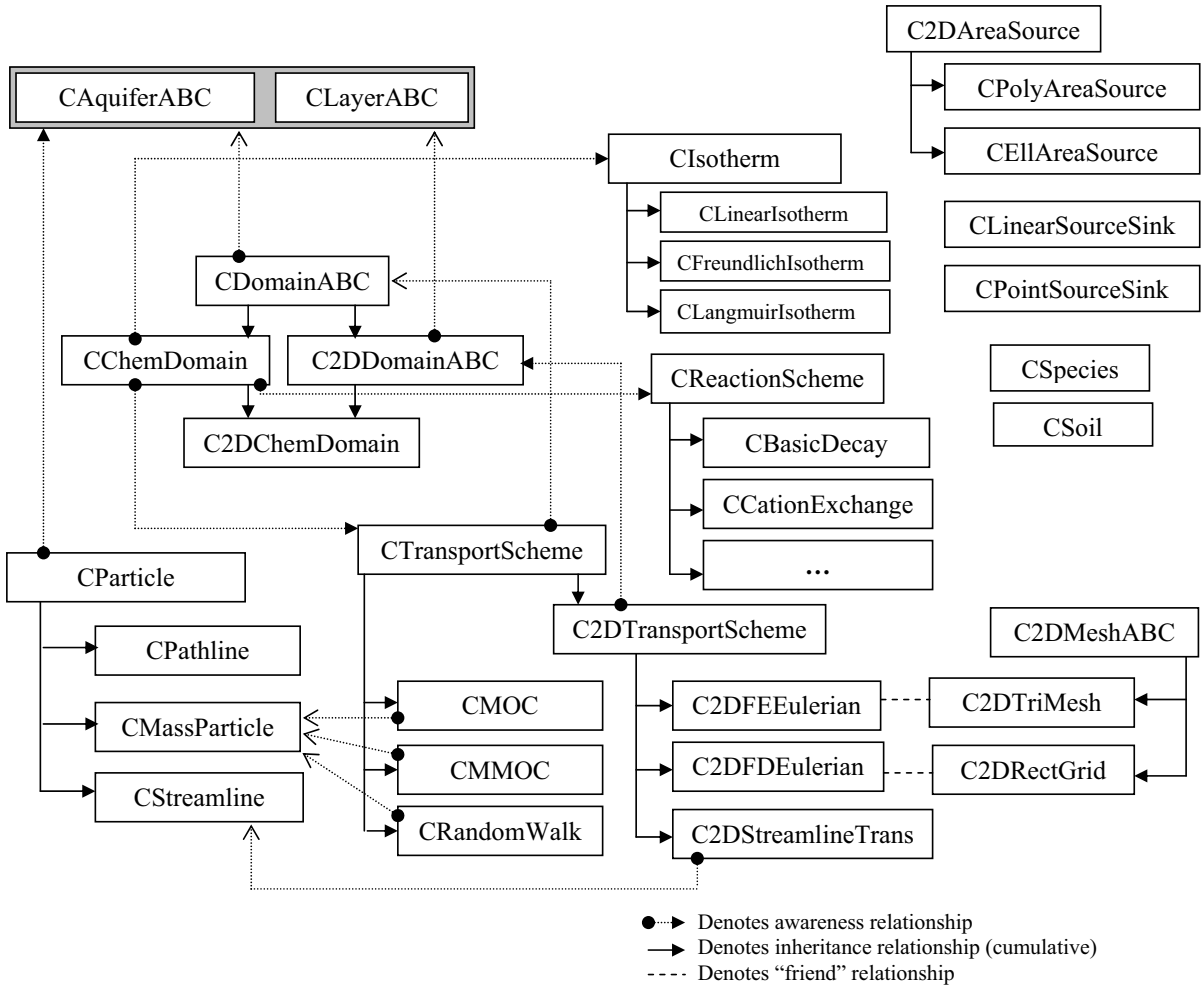

Figure 3.7: The CARDINAL library class organization.

Simulation of hydrodynamic transport of contaminant requires information about the spatial distribution of groundwater velocities and saturated thicknesses, which are generally obtained via a numerical flow model. Access to this information in CARDINAL is limited to select knowledge of only two classes in the connected BLUEBIRD library (see section 3.1.2), the abstract aquifer class,

CAquiferABC and the abstract layer class, CLayerABC, as shown in figure 3.7. While these entities currently represent flow fields associated with analytic element flow solutions, finite difference or finite element solutions may also be used. CARDINAL does not "know" the source of its velocity information. Thus the flow engine and transport engine are only loosely bound to each other, but the essential communication of information is fully preserved.

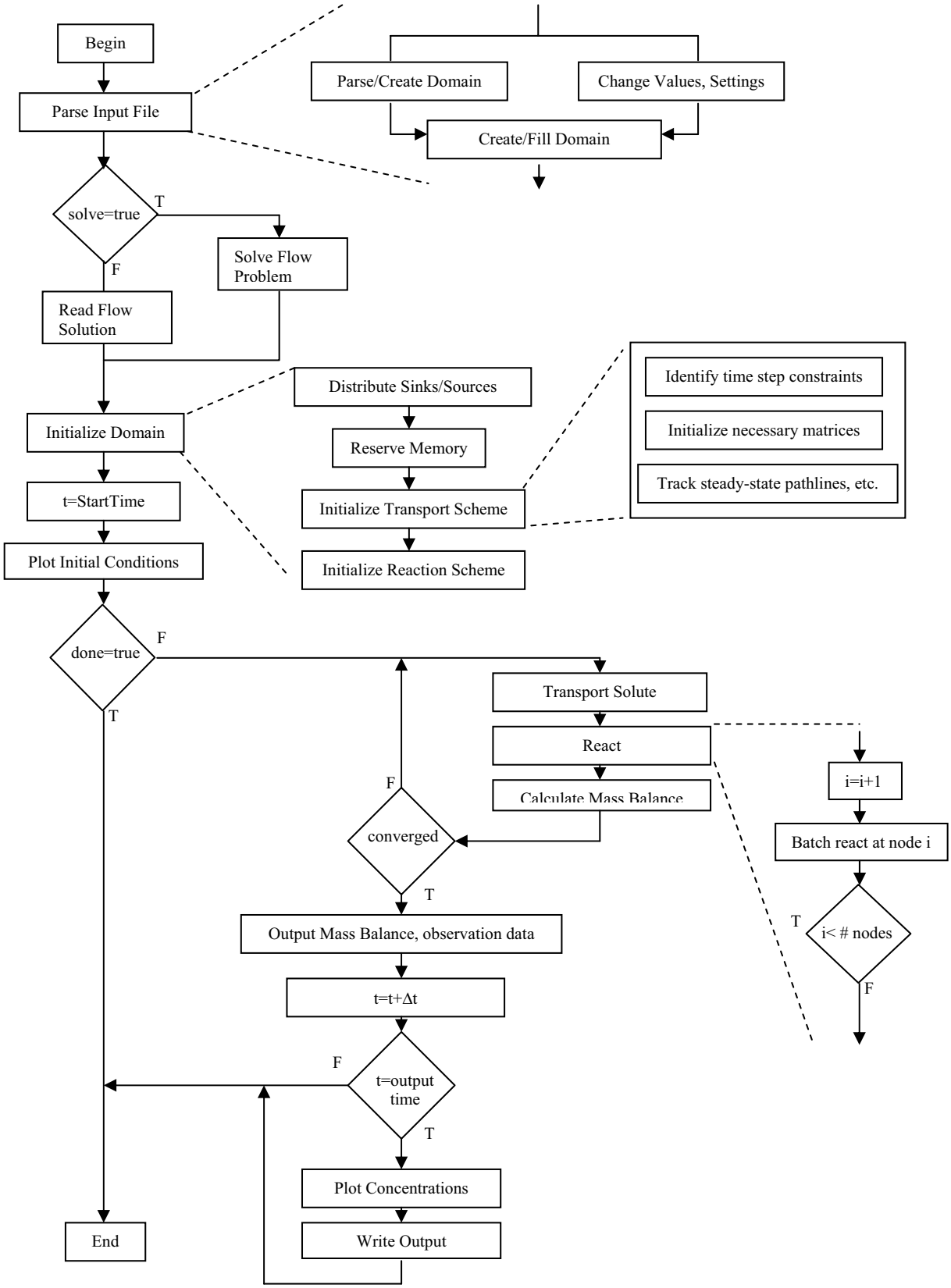

Figure 3.8: Flow chart of generic CARDINAL transport algorithm

3.2 Mass Balance Accounting

For numerical contaminant transport models that are used for regulatory or management decisions, it is important to provide an assessment of model quality. A particularly useful measure of numerical performance is the mass balance of aqueous and sorbed species. If a numerical approach does not preserve this mass balance, it is unclear whether predicted changes in concentration are due to the modeled process or the numerical method used. For this reason, a comprehensive suite of mass balance accounting tools have been implemented in CARDINAL. These tools are used primarily to quantify the mass balance error in a given model, and are particularly important for rigorously evaluating the new methods introduced within this dissertation.

In a typical contaminant transport model, there are a variety of sinks and sources of contaminant mass. Mass may be lost or gained by the following means:

- Advection and dispersion across system boundaries
- Addition by source terms, which may be specified mass influx ("dry" condition), specified influx concentration ("wet" condition), or Dirichlet boundary conditions
- Removal by sink terms, which may be "natural" mass outflux or Dirichlet boundary condition
- Chemical reaction (e.g., decay)

Each transport algorithm represents concentration, sources, sinks, and advection in different ways. Therefore, the appropriate means of calculating contaminant loss must be developed specifically for each method. However, the cumulative mass balance error for a single species, ε_{MB}, for all methods is calculated as follows for time n:

$$\varepsilon_{MB} = 2\frac{(M^n - M^0) + \sum_{n=0}^{n} \left(\Delta M^n_{bound} + \Delta M^n_{source} + \Delta M^n_{sink} + \Delta M^n_{dir} + \Delta M^n_{rxn}\right)}{M^n + \sum_{n=0}^{n} \left(\Delta M^n_{source} + \Delta M^n_{dir}\right) + M^0 - \sum_{n=0}^{n} \left(\Delta M^n_{sink} + \Delta M^n_{rxn} + \Delta M^n_{bound}\right)} \tag{3.1}$$

Where M^n is the mass in the system at time n, Δt_n is the simulation time step, and the ΔM^n terms correspond to the change in mass over time step n for the various loss/gain terms (*bound*=boundary loss (-); *source*=source gain (+); *sink*=sink loss (-); *dir*=dirichlet source gain (+); *rxn*=mass lost to reaction(-)).

The mass balance error expression given above is not particular to any contaminant transport simulation algorithm. The expressions for the various terms in equation 3.1 are provided in appendix E for both finite difference methods and finite element methods.

3.3 Using AEM for Finite Difference Transport Simulation

Eulerian and Eulerian-Lagrangian finite difference-based transport models (e.g., those found in MT3DMS (Zheng and Wang 1999)) are the prevailing technique for simulating contaminant transport in aquifers. Finite difference methods are mathematically simpler than finite element or finite volume methods, yet robust in their treatment of many complex transport systems. Finite difference models solve a discretized version of the governing advection-dispersion equation shown in equation 2.2 on a finite difference grid, with face- and cell-averaged fluxes of water as input. This typically requires a finite difference-style representation of the flow system (e.g., that of MODFLOW (McDonald and Harbaugh 1988)). Therefore, the first (and most basic) step towards using AEM as a basis for contaminant transport is to translate analytic element fluxes into a finite difference analogue. These discretized fluxes can then be used as input into an existing two- or three-dimensional finite difference transport simulator (e.g., MT3DMS), or they may be used within a new vertically-averaged finite difference formulation, as done here.

The following subsections describe a new Eulerian algorithm for solving the vertically-averaged transport equation (equation 2.16) using a finite difference method on a rectangular grid with uneven spacing and arbitrary angular orientation. The first subsection (3.3.1) describes how to use the finite difference method to discretize and solve the governing equation given initial and boundary conditions. The second subsection (3.3.2) describes the steps required to translate the AEM flow solution (fluxes and saturated thicknesses) so that it may be used as input to this finite difference transport model. This translation process is primarily focused upon preserving the highly accurate water balance provided by the analytic element method. While the stability and accuracy of finite difference methods are important, they are discussed only briefly here, as they are only minimally affected by the use of analytic element flow solutions, once the water balance is maintained.

The methods discussed below have been implemented in BLUEBIRD and CARDINAL and benchmarked against analytic solutions (subsections 4.1.1and 4.1.2) and the numerical model MT3DMS (subsection 4.1.3). In addition, a translator has been developed (based upon the methods in section 3.3.2) to export highly accurate AEM fluxes calculated by BLUEBIRD into MT3DMS input files.

The finite difference transport implementation discussed here is the first to fully utilize the analytic element method. In addition, to the authors knowledge, it is the first finite difference

simulator designed specifically to solve the vertically-averaged transport equation.

3.3.1 Finite Difference Approximation of the Vertically-Averaged ADE

The vertically-averaged transport equation (equation 2.13) is rewritten here as

$$\begin{aligned} R_f \frac{\partial C}{\partial t} = & -\frac{1}{h\theta}\frac{\partial Q_x C}{\partial x} - \frac{1}{h\theta}\frac{\partial Q_y C}{\partial x} \\ & + \frac{1}{h\theta}\frac{\partial}{\partial x}\left(h\theta D_{xx}\frac{\partial C}{\partial x}\right) + \frac{1}{h\theta}\frac{\partial}{\partial x}\left(h\theta D_{xy}\frac{\partial C}{\partial y}\right) \\ & + \frac{1}{h\theta}\frac{\partial}{\partial y}\left(h\theta D_{yx}\frac{\partial C}{\partial x}\right) + \frac{1}{h\theta}\frac{\partial}{\partial y}\left(h\theta D_{yy}\frac{\partial C}{\partial y}\right) \\ & + \frac{N_t^+}{h\theta}c_t^+ + \frac{N_b^+}{h\theta}c_b^+ - \frac{N_t^-}{h\theta}C - \frac{N_b^-}{h\theta}C \end{aligned} \tag{3.2}$$

Where the notation is the same as that defined in section 2.2.

Note that the "divergent" formulation of the transport equation (rather than the equivalent "convective" formulation shown in equation 2.16) is chosen for approximation by finite differences. By handling the advective and dispersive parameters from inside the partial derivative terms, consistency of mass flux between cells is ensured, thereby maintaining mass balance.

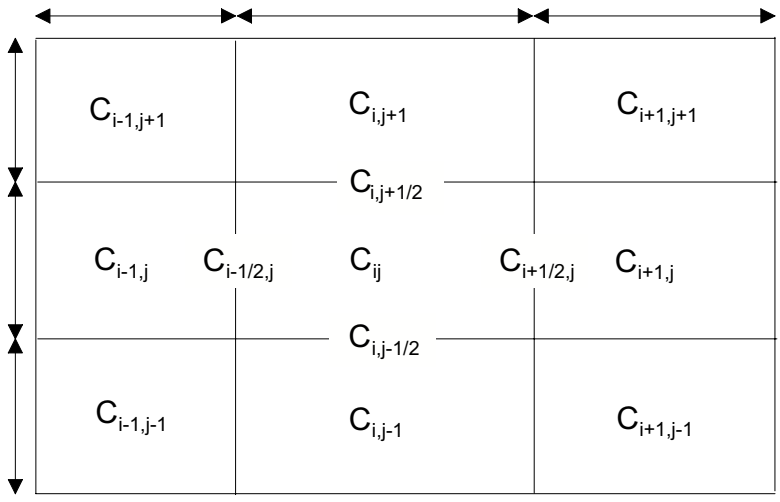

Figure 3.9: Grid notation for irregular finite difference grid. Row values are indexed with j and columns are indexed with i. Interfacial values are noted with subscripts of 1/2 (e.g., $C_{i+1/2,j}$ is the face-averaged concentration at the interface between cells (i, j) and $(i + 1, j)$)

In the finite difference method, each of the partial derivative terms of 3.2 are expressed as finite difference approximations, which may be obtained from truncated Taylor series of the continuous terms. These finite difference approximations are linked to the structure of the finite difference grid

(shown in figure 3.9). The independent parameters (Q_x, Q_y, h, θ, etc.) are similarly discretized on this grid, allowing a single equation to be written for each cell in the system. With *NC* cells, there are *NC* equations, each corresponding to the *NC* unknowns of cell-averaged concentrations. This sparse system of equations may be solved using conventional linear algebraic methods for each time step in the transport simulation. In the CARDINAL implementation, a biconjugate gradient method is used based upon the algorithm presented by Press et al. (2002).

Each derivative term of equation 3.2 may be replaced by its finite difference equivalent. A first-order approximation of the time derivative is given by:

$$\left.\frac{\partial C}{\partial t}\right|_{ij} \approx \frac{C_{ij}^{n+1} - C_{ij}^{n}}{\Delta t} \tag{3.3}$$

where the superscript n refers to the time step used and Δt is the time interval.

The advective term may be expressed using an upstream weighting scheme, which only includes the concentrations upstream of the cell, or a central weighting scheme, which includes both downstream and upstream values (e.g., Zheng and Bennett (2002)). A general expression for the advective derivative terms in the x-direction is

$$\begin{aligned}
&\frac{1}{h\theta}\left.\frac{\partial Q_x C}{\partial x}\right|_{n}^{n+1} \approx \\
&(1-\omega)\left(\frac{Q_{x(i+1/2,j)}[(1-\alpha)C_{i,j}^{n} + \alpha C_{i+1,j}^{n}] - Q_{x(i-1/2,j)}[(1-\alpha)C_{i-1,j}^{n} + \alpha C_{i,j}^{n}]}{h_i\theta_i[(1-\alpha)\Delta x_{i-1} + \Delta x_i + \alpha\Delta x_{i+1}]}\right) + \\
&(\omega)\left(\frac{Q_{x(i+1/2,j)}[(1-\alpha)C_{i,j}^{n+1} + \alpha C_{i+1,j}^{n+1}] - Q_{x(i-1/2,j)}[(1-\alpha)C_{i-1,j}^{n+1} + \alpha C_{i,j}^{n+1}]}{h_i\theta_i[(1-\alpha)\Delta x_{i-1} + \Delta x_i + \alpha\Delta x_{i+1}]}\right)
\end{aligned} \tag{3.4}$$

Where the subscripts $(i \pm 1/2, j)$ denote face-averaged quantities.

A similar expression is available for the advective derivative terms in the y-direction:

$$\begin{aligned}
&\frac{1}{h\theta}\left.\frac{\partial Q_y C}{\partial y}\right|_{n}^{n+1} \approx \\
&(1-\omega)\left(\frac{Q_{y(i,j+1/2)}[(1-\alpha)C_{i,j}^{n} + \alpha C_{i,j+1}^{n}] - Q_{y(i,j-1/2)}[(1-\alpha)C_{i,j-1}^{n} + \alpha C_{i,j}^{n}]}{h_{(i,j)}\theta_{(i,j)}[(1-\alpha)\Delta y_{j-1} + \Delta y_j + \alpha\Delta y_{j+1}]}\right) + \\
&(\omega)\left(\frac{Q_{y(i,j+1/2)}[(1-\alpha)C_{i,j}^{n+1} + \alpha C_{i,j+1}^{n+1}] - Q_{y(i,j-1/2)}[(1-\alpha)C_{i,j-1}^{n+1} + \alpha C_{i,j}^{n+1}]}{h_{(i,j)}\theta_{(i,j)}[(1-\alpha)\Delta y_{j-1} + \Delta y_j + \alpha\Delta y_{j+1}]}\right)
\end{aligned} \tag{3.5}$$

Here the spatial weighting factor, α, is equal to 0.5 for the central weighting scheme and either zero or one (depending upon the flow direction in the cell) if the upstream weighting scheme is

used. In addition to this spatial weighting, the spatial derivatives may be expressed in terms of a weighted average of the cell values C_{ij} from the previous time step (n) and the current time step ($n+1$). The temporal weighting factor, ω, is 0.5 for the unconditionally stable Crank-Nicholson scheme, zero for a fully explicit scheme (one that is only expressed in terms of known concentrations from the previous time step), or one for a fully implicit scheme (one that is expressed completely in terms of unknown concentrations). The strengths and weaknesses of each of these numerical schemes are discussed elsewhere (e.g., Zheng and Bennett (2002) or Hoffman (1992)). Note that this finite difference expression does not assume a regular grid spacing. Also, for simplicity of derivation, it is assumed that the grid is aligned with the global coordinate system of the analytic element solution (i.e., Q_x is normal to the face $(i+1/2, j)$). However, in CARDINAL the method has been implemented for arbitrary grid orientation.

The interfacial normal fluxes, denoted by $Q_{x(i\pm1/2,j)}$ and $Q_{y(i,j\pm1/2)}$, represent the average integrated discharge across the cell face between cells i and $i+1$ or i and $i-1$. If a finite difference method is used to solve the flow problem, these values are known explicitly as a byproduct of the flow solution. However, if the analytic element method is used, an alternative method is required to evaluate the magnitude of these terms. If poor approximations of these average intercell fluxes are used, the water balance (and thus the solute mass balance) will not be maintained.

The dispersion terms of equation 3.2 are represented using a central in space weighting and the same temporal weighting ω, as the advective terms:

$$\begin{aligned}
&\frac{1}{h\theta}\frac{\partial}{\partial x}\left(h\theta D_{xx}\frac{\partial C}{\partial x}\right)\Bigg|_{n}^{n+1} \approx \\
&(1-\omega)\left(\frac{(h\theta D_{xx})_{(i+1/2,j)}[C^{n}_{i+1,j}-C^{n}_{i,j}]}{h_{(i,j)}\theta_{(i,j)}\frac{1}{2}\Delta x_i(\Delta x_i+\Delta x_{i+1})}-\frac{(h\theta D_{xx})_{(i-1/2,j)}[C^{n}_{i,j}-C^{n}_{i-1,j}]}{h_{(i,j)}\theta_{(i,j)}\frac{1}{2}\Delta x_i(\Delta x_i+\Delta x_{i-1})}\right)+ \\
&(\omega)\left(\frac{(h\theta D_{xx})_{(i+1/2,j)}[C^{n+1}_{i+1,j}-C^{n+1}_{i,j}]}{h_{(i,j)}\theta_{(i,j)}\frac{1}{2}\Delta x_i(\Delta x_i+\Delta x_{i+1})}-\frac{(h\theta D_{xx})_{(i-1/2,j)}[C^{n+1}_{i,j}-C^{n+1}_{i-1,j}]}{h_{(i,j)}\theta_{(i,j)}\frac{1}{2}\Delta x_i(\Delta x_i+\Delta x_{i-1})}\right)
\end{aligned} \tag{3.6}$$

$$\begin{aligned}
&\frac{1}{h\theta}\frac{\partial}{\partial y}\left(h\theta D_{yy}\frac{\partial C}{\partial y}\right)\Bigg|_{n}^{n+1} \approx \\
&(1-\omega)\left(\frac{(h\theta D_{yy})_{(i,j+1/2)}[C^{n}_{i,j+1}-C^{n}_{i,j}]}{h_{(i,j)}\theta_{(i,j)}\frac{1}{2}\Delta y_j(\Delta y_j+\Delta y_{j+1})}-\frac{(h\theta D_{yy})_{(i,j-1/2)}[C^{n}_{i,j}-C^{n}_{i,j-1}]}{h_{(i,j)}\theta_{(i,j)}\frac{1}{2}\Delta y_j(\Delta y_j+\Delta y_{j-1})}\right)+ \\
&(\omega)\left(\frac{(h\theta D_{yy})_{(i,j+1/2)}[C^{n+1}_{i,j+1}-C^{n+1}_{i,j}]}{h_{(i,j)}\theta_{(i,j)}\frac{1}{2}\Delta y_j(\Delta y_j+\Delta y_{j+1})}-\frac{(h\theta D_{yy})_{(i,j-1/2)}[C^{n+1}_{i,j}-C^{n+1}_{i,j-1}]}{h_{(i,j)}\theta_{(i,j)}\frac{1}{2}\Delta y_j(\Delta y_j+\Delta y_{j-1})}\right)
\end{aligned} \tag{3.7}$$

As with the interfacial integrated discharge terms of equations 3.4 and 3.5, both the interfacial

dispersion coefficients ($D_{xx(i\pm1/2,j)}$ and $D_{yy(i,j\pm1/2)}$) and the average interfacial saturated thickness, ($h_{(i\pm1/2,j)}$ and $h_{(i,j\pm1/2)}$) must be evaluated based upon the analytic element solution. Methods for calculating these variables are significantly different from those of conventional finite difference transport models (e.g., MT3DMS (Zheng and Wang 1999)), and are discussed in the following subsection.

The cross-dispersion terms are expressed with variable time weighting and non-uniform grid spacing as follows:

$$\begin{aligned}
&\frac{1}{h\theta}\frac{\partial}{\partial x}\left(h\theta D_{xy}\frac{\partial C}{\partial y}\right)\Bigg|_{n}^{n+1} \approx \\
&(1-\omega)\left(\frac{(h\theta D_{xy})_{(i+1/2,j)}[\Delta x_i C^n_{i+1,j+1}+\Delta x_{i+1}C^n_{i,j+1}-\Delta x_i C^n_{i+1,j-1}-\Delta x_{i+1}C^n_{i,j-1}]}{h_{(i,j)}\theta_{(i,j)}\frac{1}{2}\Delta x_i(\Delta x_{i+1}+\Delta x_i)(\Delta y_{j-1}+2\Delta y_j+\Delta y_{j+1})}\right)- \\
&(1-\omega)\left(\frac{(h\theta D_{xy})_{(i-1/2,j)}[\Delta x_i C^n_{i-1,j+1}+\Delta x_{i-1}C^n_{i,j+1}-\Delta x_i C^n_{i-1,j-1}-\Delta x_{i-1}C^n_{i,j-1}]}{h_{(i,j)}\theta_{(i,j)}\frac{1}{2}\Delta x_i(\Delta x_{i-1}+\Delta x_i)(\Delta y_{j-1}+2\Delta y_j+\Delta y_{j+1})}\right)+ \\
&(\omega)\left(\frac{(h\theta D_{xy})_{(i+1/2,j)}[\Delta x_i C^{n+1}_{i+1,j+1}+\Delta x_{i+1}C^{n+1}_{i,j+1}-\Delta x_i C^{n+1}_{i+1,j-1}-\Delta x_{i+1}C^{n+1}_{i,j-1}]}{h_{(i,j)}\theta_{(i,j)}\frac{1}{2}\Delta x_i(\Delta x_{i+1}+\Delta x_i)(\Delta y_{j-1}+2\Delta y_j+\Delta y_{j+1})}\right)- \\
&(\omega)\left(\frac{(h\theta D_{xy})_{(i-1/2,j)}[\Delta x_i C^{n+1}_{i-1,j+1}+\Delta x_{i-1}C^{n+1}_{i,j+1}-\Delta x_i C^{n+1}_{i-1,j-1}-\Delta x_{i-1}C^{n+1}_{i,j-1}]}{h_{(i,j)}\theta_{(i,j)}\frac{1}{2}\Delta x_i(\Delta x_{i-1}+\Delta x_i)(\Delta y_{j-1}+2\Delta y_j+\Delta y_{j+1})}\right)
\end{aligned} \tag{3.8}$$

$$\begin{aligned}
&\frac{1}{h\theta}\frac{\partial}{\partial y}\left(h\theta D_{yx}\frac{\partial C}{\partial x}\right)\Bigg|_{n}^{n+1} \approx \\
&(1-\omega)\left(\frac{(h\theta D_{yx})_{(i,j+1/2)}[\Delta y_j C^n_{i+1,j+1}+\Delta y_{j+1}C^n_{i+1,j}-\Delta y_j C^n_{i-1,j+1}-\Delta y_{j+1}C^n_{i-1,j}]}{h_{(i,j)}\theta_{(i,j)}\frac{1}{2}\Delta y_j(\Delta y_{j+1}+\Delta y_j)(\Delta x_{i-1}+2\Delta x_i+\Delta x_{i+1})}\right)- \\
&(1-\omega)\left(\frac{(h\theta D_{yx})_{(i,j-1/2)}[\Delta y_j C^n_{i+1,j-1}+\Delta y_{j-1}C^n_{i+1,j}-\Delta y_j C^n_{i-1,j-1}-\Delta y_{j-1}C^n_{i-1,j}]}{h_{(i,j)}\theta_{(i,j)}\frac{1}{2}\Delta y_j(\Delta y_{j-1}+\Delta y_j)(\Delta x_{i-1}+2\Delta x_i+\Delta x_{i+1})}\right)+ \\
&(\omega)\left(\frac{(h\theta D_{yx})_{(i,j+1/2)}[\Delta y_j C^{n+1}_{i+1,j+1}+\Delta y_{j+1}C^{n+1}_{i+1,j}-\Delta y_j C^{n+1}_{i-1,j+1}-\Delta y_{j+1}C^{n+1}_{i-1,j}]}{h_{(i,j)}\theta_{(i,j)}\frac{1}{2}\Delta y_j(\Delta y_{j+1}+\Delta y_j)(\Delta x_{i-1}+2\Delta x_i+\Delta x_{i+1})}\right)- \\
&(\omega)\left(\frac{(h\theta D_{yx})_{(i,j-1/2)}[\Delta y_j C^{n+1}_{i+1,j-1}+\Delta y_{j-1}C^{n+1}_{i+1,j}-\Delta y_j C^{n+1}_{i-1,j-1}-\Delta y_{j-1}C^{n+1}_{i-1,j}]}{h_{(i,j)}\theta_{(i,j)}\frac{1}{2}\Delta y_j(\Delta y_{j-1}+\Delta y_j)(\Delta x_{i-1}+2\Delta x_i+\Delta x_{i+1})}\right)
\end{aligned} \tag{3.9}$$

Finally, the recharge and leakage source/sink term of 3.2 may be expressed in terms of cell-averaged quantities as:

$$\begin{aligned}
&\frac{N^+_t}{h\theta}c^+_t+\frac{N^+_b}{h\theta}c^+_b-\frac{N^-_t}{h\theta}C-\frac{N^-_b}{h\theta}C= \\
&\qquad\frac{N^+_{t(i,j)}}{h_{(i,j)}\theta_{(i,j)}}c^+_{t(i,j)}+\frac{N^+_{b(i,j)}}{h_{(i,j)}\theta_{(i,j)}}c^+_{b(i,j)}-\frac{N^-_{t(i,j)}}{h_{(i,j)}\theta_{(i,j)}}C_{i,j}-\frac{N^-_{b(i,j)}}{h_{(i,j)}\theta_{(i,j)}}C_{i,j}
\end{aligned} \tag{3.10}$$

The preceding finite difference approximations of the terms in 3.2 may be rearranged and assembled into a single equation for each cell (i, j) of the following form:

$$\begin{aligned} &\underset{ij}{a_1} C^{n+1}_{i-1,j-1} + \underset{ij}{a_2} C^{n+1}_{i-1,j} + \underset{ij}{a_3} C^{n+1}_{i-1,j+1} + \\ &\underset{ij}{a_4} C^{n+1}_{i,j-1} + \underset{ij}{a_5} C^{n+1}_{i,j} + \underset{ij}{a_6} C^{n+1}_{i,j+1} + \\ &\underset{ij}{a_7} C^{n+1}_{i+1,j-1} + \underset{ij}{a_8} C^{n+1}_{i+1,j} + \underset{ij}{a_9} C^{n+1}_{i+1,j+1} = RHS_{ij} \end{aligned} \tag{3.11}$$

where $\underset{ij}{a_1} ... \underset{ij}{a_9}$ are coefficients assembled from the previous expressions, and RHS_{ij} is the known right hand side of the equation. Similar equations may be written for each cell.

Given a set of initial conditions (e.g., C^0_{ij} for each ij) and a set of boundary conditions, this system of equations may be solved for each time step, Δt. This process is repeated over and over again for each time step. Particular issues related to boundary condition implementation and numerical accuracy/stability are not discussed here, as the issues are the same with fluxes derived from analytic flow solutions as they are with fluxes obtained from finite difference solutions. The user is referred to Zheng and Bennett (2002) for a more complete discussion of the numerical accuracy and stability requirements of finite difference methods for transport. In this dissertation, the primary goal is to find methods with which to accurately "discretize" the interfacial fluxes, cell-averaged leakage/reacharge, dispersion coefficients, and saturated thicknesses.

3.3.2 Flux Discretization

As apparent from the derivation of the vertically-averaged transport equation in the previous section, there are four necessary flow-based inputs to a finite difference transport model:

1. Average integrated Darcian flux across each cell interface, $Q_{x(i\pm1/2,j)}$ and $Q_{y(i,j\pm1/2)}$[L/T]
2. Cell-averaged vertical fluxes, $N^+_{t(i,j)}$, $N^-_{t(i,j)}$, $N^+_{b(i,j)}$, and $N^-_{b(i,j)}$ $[L/T]$
3. Volumetric source/sink fluxes to each cell, $Q^+|_{i,j}$, $Q^-|_{i,j}$ $[L^3/T]$
4. Cell-averaged saturated thickness, h_{ij}, and face-averaged saturated thicknesses, $h_{i,j\pm1/2}$ and $h_{i\pm1/2,j}$ $[L]$

An additional quantity, often interpolated from adjacent normal fluxes in typical finite difference methods for flow (e.g., MODFLOW), but available directly from analytic element solutions, are the

average tangential integrated discharges along a cell interface ($Q_{y(i\pm1/2,j)}$ and $Q_{x(i,j\pm1/2)}$), which may be used to quantify the dispersion coefficient at that interface.

The distinction made here between typical source/sinks (e.g., wells, rivers) and recharge/leakage, is based upon the different handling of the two concepts in the AEM. The remainder of this subsection is devoted to obtaining precise and robust expressions for these five variables. Once these variables are calculated in such a way that the local water balance is maintained, they may be easily exported to any of the transport simulators that rely upon an integrated finite difference (e.g., MODFLOW) input structure. These derivations are general, and are useful for other uses of analytic element flow solutions as well.

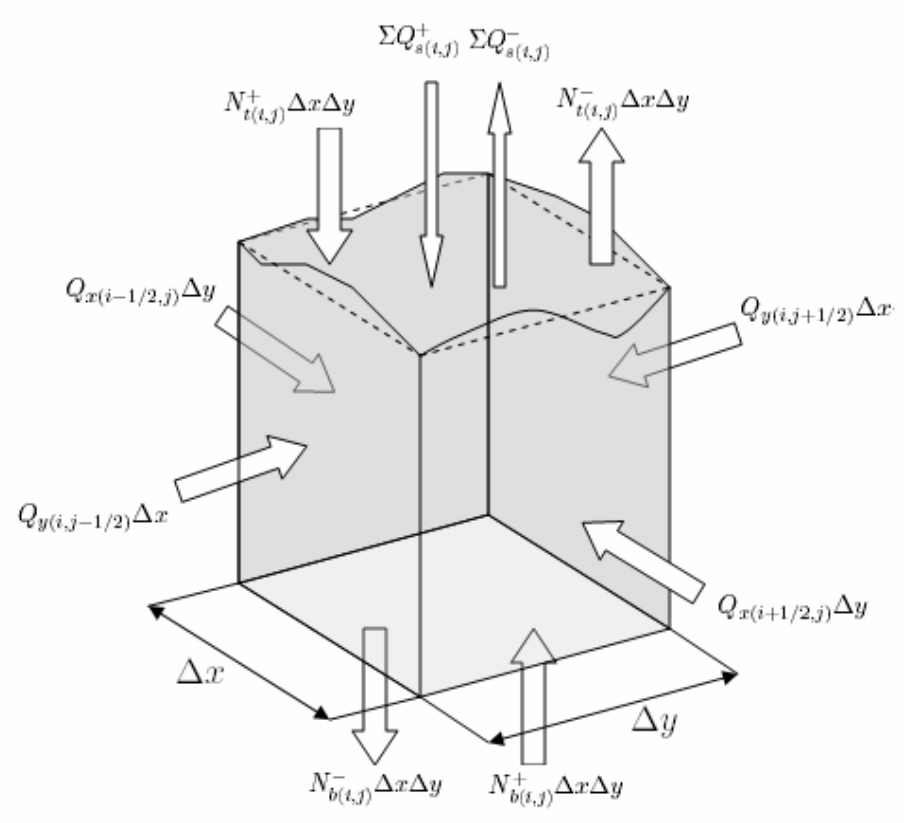

Figure 3.10: Single layer finite difference mass balance on water in a cell

A water balance may be written for the finite difference cell shown in Figure 3.10:

$$\begin{aligned} &Q_{x(i-1/2,j)}\Delta y + Q_{x(i+1/2,j)}\Delta y + Q_{y(i,j-1/2)}\Delta x + Q_{y(i,j+1/2)}\Delta x + \\ &N^+_{t(i,j)}\Delta x\Delta y + N^+_{b(i,j)}\Delta x\Delta y - N^-_{t(i,j)}\Delta x\Delta y - N^-_{b(i,j)}\Delta x\Delta y + \\ &\Sigma Q^+_{(i,j)} - \Sigma Q^-_{(i,j)} = 0 \end{aligned} \tag{3.12}$$

where N_t^+, N_b^+, N_t^-, and N_b^- are vertical influx/outflux terms defined in section 2.2.1, averaged over the cell.

The water balance condition of 3.12 may be expressed in terms of integrated AEM variables as:

$$\begin{aligned}
&\int_y^{y+\Delta y} Q_x(x_{i-1/2}, y)dy + \int_y^{y+\Delta y} Q_x(x_{i+1/2}, y)dy + \\
&\int_x^{x+\Delta x} Q_y(x, y_{j-1/2})dx + \int_x^{x+\Delta x} Q_y(x, y_{j+1/2})dx + \\
&\int_y \int_x [N_t^+(x,y) + N_b^+(x,y)]dxdy - \int_y \int_x [N_t^-(x,y) + N_b^-(x,y)]dxdy + \\
&\Sigma Q^+|_{i,j} - \Sigma Q^-|_{i,j} = 0
\end{aligned} \tag{3.13}$$

Here, the first four terms represent the net influx through each of the four sides of the cell, the fifth and sixth term represent the influence of recharge and leakage, and the final terms represent the source and sink fluxes to that cell. As will be shown, all of these integral terms can be evaluated analytically, not only ensuring that water balance is met regardless of discretization, but also ensuring a more accurate representation of average interfacial dispersion coefficients, which are functions of flow velocity. Closed-form expressions for many of the integrals in equation 3.13 will prove valuable for translation to non-finite-difference discretization schemes as well.

The following subsections describe the means of evaluating the three types of cell- and face-integrated fluxes in equation 3.13. In addition, a means for evaluating the face-averaged dispersion coefficients (required by the finite difference approximations of equations 3.6 through 3.9) is presented.

3.3.2-A Integrated (Net) Flux Through a Face

The net flux of water through a vertical strip of the aquifer may be calculated to an arbitrary precision with the analytic element method. The stream function, Ψ, is a byproduct of an AEM flow solution, and requires no postprocessing to obtain. In non-divergent domains (domains without recharge or leakage), the stream function provides a relatively simple method for calculating the integrated flux. If there are no discontinuities in the stream function intersecting an arbitrarily oriented vertical face from z_1 to z_2, the net flux through the face may be calculated as the difference

in the stream function calculated at its two endpoints (Bear 1972; Strack 1989):

$$\int_{z_1}^{z_2} Q_\eta(z)dz = \Psi(z_2) - \Psi(z_1) \tag{3.14}$$

where Q_η is the flux normal to the face. This expression is a generalization of the integrals found in equation 3.13. Unfortunately, this simple calculation is often complicated by the existence of "branch cuts", element boundaries, and divergent flow along the line defined by z_1 and z_2. Each of these three cases correspond to discontinuities or undefined regions of the stream function. Therefore, three steps must be taken to properly calculate net integrated flux using the stream function:

1. Intersecting branch cuts must be re-oriented
2. The integrated flux due to divergent elements (e.g., area sinks) must be evaluated directly (i.e., without use of the stream function)
3. Cell face/ analytic element intersections must be identified and specially handled

To simplify the above operations for arbitrary element geometry, the integral defined in (3.14) is redefined using the principle of superposition, and subdivided based on the influence of each element. The resulting integral may be calculated on an element-by-element basis as:

$$\int_{z_1}^{z_2} Q_\eta(z)dz = \sum_{i=1}^{N_E} \int_{z_1}^{z_2} \underset{i}{Q_\eta}(z)dz \tag{3.15}$$

where N_E is the number of elements and $\underset{i}{Q_\eta}$ is the flux normal to the face due to element i. The total flux due to any single non-divergent, non-intersecting element is evaluated using the element stream function at the endpoints, $\int \underset{i}{Q_\eta} = \underset{i}{\Psi}(z_2) - \underset{i}{\Psi}(z_1)$. However, elements that extract or inject water into the system must first have their branch cuts redirected.

In AEM, for every element that extracts or contributes water to the system (e.g., linesinks and point sinks), there exists a "branch cut" emanating from part of the element ($z_{singularity}$) to infinity. This branch cut is a discontinuity in the stream function that is equal to the net flux of the element, Q^{net}. The orientation of this branch cut is arbitrary, and has no effect upon the flow solution. To reorient all branch cuts away from a given point, z_p, (the center of the face where we

are calculating flux, in this case), the element stream function may be modified using the algorithm in Fig. 3.11.

$\theta_1 = \arg(z - z_{singularity})$
$\theta_2 = \arg(z - z_p)$
if ($\theta_2 >= 0$ and $\theta_1 >= 0$ and $\theta_1 > \theta_2$) then $\Psi(z) = \Psi(z) - Q^{net}$
if ($\theta_2 < 0$ and $\theta_1 < 0$ and $\theta_1 < \theta_2$) then $\Psi(z) = \Psi(z) + Q^{net}$

Figure 3.11: Branch cut re-orientation algorithm

The branch cuts (which by default are directed to the left of the singularity in local element coordinates) will point in the opposite direction from the point z_p. This ensures that there is no branch cut discontinuity in the stream function intersecting the face. Thus the difference in the stream function reflects the actual flux through the face. The results of this operation are shown in Fig. 3.12.

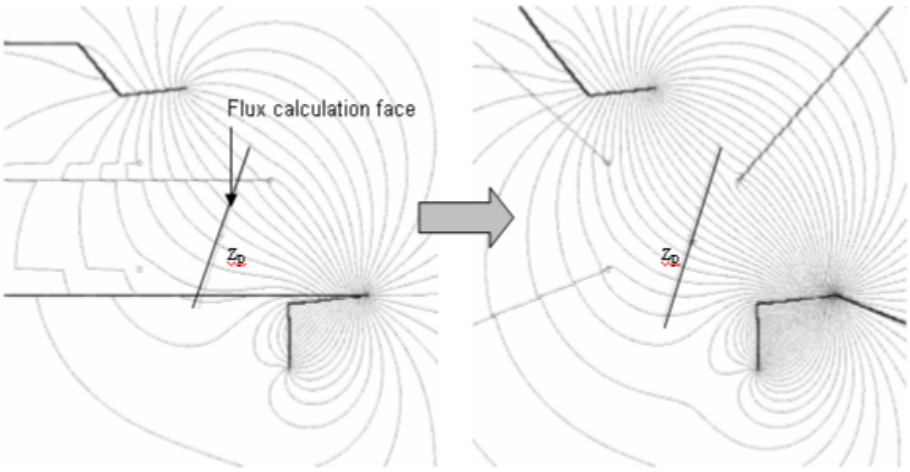

Figure 3.12: Branch cuts are realigned to avoid discontinuities in the stream function through a specified linear region

The second required modification to ensure accurate flux calculation is to incorporate the unique effects of area-sinks. The stream function is undefined within divergent areas, and, for ease of calculation, often assumed to be zero. However, the integrated flux can still be calculated without use of the stream function. The element integral in (3.15) may be evaluated analytically for the two most common area-sinks, the multi-quadric area-sink (Strack and Janković 1999) and uniform leakage area sink. The integrated flux across a face internal to the multi-quadric area sink is (Strack

and Janković 1999):

$$\int_{z_1}^{z_2} Q_\eta(z)dz = -N_{ave}\frac{L^2 Y_c}{4} + \sum_{n=0}^{N_{AS}} a_n \frac{Y_n}{6}\left(\frac{L}{2}\right)^3 \left[\begin{array}{l} (-1-X_n)\sqrt{(-1-X_n)^2+Y_n^2} - \\ (1-X_n)\sqrt{(1-X_n)^2+Y_n^2} + \\ Y_n^2 \ln\left(\sqrt{(-1-X_n)^2+Y_n^2} - X_n - 1\right) - \\ Y_n^2 \ln\left(\sqrt{(1-X_n)^2+Y_n^2} - X_n + 1\right) \end{array}\right] \quad (3.16)$$

where L is the length of the face, Y_c is the y-location of the area sink centroid in local coordinates, N_{AS} is the order of the multiquadric leakage function with coefficients a_n and average leakage N_{ave}, and X_n and Y_n denote the location of the multiquadric basis points in local face coordinates. The local face coordinate system is defined as:

$$Z = X + iY = \frac{z - \frac{1}{2}(z_2 + z + 1)}{\frac{1}{2}(z_2 - z + 1)} \quad (3.17)$$

In the case that the cell face intersects the area sink boundary, this integration is only performed between the intersection point and the internal point.

The final "special case" occurs when an analytic element intersects the cell face. For each element that exhibits a discontinuity in the stream function across the cell face (e.g., linesinks or doublets), the points of discontinuity are calculated using simple geometric algorithms. The element influence in (3.15) is obtained as a summation of the integrals evaluated between discontinuities. For N_{INT} intersections of the face and the element, the flux integral is evaluated by:

$$\int_{z_1}^{z_2} \underset{i}{Q_\eta}(z)dz = \left[\underset{i}{\Psi}(z_2) - \underset{i}{\Psi}(z_{j=1}^-)\right] + \sum_{j=1}^{N_{INT}-1}\left[\underset{i}{\Psi}(z_j^+) - \underset{i}{\Psi}(z_{j+1}^+)\right] + \left[\underset{i}{\Psi}(z_{j=N_{INT}}^+) - \underset{i}{\Psi}(z_1)\right] \quad (3.18)$$

where z_j^+ and z_j^- are the locations along the face just to the right and left of discontinuity j. These locations are ordered along the face (i.e., $|z_j^- - z_1| < |z_j^+ - z_1| < |z_{j+1}^- - z_1| < ...$). The particular case where the stream function is singular along the entire line from z_1 to z_2 (i.e., the transect coincides with a linesink border) requires special treatment, because the normal component of flux is doubly valued along such a border. In that case, the integral is evaluated along a slightly offset transect.

3.3.2-B Calculating Cell-Averaged Recharge and Leakage

In addition to calculating cell-wise interfacial fluxes, the continuous multi-quadric leakage terms used in the analytic element method must be integrated over the cell area to obtain the appropriate quantity of flux entering and/or leaving the cell from leakage or recharge. In typical finite difference methods, this cell-averaged leakage is user-specified or calculated on a cell-by-cell basis. However, AEM allows leakage to be represented as a continuous function of space. Cell-averaged vertical flux rates can be represented in integral form as

$$\bar{N} = \frac{1}{A} \int_A N(z) dA \tag{3.19}$$

where A is the area of the cell and $N(z)$ $[L/T]$ is the vertical leakage from the aquifer. Each area sink element generally only represents a single component of this vertical flux (i.e., N_t^+ or N_b^-, etc.). To ensure that this is the case, BLUEBIRD requires separate elements to be used for positive leakage, negative leakage, and recharge. Vertical flux components may therefore be distinguished without numerical intervention. The integral of equation 3.19 can be evaluated for any area sink numerically using Gaussian quadrature. In most cases, such a numerical implementation could be more efficient than the analytic solution, but less precise. To preserve mass balance exactly, the analytic solution is evaluated below.

The analytic solution for the integrated recharge/leakage flux is obtained by equating the flux of water into any internal portion of an area sink with the net flux out through that portion's sides, i.e.:

$$\int_A N(z) dA = \int_s \underset{AS}{Q_\eta}(z) ds \tag{3.20}$$

where s is the perimeter of the internal area over which integration is being performed. For an area boundary defined by linear segments, this integral is a summation of the expression found in (3.16) over the linear sides of the area, and may be evaluated analytically for each side of the cell perimeter. For any cell fully internal to the area sink, this result is exact. Likewise, cells fully external to the area sink will have an exact net leakage/recharge flux of zero. However, if a cell is only partially contained by the area sink, the integral must be carefully evaluated as a summation of carefully delineated sub-integrals to maintain the quality of the solution.

Exact flux results may be obtained for cells partially contained within an area sink by simple

geometric calculations to obtain the integration subareas. The algorithm described below performs integration of the leakage over an arbitrary triangular area (e.g., half a finite difference cell), assuming only that only a single connected portion of the area sink overlaps the triangular cell. This assumption is always valid if the smallest distance between area sink vertices is less than the maximum triangular side lengths. This will be the case for typical models of flow and contaminant transport.

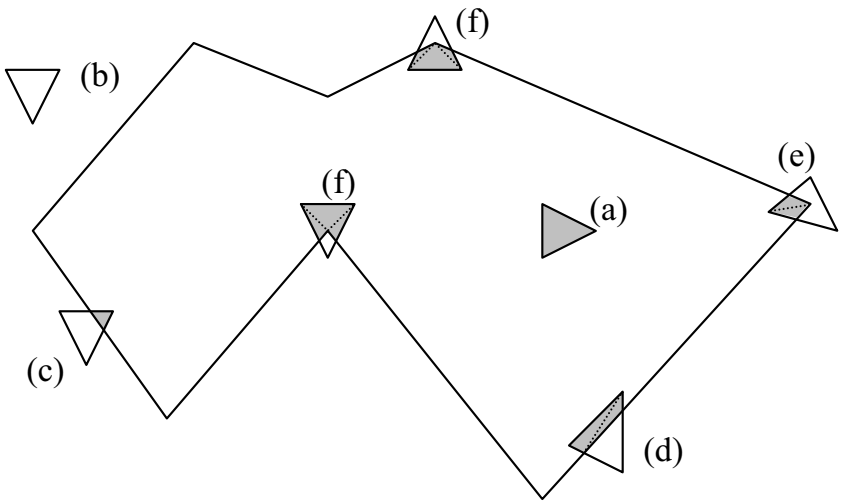

Figure 3.13: Six polygon/triangle overlap cases. Sub-triangles used for integration are denoted by dashed lines

Fig 3.13 displays the six possible configurations of triangle overlap on a polygon given the above assumption about relative triangle and area sink dimensions. The particular configurations are related by the number of triangle vertices inside the polygon (N_Δ) and the number of polygon vertices in the triangle (M_Δ). The cases depicted in Fig. 3.13 are handled as follows:

(a) $N_\Delta = 3$; $M_\Delta = 0$; (the triangle is completely inside of the area sink),

$$\int_\Delta \underset{AS}{N(z)} dA = \sum_{k=1}^{3} \int_{z_k}^{z_{k+1}} \underset{AS}{Q_\eta(z)} dz \tag{3.21}$$

where the integrals on the right hand side are given by (3.16)

(b) $N_\Delta = 0$; $M_\Delta = 0$; (the triangle is completely outside of the area sink)

$$\int_\Delta \underset{AS}{N(z)} dA = 0 \tag{3.22}$$

(c) $N_\Delta = 1$; $M_\Delta = 0$; A new triangle is defined by the two intersection points and the interior point. Equation 3.21 is evaluated over this sub-triangle only.

(d) $N_\Delta = 2$; $M_\Delta = 0$; Two sub-triangles are defined by the two interior points and the two intersection points. Equation 3.21 is applied to these sub-triangles and the net fluxes are summed.

(e) $N_\Delta = 1$; $M_\Delta = 1$; Two sub-triangles are defined by the interior point and the two intersection points. Equation 3.21 is applied to these sub-triangles and the net fluxes are summed.

(f) $N_\Delta = 1$; $M_\Delta = 2$; Three sub-triangles are defined by the interior points and the two intersection points. Equation 3.21 is applied to these sub-triangles and the net fluxes are summed.

3.3.2-C Calculating Source/Sink Distribution To Cells

As with leakage distribution, calculating the source/sink distribution to individual grid cells requires geometric manipulations. Along each analytic element that contributes to or removes water from the domain, the distribution of flux is known explicitly, usually as a polynomial function. However, this flux is not cell-averaged, as with finite difference boundary conditions. Instead, it is provided as the flux per unit length of the element boundary, which may be linear, curvilinear, circular, or elliptical. For example, the flux distribution along a (linear) high-order linesink (Janković 1997; Janković and Barnes 1999a) is given by a Chebyshev polynomial:

$$Q_X(X) = -\frac{2}{L}\sum_{n=0}^{N-1} d_n T_n(X) \tag{3.23}$$

where Q_X is the extraction per unit length of the linesink, the $N-1$ coefficients d_n are based upon the element strength coefficients, T_n is an order n Chebyshev polynomial, and X is the location along the linesink in local coordinates ($X = -1$ on one end of the linesink, $X = 1$ on the other). This high-order linesink is used to model head-specified or general head boundary conditions in the analytic element method. To obtain the net flux, Q^{net}, from any arbitrary segment of the linesink, this expression may be integrated over that segment to obtain:

$$Q^{net} = \int_{X_1}^{X_2} \frac{2}{L}\sum_{n=0}^{N-1} d_n T_n(X) dX = \frac{2}{L}\sum_{n=0}^{N} a_n \left[T_n(X_2) - T_n(X_1)\right] \tag{3.24}$$

where a_n are the known element jump coefficients (see (Janković 1997) for details on the high order implementation). Unfortunately, dividing this net flux into influx (Q^+) and outflux (Q^-) components requires separating the integral into its positive and negative parts, which cannot be done analytically. The following equations identify and separate the positive and negative portions of the integral in (3.24):

$$\begin{aligned} Q^+ &= \frac{1}{L}\int_{X_1}^{X_2}\sum_{n=0}^{N}|d_nT_n(X)| - d_nT_n(X)dX \\ Q^- &= \frac{1}{L}\int_{X_1}^{X_2}\sum_{n=0}^{N}|d_nT_n(X)| + d_nT_n(X)dX \end{aligned} \tag{3.25}$$

These integrals are calculated using quadrature and corrected with the analytic net flux so that the mass balance over the segment from X_1 to X_2 is maintained. If the segment extracts only or injects only (i.e., $Q^+ = Q^{net}$ or $Q^- = -Q^{net}$), the analytic solution is used directly (this is the most common case). Otherwise, adjustments to the numerically calculated extraction and injection fluxes are made based upon the segment mass balance error due to numerical integration, $\Delta Q = Q^{net} - (Q^+)_{NUM} + (Q^-)_{NUM}$ as follows:

$$\begin{aligned} Q^+ &= (Q^+)_{NUM}\left(1 + \frac{\Delta Q}{(Q^+)_{NUM} + (Q^-)_{NUM}}\right) \\ Q^- &= (Q^-)_{NUM}\left(1 - \frac{\Delta Q}{(Q^+)_{NUM} + (Q^-)_{NUM}}\right) \end{aligned} \tag{3.26}$$

As before, triangles (two per cell) may be used to identify the intercepts between the cell and the element. The intersection points (in local element coordinates) are used as the integration bounds X_1 and X_2.

The above analysis was illustrated for a linear element; similar expressions may in the future be obtained for circular, elliptical, and curvilinear elements. The functional form of the flux distributions along the element boundaries for these geometries is either a Fourier series (circular and elliptical elements) or Chebyshev series (curvilinear elements).

The final type of source/sink to be considered is that of a pumping well (point sink). The net flux from this element is obtained exactly as in conventional finite difference methods: if the well is located within a cell, the flux is linked to that cell. No geometric manipulation or integration is necessary.

3.3.2-D Calculating Face-averaged Dispersion coefficients

A generic expression for the dispersion coefficients in terms of longitudinal and transverse dispersivities, α_l [L] and α_t [L], and species-specific diffusion coefficients is given as (Zheng and Bennett 2002):

$$D_{xx} = \alpha_l \frac{v_x^2}{|v|} + \alpha_t \frac{v_y^2}{|v|} + D^* \tag{3.27}$$

$$D_{yy} = \alpha_l \frac{v_y^2}{|v|} + \alpha_t \frac{v_x^2}{|v|} + D^* \tag{3.28}$$

$$D_{xy} = D_{yx} = (\alpha_l - \alpha_t) \frac{v_x v_y}{|v|} \tag{3.29}$$

where α_l, α_t are the longitudinal and transverse dispersivities, and D^* is the species-specific diffusion coefficient. As shown in subsection 3.3.1, each of these dispersion coefficients must be calculated (in an average sense) across each cell face to develop the system of finite difference equations. Typically, this has been done directly from the (known) normal discharge through the face– the values for $v_{x(i\pm1/2,j)}$ are easily obtained from the integrated flux $Q_{x(i\pm1/2,j)}$ and the values for $v_{y(i,j\pm1/2)}$ are easily obtained from the integrated flux $Q_{y(i,j\pm1/2)}$. However, face-averaged dispersion coefficients require estimates for $|v|_{(i,j\pm1/2)}$, which requires estimates of the face-averaged tangential fluxes. Tangential flux values are not available as a byproduct of traditional finite difference flow solution. Therefore, the tangential component of flux along a cell face is typically estimated as the average of the four normal fluxes calculated at the adjacent perpendicular cell faces. These calculations are discussed at length by Zheng and Bennett (Zheng and Bennett 2002).

With the analytic element method, the velocity is known as a continuous function of space, and this averaging process, which may introduce minor parameter evaluation errors in zones with rapidly changing velocity or low-resolution spatial discretization, is not necessary. As an alternative to the method of Zheng and Bennett (Zheng and Bennett 2002), the following formulation for the face-averaged dispersion coefficients is derived:

$$D_{xx(i+1/2,j)} = \alpha_l \frac{v_{x(i+1/2,j)}^2}{|v|_{(i+1/2,j)}} + \alpha_t \frac{v_{y(i+1/2,j)}^2}{|v|_{(i+1/2,j)}} + D^* \tag{3.30}$$

$$D_{xy} = (\alpha_l - \alpha_t) \frac{v_{x(i+1/2,j)} v_{y(i+1/2,j)}}{|v|_{(i+1/2,j)}} \tag{3.31}$$

where

$$v_{x(i+1/2,j)} = \frac{Q_{x(i+1/2,j)}}{h_{(i+1/2,j)}\theta_{(i+1/2,j)}} \tag{3.32}$$

$$v_{y(i+1/2,j)} = \frac{Q_{y(i+1/2,j)}}{h_{(i+1/2,j)}\theta_{(i+1/2,j)}} \tag{3.33}$$

$$|v|_{(i+1/2,j)} = \sqrt{v^2_{x(i+1/2,j)} + v^2_{y(i+1/2,j)}} \tag{3.34}$$

The magnitude of $Q_{x(i+1/2,j)}$ is calculated using the divergence-corrected version of equation 3.14. The magnitudes of $h_{(i+1/2,j)}$ and $\theta_{(i+1/2,j)}$ may be calculated using low-order numerical integration, and the magnitude of $Q_{y(i+1/2,j)}$ requires evaluation of the average tangential discharge along the cell face (since the y-direction is not normal to the cell face). Such a calculation is briefly described in the next subsection.

3.3.2-E Average Tangential Discharge along a Face

The average tangential discharge, as shown in the previous section, is useful for calculating the face-averaged dispersion coefficient. As with the net flux of water through a vertical strip of the aquifer, the average tangential discharge normal to a vertical strip may also be calculated to an arbitrary level of precision in AEM. In irrotational domains (i.e., domains where the discharge potential, Φ, is defined because the aquifer conductivity, base elevation, and thickness are piecewise continuous), the integrated tangential flux may be calculated in a manner analogous to that used for the normal discharge. If there are no discontinuities in the potential function intersecting an arbitrary face from z_1 to z_2, the average tangential flux through the face may be calculated as the difference in the potential function calculated at its two endpoints, normalized by the length of the segment.

$$\bar{Q_t} = \frac{1}{|z_2 - z_1|}\int_{z_1}^{z_2} Q_t(z)dz = \frac{1}{|z_2 - z_1|}\left(\Phi(z_2) - \Phi(z_1)\right) \tag{3.35}$$

where Q_t is the integrated discharge tangential to the face defined by z_1 and z_2. Note the similarity between this formulation and equation 3.14. In fact, this calculation is subject to the same problems ascribed to intersecting elements (line doublets in this case) and undefined zones of the potential function (e.g., area vortices). These problems may be handled in a manner analogous to their treatment during the calculation of net flux.

3.3.3 Pseudo-3D Flux Discretization

The above analysis was carried out for vertically-averaged flow systems linked to a vertically-averaged transport algorithm. For transport simulations in shallow aquifers (those approximated with the Dupuit-Forcheimer assumption), the aquifer system may also be discretized vertically, and solved using a three-dimensional finite difference approximation. Vertical flow components are approximated using an approach developed by Strack (Strack 1984). This analogous finite difference discretization of the fully 3D governing equation (equation 2.2) will not be discussed here, as it has been rigorously derived elsewhere (Zheng and Bennett 2002; Zheng and Wang 1999). However, the following section will discuss the appropriate measures for discretizing the horizontal and vertical fluxes in pseudo-3D Dupuit-Forcheimer models.

3.3.3-A Horizontal flux across a Face

In Dupuit-Forcheimer models, one of the common assumptions is that horizontal discharge is uniform across the saturated thickness. Making this assumption, the horizontal flux across a vertical cell face in the aquifer may be calculated as a fraction of the integrated flux across a face in 2D. Unfortunately, if the height of each 3D grid cell is constant in space, the integral must be evaluated as

$$q^{net} = \int_{z_1}^{z_2} \int_{z'}^{min(z'+\Delta z', h)} \frac{Q_\eta(z)}{h} dz \tag{3.36}$$

where z' is the vertical coordinate measured from the aquifer base, $\Delta z'$ is the height of the three-dimensional finite difference cell, and the face is oriented vertically from z_1 to z_2. If $h(z)$ is non-uniform (as is the case for unconfined flow), numerical integration is required.

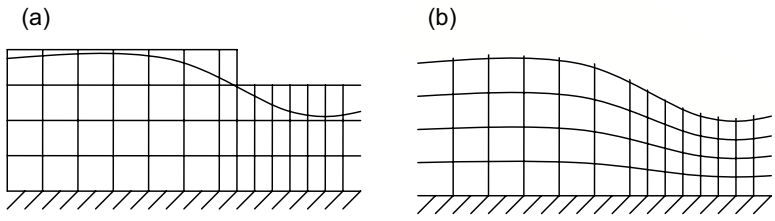

Figure 3.14: Vertical discretization schemes for Pseudo-3D simulations. (a) Uniform discretization (b) Smooth vertical discretization

However, if the system is discretized so that planes of constant z'/h are used to subdivide the

domain in the vertical (as shown in figure 3.14), the horizontal flux through the face will simply be some fraction of the net integrated flux through the saturated thickness:

$$q^{net} = \frac{\Delta z'}{h} \int_{z_1}^{z_2} Q_\eta(z) dz \tag{3.37}$$

Here, the uniformity of the specific discharge vector in the vertical was used to simplify the expression for horizontal flux. The integral in equation 3.37 may be evaluated exactly as presented above in subsection 3.3.2-A. Caution must be used with this formulation, as the finite difference approximation must be revised to account for the curved geometry of each grid cell.

3.3.3-B Vertical flux across a horizontal face

The vertical flux in a shallow aquifer may be approximated with the following formula (developed in appendix B:

$$q_z(z, z') = \zeta \frac{|W|^2}{kh^3} z' - \frac{N(z)}{h} z' + N_b(z) \tag{3.38}$$

Integrating this over an arbitrary triangle,

$$\int_\Delta q_z(z, z') dz = \zeta z' \int_\Delta \frac{|W|^2}{kh^3} - z' \int_\Delta \frac{N(z)}{h} dz + \int_\Delta N_b(z) dz \tag{3.39}$$

If the vertical discretization of the aquifer system is uniform in space (as in figure 3.14a), this integral may only be evaluated exactly if the aquifer is confined (i.e., $\zeta = 0$ and $h = H$). However, if the system is discretized such that the vertical discretization follows surfaces of constant z'/h (as shown in figure 3.14b), the integrated flux normal to the face simplifies to:

$$\int_{\Delta'} q_z(z, z') dz = -\frac{z'}{h} \int_\Delta N(z) dz + \int_\Delta N_b(z) dz \tag{3.40}$$

Note that Δ' is now a curved surface. Here, both integrals may be evaluated analytically, and the projection of the curved surface Δ' back into the z plane may be used as a surrogate for the exact integral, because the fluxes $N(z)$ and $N_b(z)$ are purely vertical.

3.3.4 Backwards Method of Characteristics

The backwards method of characteristics (BMOC) uses a Lagrangian approach to model the influence of advection and an Eulerian approach to model the influence of dispersion. The method, as implemented for this dissertation, has been configured to be used with both finite difference and finite element methods for simulating dispersion, and is briefly described here.

The AEM-based BMOC algorithm, briefly introduced in chapter 2, simulates advection by backtracking a particle along a flow path (or "characteristic" path) from the nodes of the computational grid or mesh. With the finite difference method, these nodes are located at the center of the grid cells. For each time step, the concentration change due to advection is calculated by simply interpolating the old concentration at the "foot" of the characteristic path and assigning this interpolated concentration to the cell. Dispersion is then simulated using the finite difference method, as described in section 3.3.1, but without including the approximations of the advective terms within the governing equation.

The primary difference between the implementation of the BMOC method within CARDINAL and previous implementations is the use of the highly accurate Runge-Kutta method (described in appendix F)to calculate the characteristic path.

.

3.4 The Effective Parameter Formulation

3.4.1 Overview

This section presents an alternative approach for formulating the two-dimensional transport problem with continuous flow parameters (velocity, dispersion coefficient) and porous media properties (porosity, sorption coefficients). The approach is independent of transport system discretization and is therefore amenable to simulation using a variety of Eulerian or Lagrangian methods. The primary difference between this new approach and existing methods is the use of the non-discrete analytic element method as the source of velocities, saturated thicknesses, dispersion coefficients, and their derivatives.

As explained previously, the analytic element method represents the flow solution via superposition of analytic functions that are continuous in space; head or flux may be obtained at any x-y location in space without the need for interpolation. Currently, the only practical method of linking an AEM flow solution to a transport model is to discretize the velocity field and export it to a transport solver such as MT3DMS (Zheng and Wang 1999) or use the revised finite difference methods discussed in section 3.3. While this approach allows the transport domain to be discretized independently of any flow grid or mesh, it results in information loss. Depending upon the model configuration, finite difference discretization can result in smoothing and clipping of local flow features and/or discontinuity of the velocity derivative. This will occur even though (1) the original AEM solution was fully conservative, high-resolution, and continuous and (2) the discretized AEM solution meets local mass balance requirements to a high degree.

In this section, continuous expressions for saturated thickness, dispersion coefficients, and dispersion coefficient spatial derivatives are derived from an AEM representation. These expressions exploit the continuous AEM flow solutions and preserve the smooth nature of the parameter fields for use in transport simulations. The information loss in translating an AEM flow solution to a discrete finite difference or finite element nodal representation is removed, leading to a potential reduction in overall spatial truncation error, particularly for Lagrangian methods. Importantly, using these continuous parameters does not prohibit the transport simulation method from "smearing" the information due to averaging of these continuous quantities over a finite element or finite difference cell. It merely provides the highest quality parameterization for the transport algorithm to then manipulate as necessary. Thus any method using these continuous parameters is still subject

to discretization error. However, if the continuous parameters are used appropriately, these errors will be smaller than if interpolated or approximated parameters were used.

In addition, an alternative "effective parameter" formulation of the vertically-averaged transport equation is here developed to facilitate robust use of continuously-represented parameters. Closed-form expressions for these effective transport parameters are derived from analytic element functions. A discussion of the difficulties of using such a formulation in an Eulerian framework is given in section 3.5.1. Implementation of this new effective parameter vertically-averaged transport approach using a revised random walk method is discussed in section 3.5.4.

With the analytic element method, the flow-solution-derived independent parameters in Equation 2.16 (and their derivatives) may be expressed as continuous functions of space. This continuity has been exploited in section 3.3 for accurate volume and facial averaging of properties in Eulerian finite difference solution schemes. Here, this continuity is exploited for highly accurate representation of subtle property changes in Eulerian, Lagrangian, or Eulerian-Lagrangian methods. By explicitly evaluating the spatial derivatives of continuous parameters, truncation and interpolation errors introduced by the transport method may be minimized or removed. In contrast, traditional methods for solving the advection-dispersion equation introduce Taylor series truncation error into parameter gradients, and interpolation error into characteristic paths.

To extend the discussion herein to continuous representation of all parameters (not just those supplied by the analytic element method), the derivations below assume that the aquifer porosity, base elevation, and aquifer thickness are represented with singly differentiable functions (e.g., polynomials; radial basis functions; kriged fields) and that the retardation factor and recharge concentration distribution may be spatially integrated. Variability of the aquifer base and thickness has not yet been fully realized in current analytic element models beyond a piecewise continuous representation, but more complex formulations are mathematically viable and considered here. The AEM flow solution requires no information about the spatial distribution of porosity, concentration, or retardation factors. Therefore, assumptions about the functional form of these properties only impact the transport solution.

To facilitate a continuous representation, the terms of the convective form of the vertically-

averaged transport equation (2.16) are expanded as follows:

$$\begin{aligned} R_f \frac{\partial C}{\partial t} = & - v_x^* \frac{\partial C}{\partial x} - v_y^* \frac{\partial C}{\partial y} \\ & + D_{xx} \frac{\partial^2 C}{\partial x^2} + 2D_{xy} \frac{\partial^2 C}{\partial x \partial y} + D_{yy} \frac{\partial^2 C}{\partial y^2} \\ & + \frac{N_t^+}{h\theta}(c_t^+ - C) + \frac{N_b^+}{h\theta}(c_b^+ - C) \end{aligned} \tag{3.41}$$

where the terms v_x^* and v_y^* are labeled the "effective velocities" because they act as multipliers of the first derivatives of concentration. These effective velocities are expressed as a combination of the actual velocities and the relative effects of independent parameter gradation:

$$v_x^* = \left[\begin{array}{l} v_x - \dfrac{\partial D_{xx}}{\partial x} - \dfrac{\partial D_{yx}}{\partial y} \\ \quad - \dfrac{D_{xx}}{\theta}\dfrac{\partial \theta}{\partial x} - \dfrac{D_{yx}}{\theta}\dfrac{\partial \theta}{\partial y} \\ \quad - \dfrac{D_{xx}}{h}\dfrac{\partial h}{\partial x} - \dfrac{D_{yx}}{h}\dfrac{\partial h}{\partial y} \end{array} \right] \tag{3.42}$$

$$v_y^* = \left[\begin{array}{l} v_y - \dfrac{\partial D_{yy}}{\partial y} - \dfrac{\partial D_{xy}}{\partial x} \\ \quad - \dfrac{D_{yy}}{\theta}\dfrac{\partial \theta}{\partial y} - \dfrac{D_{xy}}{\theta}\dfrac{\partial \theta}{\partial x} \\ \quad - \dfrac{D_{xy}}{h}\dfrac{\partial h}{\partial x} - \dfrac{D_{yy}}{h}\dfrac{\partial h}{\partial y} \end{array} \right] \tag{3.43}$$

The preceding formulation of the vertically-averaged transport equation is henceforth labeled the "effective parameter vertically-averaged" (EPVA) formulation. The remainder of this section deals with identifying closed-form continuous expressions for (3.42) in terms of superimposed analytic element functions and generic differentiable expressions for the flow system and porous media properties (porosity, recharge, retardation factor, base, and thickness).

3.4.2 The Discharge Derivative

Developing a closed-form expression for effective velocity requires evaluation of the spatial derivatives of velocity. These spatial derivatives may be obtained by use of a newly defined analytic function, the discharge derivative, G_x [LT^{-1}], which is defined as follows:

$$G_x = \frac{\partial W}{\partial z} = \frac{\partial Qx}{\partial x} - i\frac{\partial Qy}{\partial x} \tag{3.44}$$

This represents the derivatives of the discharge vector with respect to the x-direction. The y-direction derivative may be obtained from application of the definition of curl and from mass continuity. From the definition of curl,

$$\frac{\partial Qx}{\partial y} = \beta + \frac{\partial Qy}{\partial x} \tag{3.45}$$

where β is the curl of the discharge vector. From mass continuity,

$$\frac{\partial Qy}{\partial y} = -N - \frac{\partial Qx}{\partial x} \tag{3.46}$$

Therefore, the y-directional discharge derivative G_y may be written,

$$G_y = \frac{\partial Qx}{\partial y} - i\frac{\partial Qy}{\partial y} = iG_x + \beta + iN \tag{3.47}$$

The functions G_x and G_y may be derived for each individual element type by differentiating the discharge function with respect to z. Most elements contribute zero curl and zero divergence to the domain, with the exception of the area-sink and area-vortex (Strack and Janković 1999; Strack 1999). The discharge derivatives for all elements in the model may be superimposed, as with the complex potential or discharge function. Discharge derivative functions for common analytic elements (point sinks, Laurent series, Taylor series, elliptical inhomogeneities, and high-order line elements) are derived in appendix C.

3.4.3 Dispersion Coefficients and Their Spatial Derivatives

The various components of the two-dimensional dispersion tensor may be written as follows (Zheng and Bennett 2002):

$$D_{xx} = \alpha_l \frac{v_x^2}{|v|} + \alpha_t \frac{v_y^2}{|v|} + D^* \tag{3.48}$$

$$D_{yy} = \alpha_l \frac{v_y^2}{|v|} + \alpha_t \frac{v_x^2}{|v|} + D^* \tag{3.49}$$

$$D_{xy} = D_{yx} = (\alpha_l - \alpha_t)\frac{v_x v_y}{|v|} \tag{3.50}$$

where α_l [L] is the longitudinal dispersivity, α_t [L] is the transverse dispersivity, and D^* [L^2T^{-1}] is the diffusion coefficient of the solute.

These coefficients are functions of velocity and, if analytic expressions are used as a basis for the velocities, are continuous functions of space. Closed-form expressions for the derivatives of dispersion coefficients are necessary for use in (3.42). For example,

$$\frac{\partial D_{xx}}{\partial x} = \frac{\partial}{\partial x}\left(\alpha_l \frac{v_x^2}{|v|} + \alpha_t \frac{v_y^2}{|v|} + D^*\right) \tag{3.51}$$

Equation 3.51 can be expanded and written as:

$$\frac{\partial D_{xx}}{\partial x} = \frac{\alpha_l v_x^2}{|v|}\frac{2}{v_x}\frac{\partial v_x}{\partial x} + \left(\alpha_l v_x^2 + \alpha_t v_y^2\right)\left(\frac{\partial |v|^{-1}}{\partial x}\right) + \frac{\alpha_t v_y^2}{|v|}\frac{2}{v_y}\frac{\partial v_y}{\partial x} \tag{3.52}$$

This formula (and similar expressions for other dispersion coefficient spatial derivatives) require closed-form expressions for the derivative of velocity and its magnitude, which are provided in appendix A. Substituting in the equations (A.8), (A.9), and (A.20), explicit closed-form expression for the x-direction dispersion derivative is obtained,

$$\frac{\partial D_{xx}}{\partial x} = \frac{\alpha_l v_x^2}{|v|}\left[2\frac{\Re(G_x)}{Q_x} - \frac{\Re(\overline{W}G_x)}{|W|^2} + \Upsilon_x\right] + \frac{\alpha_t v_y^2}{|v|}\left[-2\frac{\Im(G_x)}{Q_y} - \frac{\Re(\overline{W}G_x)}{|W|^2} + \Upsilon_x\right] \tag{3.53}$$

where the Υ terms $[L^{-1}]$, derived in appendix A, represent the combined influence of spatial gradients in saturated thickness and porosity. Similar analysis for the y-derivative of D_{yy} provides:

$$\frac{\partial D_{yy}}{\partial y} = \frac{\alpha_t v_x^2}{|v|}\left[2\frac{\Re(G_y)}{Q_x} - \frac{\Re(\overline{W}G_y)}{|W|^2} + \Upsilon_y\right] + \frac{\alpha_l v_y^2}{|v|}\left[-2\frac{\Im(G_y)}{Q_y} - \frac{\Re(\overline{W}G_y)}{|W|^2} + \Upsilon_y\right] \tag{3.54}$$

The cross-dispersion terms are similarly developed as:

$$\begin{aligned}&\frac{\partial D_{xy}}{\partial x} = \frac{\partial D_{yx}}{\partial x} = \\ &(\alpha_l - \alpha_t)\frac{v_x v_y}{|v|}\left[\frac{\Re(G_x)}{Q_x} - \frac{\Im(G_x)}{Q_y} - \frac{\Re(\overline{W}G_x)}{|W|^2} + \Upsilon_x\right]\end{aligned} \tag{3.55}$$

$$\begin{aligned}&\frac{\partial D_{xy}}{\partial y} = \frac{\partial D_{yx}}{\partial y} = \\ &(\alpha_l - \alpha_t)\frac{v_x v_y}{|v|}\left[\frac{\Re(G_y)}{Q_x} - \frac{\Im(G_y)}{Q_y} - \frac{\Re(\overline{W}G_y)}{|W|^2} + \Upsilon_y\right]\end{aligned} \tag{3.56}$$

These expressions are exact- the only numerical error introduced is that induced by the truncation of polynomials in some of the analytic element expressions (high-order AEM implementations suffer from piezometric head errors on the order of millimeters or less (Janković and Barnes 1999a); a

similar order of errors is expected here).

If the derivatives of Equations 3.55 and 3.56 are approximated using finite differences, Taylor series truncation errors are generated. For example, the standard central difference truncation errors are on the order of Δx^2, where Δx is the representative spacing between nodes. This error is in addition to any velocity errors resulting from discretization of the flow model.

This dispersion derivative truncation error is rarely discussed in the context of transport modeling in part because the errors affect only regions with significant velocity gradients. Also, researchers tend to be primarily concerned with truncation error of the dependent variable, because it controls the stability of the solution. However, truncation of any input parameter contributes to overall model error.

3.4.4 Effective Velocities

The expressions for the dispersion coefficients and their derivatives (equations 3.48; 3.53-3.56) are combined with expressions for the influence of variable saturated thickness and porosity (equations A.4 and A.5 from appendix A) to obtain closed-form solutions for the effective velocities as an explicit function of space (note that v_x and v_y are also closed-form). Substitution of these expressions into equation 3.42 with minor rearrangement leads to:

$$\begin{aligned} v_x^* = & v_x \\ & - \frac{\alpha_l v_x^2}{|v|}\left[2\frac{\Re(G_x)}{Q_x} - \frac{\Re(\overline{W}G_x)}{|W|^2}\right] \\ & - \frac{\alpha_t v_y^2}{|v|}\left[-2\frac{\Im(G_y)}{Q_y} - \frac{\Re(\overline{W}G_x)}{|W|^2} - (\Upsilon_x - \Upsilon_y)\right] \\ & - (\alpha_l - \alpha_t)\frac{v_x v_y}{|v|}\left[\frac{\Re(G_y)}{Q_x} - \frac{\Im(G_y)}{Q_y} - \frac{\Re(\overline{W}G_y)}{|W|^2}\right] \\ & + D^*\left[\Upsilon_x - \Upsilon_y\right] \end{aligned} \tag{3.57}$$

$$
\begin{aligned}
v_y^* = & v_y \\
& - \frac{\alpha_l v_y^2}{|v|}\left[2\frac{\Re(G_y)}{Q_x} - \frac{\Re(\overline{W}G_y)}{|W|^2}\right] \\
& - \frac{\alpha_t v_x^2}{|v|}\left[-2\frac{\Im(G_y)}{Q_y} - \frac{\Re(\overline{W}G_y)}{|W|^2} - (\Upsilon_y - \Upsilon_x)\right] \\
& - (\alpha_l - \alpha_t)\frac{v_x v_y}{|v|}\left[\frac{\Re(G_x)}{Q_x} - \frac{\Im(G_x)}{Q_y} - \frac{\Re(\overline{W}G_x)}{|W|^2}\right] \\
& + D^*\left[\Upsilon_y - \Upsilon_x\right]
\end{aligned}
\tag{3.58}
$$

As with the dispersion coefficient derivatives, equations 3.57 and 3.58 are nearly exact, limited only by the accuracy of the AEM solution. However, these effective velocities are independent of the numerical technique used to obtain the flow parameters. The discharge derivatives G_x and G_y may, in fact, be obtained using discrete flow solutions with first or higher order derivatives of flux. However, it is likely that this will not be very advantageous, particularly if fluxes are obtained as a byproduct of the solution for hydraulic head (as is often the case). Cumulative truncation error will likely invalidate the accuracy of the expression, and the traditional handling of parameter derivatives within the vertically-averaged ADR will provide similar results.

The difference between the effective velocity and the flow velocity will normally be small, except for systems characterized by (1) large dispersivities, (2) large gradients in flux (e.g., close to hydrologic features such as wells), and (3) small saturated thicknesses. Most of the terms in equations 3.57 and 3.58 represent relative changes of parameters (i.e., the change in parameter normalized by the value of that parameter). Therefore, locations with small property magnitudes and high property gradients are particularly sensitive to the additional effective velocity terms. For example, the effective velocity will be appreciably different from the flow velocity on the edge of an engineered vertical barrier where the porosity is low but the porosity gradient is high. For the most part, however, the additional effective velocity terms will have values that are a small fraction of the velocity. One of the benefits of the EPVA formulation is that the relative influence of parameter gradients (in dispersion coefficients, porosity, and saturated thickness) may be directly analyzed and visualized using the function $(v^* - v)$, which controls the hyperbolic behavior of the dispersive portion of the PDE.

3.4.5 Effective velocities in 3D

Analytic element method flow solutions, based upon a 2-dimensional approximation for simulating groundwater flow, may nonetheless be used to calculate vertical fluxes in an approximate fashion (Strack 1989). For "pseudo-three-dimensional" flow in Dupuit-Forcheimer models, a vertical component of the velocity vector may be estimated as (revised from Strack (1989), as shown in appendix B):

$$v_z(z,z') = \zeta\frac{|W|^2}{kh^3\theta}z' - \frac{N(z)}{h\theta}z' + \frac{N_b(z)}{\theta} \tag{3.59}$$

where z' is the vertical coordinate measured from the aquifer base (the superscript is used to differentiate it from the complex coordinate, z), and ζ is a boolean variable equal to one for unconfined flow, zero otherwise. The above expression is particular to irrotational systems (where the base and thickness of the aquifer are piecewise constant). The general expression may be found in appendix B.

For three-dimensional transport simulations within Dupuit-Forcheimer flow systems, the expressions for effective velocities must be modified. The effective formulation of the governing equation for contaminant transport in saturated three-dimensional aquifer systems (neglecting source/sink and reaction terms) is given as:

$$\frac{\partial c}{\partial t} = -\vec{v^*}\nabla c + \mathbf{D}\nabla^2 c \tag{3.60}$$

where the components of the effective velocity vector, $\vec{v^*}$, only include the influence of variable porosity and dispersion coefficients:

$$v_x^* = \left[\begin{array}{l} v_x - \dfrac{\partial D_{xx}}{\partial x} - \dfrac{\partial D_{yx}}{\partial y} - \dfrac{\partial D_{zx}}{\partial z'} \\ \quad - \dfrac{D_{xx}}{\theta}\dfrac{\partial\theta}{\partial x} - \dfrac{D_{yx}}{\theta}\dfrac{\partial\theta}{\partial y} - \dfrac{D_{zx}}{\theta}\dfrac{\partial\theta}{\partial z'} \end{array}\right] \tag{3.61}$$

$$v_y^* = \left[\begin{array}{l} v_y - \dfrac{\partial D_{yy}}{\partial y} - \dfrac{\partial D_{xy}}{\partial x} - \dfrac{\partial D_{zy}}{\partial z'} \\ \quad - \dfrac{D_{yy}}{\theta}\dfrac{\partial\theta}{\partial y} - \dfrac{D_{xy}}{\theta}\dfrac{\partial\theta}{\partial x} - \dfrac{D_{zy}}{\theta}\dfrac{\partial\theta}{\partial z'} \end{array}\right] \tag{3.62}$$

$$v_z^* = \left[\begin{array}{l} v_z - \dfrac{\partial D_{zz}}{\partial z'} - \dfrac{\partial D_{xz}}{\partial x} - \dfrac{\partial D_{yz}}{\partial y} \\ \quad - \dfrac{D_{zz}}{\theta}\dfrac{\partial\theta}{\partial z'} - \dfrac{D_{xz}}{\theta}\dfrac{\partial\theta}{\partial x} - \dfrac{D_{yz}}{\theta}\dfrac{\partial\theta}{\partial y} \end{array}\right] \tag{3.63}$$

where the diagonal components of the dispersion tensor are modified in definition to account for a

non-zero velocity in the vertical direction (ignored in the vertically-averaged transport formulation):

$$D_{xx} = \alpha_l \frac{v_x^2}{|v|} + \alpha_t \frac{v_y^2}{|v|} + \alpha_{tv} \frac{v_z^2}{|v|} + D^* \tag{3.64}$$

$$D_{yy} = \alpha_l \frac{v_y^2}{|v|} + \alpha_t \frac{v_x^2}{|v|} + \alpha_{tv} \frac{v_z^2}{|v|} + D^* \tag{3.65}$$

$$D_{xy} = D_{yx} = (\alpha_l - \alpha_t) \frac{v_x v_y}{|v|} \tag{3.66}$$

where α_{tv} [L] is the vertical transverse dispersivity and $|v|$ is now defined as the magnitude of the three-dimensional velocity vector ($|v| = \sqrt{v_x^2 + v_y^2 + v_z^2}$), but approximated with the two-dimensional velocity vector (nearly equivalent in shallow flow systems well described by the Dupuit-Forcheimer assumption). The additional five dispersion tensor components related to the third dimension are given as (from (Zheng and Bennett 2002)):

$$D_{zz} = \alpha_l \frac{v_z^2}{|v|} + \alpha_{tv} \frac{v_x^2}{|v|} + \alpha_{tv} \frac{v_y^2}{|v|} + D^* \tag{3.67}$$

$$D_{zx} = D_{xz} = (\alpha_l - \alpha_{tv}) \frac{v_x v_z}{|v|} \tag{3.68}$$

$$D_{zy} = D_{yz} = (\alpha_l - \alpha_{tv}) \frac{v_y v_z}{|v|} \tag{3.69}$$

As was done for the 2D vertically-averaged formulation, velocity spatial derivatives have been calculated for any general pseudo-3D Dupuit-Forcheimer flow solution in appendix B. Together with the definitions in 3.64 and 3.67, they may be assembled into closed-form solutions for effective velocities. Because both the vertical transverse dispersivities and vertical velocities are small in relation to longitudinal and horizontal transverse dispersivities, the expressions for the spatial derivatives of D_{xx}, D_{yy}, D_{xy}, and D_{yx} derived in equations 3.53 though 3.56 can be used as surrogates for an exact expression obtained from taking the derivatives of their 3D expressions (equation 3.64). The expressions for the derivatives of the vertical dispersion coefficient are:

$$\frac{\partial D_{zz}}{\partial z'} = \alpha_l \frac{v_z^2}{|v|} \frac{2}{v_z} \frac{\partial v_z}{\partial z} \tag{3.70}$$

$$\frac{\partial D_{zz}}{\partial z'} = \alpha_l \frac{v_z^2}{|v|} \frac{2}{v_z} \left(\zeta \frac{|W|^2}{kh^3\theta} \left(1 - \frac{\theta_z'}{\theta} \right) - \frac{N}{h\theta} - N_b \frac{\theta_z'}{\theta} \right) \tag{3.71}$$

Similar expressions may be obtained for the vertical spatial derivatives of D_{zx} and D_{zy}:

$$\frac{\partial D_{zx}}{\partial z'} = \frac{\partial D_{xz}}{\partial z'} = (\alpha_l - \alpha_{tv})\frac{v_x}{|v|}\left(\zeta\frac{|W|^2}{kh^3\theta}\left(1 - \frac{\theta'_z}{\theta}\right) - \frac{N}{h\theta} - N_b\frac{\theta'_z}{\theta}\right) \tag{3.72}$$

$$\frac{\partial D_{zy}}{\partial z'} = \frac{\partial D_{yz}}{\partial z'} = (\alpha_l - \alpha_{tv})\frac{v_y}{|v|}\left(\zeta\frac{|W|^2}{kh^3\theta}\left(1 - \frac{\theta'_z}{\theta}\right) - \frac{N}{h\theta} - N_b\frac{\theta'_z}{\theta}\right) \tag{3.73}$$

And for the horizontal spatial derivatives of D_{xz} and D_{yz}:

$$\frac{\partial D_{xz}}{\partial x} = \frac{\partial D_{zx}}{\partial x} = (\alpha_l - \alpha_{tv})\frac{v_x}{|v|}\left(\frac{\partial v_z}{\partial x} + v_z\left(\frac{\Re(G_x)}{Q_x} - \frac{\Re(\overline{W}G_x)}{|W|^2} + 2\Upsilon_x\right)\right) \tag{3.74}$$

$$\frac{\partial D_{yz}}{\partial y} = \frac{\partial D_{zy}}{\partial y} = (\alpha_l - \alpha_{tv})\frac{v_y}{|v|}\left(\frac{\partial v_z}{\partial y} + v_z\left(\frac{\Re(G_y)}{Q_y} - \frac{\Re(\overline{W}G_y)}{|W|^2} + 2\Upsilon_y\right)\right) \tag{3.75}$$

where $\frac{\partial v_z}{\partial y}$ and $\frac{\partial v_z}{\partial y}$ are too complicated to be included here, but are also closed-form expressions (derived in appendix B). The full expression for effective velocities may be assembled by substitution of equations 3.52-3.56 and 3.71-3.75 into equation 3.61.

Note that these closed-form solutions for effective velocity are only valid for Dupuit-Forcheimer flow using the estimated v_z of equation 3.59. Similar expressions may be obtained from fully three-dimensional analytic element models, given redefined elementary solutions for the analogous 3D discharge derivatives G_x, G_y, and G_z (each vectors with three components).

3.4.6 Computational Considerations

Computation of the effective velocity, v^*, requires about fifty percent more calculations than standard velocity terms derived from the analytic element method. To calculate the velocity at a given spatial location, computation of all element discharge potential functions (for the saturated thickness) and all element discharge functions (for the integrated discharge) is required. The effective velocity term requires additional computation of all element discharge derivatives. Each of these calculations are roughly of order n, where n is the number of degrees of freedom in the model. The cost of calculating v_x and v_y is roughly $2n$, and the cost for the effective velocities is $3n$. For Eulerian methods, where such values need only be calculated a few times per degree of freedom, this is a minor computational limitation. This additional cost may be inhibitive, however, for Lagrangian simulations where the characteristic paths of the effective velocity are tracked using higher-order Runge-Kutta methods.

3.5 Implementation of EPVA Methods

3.5.1 EPVA Applicability

While the EPVA approach is attractive due to its rigor and its reduced dependence upon numerical differentiation of independent parameters, the successful solution of the revised differential equation (equation 3.41) using standard Eulerian or Eulerian-Lagrangian numerical methods proved either problematic or impossible in practice, as discussed below. In this dissertation the EPVA approach was applied only to purely Lagrangian simulation. However, it may eventually prove valuable for solution of transport problems using mesh-free methods.

The initial motivation for deriving the effective parameter formulation was to solve an *identical* differential equation where the parameter derivatives were decoupled from the derivatives of concentration, the dependent parameter. The concentration derivatives *must* be numerically discretized and approximated to solve the governing equation; the independent parameters should ideally have no such limitations. It was expected that the effects of continuous parameter gradation would likely be averaged in some way, but the averaging technique would ideally be flexible, and errors from the averaging could be reduced in the traditional fashion, with increased grid or mesh resolution. However, unforeseen limitations of finite element and finite difference methods impede the successful numerical solution of the EPVA formulation of the governing equation. This is despite the fact that the EPVA formulation, in a purely mathematical sense, is identical to the classical governing equation successfully solved by both methods. The sources of these limitations are presented in this section, as is the successful EPVA implementation of a purely Lagrangian technique, the random walk method.

3.5.2 EPVA Limitations: Finite Difference Methods

Finite difference methods are limited not by their ability to solve the effective parameter formulation of vertically-averaged transport, but rather by their ability to conserve mass with this particular formulation. Simply stated, partial differential equations of the "divergence" form:

$$\frac{\partial f}{\partial t} = \nabla \cdot (af) + \nabla \cdot (b \nabla \cdot f) \tag{3.76}$$

Where f is the dependent variable and a and b are spatially variable independent parameters, are conservative when approximated with finite differences. The mathematically equivalent formulation of the partial differential equation,

$$\frac{\partial f}{\partial t} = a\nabla f + f\nabla a + (\nabla b)(\nabla f) + b\nabla^2 f \tag{3.77}$$

is not conservative, due to the different methods of handling the spatially variable parameters a, b, ∇a, and ∇b. In the first case, the parameters a and b are face averaged, in the second case they are cell-averaged. The EPVA formulation, equivalent to equation 3.77, thus cannot be implemented in a conservative manner using finite difference techniques.

3.5.3 EPVA Limitations: Finite Element Methods

The difficulty with solving equation 3.41 using finite element methods is not one of accuracy, as with finite difference methods. Rather, it results from the inability of FE methods to mathematically separate out the influence of graded parameters in the "weak" form of the governing equation (for a discussion of the significance of the weak form in finite element methods, the reader is referred to Gresho and Sani (1998)). To illustrate this point, the appropriate weak form of an effective parameter formulation for 1-dimensional transport is derived below.

Essentially, the use of the weak form enables a partial differential equation to explicitly include the influence of discontinuities and boundaries (PDEs, expressed in their general "strong" form are applicable to a continuous non-bounded system). The weak form is obtained by first integrating the governing PDE multiplied by a weighting function, $w(x)$ over the model domain:

$$\int w(x)\left(\frac{\partial C}{\partial t} + [v(x) - \nabla D(x)] \cdot \nabla C - D(x)\nabla^2 C\right) = 0 \tag{3.78}$$

The term in square brackets is the effective velocity for the simple 1D case. If $w(x)$ is once differentiable, the following identity is valid (using the chain rule):

$$\nabla[wD(x)\nabla C] = wD(x)\nabla^2 C + w\nabla D(x) \cdot \nabla C + D(x)\nabla w \cdot \nabla C \tag{3.79}$$

By integrating equation 3.79 over the model domain and applying the divergence theorem, the second partial derivative term in equation 3.78 may be redefined in terms of both internal and

boundary integrals, which only involve first order derivatives of concentration.

$$\int wD(x)\nabla^2 C = \int_\Gamma wD(x)\mathbf{n}\nabla C - \int w\nabla D(x)\cdot\nabla C - \int D(x)\nabla w\cdot\nabla C \tag{3.80}$$

where Γ is the system boundary. Using the relationship in 3.80, equation 3.78 becomes:

$$\int w\frac{\partial C}{\partial t} + \int w\left[v(x) - \nabla D(x)\right]\cdot\nabla C - \int_\Gamma wD(x)\mathbf{n}\nabla C + \int w\nabla D(x)\cdot\nabla C + \int D(x)\nabla w\cdot\nabla C = 0 \tag{3.81}$$

Here, the spatial derivative of the dispersion coefficient in the second term cancels the fourth term, giving

$$\int w\frac{\partial C}{\partial t} - \int wv(x)\cdot\nabla C - \int_\Gamma wD(x)\mathbf{n}\nabla C + \int D(x)\nabla w\cdot\nabla C = 0 \tag{3.82}$$

This weak form is equivalent to the weak form of the traditional 1-dimensional ADE, despite the attempt to restate the governing equation. Because of approximations induced by the removal of the second partial derivative term of equation 3.78, the closed-form expressions for gradients in continuous parameters may not be handled explicitly in standard finite element methods, and the EPVA approach may not be used. Instead the gradients in spatial derivatives are handled using the the numerical derivatives of the weighting function, an approximation apparently induced by the application of the divergence theorem. This derivation extends to the two-dimensional case.

It is possible that alternative formulations of the EPVA weak form may be used that do not suffer from the drawbacks of the above approach. The development of such alternate formulations were considered beyond the scope of this research.

3.5.4 Effective Parameter Random Walk Technique

The random walk method (Prickett et al. 1981; Kinzelbach 1986; Kinzelbach and Uffink 1991)is a fully Lagrangian approach for simulating advective and dispersive transport of solute in an aquifer. Dissolved species in the aquifer are represented by a set of discrete particles, each associated with some solute mass. The method simulates advection of the plume via particle tracking techniques. The effects of hydrodynamic dispersion and diffusion are modeled by adding a random displacement of the particle location (correlated to the local dispersion coefficient).

For each time step Δt in the transport simulation, the two-dimensional random walk method moves each particle, initially located at the point $z_p(t)$ to an updated location, $z_p(t+\Delta t)$, according

to the following equation (modified from Zheng and Bennett (2002)):

$$z_p(t+\Delta t) = z_p(t) + \Delta z_a + \Delta z_d \tag{3.83}$$

Where Δz_a is the advective displacement over the time step, Δt, (from particle tracking) and Δz_d is the dispersive displacement over the time step, given by:

$$\Delta z_d = \left[\left(2\alpha_l \frac{v_x^2}{|v|} \Delta t \right)^{\frac{1}{2}} \kappa' + \left(2\alpha_t \frac{v_y^2}{|v|} \Delta t \right)^{\frac{1}{2}} \kappa'' \right] + i \left[\left(2\alpha_l \frac{v_y^2}{|v|} \Delta t \right)^{\frac{1}{2}} \kappa' + \left(2\alpha_t \frac{v_x^2}{|v|} \Delta t \right)^{\frac{1}{2}} \kappa'' \right] \tag{3.84}$$

Here, the values κ' and κ'' are two distinct normally distributed random numbers with a mean of zero and a standard deviation of 1. This expression for dispersive displacement is obtained via analogy between purely dispersive transport of a point source and the functional form of a normally distributed random variable.

As described by Kinzelbach (1986), the preceding approach causes the density of the particles to satisfy the Fokker-Plank equation, not the advection-dispersion equation. In order to properly account for this deviation, Kinzelbach (Kinzelbach 1988) proposed using a corrected velocity during the particle tracking, v', given as (for the two-dimensional non-vertically-averaged case without spatial variation in porosity):

$$\begin{aligned} v_x' &= v_x + \frac{\partial D_{xx}}{\partial x} + \frac{\partial D_{xy}}{\partial y} \\ v_y' &= v_y + \frac{\partial D_{yy}}{\partial y} + \frac{\partial D_{yx}}{\partial x} \end{aligned} \tag{3.85}$$

This additional term is often referred to as the drift term (e.g., as in (LaBolle et al. 1996)). Notice the similarity to the effective velocities presented in equation 3.42. The only difference is that the spatial gradients are added, rather than subtracted from, the seepage velocity. When accounting for vertical averaging, the correction assumes a form directly related to that of the effective velocities:

$$\begin{aligned} v_x' &= 2v_x - v_x^* \\ v_y' &= 2v_y - v_y^* \end{aligned} \tag{3.86}$$

This particular use of the closed-form dispersion derivatives and saturated thickness derivatives does not suffer from the numerical limitations associated with finite element or finite difference

methods. The random walk method allows these derivatives to be utilized directly, and there are no mass balance errors or mathematical cancellations to impede their direct use. It is for this reason that the random walk method is the only numerical technique tested herein that is well-suited for *directly* using continuous parameters in the form presented in section 3.4. This is not surprising, since the fully Lagrangian method lacks any fixed grid over which to average continuous parameters, and the method is globally mass conservative regardless of the particular formulation of the differential equation.

The EPVA random walk method has been implemented in CARDINAL and tested in section 4.2.2.

3.6 Implementation of a Graded Finite Element Method

The following section discusses the solution of the standard vertically-averaged formulation of the advective-dispersive equation presented in section 2.2.2 using a revised finite element method. Unlike the EPVA formulation, the solution of equation 2.16 is feasible using finite difference, finite volume, or streamline methods. However, finite element methods (FEMs) offer three distinct advantages: (1) the FEM more easily accommodates continuously varying aquifer properties, (2) FEM provides the mesh flexibility needed to conform to AEM geometries, and (3) FEMs may be more easily configured to simulate transport at regional and local scales simultaneously. The fully Eulerian graded-parameter finite element approach outlined below and in the following section has all of these properties. This approach has also been extended to use Eulerian finite element schemes for the dispersive portion of the ADR and a Lagrangian scheme (BMOC) for the advective portion.

The graded parameter finite element solution technique has been implemented in CARDINAL, benchmarked against analytic solutions (section 4.1), and applied to test cases (sections 4.2.3 and 4.4) to verify its numerical accuracy. A discussion of its advantages and disadvantages may be found in chapter 5. The following section only outlines its mathematical formulation.

3.6.1 Finite Element Formulation

The vertically-averaged advective-dispersive equation (equation 2.16) may be solved using triangular finite elements by approximating the concentration field with a function $\hat{C}$ of the following form

$$\hat{C}(\mathbf{x}, \mathrm{t}) = \sum_{\mathrm{e}=1}^{\mathrm{NE}} \sum_{\mathrm{i}=1}^{3} \mathrm{N}_{\mathrm{i}}^{(\mathrm{e})}(\mathbf{x}, \mathrm{t}) \hat{\mathrm{C}}_{\mathrm{i}} \tag{3.87}$$

where NE is the number of linear triangle finite elements, $N_i^{(e)}$ are the basis functions associated with the i^{th} node of element e (see appendix D for details) and $\hat{C}_i$ is the vertically-averaged concentration at node i. Within this dissertation, only linear triangle finite elements are used. While more advanced element geometries are available (Istok 1989; Akin 1994), the process of linking alternative element types to AEM flow solutions is similar to the approaches proposed here.

The finite element method solves the divergence form of the transport equation (2.16) by min-

imizing the following system residual (as in Yeh (2000)):

$$\int_{\Omega} \left[\begin{array}{l} -Q_x \dfrac{\partial C}{\partial x} - Q_y \dfrac{\partial C}{\partial y} \\ + \dfrac{\partial}{\partial x}\left(h\theta D_{xx}\dfrac{\partial C}{\partial x}\right) + \dfrac{\partial}{\partial x}\left(h\theta D_{xy}\dfrac{\partial C}{\partial y}\right) \\ + \dfrac{\partial}{\partial y}\left(h\theta D_{yx}\dfrac{\partial C}{\partial x}\right) + \dfrac{\partial}{\partial y}\left(h\theta D_{yy}\dfrac{\partial C}{\partial y}\right) \\ + \left(N_t^+(c_t^+ - C) + N_b^+(c_b^+ - C)\right) - R_f h\theta \dfrac{\partial C}{\partial t} \end{array} \right] dA \tag{3.88}$$

where $\hat{C}(\mathbf{x}, \mathrm{t})$ has been rewritten as C for simplicity of notation. This residual expression is temporally discretized using a finite difference approximation of the time derivative. This discrete approximation to the residual expression is minimized over each time step by solving a single system of equations. Similar to Yeh (2000) and Istok (1989), this system may be expressed as:

$$\begin{aligned} &\left[[A] + (\omega)\Delta t\left([D]^{n+1} + [K]^{n+1}\right)\right]\{C\}^{n+1} = \\ &\quad [[A] - (1-\omega)\Delta t\left([D]^n + [K]^n\right)]\{C\}^n \\ &\qquad\qquad + \Delta t\left[(\omega)[\{Q\}^n + \{F\}^n] + (1-\omega)[\{Q\}^{n+1} + \{F\}^{n+1}]\right] \end{aligned} \tag{3.89}$$

where the temporal weighting factor ($0 < \omega \leq 1$) determines whether an explicit, implicit, or Crank-Nicholson scheme is used. These schemes are analogous to those used in the finite difference algorithm.

Each equation in the system of *NN* equations represented by 3.89 corresponds to a single unknown value of concentration at each of the *NN* nodes in the mesh. The various matrices in this system are assembled on a node-by-node basis based upon the properties of the adjacent elements. The entries of the *NN* x *NN* "sorption matrix" or "mass matrix" $[A]$ are given by (e.g., Yeh (2000)):

$$A_{ij} = \sum_{e=1}^{NE_i} \int_{A^{(e)}} N_i^{(e)} R_f h\theta N_j^{(e)} dA \tag{3.90}$$

where NE_i are the number of elements within the region where the basis function N_i for node i is non-zero (element basis functions are defined in appendix D) and $A^{(e)}$ is the element area. With the exception of the advection term, the weighting functions are equivalent to the basis functions (this is referred to as the Petrov-Galerkin formulation).

The entries in the global "dispersion matrix" or "stiffness matrix" $[D]$ are given by (Yeh 2000)

$$D_{ij} = \sum_{e=1}^{NE_i} \int_{A^{(e)}} w_i^{(e)} \mathbf{Q} \cdot \nabla N_j^{(e)} - \sum_{e=1}^{NE_i} \int_{A^{(e)}} \nabla N_i^{(e)} h\theta \mathbf{D} \cdot \nabla N_j^{(e)} dA \tag{3.91}$$

where $w_i^{(e)}$ are the upstream weighting functions for node i, applied only to the advective terms and $\mathbf{Q}$ is the integrated discharge vector (in vector form). Three alternative FEM formulations for the upstream weighting terms were implemented in CARDINAL: (1) standard upstream weighting (defined by equation D.11 in appendix D), (2) streamline upwind weighting (defined by equation D.13), and (3) standard Galerkin weighting (where $w_i^{(e)}$=$N_i^{(e)}$).

The influence of distributed linear and point sink terms (the sink "load vector"), is expressed as

$$K_{ii} = \sum_{s=1}^{NS_i} \int_{L^{(s)}} N_i^{(s)} Q_X^- dX + Q_i^- \tag{3.92}$$

where Q_i^- is a point flux of water from the system at node i, NS_i is the number of element sides intersecting node i and Q_X^- [$\mathrm{L^2T^{-1}}$] is the distributed loss of water along element side s (of length $L^{(s)}$). These terms may be obtained directly from an analytic element flow solution, as shown later in section 3.6.3.

The influence of point, linear, and areal source terms (the source "load vector", $\{Q\}$) is given by

$$Q_i = \sum_{e=1}^{NE_i} \int_{A^{(e)}} N_i^{(e)} \left[N_t^+ c_t^+ + N_b^+ c_b^+ + q_s \right] dA + \sum_{s=1}^{NS_i} \int_{L^{(s)}} N_i^{(s)} Q_X^+ c_s^+ dX + Q_i^+ c_i^+ \tag{3.93}$$

where $q_s(x, y)$ is a distributed "dry" influx of mass per unit area [$\mathrm{MT^{-1}L^{-2}}$], Q_X^+ [$\mathrm{L^2T^{-1}}$] is the distributed gain of water with concentration c_s^+ along finite element side s (of length $L^{(s)}$), $N_b^+(x, y)$ and $N_b^+(x, y)$ are areal fluxes of water to the aquifer with concentrations of c_t^+ and c_b^+, respectively, and Q_i^+ is a point flux of water into the aquifer at node i with concentration c_i^+. These areal, linear distributed, and point source fluxes are also directly obtained from an analytic element flow solution as shown in section 3.6.3.

The $\{F\}$ vector is the "flux" vector and is used to handle specified flux boundary conditions and special flux conditions not explicitly associated with conventional sources and sinks and not typically used in traditional finite element methods (such special conditions are outlined later in section 3.7).

The above sparse system of equations, solved using a biconjugate gradient method based upon Press et al. (2002), may be modified to meet Dirichlet (specified concentration), Neumann (specified flux), or Dankwerts (mixed) conditions at nodes or along element sides. Most models are additionally subject to the "natural" boundary condition along the mesh boundary Γ:

$$\begin{aligned} -h\theta D_\eta \frac{\partial C}{\partial \eta} &= 0 \quad \text{if } Q_\eta < 0 \\ -\left(Q_\eta C - h\theta D_\eta \frac{\partial C}{\partial \eta} \right) &= 0 \quad \text{if } Q_\eta > 0 \end{aligned} \tag{3.94}$$

where η is the vector normal to the boundary. The first (outflux) condition of equation 3.94 ensures that there is no dispersive flux through outflow boundaries. This is equivalent to a zero concentration gradient across the boundary. The second (influx) condition of 3.94 ensures that there is no net flux of mass through inflow boundaries.

The primary revision to existing finite element approaches for solving the vertically-averaged transport equation (e.g., Yeh (2000)) is the use of an continuous AEM-based representation of flow parameters. By integrating continuous parameters ($\mathbf{V}$, $\mathbf{D}$, R_f, θ, h etc.) in the finite element residuals, the variation of these parameters on a sub-element scale is accounted for (something that standard FE methods do not do). Because the variation of these parameters within an element is known precisely, the residual expressions are evaluated to a higher degree of accuracy, without addition of nodes. In addition, the sink and source flux integrals of equations 3.92 and 3.93 may be evaluated to an arbitrary degree of precision using analytic element flow solutions, as shown in section 3.6.3.

The second revision to conventional finite element methods is the use of specialized "discontinuous" internal boundary conditions along certain analytic elements. These special physics-based flux conditions are enforced at sharp discontinuities in the dependent variable of vertically-averaged concentration, allowing for the influence of local scale features to be explicitly modeled without excessive overdiscretization. These approximate discontinuous boundary conditions are described in section 3.7.

3.6.2 Finite Element Discretization

Unlike with finite difference methods for flow modeling, finite element methods are not inherently mass conservative. Rather, they approach perfect global mass balance as the mesh resolution is

increased (Huyakorn and Pinder 1983; Yeh 2000). Likewise, local mass balance is not mathematically ensured, but is a likely byproduct of a successful global solution. The magnitude of this global and local mass balance error is directly related to the quality of the flow solution: the discretized AEM solution must satisfy the water balance ($\nabla \cdot \mathbf{Q}$=0) (Gresho and Sani 1998). Therefore, just as with FD methods, the manner in which the flow system is discretized is of paramount importance. In addition, the accuracy of the finite element method increases as the accuracy of the residual expression is improved. Such improvements may be attained by (1) increasing mesh resolution or (2) more accurately evaluating the residual integrals in the FE formulation of the transport method. When using a flow solution obtained from a finite element technique, these integrals are limited in accuracy by the quality of the flow solution. With the analytic element method, these integral expressions may be evaluated numerically (using standard Gaussian quadrature) to a high level of precision. In a few particular cases, they may be evaluated exactly.

The improved material and flux integral evaluation, directly attributed to the use of analytic element solutions, reduces the mesh resolution required to reach a specified level of solution accuracy. Ideally, this will enable the development of chemically complex models with fewer degrees of freedom, and therefore lesser computational cost. However, certain constraints on mesh geometry are required to ensure numerical stability of the solution. These constraints, which are dictated by the need to accurately calculate residual expressions, are as follows:

- Analytic elements may not intersect finite element sides. Fluxes from linesinks, wells, etc. are constrained to be distributed along finite element sides. This also ensures that discontinuities in saturated thickness, normal flux, or tangential flux do not occur within a finite elements interior.

- Analytic elements that enforce a sharp discontinuity in saturated thickness or normal flux that results necessarily in a discontinuity in vertically-averaged concentration require an internal "hole" in the mesh so that the discontinuity may be handled using special flux conditions or constraints (described in section 3.7).

- Sharp discontinuities in porosity and retardation factor must be located along finite element sides.

The reasons for these constraints are well founded. Analytic element models are vector-based: the underlying geometry is not based on a grid or mesh, by rather on polylines, polygons, points,

ellipses, and, in some cases, splines. The formulation of the method is such that all important discontinuities in the flow field occur along these boundaries. Important discontinuities include influx/outflux boundaries or spatial changes in conductivity, base, or thickness. Many parameters required for transport simulation (velocity, dispersion coefficients, saturated thickness, etc.) are derived from these flow parameters, and are therefore perfectly continuous between elements, but discontinuous across them. It is for this reason that the transport mesh must be discretized in a way such that finite elements are not intersected by analytic elements. By discretizing with this constraint, numerical or analytic integration of finite element residuals is more accurate (Gaussian integration of continuous functions is significantly more effective than that of discontinuous ones). In addition the specialized spatial discretization constraints outlined above, Peclet constraints (as described by Yeh (2000)) must still be met to ensure the accuracy of the numerical solution. Such constraints are independent of the particular style of flow solution used.

3.6.3 Finite Element Flux Discretization

As with finite difference methods, accurate translation of fluxes from an analytic representation to a discrete representation requires intelligent manipulation of information. In standard finite element methods for transport, fluxes of water are of three primary types:

1. Point fluxes, either those that occur at a node or within an element
2. Area fluxes, which are distributed over an entire element. Their influence is distributed to the three (or more) element nodes, and
3. Linear distributed fluxes, which are distributed over an element side. Their influence is distributed to the two nodes along that side.

Each of these three flux terms impacts the contaminant transport simulation and must therefore be properly identified and calculated.

Material fluxes are generally handled in finite element methods via a source/sink term added to the vertically-averaged ADR (equation 2.16). This flux is distributed to nodes of the finite element mesh and incorporated into the system of equations used to represent the governing equation (as shown in equations 3.92 and 3.93). The material flux term associated with each finite element node

i may be generally expressed as:

$$Q_i = \sum_{e=1}^{NE_i} \int_{A^{(e)}} N_i^{(e)}(x,y) q(x,y,t) dA \tag{3.95}$$

where NE_i is the number of elements adjacent to the node, $A^{(e)}$ is the area of each element, $N_i^{(e)}$ is the basis function within element e associated with node i (see appendix D for details), and $q(x,y,t)$ $[M/TL^2]$ is the spatially distributed mass flux per unit area. This spatially distributed flux term is a function of local concentrations (the dependent variable) for sinks, but generally independent of concentration for sources. Therefore, flux components show up on both the left and right hand side of the system of equations in 3.89.

For "dry" fluxes (mass added independently from the influx of water), the integral in equation 3.95 may be evaluated directly using Gaussian quadrature. For "wet" fluxes, which are linked to the analytic element method representation, a formal method for flux discretization is desirable. The following subsections discuss the evaluation of these "wet" fluxes for point features (wells), area features (e.g., contaminated recharge) and polylinear features.

Point Fluxes

The mesh generation constraints discussed earlier in this section requires that pumping wells (the only point flux dealt with here) are located at nodes of the mesh. Any material flux to or from the domain may be written as a component of the finite element flux vector:

$$Q_i = \begin{cases} Q_{well}\hat{C}_i & \text{if } Q_{well} < 0 \\ Q_{well}c_s^+ & \text{if } Q_{well} > 0 \end{cases} \tag{3.96}$$

where Q_{well} is the pumping rate of the well, $\hat{C}_i$ is the vertically-averaged concentration at the node, c_s^+ is the concentration of solute in the injected fluid, and F_i is an element of the FE material flux vector, defined as in (Istok 1989). This formulation is equivalent to that of standard finite element methods.

Area Fluxes

In the traditional 2-D finite element method for flow, areal fluxes (recharge or leakage) are often specified as piecewise constant on an element-by-element basis. However, the analytic element

method allows these fluxes to be represented in a continuous manner (e.g., multi-quadric basis functions (Strack and Janković 1999)). The contaminant flux due to an areal element may be distributed to the adjacent nodes via the following expression:

$$Q_i = \sum_{e=1}^{NE_i} \int_{A^{(e)}} N_i^{(e)} N^-(x,y) \hat{C}_i dA + \sum_{e=1}^{NE_i} \int_{A^{(e)}} N_i^{(e)} N^+(x,y) c_s^+ dA \tag{3.97}$$

These integrals are best evaluated using Gaussian quadrature. However, in domains with uniform source (recharge or leakage) concentration, the area integrals may be evaluated exactly (as shown in the finite difference analysis of section 3.3.2).

Linear Fluxes

Linear fluxes are those fluxes associated with linesinks. Such features are used to represent head-specified or flux boundaries in the analytic element method. Since these features are polylinear, they produce a concentrated flux per unit length along their boundaries, Q_X [$\mathrm{L^2T^{-1}}$], which may be an outflux from the aquifer (Q_X^-) or and influx to the aquifer (Q_X^+) with associated concentration linked to the feature c_s^+. These fluxes may be distributed to adjacent nodes via the following relationship:

$$Q_i = -\sum_{s=1}^{NS_i} \int_{L^{(s)}} N_i^{(s)} Q_X^- \hat{C} dX + \sum_{s=1}^{NS_i} \int_{L^{(s)}} N_i^{(s)} Q_X^+ c_s^+ dX \tag{3.98}$$

where NS_i is the number of sides (finite element edges) linked to node i, and $S^{(s)}$ is the side length. Neither Q_X^- nor Q_X^+ are defined along sides that are not along linesink borders. The effect of flux redistribution is shown in figure 3.15. Note that this formulation of linesink fluxes may be expanded to include other (elliptical or curvilinear) features that distribute concentrated fluxes of water to the domain.

3.6.4 Finite Element Material Integral Evaluation

The global matrices discussed in section 3.6.1 are usually assembled on an element-by-element basis. The contribution of node i to the residual within element e, $R_i^{(e)}$, for the vertically-averaged

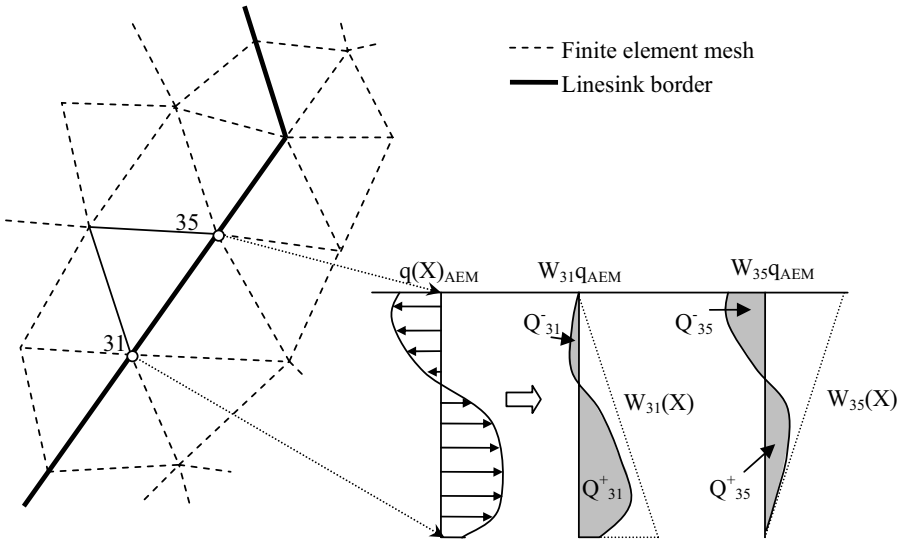

Figure 3.15: Fluxes from analytic elements are evaluated analytically along finite element sides. These fluxes are distributed to nodes using the same basis functions (N_i) as used for solution.

transport equation may be divided into the multiple integral terms and expressed as:

$$
\begin{aligned}
R_i^{(e)} = & \int_{A^{(e)}} -w_i^{(e)} \left[Q_x \frac{\partial \hat{C}^{(e)}}{\partial x} + Q_y \frac{\partial \hat{C}^{(e)}}{\partial y} \right] dA \\
& + \int_{A^{(e)}} N_i^{(e)} \left[h\theta D_{xx} \frac{\partial^2 \hat{C}^{(e)}}{\partial x^2} + h\theta D_{xy} \frac{\partial^2 \hat{C}^{(e)}}{\partial x \partial y} + h\theta D_{yy} \frac{\partial^2 \hat{C}^{(e)}}{\partial y^2} \right] dA \\
& + \int_{A^{(e)}} N_i^{(e)} \left[N_t^+ \left(c_t^+ - \hat{C}^{(e)} \right) + N_b^+ \left(c_b^+ - \hat{C}^{(e)} \right) \right] dA \\
& - \int_{A^{(e)}} N_i^{(e)} \left[R_f h\theta \frac{\partial \hat{C}^{(e)}}{\partial t} \right] dA
\end{aligned}
\tag{3.99}
$$

This may be written as a local system of equations (as in Istok (1989)) as:

$$
\begin{Bmatrix} R_1^{(e)} \\ \vdots \\ R_M^{(e)} \end{Bmatrix} = \left[D^{(e)} \right] \begin{Bmatrix} C_1 \\ \vdots \\ C_M \end{Bmatrix} - \left[K^{(e)} \right] \begin{Bmatrix} C_1 \\ \vdots \\ C_M \end{Bmatrix} + \left[Q^{(e)} \right] + \left[A^{(e)} \right] \begin{Bmatrix} \frac{\partial C_1}{\partial t} \\ \vdots \\ \frac{\partial C_M}{\partial t} \end{Bmatrix} \tag{3.100}
$$

where M is the number of nodes that define the element (3 for linear triangle elements) $\left[D^{(e)} \right]$ is the element dispersion matrix (composed of the first two terms on the RHS of equation 3.99, $\left[K^{(e)} \right]$ is the element sink load matrix, $\left[Q^{(e)} \right]$ is the element source load matrix, and $\left[A^{(e)} \right]$ is the element sorption matrix. Each of these is defined differently, and is closely related to the expression of the

global matrix. In fact, the global matrix may be assembled as a summation of individual element contributions, as shown by Istok (1989). This dissertation will only present means of evaluating the element dispersion matrix for linear triangle elements. Similar representations for more complicated finite element basis functions are available.

The element dispersion matrix is generically defined for linear triangular finite elements as:

$$\left[D^{(e)}\right] = \int_{A^{(e)}} \left[N'\right]^T \begin{bmatrix} h\theta D_{xx} & h\theta D_{xy} \\ h\theta D_{xy} & h\theta D_{yy} \end{bmatrix} \left[N'\right] + [w] \begin{bmatrix} Q_x & 0 \\ 0 & Q_y \end{bmatrix} \left[N'\right] dA \tag{3.101}$$

where

$$\left[N'\right] = \begin{bmatrix} \frac{\partial N_i^{(e)}}{\partial x} & \frac{\partial N_j^{(e)}}{\partial x} & \frac{\partial N_k^{(e)}}{\partial x} \\ \frac{\partial N_i^{(e)}}{\partial y} & \frac{\partial N_j^{(e)}}{\partial y} & \frac{\partial N_k^{(e)}}{\partial y} \end{bmatrix} \tag{3.102}$$

and

$$[w] = \begin{bmatrix} w_i^{(e)} & w_i^{(e)} \\ w_j^{(e)} & w_j^{(e)} \\ w_k^{(e)} & w_k^{(e)} \end{bmatrix} \tag{3.103}$$

Depending upon the functional form of the parameters (Q_x, D_{xx}, etc.), this residual will be evaluated in a different manner. Three cases, that of uniform (or averaged) parameterization within an element, linearly varying parameterization, or continuous parameterization are considered here. The three cases are shown in figure 3.16.

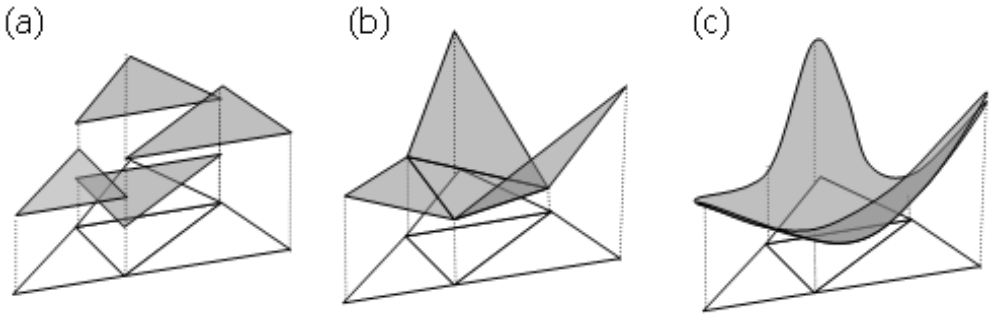

Figure 3.16: Three forms of parameterization for finite element integral evaluation. (a) Element-averaged parameters (b) Linearly-varying (nodal) parameters (c) Continuous parameters

3.6.4-A Element-averaged Parameters

In finite elements, independent parameters (e.g., velocity, dispersion coefficients) are generally assumed to be piecewise constant over the element. Often this is because the velocity is obtained from conventional FE flow models that solve for hydraulic head with linear basis functions, and calculate velocity as a byproduct of this solution. Assuming uniform parameter values and a weighting function $w_i^{(e)}$ equal to the basis function, the integrals in equation 3.101) may be obtained analytically, and the matrix is expressed as (Istok 1989):

$$\begin{aligned}\left[D^{(e)}\right] = &\frac{h\theta D_{xx}^{(e)}}{4A^{(e)}}\begin{bmatrix} b_i^2 & b_ib_j & b_ib_k \\ b_jb_i & b_j^2 & b_jb_k \\ b_kb_i & b_kb_j & b_k^2 \end{bmatrix} + \frac{h\theta D_{yy}^{(e)}}{4A^{(e)}}\begin{bmatrix} c_i^2 & c_ic_j & c_ic_k \\ c_jc_i & c_j^2 & c_jc_k \\ c_kc_i & c_kc_j & c_k^2 \end{bmatrix} + \\ &\frac{h\theta D_{xy}^{(e)}}{4A^{(e)}}\begin{bmatrix} b_ic_i & b_ic_j & b_ic_k \\ b_jc_i & b_jc_j & b_jc_k \\ b_kc_i & b_kc_j & b_kc_k \end{bmatrix} + \frac{h\theta D_{yx}^{(e)}}{4A^{(e)}}\begin{bmatrix} c_ib_i & c_ib_j & c_ib_k \\ c_jb_i & c_jb_j & c_jb_k \\ c_kb_i & c_kb_j & c_kb_k \end{bmatrix} + \\ &\frac{Q_x^{(e)}}{6}\begin{bmatrix} b_i & b_j & b_k \\ b_i & b_j & b_k \\ b_i & b_j & b_k \end{bmatrix} + \frac{Q_y^{(e)}}{6}\begin{bmatrix} c_i & c_j & c_k \\ c_i & c_j & c_k \\ c_i & c_j & c_k \end{bmatrix}\end{aligned} \tag{3.104}$$

where b_i and c_i are related to the spatial derivatives of the basis function, $b_i = 2A^{(e)}\frac{\partial N_i}{\partial x}$ and $c_i = 2A^{(e)}\frac{\partial N_i}{\partial y}$. Notice that in this particular formulation, the continuous parameters D_{ij}, and v_i^* are represented in a piecewise constant fashion by their average value over the element, $D_{ij}^{(e)}$ and $v_i^{(e)}$, respectively. This approach will be less accurate for regions with large variations of these properties. The following sub-section presents a formulation that allows these parameters to vary linearly across the element, using the same representation as the concentration field, $\hat{C}$.

3.6.4-B Linearly Graded Parameters

The averaging of $(h\theta D)^{(e)}$ and $v^{(e)}$ over a whole element is adequate for fine discretization, but can introduce some errors at coarser discretization when the parameters vary across the element. A better approximation (since these AEM-based parameters are changing over an element) to allow the parameters to vary across the element in a linear fashion. Note that the following derivation is not used elsewhere in the dissertation (because it does not allow for upstream weighting), but is

novel and closed-form, and thus a worthy contribution. With this formulation (once again assuming that the weighting function is equivalent to the basis function), our residual becomes:

$$R_i^{(e)} = -\int_{A^{(e)}} N_i \begin{bmatrix} \left(\sum_{j=1}^{3} N_j \left(h\theta D_{xx}\right)_j\right) \frac{\partial^2 \hat{C}^{(e)}}{\partial x^2} + \\ \left(2\sum_{j=1}^{3} N_j \left(h\theta D_{xy}\right)_j\right) \frac{\partial^2 \hat{C}^{(e)}}{\partial x \partial y} + \\ \left(\sum_{j=1}^{3} N_j \left(h\theta D_{yy}\right)_j\right) \frac{\partial^2 \hat{C}^{(e)}}{\partial y^2} \end{bmatrix} dA - \int_{A^{(e)}} N_i \begin{bmatrix} \left(\sum_{j=1}^{3} N_j \left(Q_x\right)_j\right) \frac{\partial \hat{C}^{(e)}}{\partial x} + \\ \left(\sum_{j=1}^{3} N_j \left(Q_y\right)_j\right) \frac{\partial \hat{C}^{(e)}}{\partial y} \end{bmatrix} dA \tag{3.105}$$

Using integration by parts,

$$\begin{aligned} -\int_{A^{(e)}} N_i \left[\left(\sum_{j=1}^{3} N_j \left(h\theta D_{xx}\right)_j\right) \frac{\partial^2 \hat{C}^{(e)}}{\partial x^2}\right] dA \\ = \int_{A^{(e)}} \frac{\partial N_i}{\partial x} \left[\left(\sum_{j=1}^{3} \frac{\partial N_j}{\partial x} \left(h\theta D_{xx}\right)_j\right) \frac{\partial \hat{C}^{(e)}}{\partial x}\right] dA \\ - \int_{S^{(e)}} N_i \left[\left(\sum_{j=1}^{3} N_j \left(h\theta D_{xx}\right)_j\right) \frac{\partial \hat{C}^{(e)}}{\partial x}\right] ds \end{aligned} \tag{3.106}$$

where S is the perimeter of the element. This last term is the dispersive flux into the element, which will be zero at system boundaries and is cancelled out along all internal element boundaries. The only time it needs to be evaluated is at specified flux (Neumann) boundaries. Similar expressions are available for the other dispersive terms in (3.105). Since

$$\frac{\partial \hat{C}^{(e)}}{\partial x} = \sum_{k=1}^{3} \frac{\partial N_k}{\partial x} \hat{C}_k \tag{3.107}$$

The new residual may be written as:

$$R_i^{(e)} = \sum_{j=1}^{3}\sum_{k=1}^{3} \hat{C}_k \int_{A^{(e)}} - \begin{bmatrix} \frac{\partial N_i}{\partial x}\frac{\partial N_j}{\partial x}\frac{\partial N_k}{\partial x} \left(h\theta D_{xx}\right)_j + \\ 2\frac{\partial N_i}{\partial x}\frac{\partial N_j}{\partial x}\frac{\partial N_k}{\partial y} \left(h\theta D_{xy}\right)_j + \\ \frac{\partial N_i}{\partial y}\frac{\partial N_j}{\partial y}\frac{\partial N_k}{\partial y} \left(h\theta D_{yy}\right)_j \end{bmatrix} - \begin{bmatrix} N_i N_j \frac{\partial N_k}{\partial x} \left(Q_x\right)_j + \\ N_i N_j \frac{\partial N_k}{\partial y} \left(Q_y\right)_j \end{bmatrix} dA \tag{3.108}$$

Using Linear finite elements, we may analytically evaluate these integrals using (D.5) and assemble our element dispersion matrix $[D^{(e)}]$:

$$\left[D^{(e)}\right] = -\frac{1}{8A^{(e)2}} \begin{bmatrix} D'^{(e)}_{11} & D'^{(e)}_{21} & D'^{(e)}_{31} \\ D'^{(e)}_{12} & D'^{(e)}_{22} & D'^{(e)}_{32} \\ D'^{(e)}_{13} & D'^{(e)}_{23} & D'^{(e)}_{33} \end{bmatrix} - \frac{1}{24} \begin{bmatrix} v'^{(e)}_{11} & v'^{(e)}_{21} & v'^{(e)}_{31} \\ v'^{(e)}_{12} & v'^{(e)}_{22} & v'^{(e)}_{32} \\ v'^{(e)}_{13} & v'^{(e)}_{23} & v'^{(e)}_{33} \end{bmatrix} \tag{3.109}$$

where

$$\begin{aligned} D'^{(e)}_{ik} &= \sum_{j=1}^{3} \left((h\theta D)_{xx_j} b_i b_j b_k + (h\theta D)_{xy_j} b_i b_j c_k + (h\theta D)_{xy_j} c_i c_j (c_k + b_k) \right) \\ v'^{(e)}_{ik} &= \sum_{j=1}^{3} \left(Q_{x_j} b_k \left(1 + \delta_{ij}\right) + Q_{y_j} c_k \left(1 + \delta_{ij}\right) \right) \end{aligned} \tag{3.110}$$

3.6.4-C Continuous Parameters

The two preceding subsections discussed how to obtain element dispersion matrices for the residual influence of node j on node i using (1) parameters that are constant in the element and (2) parameters that vary linearly within the element. Both assumed a fully Galerkin representation, where the weighting function was equivalent to the basis function. The first case is that most commonly used in linear finite element representations, because they are based upon groundwater flow models that provide piecewise-constant expressions for velocity within elements. The second case may be considered an expansion of the representation available from "mixed" finite element groundwater flow models (Chavent and Jaffre 1986). Within this dissertation however, we are primarily concerned with obtaining highly accurate residual expressions for parameters that vary continuously within elements. The following subsection describes the means for evaluating the terms of the *Petrov*-Galerkin element dispersion matrix using Gaussian integration.

We can write each term of the element dispersion matrix as (i=col,j=row):

$$D^{(e)}_{ij} = \int_{A^{(e)}} \begin{pmatrix} \frac{\partial N_j}{\partial x} \left[\left(h\theta D_{xx} \frac{\partial N_i}{\partial x} + h\theta D_{xy} \frac{\partial N_i}{\partial y} \right) \right] + \\ \frac{\partial N_j}{\partial y} \left[\left(h\theta D_{xx} \frac{\partial N_i}{\partial x} + h\theta D_{xy} \frac{\partial N_i}{\partial y} \right) \right] + \\ w_j \left[Q_x \frac{\partial N_i}{\partial x} + Q_y \frac{\partial N_i}{\partial y} \right] \end{pmatrix} dA \tag{3.111}$$

Defining the bracketed term in 3.111 as $F_{ij}(z)$, we may evaluate the terms using Gaussian quadra-

ture as:

$$D_{ij}^{(e)} = A^{(e)} \sum_{k=0}^{N} \omega_k F_{ij}(z_k) \tag{3.112}$$

where ω_k are the Gaussian weights and z_k are the Gauss points at which the values of v_x, v_y, $h\theta D_{xx}$, $h\theta D_{xy}$, $h\theta D_{yx}$, $h\theta D_{xy}$, w_i, w_j and w_k must be evaluated.

The benefit of the above approach is that loss of information from the continuous AEM flow model to the discrete transport model is minimized. The information loss that does occur is due solely to the order of the numerical integration scheme used, which may be improved to an arbitrary level of precision. Numerical error that occurs in the evaluation of the residual of the partial differential equation may only be ascribed to the mesh resolution and the functional form of the basis functions and weighting functions. Previously, evaluation of the residual was also subject to numerical discretization error within the flow solution. This method, as opposed to the element-averaged or linear parameter scheme is the preferred approach for analytic element-based transport modeling.

3.6.5 Mesh Generation

For the purposes of meeting the mesh constraints outlined in section 3.6.2, a robust two-dimensional unstructured triangular finite element mesh generator was developed within CARDINAL. The mesh generator is based upon previously developed automatic node placement algorithms (Frey 1987; Frey and Field 1991; Rebay 1993). Node locations and/or node spacing along system boundaries and internal boundaries (i.e., analytic elements) are specified, and a system-wide "spacing function" is interpolated between internal nodes as they are added to the mesh. Fig. 3.17 depicts the automated process of mesh delineation over an analytic element flow domain.

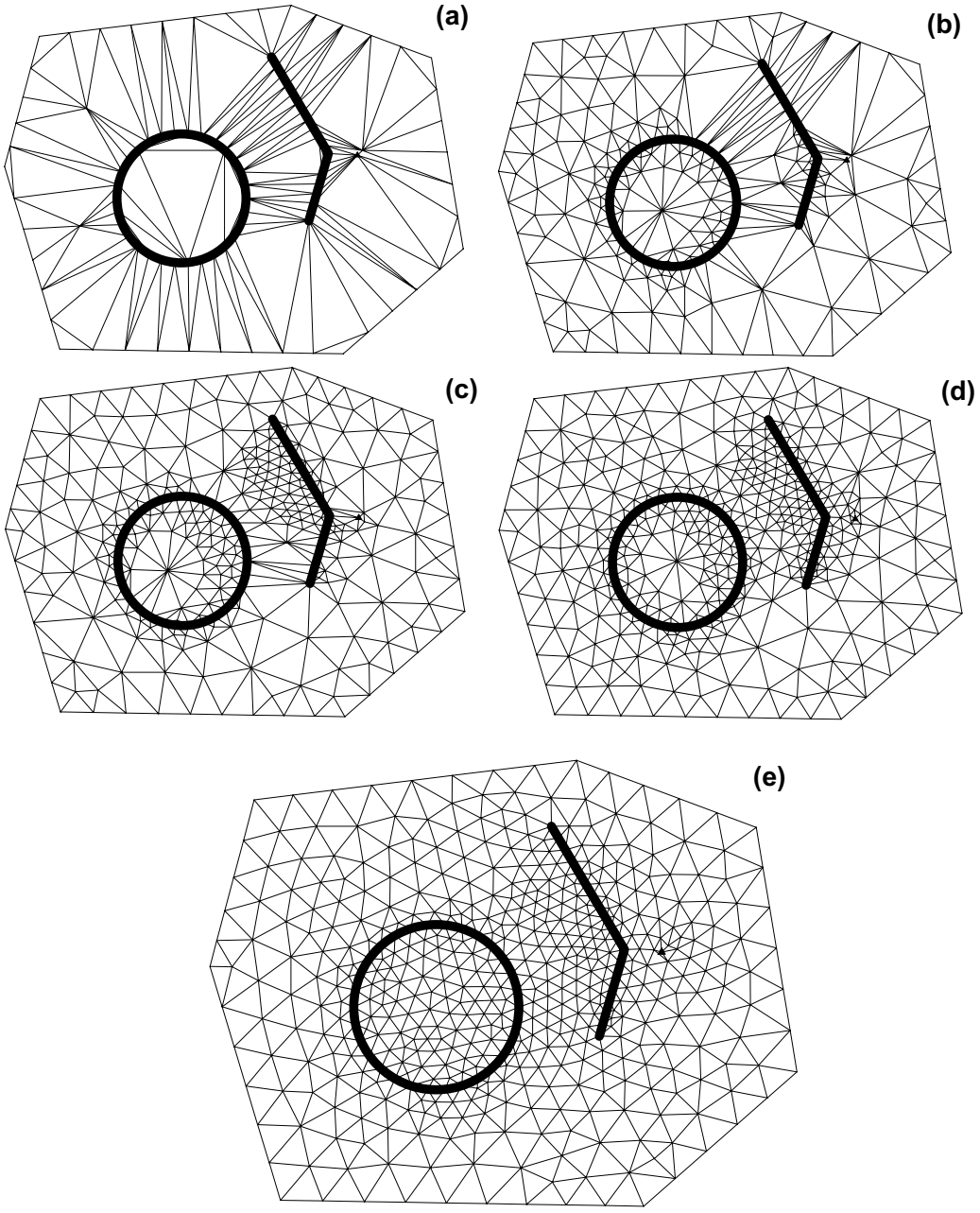

Figure 3.17: The automated mesh generation process as implemented in CARDINAL. The specified node spacings along the inhomogeneity (circle), leaky wall (polyline), well (triangle), and the boundary are 2.94m, 2.31m, 2.8m and 7m, respectively. (a)-(e) represent different stages of the generation process: (a) depicts the initial specified boundary spacing and triangulation (100 nodes). (b) the intermediate mesh with 200 nodes (c) with 300 nodes (d) with 400 nodes, and (e) the final mesh with 505 nodes after Laplacian smoothing and relaxation

The mesh generation process implemented in the CARDINAL library primarily echoes that of Rebay (1993). The basic process is as follows:

1. The geometry of external (domain) and internal (element) boundaries are specified by the modeler.

2. The spacing of boundary nodes along features is specified by the user (for the mesh generation in this dissertation, this specification process is automated through the graphical user interface to BLUEBIRD and CARDINAL, VISUAL BLUEBIRD (Craig and Matott 2004)). This results in a Delunay mesh of boundary nodes only.

3. The following sequence of events is repeated until the maximum number of nodes is reached or the mesh is fully populated with desirable elements:

    - The triangular elements are classified by their quality (judged by the angles of the triangle, the relative location of their circumcenter, and their side lengths with reference to the domain-wide spacing function).
    - New nodes are inserted in the "worst" triangular element. The details of the node insertion algorithm are outlined elsewhere (Watson 1981; Bowyer 1981; Rebay 1993).

4. The final mesh is relaxed and smoothed (Frey and Field 1991).

5. New connections along "special" element boundaries at important physical discontinuities are created (as discussed in section 3.7).

6. The ordering of mesh node indices is rearranged to obtain the optimal bandwidth of the resultant finite element matrix.

The preceding algorithm has been robustly implemented using complex arithmetic and fully optimized for rapid use with nearly any arbitrary configuration of analytic elements. The finite element meshes used for testing of the methods and algorithms for this dissertation were all generated using the above methods.

3.7 Discontinuous Concentration Conditions

In most cases, a finite element mesh linked to analytic element geometry will have a structure similar to that used for any traditional finite element method. However, particular difficulties (and opportunities) arise when analytic elements enforce flow boundary conditions that cause a discontinuity in the vertically-averaged concentration. This may occur where there is a discontinuity in the saturated thickness of the aquifer (the definition of vertically-averaged concentration changes) or a discontinuity in the normal component of flow (i.e., mass is lost from the aquifer to partially-penetrating surface water features).

Classical FEMs for flow problems model head as the dependent variable. Because of this, discontinuities in head (e.g., as found across a vertical barrier such as a slurry wall) are typically spread out along element sides, i.e., the head is interpolated from one node to the next, and the grid spacing dictates the gradient between. The accuracy of the flow model depends in part upon the spatial discretization near the feature. However, analytic elements will enforce a discontinuity in head over an infinitesimally small distance, with a singularity in the head gradient across the barrier (as shown in figure 3.18a). Head (and thus saturated thickness in unconfined aquifers) may be multi-valued at a node that lies along the barrier. Importantly, this requires that the dependent variable of vertically-averaged concentration is multi-valued along the barrier.

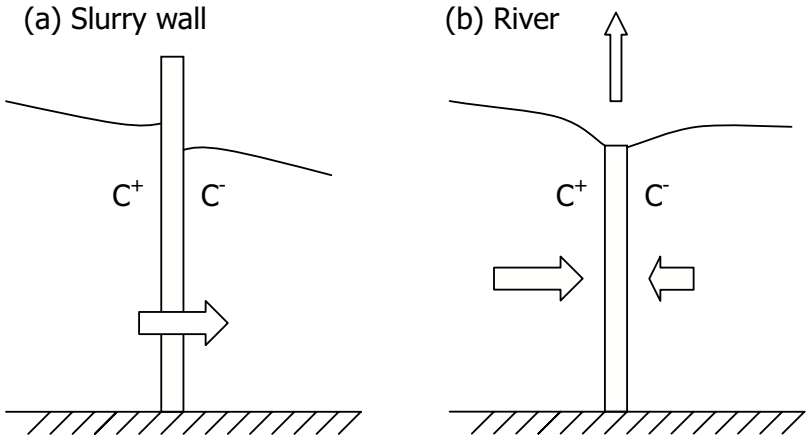

Figure 3.18: Discontinuous concentration conditions. (a) an infinitesimally thin inhomogeneity (slurry wall) enforces a discontinuity in saturated thickness across the inhomogeneity, which causes a discontinuity in vertically-averaged concentration. (b) a river removes all or part of the contaminant from the aquifer so that the concentration on one bank is different from that on the other bank.

A similar situation occurs with a fully penetrating river (figure 3.18b). In this case, the saturated

thickness is the same on both sides of the river, but the concentration is discontinuous because there is mass lost to the river. Solute may be present on one side of the river, but absent on the other.

These special cases of discontinuous vertically-averaged concentration may be modeled using an internal gap in the finite element mesh. Finite elements on either side of this gap cannot be mathematically connected in the typical manner, because they do not have shared nodes. The boundary condition along the border of this "hole" requires "coincident" nodes (nodes sharing the "same" mesh location) to communicate with each other without a shared element, as is typically done in FE methods. Flux conditions, equivalence conditions, or some other correspondence may be used to specify the functional form of the relationship between the concentration on either side of the discontinuity. While the approach is rather simple in concept, the author has found no published implementation similar to the one presented here.

Two revisions to the existing finite element formulation of section 3.6 are necessary to account for these local discontinuities in concentration. First, the automatic mesh generation algorithm must be able to introduce the discontinuities in the mesh. Additional coincident nodes and sides must be added, and the topological connections between elements, sides, and these new nodes must be properly revised and stored in memory. Second, flux- or concentration-based boundary conditions and constraints must be developed that maintain the appropriate physical relationship between the dependent variable of vertically-averaged aqueous concentration at the nodes on either side of the hydrogeologic feature. Possible conditions are here evaluated for thin, low-conductivity inhomogeneity elements (the "Leaky wall" condition), and for pseudo-partially-penetrating river elements. Both conditions naturally arise from AEM flow solutions. These discontinuous internal boundary conditions have been implemented in CARDINAL and are demonstrated in section 4.3.

Importantly, this approach allows for some scale-independence by removing the adjacency constraints associated with standard finite element models. For example, the mesh along an engineered barrier does not require elements on the same scale as the thickness of the barrier. Using AEM flow solutions facilitates the development of transport models that are not discretized based upon the smallest feature in the model.

NOTE: The boundary conditions and constraints discussed below are by no means the only possible means of handling the variety of discontinuous hydrogeologic conditions encountered in practice. Many of the simplifications needed for the following numerical formulations are only applicable in a subset of cases, and were primarily developed to (1) maintain the applicability of

the AEM-based FEM methods for domains that contain these problematic features, (2) provide results that avoid violating certain important behavioral constraints across the discontinuity, and (3) maintain global mass balance.

3.7.1 Mesh Splitting

As stated above, the first necessary step for handling discontinuous conditions in a finite element method linked to an analytic element flow solution is to reconfigure the mesh topology to account for coincident nodes. The initial phase of discontinuous mesh generation may proceed in the same manner as described in section 3.6.5 with a continuous mesh, as long as element sides are constrained to fall along the discontinuity boundary. In fact, any standard mesh generation algorithm may be used. This initial mesh (with only single-valued nodes along the discontinuity) is modified by (1) creating new nodes and finite element sides along the discontinuity and (2) reevaluating the connections between all nodes, elements, and sides linked to the discontinuous boundary. While conceptually simple, the details of implementing this procedure in a robust fashion are tedious.

Triangular finite element meshes must contain a significant amount of information. Along with information about the geometry of a mesh, topological information must also be preserved in an internal program structure or database. The connections between nodes, sides, and elements are as important (if not more important) than their location. Topologic information is here stored with the sides and the elements, using the nodes as reference. Elements are "aware of" their 3 adjacent sides, 3 corner nodes, and up to 3 adjacent elements. Sides are "aware of" their two end nodes, up to two adjacent elements, and up to 2 opposing nodes. This storage criteria is sufficient to completely explain the topology of a standard mesh. During the splitting procedure, this information must be reevaluated correctly. In addition, new topological information must be preserved (the connection between the nodes on either side of the discontinuity). Otherwise, the development of the finite element system of equations will be flawed.

The "Mesh-splitting" procedure may be decomposed into a single operation applied to one discontinuous node flanked by two discontinuous sides (henceforth a "wing"). This splitting operation is applied repeatedly until all multi-valued nodes have been created. If it is assumed that only a single discontinuity is allowed (i.e., the variable represented on the mesh may be double-valued at a location but not triple- or quadruple-valued), then there are only three geometric cases to consider. Firstly, the node may be flanked by two sides that have not yet been split (fig. 3.19a). The node

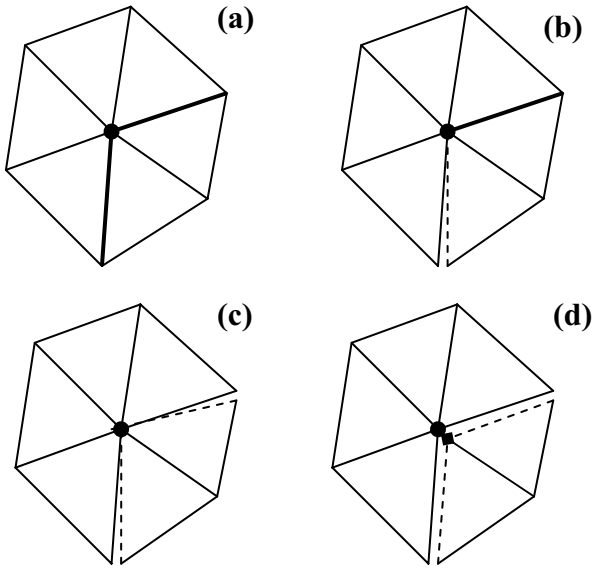

Figure 3.19: Wing-by-wing mesh splitting cases. (a) unsplit node flanked by unsplit sides (b) unsplit node flanked by one split side (c) unsplit node flanked by two split sides (d) resultant split node flanked by split side

may be flanked by two sides that have already been split (fig. 3.19c), or the node may be flanked by one split side and one unsplit side (fig. 3.19b).

The single wing mesh-splitting algorithm that corresponds to case (a) of figure 3.19 is shown in figure 3.20.

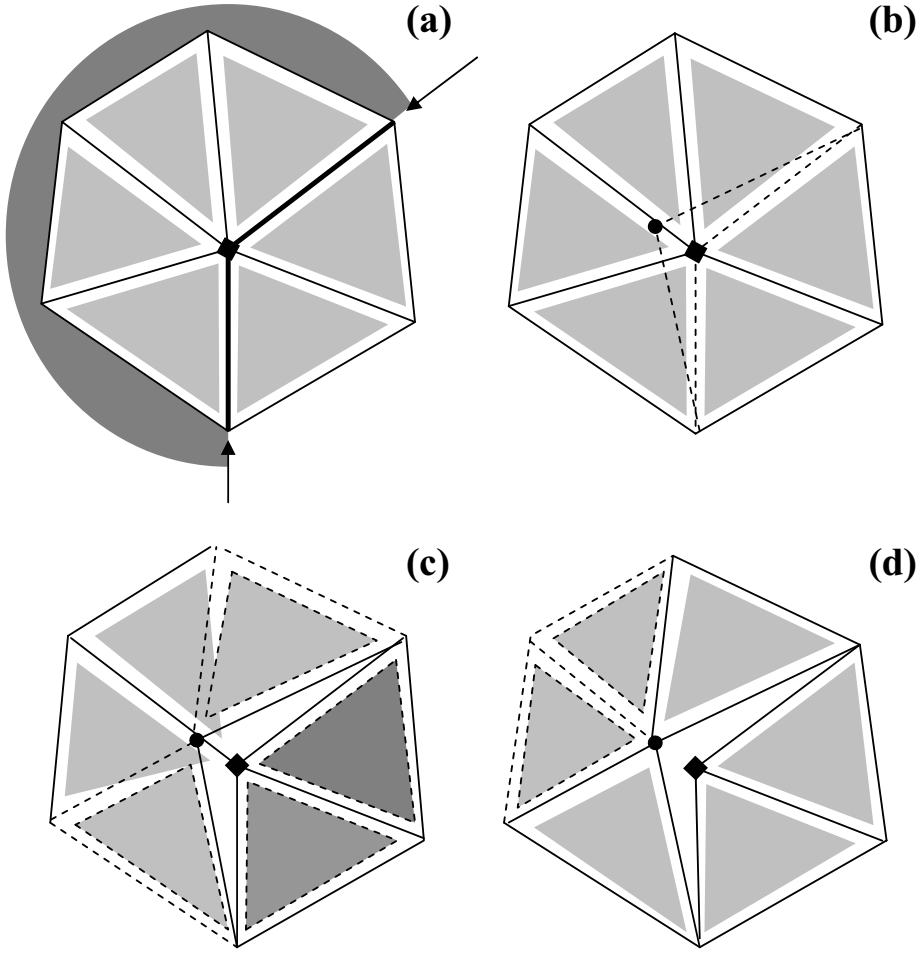

Figure 3.20: Mesh splitting procedure. The algorithm for mesh splitting may be simplified to the repeated splitting of the mesh along a "wing" (a node flanked by two sides). If neither side (shown in bold in (a)) has yet been split, the process operates as follows. (a) the "internal" area to the wing is identified (dark background circle). (b) The new sides and node are created as copies of the existing nodes and sides, with all references to formerly adjacent elements omitted. (c) The "internal" (lighter) and "external" (darker) elements adjacent to the split are updated, as are all sides associated with these internal elements. (d) Finally, all other elements are sifted through. If they are "internal" and associated with the old node, they are updated (as are their sides)

3.7.2 Leaky Wall Flux Conditions

A element commonly used in AEM that enforces a discontinuity in saturated thickness is the "Leaky Wall" element (Strack 1989), which represents a relatively thin inhomogeneity in hydraulic conductivity as a polyline or curvilinear shape. The normal flux, Q_η, across the barrier is known as a function of position along the element border, as are the saturated thicknesses on either side of the wall. There are multiple approaches available for modeling transport of solute across this boundary, of varying complexity.

The simplest manner in which to represent mass flux across the barrier is as a Dankwerts type boundary condition applied to either side of the barrier. With this approximate condition, the wall is assumed to store no mass, the concentration varies linearly across the wall, the flux across the barrier is both advective and dispersive, where the dispersive flux is determined by the single gradient across the wall. The flux across the barrier associated with nodes i^+ and i^- is given as:

$$F_i = \sum_{s=1}^{2} \int_{L^{(s)}} N_i \left[-Q_\eta C_i^+ + \bar{h}\bar{\theta} D_\eta^+ \frac{\partial \hat{C}}{\partial \eta} \right] dX \tag{3.113}$$

where $\partial \hat{C}/\partial \eta = (C_i^+ - C_i^-)/b_w$, b_w is the thickness of the wall, and two finite element sides (s=1; s=2) are along the wall adjacent to node i. This flux condition connects the behavior of two "coincident" nodes on either side of the infinitely thin wall. Neither continuity of concentration or continuity of vertically-averaged concentration are required along such a boundary. However, inherent in this formulation is the continuity of mass flux across the wall; what enters the wall through one side leaves through the other side. No mass is stored within the wall itself, and the gradient of concentration across the wall is assumed to be an adequate representation of the average gradient within the wall. These assumptions are invalid if the wall is sufficiently thick or if transport is dominated by diffusion, as is often the case for engineered slurry walls. However, for preliminary transport investigations, this approximation may adequately capture the behavior of a plume. Also, with this particular formulation, the wall meets the zero mass flux condition in the limiting case where the barrier is impermeable.

A more sophisticated approach to handling the slurry wall condition, likely more accurate for diffusion-dominated transport prevalent in barrier systems, is to allow the wall to retain mass, and explicitly model the transport behavior within the wall using a separate 1-dimensional model. The fluxes from the external model could act as boundary conditions to the model of the wall and

vice versa. Because transport within the wall occurs on a much longer timescale than transport outside of the wall, this process may be decoupled via operator-splitting, and the flux boundary conditions for the internal transport model may be obtained from the concentrations upgradient and downgradient of the barrier. This more sophisticated numerical approach has not been implemented in CARDINAL, and remains an open research problem.

3.7.3 Transport Beneath a Pseudo-Partially Penetrating River

The final discontinuous condition considered here is that of vertically-averaged contaminant transport beneath a river. Note that river conditions in the 2D AEM are typically assumed to be fully penetrating. However, the same boundary conditions used to model a fully-penetrating river are roughly valid for partially penetrating rivers where the head below the river is assumed uniform and the vertical flux directly beneath the river is negligible. For transport models, this description of the river condition (in the flow model) may be more apt for realistic simulation of the actual mass transfer processes occurring (even if the exact vertical distribution of mass and water flux to the river is not explicitly represented by the flow model).

For a partially-penetrating river (as shown in figure 3.21), the concentration is discontinuous at the river boundary because some percentage of the mass upgradient of the river is lost from the aquifer system to the river itself. Typically, with the Dupuit-Forcheimer approximation, a river will remove all of the water moving towards it (because the 2-dimensional hydraulic gradient "points" towards the river on both banks). This "strong extraction" condition is well-treated using typical specified mass flux conditions in the transport model (as derived in section 3.6.3), and no discontinuity has to be explicitly modeled. If modeled with a mass flux condition, the concentration at a node along the strongly extracting river roughly represents the concentration on the upstream bank of the river. The same is true for a river that loses water to the aquifer at a sufficient rate that the hydraulic gradient points away from the river on both banks (a "strong injection" condition). However, if the hydraulic gradient is towards the river on one side and away from the river on the other (as in figure 3.21), some of the aquifer water (and the solute contained within) moves either (a) into the river and subsequently out of the river (for a fully-penetrating river) or (b) underneath the river (partially-penetrating conditions).

For the fully penetrating conditions, all of the mass removed by the river is assumed lost to the river. In actuality, this mass would be tranported downstream, and without conjunctive surface

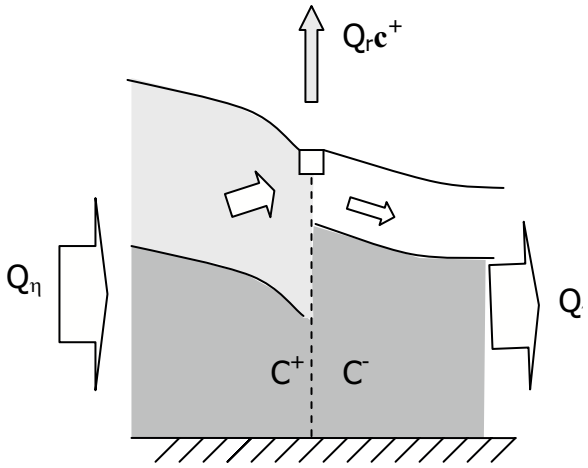

Figure 3.21: Discontinuous Condition: Partially Penetrating River

water/ground water transport simulation (beyond the scope of this dissertation), simulating this transport phenomenon is impossible. For the pseudo-partially penetrating conditions, a discontinuous vertically-averaged concentration condition occurs, and mass flux conditions may be developed to couple the concentrations at the nodes on either side of the river.

To appropriately model this discontinuous condition within the confines of the Dupuit-Forcheimer approximation, certain assumptions are made about the vertical distribution of flux to the river. As shown in figure 3.21, it is assumed that only the upper portion of the saturated thickness is extracted by the river, and the percentage of the saturated thickness removed is directly proportional to the jump in integrated discharge across the river. The water (and solute) in the lower part of the saturated thickness is assumed to move underneath the river. Thus the mass flux from one side of the river to the other may be calculated as:

$$F_i = \sum_{s=1}^{2} \int_{L^{(s)}} N_i \left[-(Q_\eta - Q_X) C_i^+ + h\theta D_\eta^+ \frac{\partial \hat{C}}{\partial \eta} \right] dX \tag{3.114}$$

Where Q_η [L^2T^{-1}] is the normal integrated discharge towards the river, and Q_X [L^2T^{-1}] is the volumetric flux of water to the river per unit length of the river. The dispersion across the boundary is controlled by the concentration gradient across the stream. This may approximated by knowing the width of the river as:

$$\frac{\partial \hat{C}}{\partial \eta} = \frac{C_i^- - C_i^+}{w_r} \tag{3.115}$$

Where w_r is the width of the river. Alternatively, if the down gradient vertical concentration distribution is assumed skewed such that the (non-vertically-averaged) concentrations are equivalent on both sides of the river, a zero-gradient condition may also be enforced such that dispersive flux is negligible beneath the river in comparison to advective flux. Neither of these approximations of the flux beneath the river are exact (many assumptions were necessary to obtain their formulations). However, for regional scale transport simulations not dominated by these features, this approximation may prove adequate.

Note that if the effect of the river is modeled in this manner, the flux conditions derived for a sink or source along a linear element in section 3.6.3 are no longer used. However, mass is still lost to the surface water feature, and this lost mass must be explicitly accounted for in the mass balance calculation.

3.8 Modular and Adaptive Reactive Transport Modeling

3.8.1 Object-Oriented Reaction Library

As was discussed in section 3.1, the use of object-orientation simplifies the process of adding and testing new algorithms and model features. In CARDINAL, one of the most powerful benefits of object-orientation is the ability to easily develop and incorporate new reaction types. Since the use of operator-splitting allows all reactions to be handled in batch mode (without reference to spatial location), each reaction process is fully defined by the time step of the reaction calculation, the initial sorbed and aqueous species concentrations, relevant chemical properties of the species or components in the reaction, and relevant properties (including the porosity, bulk density, and chemical properties) of the soil type in which the reaction occurs. By making all other information about the aquifer invisible to the reaction process, non-linear/linear and kinetic/equilibrium reactions may be connected to the overall reactive transport algorithm with equal ease. In addition, different isotherm types (for modeling non-competitive equilibrium sorption) may be implemented as subsets of the class CIsotherm.

At the time of this writing, four types of equilibrium sorption have been implemented in CARDINAL: a general cation exchange class (details in appendix G), and three types of single-solute isotherm (linear, Langmuir, and Freundlich). Sequential parent-daugther first-order decay reactions have also been implemented (based upon the solution of Sun et al. (1999)), but testing is ongoing and this type of reaction is not discussed in this dissertation.

3.8.2 Adaptive Enabling of Reactions

For transport problems characterized by complex reactions, the primary computational cost is often the cost of solving the reaction equations for each node of the grid or mesh at each time step. The time step constraints for reactive transport are a function of the speed of the reaction in relation to the speed of transport and the simulation period is likely a function of the application of interest. Thus, the total number of time steps is generally fixed by a combination of Courant constraints and the needs of the modeler. The Courant constraints may be somewhat relaxed by using a lower-resolution grid or mesh (this is facilitated via use of AEM solutions). However, Peclet constraints (for Eulerian methods) may require higher resolution. An alternative is to allow for adaptive enabling of reactions in which the reactive portion of the transport problem is solved only

when it is important to do so. This approach reduces the size of the transport problem.

Multiple methods of adaptive enabling have been conceived, all of which fall under two general categories:

Spatial Adaptivity

- Vary reaction applicability by soil zone. Reactions can be enabled or disabled based upon soil type.
- User-specified. The user may specify areas of reaction applicability that are consistent with their observations of the system (i.e., the effects of a given reaction may have little importance downgradient of a remediation process).

Model-Constrained Adaptivity

- Vary reaction applicability based upon the magnitude of concentration. Oftentimes, reactions only occur at a non-negligible rate if there is a significant amount of catalyst or a small concentration of reaction-inhibiting solute. For instance, redox reactions may require anaerobic conditions, and reactions may only have a significant impact upon results if the modeled concentration of oxygen is below a certain threshold.
- Vary reaction applicability based upon flow velocity. In some classes of kinetic sorption reactions, the aqueous phase may be assumed to be at equilibrium if given a sufficient amount of contact time. Therefore, a sorption reaction may be treated as an equilibrium reaction in stagnation zones, and a kinetic reaction in faster moving areas. This is a conceptual advantage of the approach and not covered within this dissertation.

The first three of these enabling constraints have been implemented in CARDINAL, and are simple to implement in any reactive transport code.

Chapter 4

Numerical Testing

The following chapter discusses the demonstration and numerical testing of the new AEM-based algorithms for solving the vertically-averaged advective-dispersive-reactive equation.

All of the methods discussed in chapter 3 are unique in their use of analytic element flow solutions, and were checked for accuracy against existing analytic and numerical solutions to the vertically-averaged transport equation. Once the general accuracy of each algorithms was confirmed, differences between using analytic element versus using discrete solutions as a source of flow information were evaluated and analyzed. Test cases were used to investigate the effectiveness of the multi-scale approach for handling discontinuous conditions of section 3.7 and the effective parameter random walk method of 3.5.4. Lastly, the finite element implementation of the new AEM-based approach was used to demonstrate the ability of the new method to effectively simulate field-scale reactive transport through an engineered barrier.

The primary contribution of this dissertation is the development and implementation of new numerical methods, rather than the analysis of contaminant transport phenomena. Therefore, the particular results of the following simulations are deemed less important than are the robustness, stability, speed, and accuracy of the numerical solution.

4.1 Comparison with Analytic and Numerical Solutions

This section describes various benchmark tests used to assess the accuracy of the transport simulators included in the CARDINAL software libraries. The BLUEBIRD flow model has previously been repeatedly tested against the numerical code SPLIT (Janković 2003) and, to a lesser extent, MODFLOW (McDonald and Harbaugh 1988). The results of these tests are not discussed here.

4.1.1 Benchmark Test 1: Cleary and Ungs Solution

To confirm the accuracy of the finite element, finite difference, and BMOC implementation in CARDINAL, numerical solutions were first compared to an analytic solution for two-dimensional transport in uniform flow with a constant concentration source. An exact solution, developed by Cleary and Ungs (1978) provides a closed-form expression for transport of an inert solute in a homogeneous, semi-infinite domain with unidirectional flow and a constant concentration source of length $2a$ located along the y-axis in the region $-a = y = a$. The boundary conditions meet specified conditions along the y-axis and zero-gradient conditions at infinity. The concentration is expressed explicitly as a function of time and position (Ségol 1994):

$$\begin{aligned} C(x,y,t) =& \frac{C_0 x}{4(\pi D_x)^{0.5}} exp\left(\frac{v_x x}{2D_x}\right) \\ & \int_0^{t/R_f} \exp\left[\frac{v_x^2}{4D_x}\tau - \frac{x^2}{4D_x\tau}\right]\tau^{-\frac{3}{2}}\cdot \\ & \left(\operatorname{erf}\left[\frac{a-y}{2(D_y\tau)^{0.5}} + \frac{v_y}{2}\left(\frac{\tau}{D_y}\right)^{0.5}\right] + \operatorname{erf}\left[\frac{a+y}{2(D_y\tau)^{0.5}} + \frac{v_y}{2}\left(\frac{\tau}{D_y}\right)^{0.5}\right]\right) d\tau \end{aligned} \tag{4.1}$$

The analytical scheme was simulated with C_0=100 mg/L, v_x=1.0 m/d, v_y=0.0 m/d, α_l=5 m, α_t=0.5 m, and a=10.0 with the analytic solution coordinate system having its origin at x=0, y=50. Numerical solutions were then obtained and compared to the analytic solution. The numerical simulations were performed using a grid Peclet number ($v\Delta x/D$) of 0.2 (FD) or a mesh Peclet number of 0.354 (FE) and a grid/mesh Courant number ($v\Delta t/\Delta x$) of 0.1. The concentration contours for the analytic and numerical solutions at t=50 d are shown in figure 4.1.1. It is important to note that this test case (and that of the following analytic benchmark test) are simulated using the simplest formulation of the vertically-averaged transport equation, with constant dispersion

coefficients, porosity, saturated thickness, and velocity. Hence, the accurate evaluation of effective velocities, the effects of spatial gradation in parameters, or cross-dispersion terms are not demonstrated by this test case. However, the simulations demonstrate the ability of finite difference, finite element, and BMOC algorithms to properly simulate advection, longitudinal dispersion, and transverse dispersion. This particular test case also demonstrates that Dirichlet (constant concentration) conditions have been correctly implemented in CARDINAL, and that both implicit and explicit systems of equations have been correctly developed.

As can be seen in figure 4.1.1, the analytic and numerical solutions are visually equivalent for the test problem. Additional testing (not shown here) confirms that increasing grid/mesh resolution reduces any discrepancies between analytic and numerical solutions. Table 4.1 and figure 4.1.1 depict the difference between the analytic and numerical simulations for six different transport algorithms and spatial weighting schemes. The root mean squared error (RMS) and median concentration are evaluated on a 100 x 100 grid of points covering the problem domain ($0 < x < 100; 0 < y < 100$) at t=50, as are the maximum concentration and median concentration. The mass balance error for each algorithm is evaluated as discussed in section 3.2.

Table 4.1: Comparison of numerical and analytic solutions to Cleary and Ungs benchmark problem

Algorithm	spatial weighting	RMS error t=50	Median Conc. t=50	MB Error t=50
AN	N/A	0.0	0.1096	0.000%
FD	UW	4.3E-5	0.1196	0.000%
FD	CW	0.0664	0.1125	0.000%
FD BMOC	N/A	0.1451	0.1183	-0.332%
FE	UW	0.2018	0.1955	-0.001%
FE	CW	0.1410	0.1834	-0.000%
FE BMOC	N/A	0.2514	0.3409	-0.782%

FD=Finite difference; FE=Finite Element; UW=Upstream weighting; CW=Central weighting; CN=Crank-Nicholson; BMOC=Backward method of characteristics; *Note: some portion of the errors in the finite element method are due to the inability to match the geometry of the initial concentration distribution near the source.

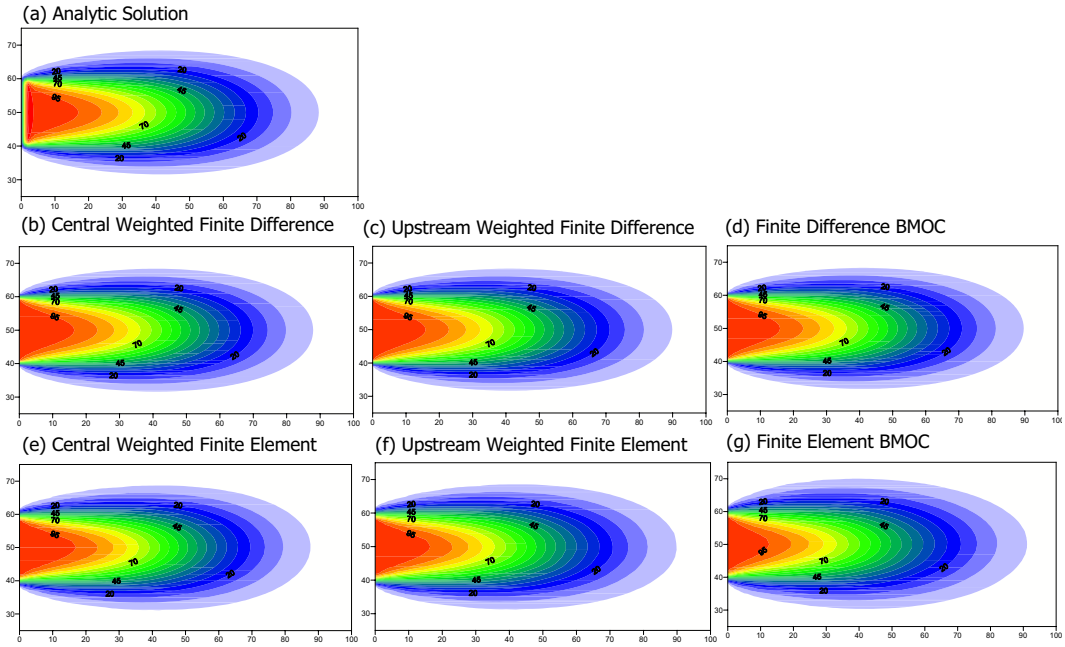

Figure 4.1: Comparison of concentration profiles for the Cleary and Ungs analytic solution at t=50 (v_x=1.0; v_y=0.0; α_l=5; α_t=0.5) with CARDINAL transport schemes. (a) analytic solution; (b,c, and d) Crank-Nicholson finite difference simulation with Δx=Δy=1.0, and Δt=0.1; (e,f, and g) Crank-Nicholson finite element simulation with a representative mesh spacing of 1.77, and Δt=0.177.

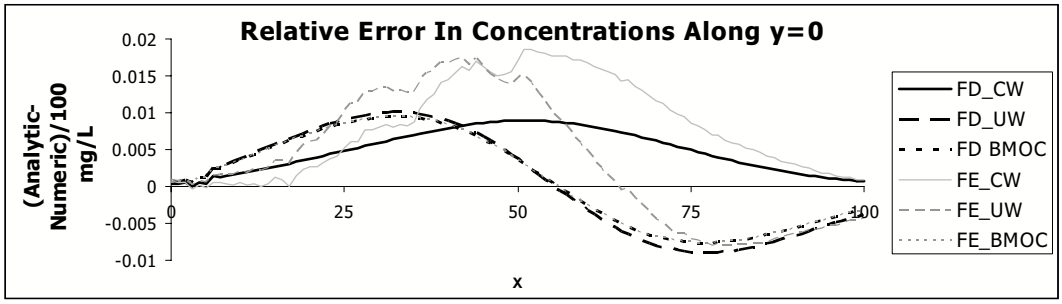

Figure 4.2: The spatial distribution of numerical solution errors for the Cleary and Ungs analytic solution with CARDINAL transport schemes. Errors are evaluated as the difference between the analytic and numerical solutions normalized by the source concentration (100 mg/L). As expected, the upstream weighted and backwards method of characteristics techniques introduce numerical dispersion (exhibited by the sinusoidal error distribution about the front of the plume.

4.1.2 Benchmark Test 2: Hunt Solution

In addition to the constant concentration source simulated in the previous section, analytical solutions developed by Hunt (Hunt 1978) are used to verify the accuracy of the CARDINAL transport model for a homogeneous, semi-infinite domain with unidirectional flow and a initial point source located at the origin. Zero concentration gradient boundary conditions are applied at an infinite distance from the point source. The solution is given as (Ségol 1994):

$$C(x,y,t) = \frac{Mexp\left[-\frac{(x-v_x t)^2}{4D_{xx}t} - \frac{y^2}{4D_{yy}t}\right]}{4\pi\theta t(D_{xx}D_{yy})^{0.5}} \tag{4.2}$$

where M is the initial mass at the origin. The analytical scheme was simulated with v_x=1.0, v_y=0.0, D_x=5, D_y=0.5, and an initial point source with a mass of 5 kg centered at x=0, y=50. The Peclet and Courant numbers for the finite difference simulations are 0.2 and 0.5, respectively. Peclet and Courant numbers for the finite element simulations (on a coarser mesh) are 0.66 and 0.152, respectively. The concentration contours for the solution at t=50 are shown in figure 4.3.

Table 4.2: Comparison of numerical and analytic solutions to Hunt point source benchmark problem

Algorithm	spatial weighting	RMS error t=50	Maximum Conc. t=50	MB Error t=50
AN	N/A	0.0	7.1169	0.000%
FD	UW	0.0690	6.8149	0.001%
FD	CW	0.0026	7.1273	0.000%
FD BMOC	N/A	0.0624	6.8446	0.000%
FE	UW	0.1116	6.6196	0.004%
FE	CW	0.0438	7.0593	0.002%
FE BMOC	N/A	0.0451	6.5388	-6.879%

FD=Finite difference; FE=Finite Element; UW=Upstream weighting; CW=Central weighting; CN=Crank-Nicholson; BMOC=Backward method of characteristics; *Note: part of the errors in the finite element method are due to the inability to match the geometry of the concentration distribution near the point source at early time periods.

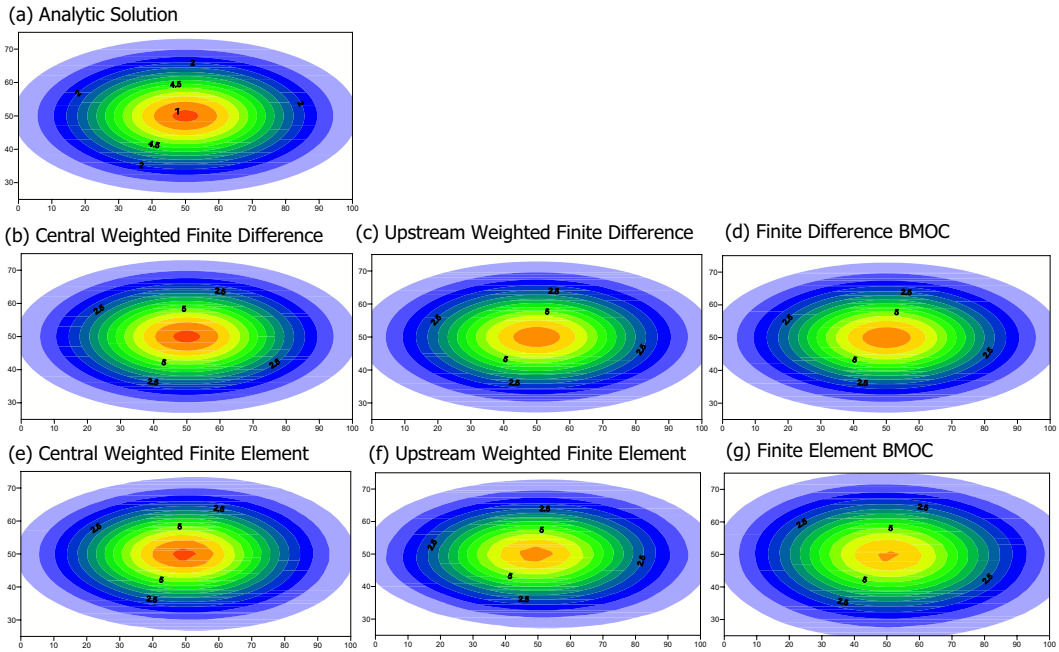

Figure 4.3: Comparison of concentration profiles for the Hunt point source analytic solution (v_x=1.0; v_y=0.0; α_l=5; α_t=1.0) simulated using CARDINAL transport algorithms. (a) analytic solution; (b,c, and d) Crank-Nicholson finite difference simulation with Δx=Δy=1.0, and Δt=0.5; (e,f, and g) Crank-Nicholson finite element simulation with a representative mesh spacing of 1.77, and Δt=0.5.

4.1.3 Benchmark Test 3: MT3DMS Comparison

The numerical model MT3DMS (Zheng and Wang 1999) is a finite difference-based simulator for three-dimensional contaminant transport. It has the capacity to solve vertically-averaged transport systems that are more complex than analytic solutions, and is here used to demonstrate that the methods used in CARDINAL are (at least) equally effective for solving the advection dispersion equation with a spatially variable velocity field, dispersion cross-terms, and non-uniform saturated thickness. Since MT3DMS has been tested against a large set of analytic solutions, this test case is considered a robust assessment of the CARDINAL transport schemes and their ability to solve problems in complex flow fields.

The configuration of the flow system for the transport test case is depicted in figure 4.4. The 1000 m by 1000 m system is defined by no-flow boundaries to the north and south, constant head boundaries of 30 m to the west and 10 m to the east, a set of square inhomogeneities with hydraulic conductivities of 0.01 m/d and 10 m/d, and a pumping well with a volumetric flow rate of -5.0 m^3/d (extraction) as shown in the figure. The background porosity is 0.3 and background conductivity is 0.1 m/d. The flow and transport system are simulated for both confined and unconfined flow. For the confined configuration, an aquifer thickness of 10 m is used. For the unconfined configuration, the flow model calculates an average saturated thickness of 20m across the domain, decreasing from west to east. The orthogonal geometry and property values for this test case were chosen because they may be simulated equally effectively using finite difference methods and the analytic element method. More complicated geometry, higher contrasts in conductivity, and mixed confined/unconfined aquifer systems may be better simulated using AEM-based transport simulators. However, the equivalence of the AEM-based and FD-based transport algorithms would be obscured in such systems due to differences in the flow solution. For the analytic element representation of the system, head-specified linesinks were used to represent the east and west boundaries, "leaky wall" (doublet) elements were used to represent the no-flow boundaries, and inhomogeneity (doublet) elements were used to represent the inhomogeneities. High order elements (Janković and Barnes 1999a) with order=10 are used in all cases. For the finite difference simulation, the flow system was defined on a 1020 m x 1020 m grid using MODFLOW, so that the no-flow and head-specified boundary conditions are applied at the borders of the flow domain, and the two flow solutions are conceptually equivalent. However, only the 1000 m by 1000 m interior of the grid is used for transport.

The transport simulations were performed using three different grid resolutions and multiple transport algorithms (both CARDINAL and MT3DMS) for four test configurations. The four test configurations are distinguished by the use of confined or unconfined flow and two different ratios of transverse to longitudinal dispersivity (α_t/α_l=0.3 and α_t/α_l=0.01). The longitudinal dispersivity was held constant at 10 m. A rectangular source zone with a concentration of 100 mg/L was placed upstream of the system center and transported over a time period of 63000 days (172.5 years). The plume configuration from both MT3DMS and CARDINAL solutions at t=63000 days are shown in figures 4.5, 4.6, 4.7, and 4.8.

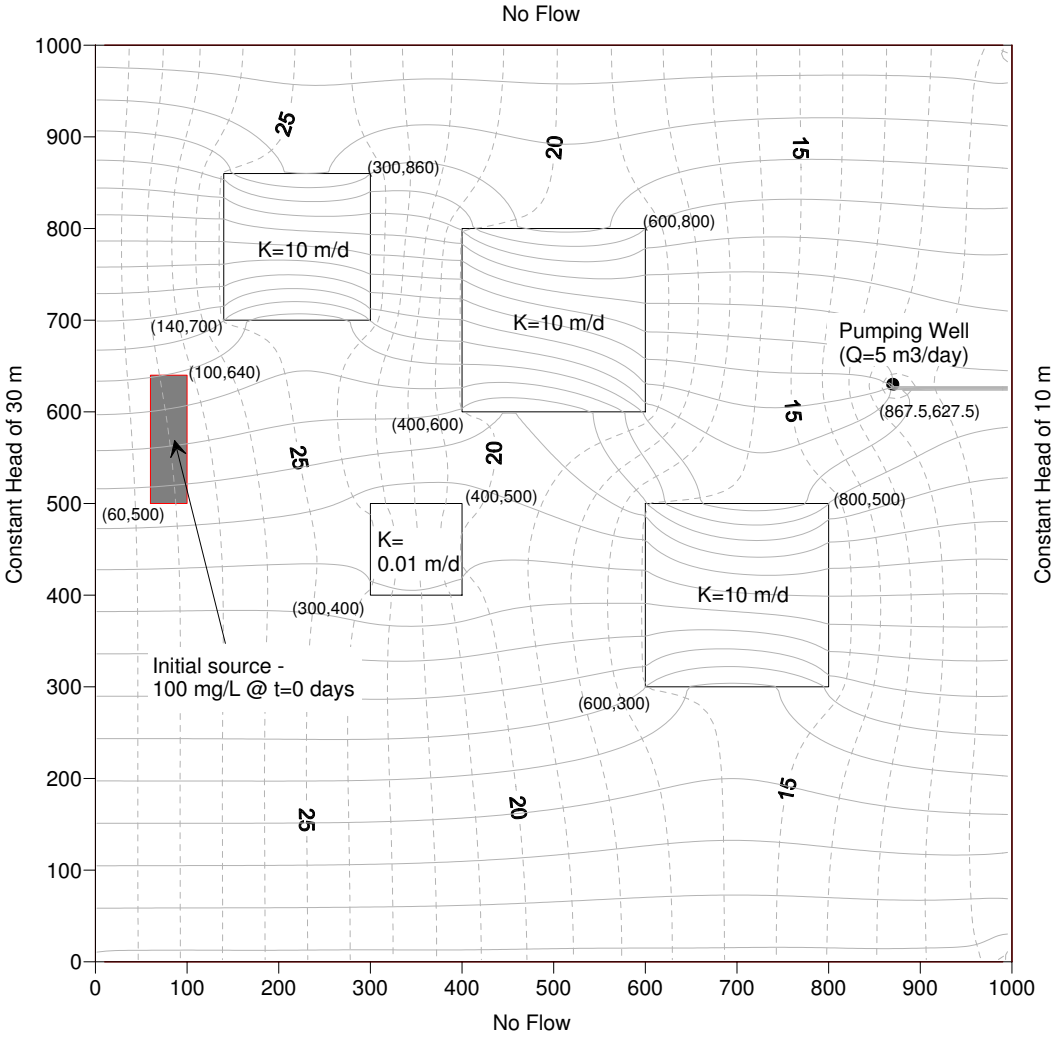

Figure 4.4: Test case setup for benchmarking against MT3DMS. The 1000 m x 1000 m system is characterized by flow from left to right through a set of square inhomogeneities oriented with the finite difference grid. The background conductivity is 0.1 m/d, and the inhomogeneity conductivities are either 10 m/d or 0.01 m/d, as depicted in the figure. The uniform aquifer porosity is 0.3. A source zone with initial concentrations of 100 mg/L is located to the left of the inhomogeneities. Average velocity in the domain is 0.0667 m/d. For the confined test case, the aquifer thickness is 10 m. The equipotential contours for the confined case are shown.

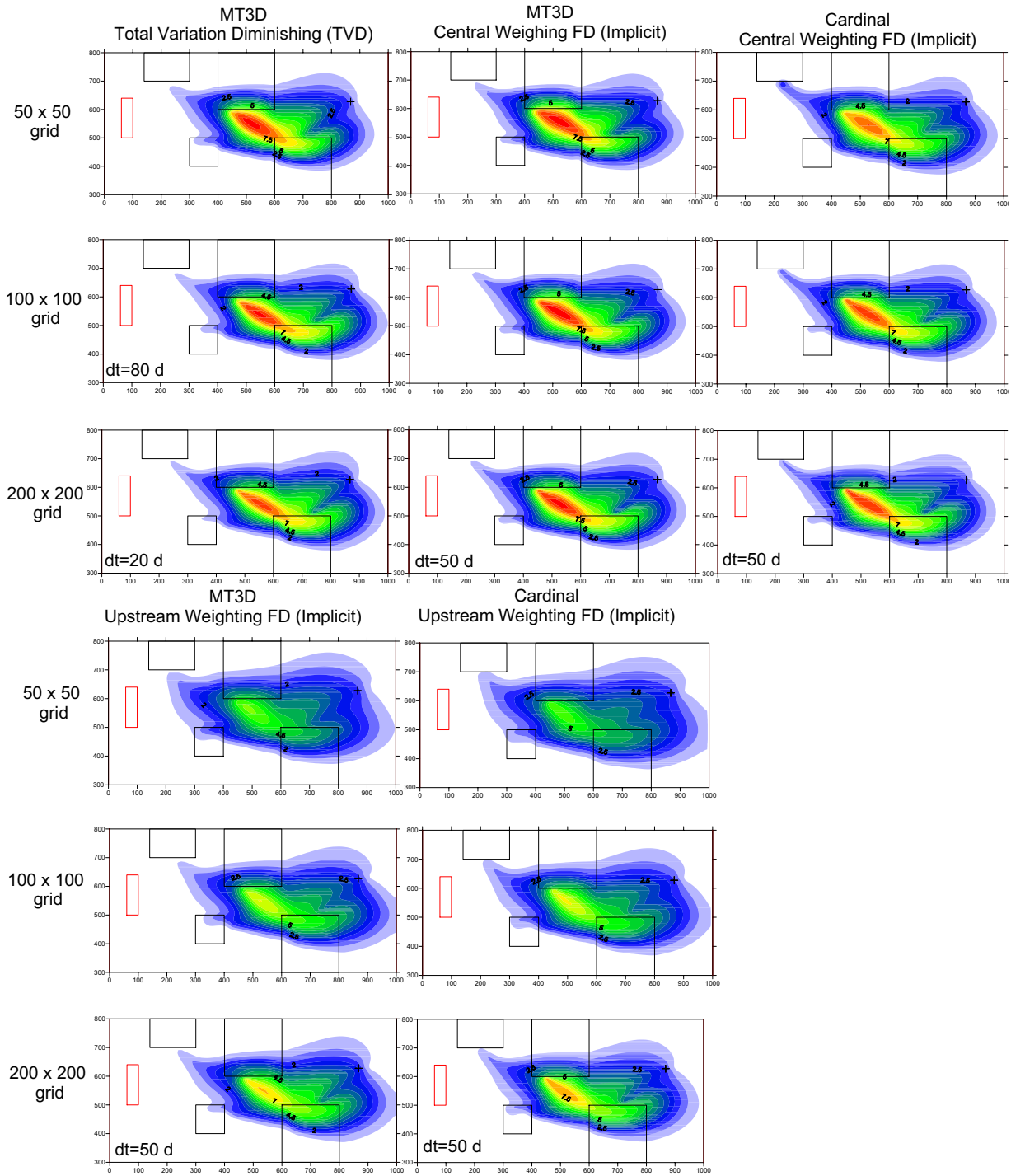

Figure 4.5: MT3DMS Benchmark (confined; α_t=0.3 m) at 63000 days

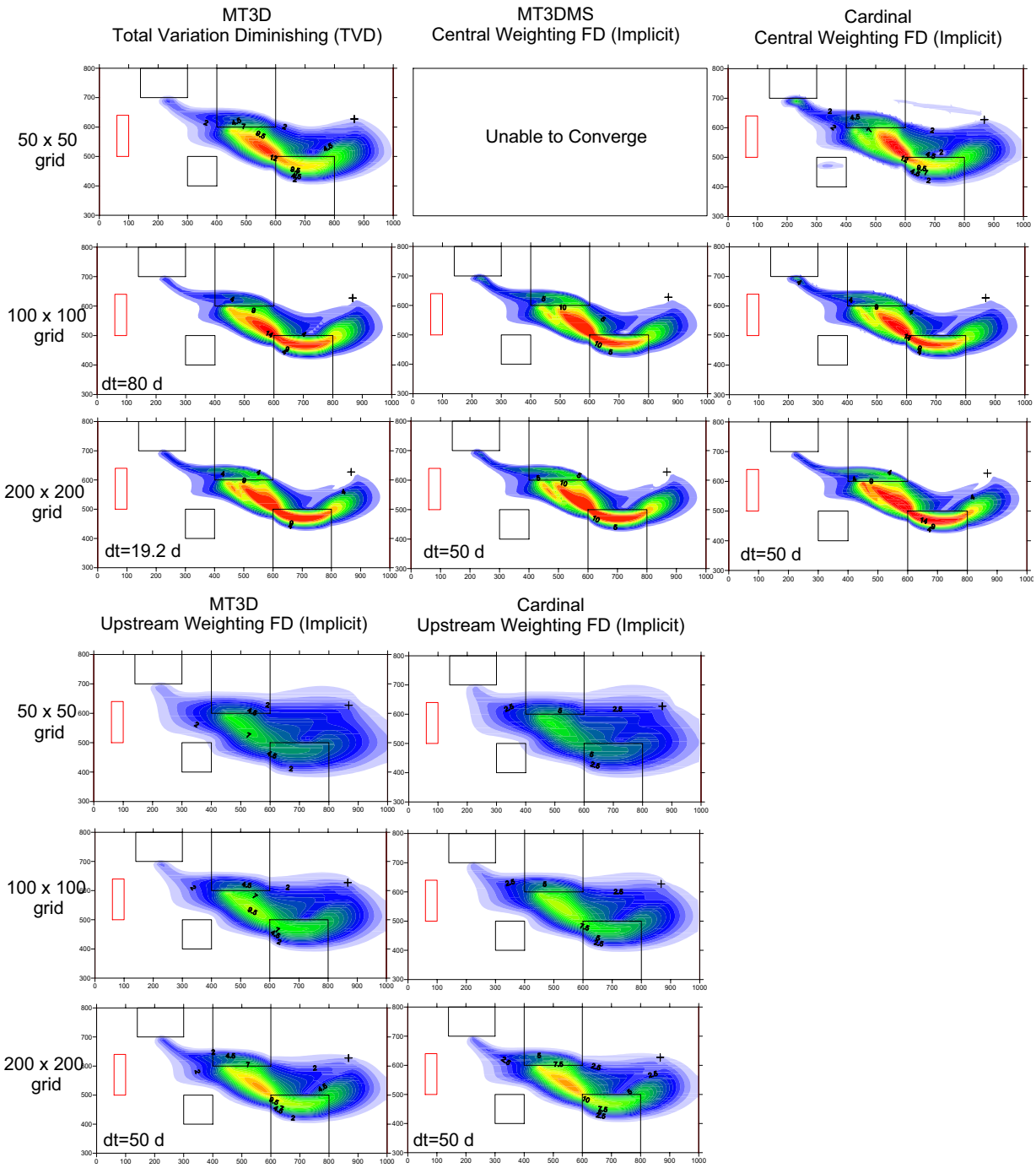

Figure 4.6: MT3DMS Benchmark (confined; α_t=0.01 m) at 63000 days

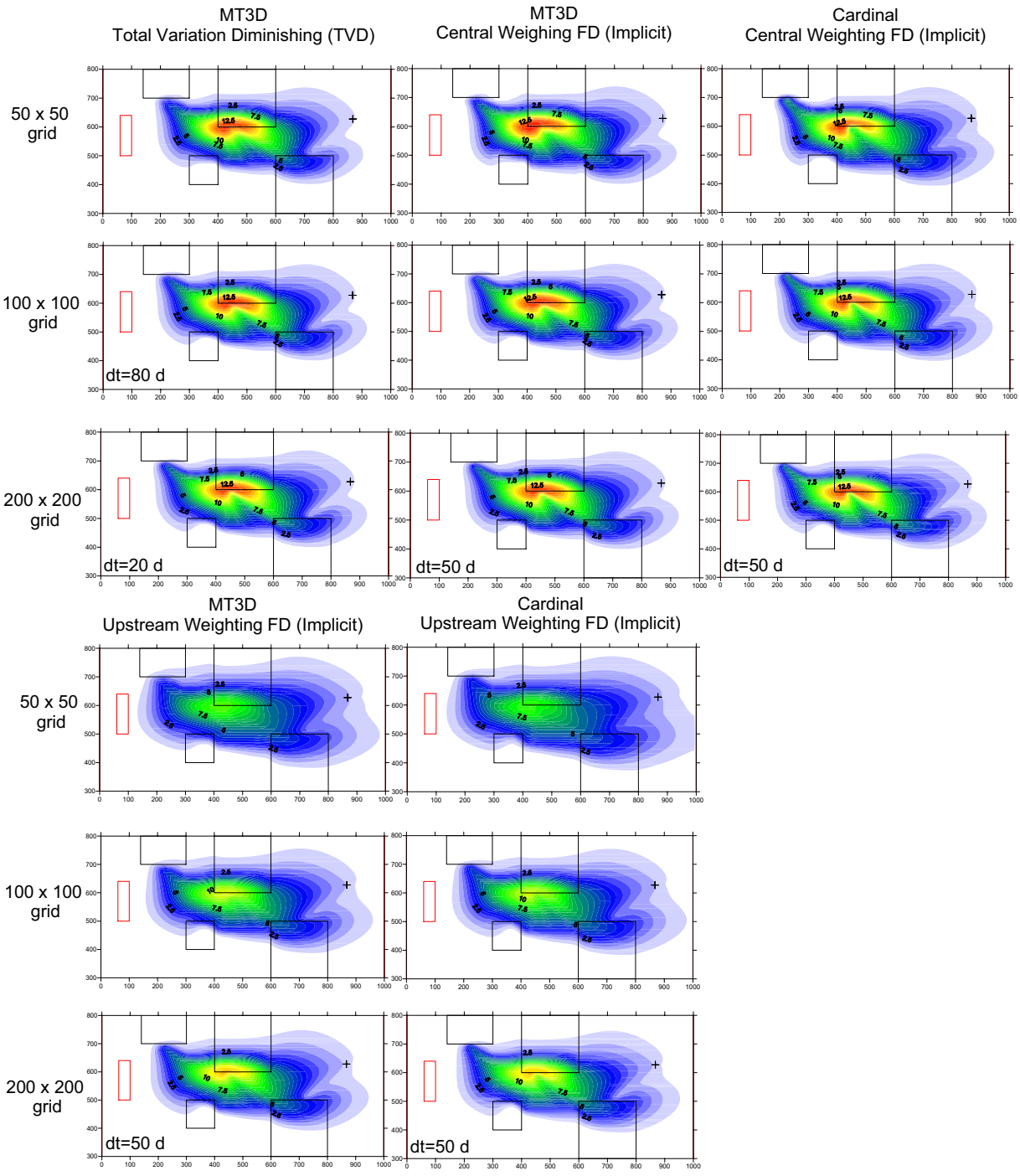

Figure 4.7: MT3DMS Benchmark (unconfined; α_t=0.3 m) at 63000 days

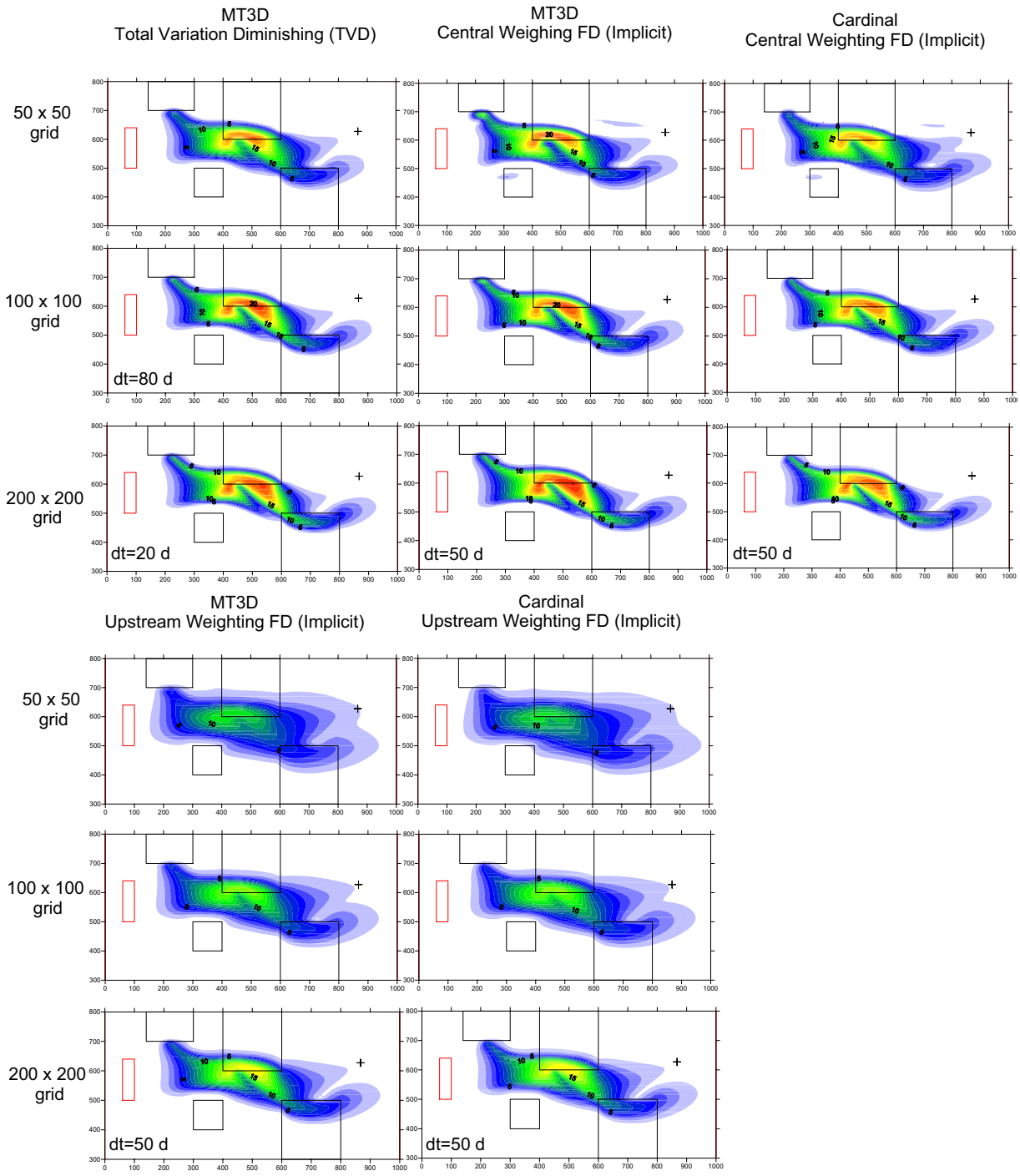

Figure 4.8: MT3DMS Benchmark (unconfined; α_t=0.01 m) at 63000 days

Table 4.3: Comparison of mass balance errors for MT3DMS and CARDINAL test cases. CARDINAL mass balance errors are calculated as described in section 3.2. The MT3DMS "alternative" mass balance calculation (Zheng and Wang 1999) is reported.

	MT3DMS			CARDINAL	
grid resolution	TVD	CW	UW	CW	UW
			Confined; α_t =3 m		
50x50	-0.002%	-0.001%	-0.003%	-0.009%	-0.007%
100x100	0.002%	0.001%	-0.003%	-0.019%	-0.018%
200x200	—%	—%	—%	—%	-0.012%
			Confined; α_t =0.1 m		
50x50	-0.003%	N/A	-0.002%	-0.004%	-0.015%
100x100	0.000%	-0.001%	-0.001%	0.004%	-0.005%
200x200	—%	—%	—%	-0.003%	-0.008%
			Unconfined; α_t =3 m		
50x50	0.000%	0.003%	0.001%	-0.007%	-0.007%
100x100	0.002%	0.003%	0.011%	-0.004%	-0.008%
200x200	—%	—%	0.004%	-0.005%	-0.005%
			Unconfined; α_t =0.1 m		
50x50	0.000%	0.003%	0.001%	-0.004%	-0.004%
100x100	-0.001%	0.003%	0.006%	-0.001%	-0.008%
200x200	-0.002%	0.004%	0.005%	-0.001%	-0.005%

TVD=Total Variation Diminishing; CW=Central weighting; UW=Upstream weighting;

As is apparent from figures 4.5 through 4.8, the solutions from the AEM-based finite difference algorithm and MT3DMS are visually nearly identical Distinct differences are apparent between the upstream and central weighting results of both MT3DMS and CARDINAL. These differences are due to the effect of numerical dispersion. All of these simulations have mass balance errors of less than 0.019% (as shown in table 4.3), and therefore may be deemed equivalent from a mass balance standpoint. This equivalence occurs because both simulations solve the divergence form of the governing equation, which, if implemented correctly, conserves mass regardless of the quality of the flow solution. However, as shown in figure 4.9, even at the highest resolution, there are still differences in the spatial distribution of concentrations.

Figure 4.9 depicts the difference between the CARDINAL and MT3DMS concentration profiles at t=63000 days for the unconfined test case simulated using the same implicit central weighting scheme on a 50 x 50 and 200 x 200 mesh with a time step of 50 days. The differences in concentration range from -3.5 mg/L to 3 mg/L on the fine mesh and -4.0 to 3.5 on the coarse mesh, where the maximum concentration at t=63000 d in both modeled systems is approximately 13.5 mg/L. These differences are concentrated at the borders of the inhomogeneities in both simulations. The locations

of these deviations correspond directly to clusters of finite difference cells with water balance errors (i.e., flow into the cell is not equal to flow out of the cell). These errors (only in the MODFLOW solution) ranged from 0.00 to 1.5% of the total flux in the cell for both simulations, with the finer resolution model having fewer cells with significant mass balance errors. In contrast, the AEM-based solution exhibited water balance errors on the order of 10^{-7}% at both resolutions. It is hypothesized, then, that the CARDINAL finite difference solution is the more accurate of the two, and the plots in figure 4.9 depicts errors in the MT3DMS transport solution that are derived from improper solution of the groundwater flow equation. This improper solution is due to insufficient default residual criterion (0.01) for the iterative solution method, solved using a preconditioned conjugate gradient method.

To validate the above assessment, an additional "zeroth-order" test was run at the coarse grid resolution. This test case is based upon similar tests run by Dawson et al. (2004) to identify compatibility between various flow and transport algorithms. The zeroth-order test case is designed to evaluate the quality of a contaminant transport solution method. The concept is stated as follows: given a system with uniform initial concentrations (C_0) bounded on all sides by constant concentration boundaries $C = C_0$ and no additional sources of solute or clean water, the concentration at all times will be that of the initial conditions (i.e., $C(x, y, t) = C(x, y, 0)$ for all t). Such a simulation was run using both the MT3DMS central weighting implicit scheme and the CARDINAL central weighting implicit scheme for the unconfined test case defined earlier in this chapter. The simulation was modified only by addition of constant concentration (Dirichlet) boundary conditions with C=100 mg/L specified along the borders of the domain and uniform initial conditions of C=100 mg/L. The simulation was run on a 50 x 50 grid with α_t=0.1. The concentration profile at t=63000 days for the MT3DMS solution is shown in figure 4.10. Concentrations range from 96.60 mg/L to 101.90 mg/L, with an average value of 100.07 mg/L and a standard deviation of 0.35 mg/L. The same simulation performed using the CARDINAL implementation was uniformly 100 mg/L, with a standard deviation of 0.00. Notably, the same simulation using CARDINAL with a non-robust flux translation algorithm (one point Gauss quadrature for each cell face) was considerably worse than the MT3DMS result, with concentrations ranging from 72 to 140 mg/L and a standard deviation of 4.2 mg/L. These results highlight the importance of a precise water balance and therefore the need for robust discretization of analytic element fluxes. The results also demonstrate the need for alternative measures of error for Eulerian transport models, as the global mass balance error

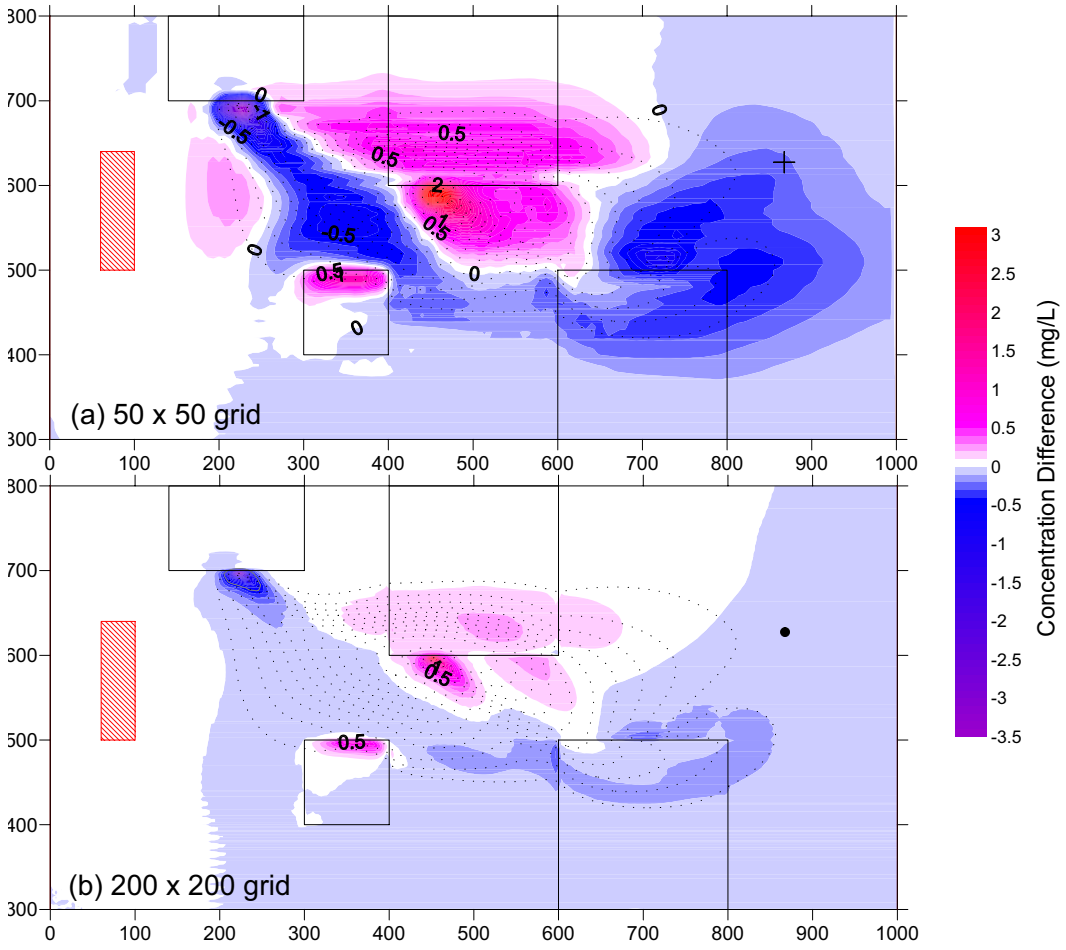

Figure 4.9: MT3DMS Benchmark comparison (unconfined; α_t=0.01 m). The differences between the CARDINAL and MT3DMS solutions at t=63000 d on (a) a 50 x 50 grid and (b) a 200 x 200 grid are plotted in space. The central-weighting implicit algorithm was used in all cases: the primary distinction between the two transport solutions is the use of AEM-based fluxes. Mass balance errors in the MODFLOW flow solution are the cause of the differences in the concentration profiles. These errors diminish as the grid resolution is increased.

(often the only error measure calculated by finite difference models) does not reflect errors in the distribution of mass.

The comparable results from both MT3DMS and CARDINAL suggest that the finite difference algorithm described in section 3.3 adequately incorporates the effects of variable saturated thickness, non-uniform velocity, and dispersion cross terms in addition to being able to replicate the simple analytic benchmark solutions. It was also shown that, because of the maintenance of the highly accurate AEM water balance, the AEM-based transport solution is more accurate. Similar accuracy may be obtained using finite difference methods by decreasing the error tolerance of the matrix

solution method used to solve the FD flow problem. However, default parameters (used by most modelers) can be insufficient for obtaining an accurate transport solution.

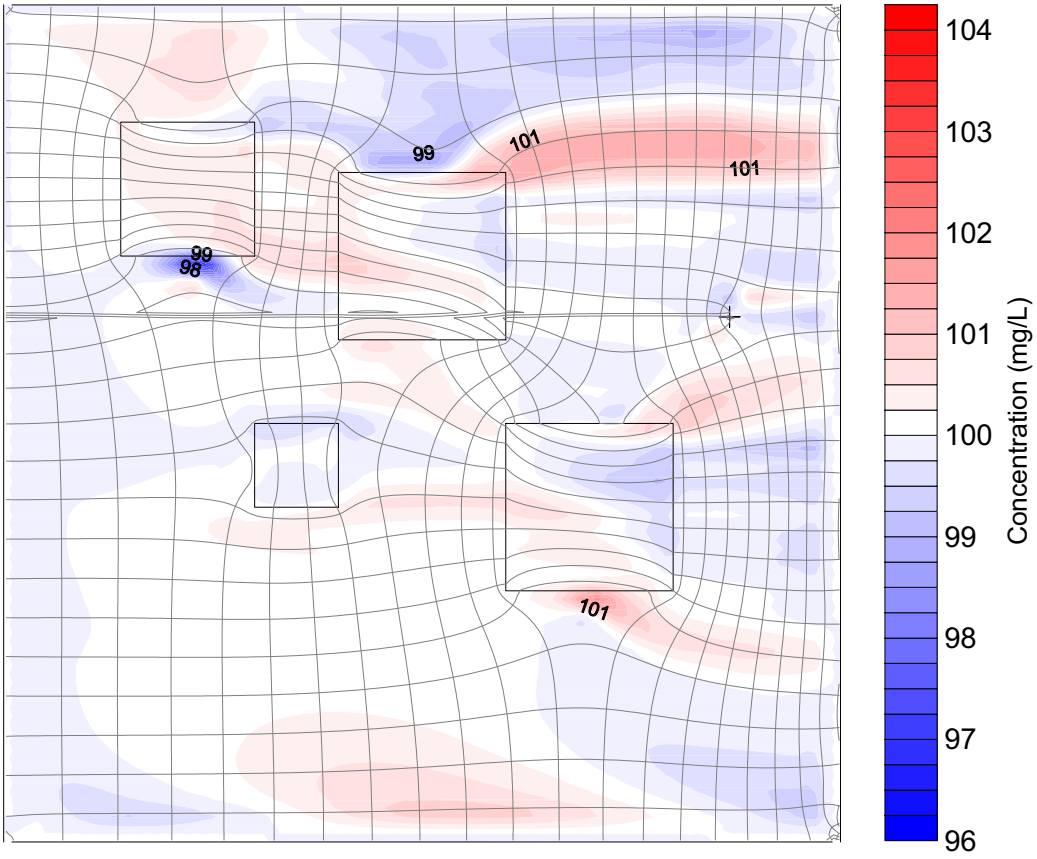

Figure 4.10: Zero-order test results for MT3DMS unconfined test case. Since the system is bounded with constant concentration (C=100 mg/L) boundaries and $C(x, y, 0)$=100 mg/L, the concentrations should be uniformly 100 mg/L for all time. The simulated concentrations (shown at t=63000 d) are non-uniform. This is attributed to the inaccuracy of the flow solution, and the non-uniformity is not exhibited in the AEM-based transport simulation.

4.2 Including Continuous Gradation in Transport Parameters

The following section examines the accuracy and efficiency of using continuous parameters, including the effective parameter method described in sections 3.4 and 3.5 and the effects of high precision integration of continuous parameters in finite element and particle-based methods. First, the results of tests run to verify the accuracy of the effective velocity and discharge derivative functions are presented. These tests show that the expressions derived for effective velocities yield correct results. Following that, the effective parameter random walk method presented in section 3.5.4 is used to simulate contaminant transport in a mildly heterogeneous domain. This is followed by tests designed to investigate the benefit of using continuous parameterization derived from AEM flow solutions in (1) characteristics methods and (2) Eulerian finite element methods.

4.2.1 Verification of Analytic Effective Velocity Expressions

The derivations of the expressions for the element discharge derivatives (appendix C) and dispersion derivatives (section 3.4 and appendix A) are lengthy. To verify their accuracy, the discharge derivatives for each element type, the various two-dimensional dispersion derivatives, and the effective velocities were evaluated both numerically and analytically, and their results were compared in a single arbitrary model that included each of the element types included in appendix C. Derivatives were evaluated numerically using the following approximation:

$$\begin{aligned} \frac{\partial f}{\partial x}(x,y) &= \frac{f(x+\epsilon,y)-f(x,y)}{\epsilon} \\ \frac{\partial f}{\partial y}(x,y) &= \frac{f(x,y+\epsilon)-f(x,y)}{\epsilon} \end{aligned} \tag{4.3}$$

For the comparison, the spatial distance ϵ was held constant as 1e-10 meters for a 100 meter by 100 meter model domain. The flow system is characterized by uniform flow from left to right through a variety of elements (a river, polygonal, elliptical, and circular inhomogeneities of varying hydraulic conductivity, an area-sink, and a well). Dispersivities of $\alpha_l = 10$ m α_t=3 m were used. Relative errors in the evaluation of the parameters were evaluated as the the maximum relative difference between the analytic and numerical calculations evaluated at 160,000 points on an evenly spaced 400 by 400 grid covering the model domain, and were consistently less than 1e-4, as shown in table 4.4.

It is important to note that this single comparison is sufficient for demonstrating the quality

of the closed-form solutions for discharge derivatives and dispersion derivatives. As long as the elements possess non-zero coefficients, the dispersivities are non-zero, any arbitrary model configuration and flow parameterization is adequate, as any derivation errors will be in evidence as spatial trends in the error. It is for this reason that the specifics of the model configuration are not discussed here. However, for completeness, the model configuration is shown in figure 4.11.

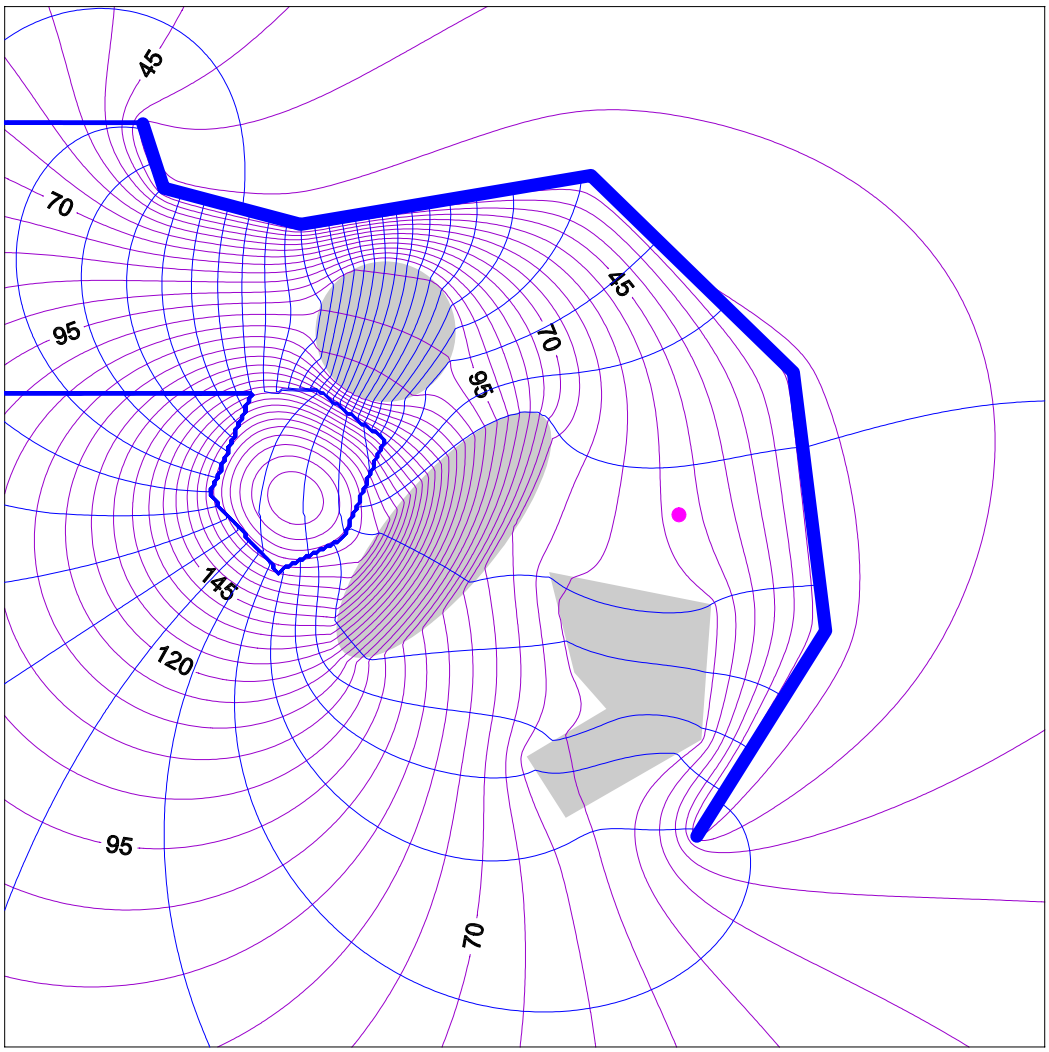

Figure 4.11: Configuration of test case used to verify the accuracy of closed-form expressions for effective parameters and discharge derivatives

The small magnitude of these maximum errors, and the fact that there was no apparent spatial trend in the errors suggests that the lengthy derivations presented in section 3.4 are accurate.

Table 4.4: Comparison of numerical and analytic evaluations of Discharge derivative, dispersion derivatives, and effective velocity. All polylinear, circular, and elliptical elements are high-order, with at least 5 degrees of freedom

Parameter	Maximum relative error
G_x (Linesink String)	3.4e-7
G_x (Area Sink)	2.1e-7
G_x (Doublet String)	9.8e-8
G_x (Well)	3.2e-7
G_x (Ellipse)	1.7e-7
G_x (Circle)	1.8e-8
$\frac{\partial D_{xx}}{\partial x}$	6.2e-6
$\frac{\partial D_{xy}}{\partial x}$	3.2e-5
$\frac{\partial D_{yy}}{\partial y}$	5.7e-6
$\frac{\partial D_{yx}}{\partial y}$	2.8e-5
v_x^*	7.8e-5
v_y^*	7.2e-5

4.2.2 EPVA Random Walk Simulation

The random walk method, the only approach deemed appropriate for using the closed-form expressions for effective parameters in section 3.4, was implemented in CARDINAL as discussed in section 3.5.4. The revised random walk method uses continuous parameters and continuous representations of parameter derivatives directly. The method solves the governing equation in a fully Lagrangian fashion, without any form of parameter discretization: the only use of a grid or mesh is for volume-averaging of mass to obtain graphical representation of the system concentrations. Advective and dispersive transport are treated in a manner that is fully consistent with the continuous governing equation and the only sources of error are (1) tracking errors (due to insufficient integration of the particle trajectories), (2) errors caused by the decoupling of advection and dispersion, and (3) the local mass distribution error (due to an insufficient number of particles tracked to resolve the plume). For the following examples it is assumed that the tracking error is negligible, as the adaptive Runge-Kutta method of appendix F is used. Global mass balance is conserved exactly for non-reactive systems modeled with random walk. With the EPVA approach, other errors due to discretization of the velocity field or truncation of the parameter derivative terms in the governing equations are removed.

To test the relative accuracy of the effective parameter random walk method, several simulations were performed of inert solute transport through the heterogeneous domain of figure 4.12. Circular inhomogeneities were used because they are uniquely represented by the analytic element method, and the resultant flow field is wholly independent of any orthogonal or linear geometry, further demonstrating the grid independence of this particular approach. An initial contaminant source of 100 mg/L was transported through this domain for 2500 days using a variety of algorithm formulations. The same model was simulated using (1) 4 different time steps (1, 5, 25, and 50 days) (the time step controls the error ascribed to the decoupling of advection and dispersion) (2) 4 different initial particle distributions (1152, 2304, 3456, or 4608 particles in the initial source zone) (this controls the resolution of the plume and local mass balance errors), and (3) either the effective parameter formulation or the traditional formulation (the traditional formulation uses a discrete representation of influence of spatial variation in dispersion coefficients). The simulation time step is independent of the tracking time step, which is calculated using the adaptive algorithm of appendix F. For the traditional formulation, the "drift" term was calculated using finite differences on an independent grid (with a spacing of 7 meters). A total of 32 simulations were run.

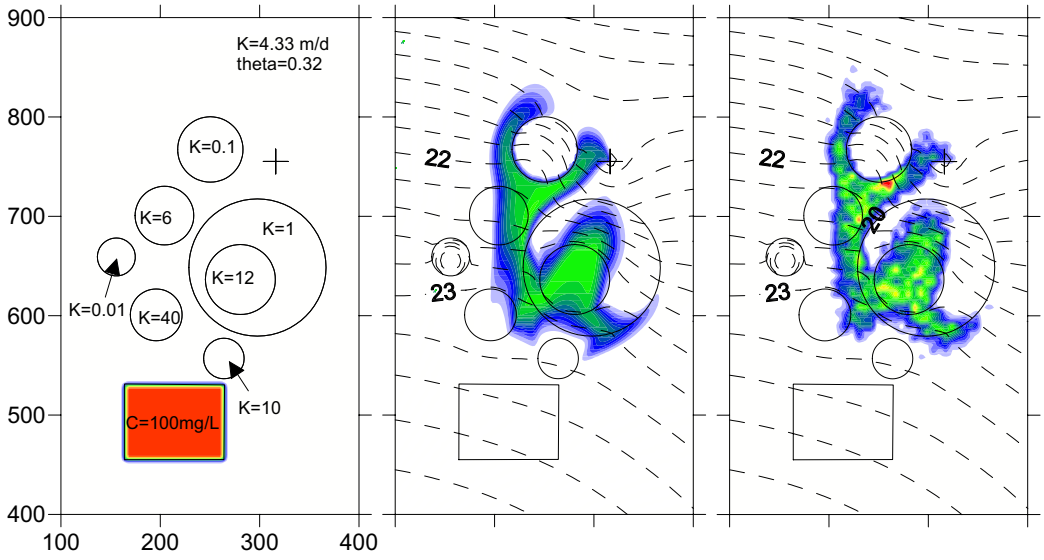

Figure 4.12: Configuration of model used for EPVA random walk test. (a) Model aquifer properties and initial condition geometry (b) Head contours and results of Eulerian finite difference simulation at 2500 days (c)Head contours and results of EPVA random walk simulation (with 4608 particles) at 2500 days

Because the random walk method uses a point-based rather than volume-averaged representation of mass (each particle represents a parcel of aqueous mass), it is more difficult to compare multiple simulations of the random walk method than the comparable Eulerian models. Additional complications arise due to the random component of the models. The global mass balance error, a useful indicator of model quality with Eulerian methods, is zero if no sinks or sources are present, and thus reveals no information about the quality of a particular simulation. Rather, random walk methods are susceptible only to errors in the distribution of this mass (LaBolle et al. 1996). To calculate the error in mass distribution, a solution for the plume distribution after 2500 days was first obtained using a finely discretized 20480 cell (160x128) finite difference model. The FD model satisfied both Courant and Peclet constraints (the model had a maximum Courant number of 0.9 and a maximum Peclet number of 1.6). Global mass balance error was less than 0.0005%, and central weighing in space was used to avoid the numerical dispersion associated with upstream weighting. The results, shown in figure 4.12b, are deemed to be an adequate representation of the true solution, and are used as the "true" distribution of mass in the aquifer at the end of the simulation.

An estimate of the mass distribution error of the random walk method was calculated at multiple levels of resolution by using five different rectangular grids (5x4,10x8,20x16,40x32,80x64) covering

the simulation domain. The point values of mass were summed over each cell volume to calculate the net mass within each cell. The plume mass calculated with the finite difference model was also distributed on the same 5 grids by integrating the concentrations over each low-resolution cell. The resultant portioning of the system mass was treated as the "true" mass distribution on each of the grids. This mass distribution error at a particular grid resolution was calculated as one half the summation of the absolute errors in each cell, where the "true" mass in the cell was calculated from the finite difference results. The error was normalized by the average mass in all grid cells at that resolution. The mass distribution error, ϵ_{NxM}, a function of resolution of the NxM averaging grid, may be expressed mathematically as:

$$\epsilon_{NxM} = \frac{1}{2} \frac{\sum_{i=1}^{N} \sum_{j=1}^{M} \left| \sum_{p=1}^{NP_{ij}} M_{ij}^{p} - M_{ij}^{FD} \right|}{\sum_{i=1}^{N} \sum_{j=1}^{M} M_{ij}^{FD}} \tag{4.4}$$

Where M_{ij}^{p} is the mass of the p^{th} particle (of NP_{ij} particles) in cell ij, M_{ij}^{FD} is the total mass of all (high-resolution) finite difference cells within cell ij, and N and M are the number of rows and columns in the grid on which the mass is distributed. This error measure can vary from 0 to 1, and quantifies the proportion of mass that has been allocated to the wrong cell. The error is smaller for the lower resolution calculations (i.e., all models will have mass distribution errors of zero if only one cell was used). Likewise, larger errors are associated with higher resolution grids. For example, if a single particle is tracked and its final location is offset from the actual location by even one cell, 100% of the mass is in the "wrong" cell. This phenomena is more prone to occur as the grid resolution is increased. While used here as an indicator of error in the distribution of mass, the measure defined by equation 4.4 actually quantifies the degree of difference in the distribution of mass between two simulation results (in this case the difference between inaccurate random walk simulations and the "true" solution). If multiple calculation grids are used, this measure also provides information about the spatial resolution of these differences in a succinct format.

Because of the complexity of the flow domain, it is computationally prohibitive to specify a sufficient number of particles to resolve the concentration distribution at the same level of accuracy as the finite difference method. As a rule of thumb, Tompson and Dougherty (1988) suggest about 20 particles per cell, or 20x80x64= 102,400 particles to appropriately match the distribution at the finest grid resolution used for analysis. No such attempt was made. Rather, the following analysis

attempts to examine the benefits of the effective parameter method without a wholly sufficient number of particles.

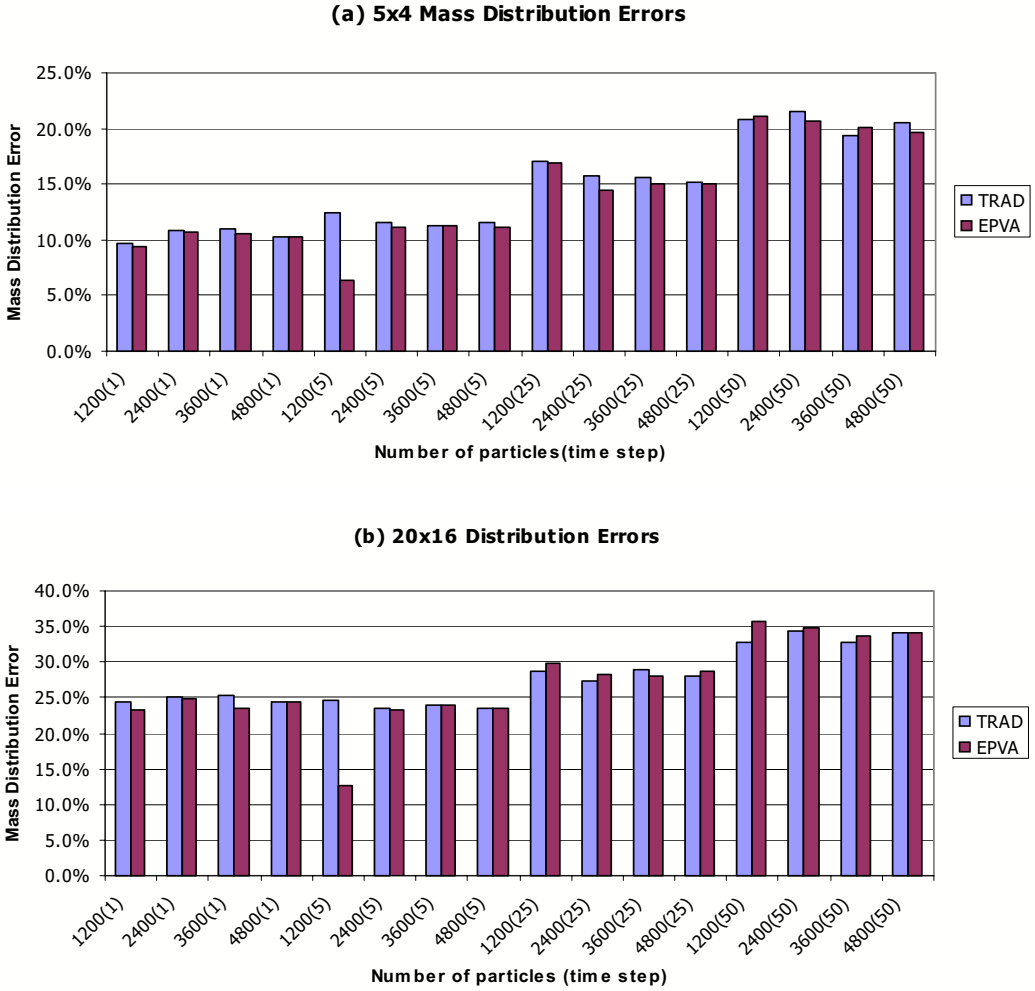

Figure 4.13: Mass distribution errors for the EPVA random walk test case. (a) Errors in the 32 simulations calculated on a coarse resolution (5x4) grid (b) Errors in the 32 simulations calculated on a finer resolution (20x16) grid

Figure 4.13 shows the mass distribution error for each of the 32 simulations performed. As expected, as more particles are added to the simulation, there is a general (though not uniform) trend towards lower mass distribution errors. In addition, it appears that the effective parameter method provides slightly better results in the majority of the simulations (87.5% of those simulations using a time step less than 10 d). However, the time step used to split the operators of advection and dispersion has the most significant influence upon the magnitude of the mass distribution error. This error, dubbed "overshoot" error by Tompson and Dougherty (1988), results from the random dispersive step being based only upon the local dispersion coefficients at the foot of the

dispersive displacement vector. If the velocity field is non-uniform, a particle may abruptly move a large distance from a high-dispersion zone to an area of low dispersion, even if the intermediate area along this displacement vector is characterized by low velocities and correspondingly low dispersion coefficients. If the time step is appropriately small, the early displacements would be small enough for the particle to "become aware of" its low-dispersion environment. The impact of this potential for overshoot error has been obscured in the past by recommendations (Prickett et al. 1981; Kinzelbach 1988) to satisfy a grid Courant criteria when determining the time step for random walk methods. However, this criteria was developed to minimize the deleterious effects of a discrete velocity field and "avoid oscillations of particle density" (Kinzelbach 1986). The results shown here demonstrate that such time step requirements are required for a less qualitative reason: they minimize the errors associated with decoupling the advection and reaction operators. In heterogenous domains, these errors have effects similar to that associated with classical numerical dispersion, as shown in figure 4.14. Researchers (e.g., (Kinzelbach 1986)) have made the claim that the random walk method is free of numerical dispersion. Such a conclusion is understandable, as the source of numerical dispersion differs from that of other numerical methods for transport simulation. With the random walk method, artificial dispersion is inversely proportional to the Peclet number (in direct contrast to Eulerian methods) and entirely absent in homogeneous domains. However, the effects of using larger time steps clearly mirrors that of traditional numerical dispersion, and is here considered to be the same phenomenon (albeit caused by considerably different factors).

It is clear from the results shown in figure 4.13 that the errors associated with the random walk method are only mildly influenced by the accuracy of the effective velocity (or "drift" term). The effect of the discretization of the drift term appears to be minor as compared to the error associated with the decoupling of the advection and dispersion operators. However, the impact of using continuous effective velocities (implied by the variation in mass distribution error) appears here to be of the same order of magnitude as the impact of the particle count. For most of the simulations, the errors due to spatial discretization are obscured by the effects of temporal discretization, the number of particles, and the random component of the results. The impact of using closed-form solution for parameters is inconsistent, varying from model to model, and lacking any consistent trend for models with few particles or large time steps. However, it appears as if the advantage of using a continuous or discrete representation of the "drift" term is not significant enough to warrant the additional computational expense of using the effective parameter method

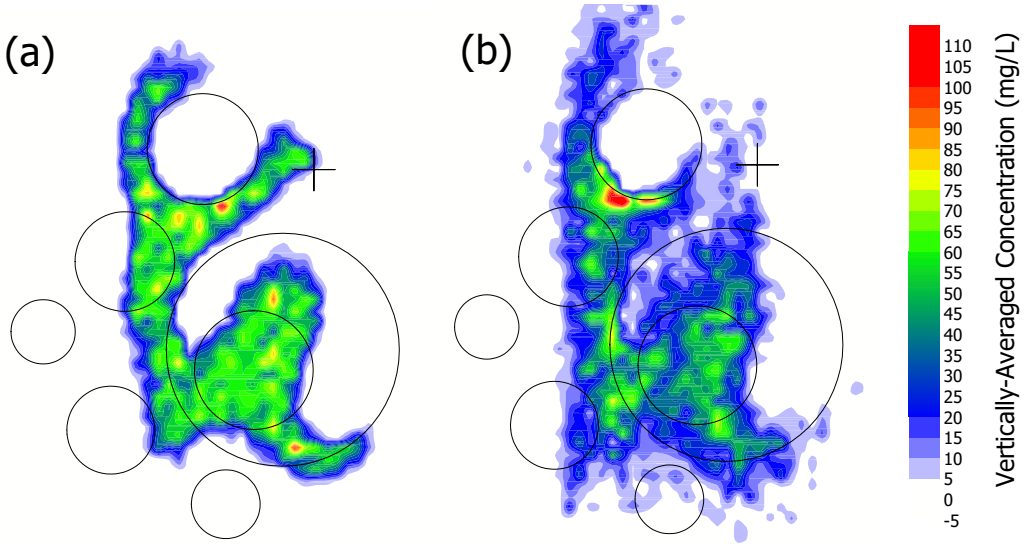

Figure 4.14: Numerical dispersion as exhibited in the random walk test case. (a) The results of the random walk method at t=2500 days using a time step of 1 day (Cr¡0.25) (b) The results of the random walk method at t=2500 days using a time step of 50 days (Cr¿10)

(discussed in section 3.4). The advantage of using a more accurate flow model (without velocity interpolation) was not addressed with this test case. However, tests performed in section 4.2.4 are used to quantify the effects of tracking error on EL methods, and the results may be extrapolated to the fully Lagrangian random walk method (with or without the use of effective parameters).

Independent of the results from this particular (challenging) test case, the simple and meaningful error measure developed here may be generally applicable for calculating the degree of mass allocation error in a transport model (given a "true" high resolution model), or for comparing the results from two different multidimensional transport problems. While there are analytical techniques for estimating the degree of artificial dispersion in one-dimensional transport models (e.g., as in Peaceman (1977)), the author is not aware of existing techniques for quantifying any type of mass distribution error in multidimensional models. Since it seems quite desirable to have quantifiable estimates of the degree of difference between two models, further research into this measure are warranted.

4.2.3 Finite Element Integral Evaluation

In section 3.6.4, three means of calculating the finite element material integral were presented, each of which incorporate the variation of transport parameters (velocity and dispersion coefficient) within an element in different ways. The first method (using element-averaged parameters) is the standard implementation for conventional finite element simulators (e.g., that of Istok (1989)). This is because element-averaged velocities are the conventional output from finite element flow solutions. The second method (nodally-interpolated parameters) uses the velocities interpolated from nodal values to calculate the material integral (as done for a similar PDE in Cooley (1992)). The third method, numerical integration of continuous parameters, was introduced within this dissertation as a means of directly incorporating the continuous inter-element variation in transport parameters, and echoes similar work done by Santare and Lambros (2000). The continuous integration method uses the velocities and other parameters evaluated at a set of representative points within the element to calculate the material integral. Here, these three distinct methods are compared using a single test configuration with variable discharge, saturated thickness, and dispersion coefficients on a single (low-resolution) mesh. As demonstrated with this series of simulation runs, the choice of how the finite element material integral is calculated (which has a relatively small impact upon the overall computational cost of the simulation) has an important effect upon the accuracy and stability of the AEM-based finite element transport solution.

The model layout, parameter values, initial conditions, and mesh used for the test simulation are shown in figure 4.15. This particular model configuration was specified because the sharp variation of hydraulic conductivity and influence of pumping wells impose high variability of the velocity within the aquifer. Specification of a lower-resolution mesh (425 nodes; 908 elements) introduces a significant degree of inter-element variation in the discharge vector, and therefore the algorithm for discretizing the analytic element flow-derived parameters has a distinct influence upon the properties of the solution. The use of a lower resolution mesh for a system with relatively high velocity variation was by design: this combination will reveal any errors linked to inappropriate incorporation of velocity information into the finite element system of equations.

Sixteen different simulations were run using different means of calculating the material integral. These sixteen simulations fall into each of the three categories discussed in section 3.6.4. Eight of the simulations used element-averaged parameters, one of them used linearly varying parameters, and seven of them used continuous parameters. The sixteen simulations are notated as follows:

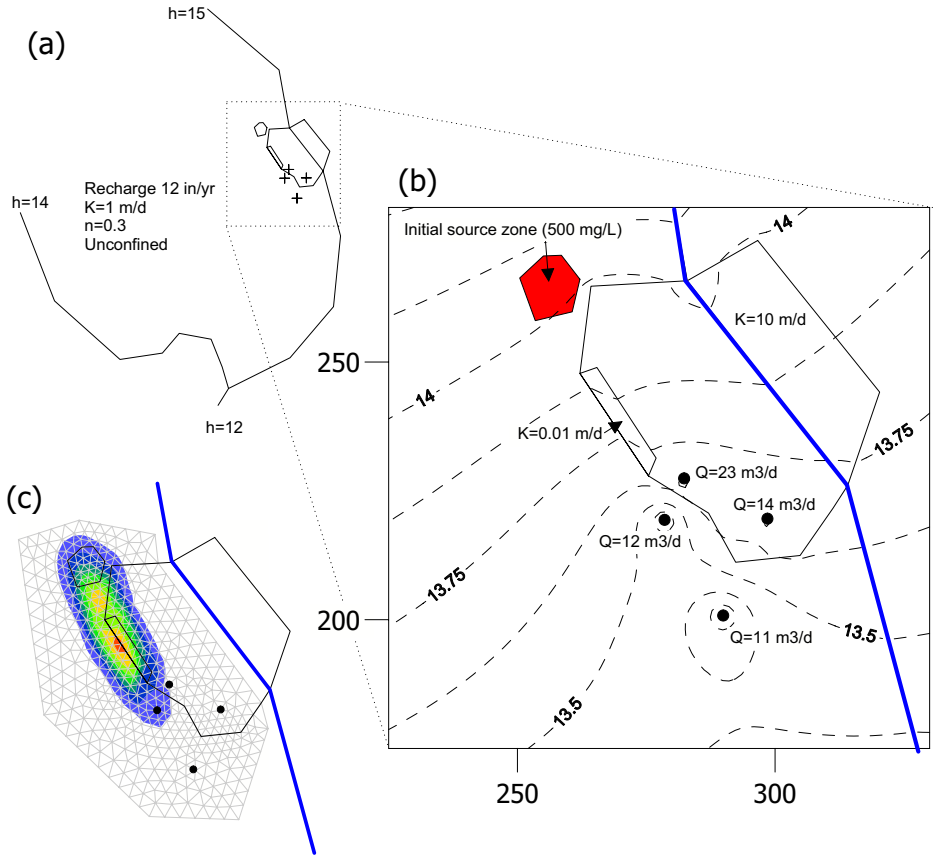

Figure 4.15: Configuration of model used for finite element integration/discretization test. (a) Zoomed out model geometry and aquifer properties. (b) Local model features, properties, and initial conditions for transport model. (c) Transport mesh used and plume results at t=2500 days.

- TRAD -The simplest, "traditional" simulation uses a uniform velocity within each element, calculated from the head at the three adjacent nodal points.

- AVG[#] -The average parameter value within the element was calculated using 1-,3-,4-,7-,9-, or 13-point Gaussian integration. The material integral itself was evaluated analytically using these element-averaged values ($Q_x^{(e)}$, z$Q_y^{(e)}$, $D_{xx}^{(e)}$, $h^{(e)}$, etc.) substituted into equation 3.104.

- NODAL -The nodal simulation used linearly varying parameters based upon the nodal values for discharge/velocity, saturated thickness, and dispersion coefficients. The material integral itself was calculated analytically using equation 3.109. The integral was also calculated numerically using linearly varying parameters to test the validity of the analytic formulation. The two were found to give comparable results.

- C[#] -The full material residual was calculated using 1-,3-,4-,7-,9-, or 13-point Gaussian

integration. The parameters were explicitly evaluated at Gauss points.

Table 4.5: Simulations used in finite element material integration test

Name	evaluation required	no. of eval. points	representation (equation)
TRAD	ϕ at nodes; k in elem.	3	average(3.104)
NODAL	W, h at nodes	3	linear(3.109)
C1	W, h at Gauss pts	1	average(3.104)
C3	W, h at Gauss pts	3	continuous(3.112)
C4	W, h at Gauss pts	4	continuous(3.112)
C7	W, h at Gauss pts	7	continuous(3.112)
C9	W, h at Gauss pts	9	continuous(3.112)
C13	W, h at Gauss pts	13	continuous(3.112)
AVG1	W, h at Gauss pts	1	average(3.104)
AVG3	W, h at Gauss pts	3	average(3.104)
AVG4	W, h at Gauss pts	4	average(3.104)
AVG7	W, h at Gauss pts	7	average(3.104)
AVG9	W, h at Gauss pts	9	average(3.104)
AVG13	W, h at Gauss pts	13	average(3.104)

Each of these simulations, summarized in table 4.5, were run for 2500 days, at which point about 40 percent of the initial mass has been extracted by the pumping wells. No upstream weighting was used and the temporal discretization was dependant upon the representative velocities obtained from each of the 13 methods. Using these representative velocities, maximum Courant number of one was used to avoid oscillations. The average and maximum Peclet number in the domain with this mesh were roughly 1.0 and 1.9, respectively (the different methods of velocity discretization produce different, but similar, Peclet numbers). The results, in terms of the estimated mass balance of section 3.2, are shown in figure 4.16.

As apparent in figure 4.16, the choice of the material integral evaluation algorithm has a significant effect upon the mass balance error for this simulation. This result has a few noteworthy ramifications for the practice of using analytic element flow solutions as the basis for finite element transport simulation.

First, it is apparent from the figure that the linearly varying parameter method for evaluating the residual (NODAL) is unacceptable, with a mass balance error greater than 10 percent for this particular simulation. The reason for this error is related to the poor approximation of the velocity field with the nodal method near sinks and sources. The nodal method evaluates the discharge function very close to singularities (e.g., wells) in the flow field, which are always located at nodes.

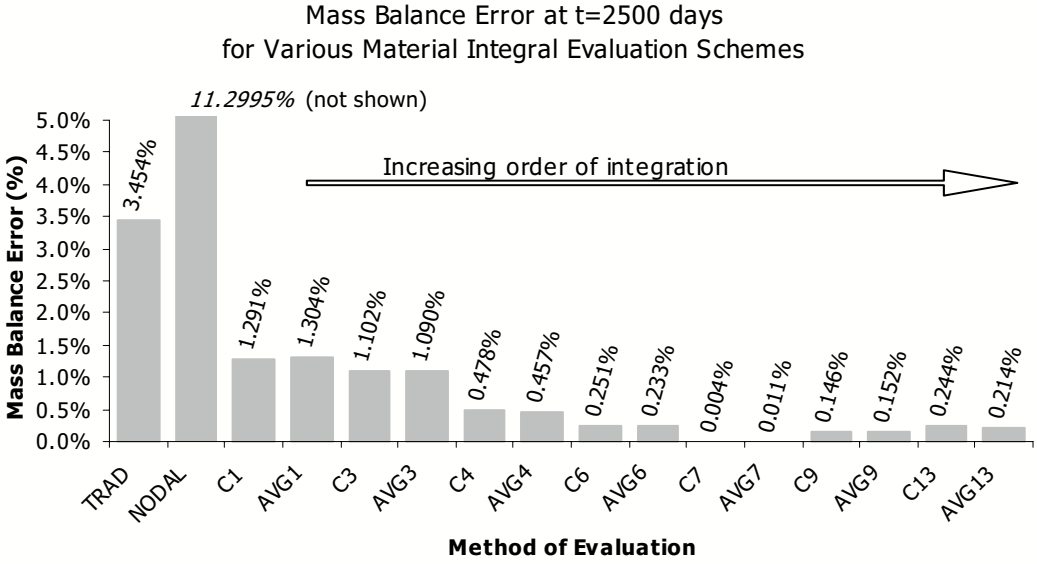

Figure 4.16: Mass balance errors for different means of discretizing continuous parameters in assembly of the finite element residual expression at time t=2500 days.

The extremely high velocity/discharge at these nodes overestimates the representative velocity within the element. For the convective form of the governing equation to be solved without mass balance errors, the *discretized* velocity field must be divergence-free (i.e., $\nabla \cdot \mathbf{Q}$=0), or in the case of systems with recharge, correspond to the specified divergence (i.e., $\nabla \cdot \mathbf{Q}$=$-N$)(Gresho and Sani 1998). Because the analytic element flow solution is divergence-free by definition, any mass balance error is due solely to the discretization process. Additional testing established that the linearly varying parameter method performs well (on par with the lower order quadrature approaches) in the case where singularities are small or nonexistent.

Second, the "traditional" means of calculating the average velocity in an element (TRAD) gives the worst performance of any of the integration schemes other than the poorly-posed nodal method. This indicates that exporting just the nodal heads from an AEM solution to a standard finite element transport solver will produce erroneous results. This is analogous to the error associated with using non-conservative flux discretization for the finite difference method, except here, where the "convective" form of the ADRE is used, the errors in discretization of the AEM solution will result in mass allocation *and* mass balance errors.

Lastly, it is apparent that for both element-averaged and continuous parameter techniques, the accuracy of the solution is directly related to the order of the Gaussian integration proce-

dure. This outcome mirrors similar results for finite elements that use higher-order basis functions (Akin 1994). One-point Gauss integration consistently performs worse than higher-order methods, and the 7-point Gauss integration procedure consistently performs the best (better than even the higher-order 9 point and 13 point methods). The improved performance of high-order methods is expected: higher order quadrature techniques are designed to evaluate the integral of more complicated functions. However, the poorer performance of the 9- and 13-point methods is less clear. The likely reason is the difficulty of integrating logarithmic functions using standard quadrature methods on the triangle. Because the discharge and potential functions are not simple polynomials of x and y, the convergence of the Gaussian quadrature formulae is not asymptotically convergent as the number of gauss points is increased (Lyness and Cools 1994). For integration of functions with logarithmic singularities, lower order quadrature may in fact produce better results. To bypass this shortcoming, "expansion" methods designed for integration of singular functions (Lyness and Cools 1994) should be used. Such an implementation in CARDINAL is beyond the scope of this dissertation.

A key result here is that there is only a minor difference between using element-averaged parameters and explicitly integrating the residual term in the material matrix, if the element-averaged parameters are calculated using quadrature methods. This indicates that integrated average element velocities and saturated thicknesses may be exported on an element-by-element basis to alternative finite element transport solvers with very little loss of accuracy. Additional tests using 4 and 7-point quadrature on the finite element simulation of the MT3DMS test case configuration (from section 4.1.3) confirms these results.

4.2.4 Velocity Interpolation Effects in Characteristic Methods

It has been shown by Oliveira and Baptista (1998) and Ruan and McLaughlin (1999) that tracking errors incurred during the forward and backtracking of characteristic paths in Eulerian-Lagrangian Methods lead to global mass balance errors. A set of simulations is used here to (1) verify these previous results using a non-discrete velocity representation and (2) demonstrate that use of analytic velocity information can remove tracking-based error but Eulerian-lagrangian methods are still subject to significant mass balance error due to interpolation of the concentration field. The test also reveals that a finite difference-based Eulerian-Lagrangian transport simulator that uses exported AEM-based velocity information will provide less accurate results than a fully integrated

AEM-transport model such as BLUEBIRD/CARDINAL.

A series of simulations were performed using the same grid and model configuration as the MT3DMS test of section 4.1.3. However, only the confined aquifer configuration was simulated, and the backward method of characteristics (BMOC) with a time step of 150 days was used. The wells in the original model were removed, because inaccuracies in the BMOC near sinks and sources (Baptista 1987) obscure the effects of velocity interpolation on global and local mass balance errors. The tests were run at multiple grid resolutions (200x200, 100x100, and 50x50). Tracking was performed in one of two ways for each simulation: using the adaptive Runge-Kutta pathline integration of appendix F (with the analytic flow field), and Pollock's semi-analytic interpolation method (Pollock 1988; Zheng and Bennett 2002). The implementation of Pollock's method relied upon discrete interfacial velocities calculated with the techniques of section 3.3.2. These discrete velocities were calculated on the same grids as used for transport.

Note that the BMOC method is susceptible to a high degree of mass balance error in systems with high spatial variation in the distribution of aqueous mass (Baptista 1987). This global mass balance error does not increase gradually, as artificial loss and gain of mass can occur through accumulation of tracking and interpolation errors. Therefore, the maximum mass balance error over the duration of the simulation (rather than the final mass balance error) is used as an indicator of the quality of the solution.

Figure 4.17 depicts the influence of using semi-analytic or analytic velocities as a source of information for particle tracking. The maximum mass balance error decreases as the grid resolution increases for both Runge-Kutta and Pollock's approaches. The use of discrete velocity information consistently performed poorer than the use of continuous velocity information. This is the consequence of using inaccurate characteristic paths, as previously found by Oliveira and Baptista (1998). What is revealing about this set of tests is that the exportation of AEM fluxes to a MOC transport simulator that only uses discrete flux information (e.g., MOC3D (Konikow et al. 1996) or MT3DMS (Zheng and Wang 1999)) will cause unnecessary errors attributed solely to discretization of the velocity field.

While using continuous rather than discrete velocities does improve the quality of the numerical solution, this improvement removes only a percentage of the overall error in the model. This small increase in accuracy comes at a significant computational cost (due to the Runge-Kutta evaluation), which the author deems unsatisfactory for most modeling simulations. Any benefits realized by

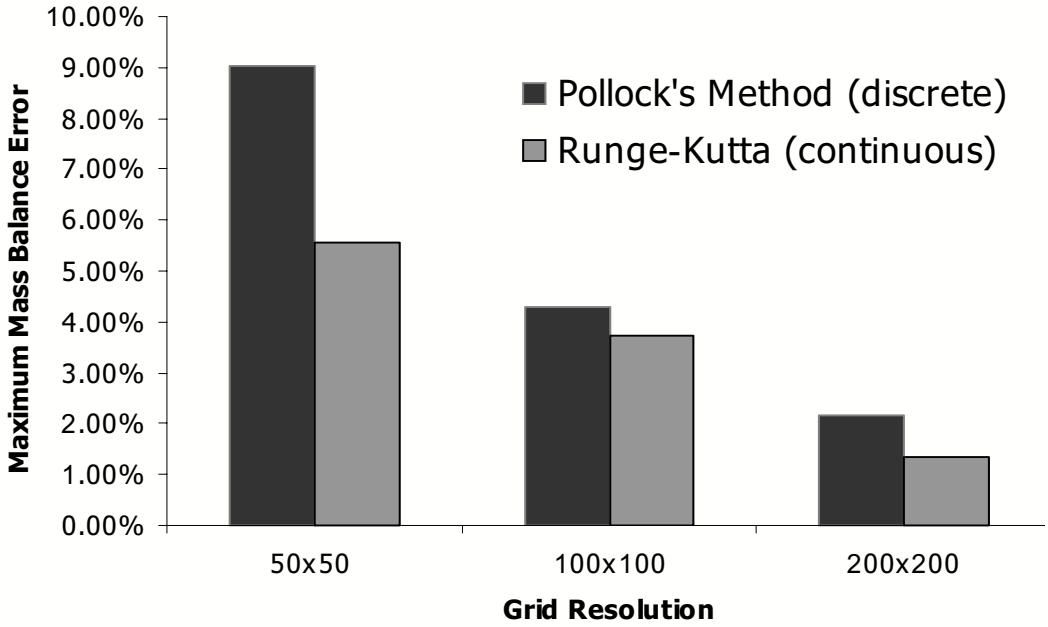

Figure 4.17: Maximum global mass balance errors for the backward method of characteristic test case. Either analytic (adaptive Runge-Kutta) or semi-analytic (Pollock's method) velocity information was used to trace backward characteristic paths.

use of a lower grid resolution are offset by the computational cost of the highly accurate Runge-Kutta method. It is expected that minor relaxation of the adaptive scheme can potentially reduce the computational cost significantly without a corresponding loss of BMOC accuracy. Less strict rules governing the adaptive time stepping, while implemented in CARDINAL, were not tested. Other intermediate alternatives, such as adaptive discretization for Pollock's method, or constant space step Runge-Kutta scheme, may prove the most beneficial tracking algorithms for use of characteristic methods. Such optimization of these algorithms is left for future research.

4.3 Discontinuous Conditions

The following section contains test results from models that incorporate the discontinuous conditions of section 3.7. These conditions are required to handle the infinitely thin internal boundary conditions in the analytic element method. This approach may prove advantageous for reducing the required mesh resolution in complex models by circumventing the adjacency constraints of standard finite element method.

4.3.1 Transport Across a Low Permeability Barrier

The following section demonstrates the successful implementation of the discontinuous mesh conditions for transport across a fully penetrating low permeability barrier. As outlined in section 3.7, using this approximate technique reduces the computational cost of the transport model by treating a barrier as an infinitely thin internal boundary condition. This internal condition does not require over-discretization along the barrier boundary, thus significantly reducing the overall number of degrees of freedom in the model.

The test case used to assess the quality of the multi-scale approximation consists of a low-permeability barrier surrounding a plume on 3 sides, with unconfined uniform flow from west to east. The model configuration is shown in figure 4.18a. The barrier was represented in the flow model using either the high order "leaky wall" condition of Strack (Strack 1989) or a high order inhomogeneity in conductivity. Parameters used in the simulation are shown in table 4.6.

Table 4.6: Parameters used in Low-conductivity barrier transport model

Flow Parameters	
aquifer conductivity (k)	0.1 m/d
aquifer base elevation (B)	0 m
barrier conductivity (k_w)	0.00001 m/d
avg. saturated thickness (k_w)	10 m
hydraulic gradient	-0.01 m/m
barrier thickness (t_w)	20 cm
downgradient barrier velocity	6.66e-5 m^2/d
Transport Parameters	
longitudinal dispersivity (α_l)	1 cm
transverse dispersivity (α_t)	1 cm
diffusion coefficient (D^*)	2e-6 m^2/d
initial source concentration	500 mg/L

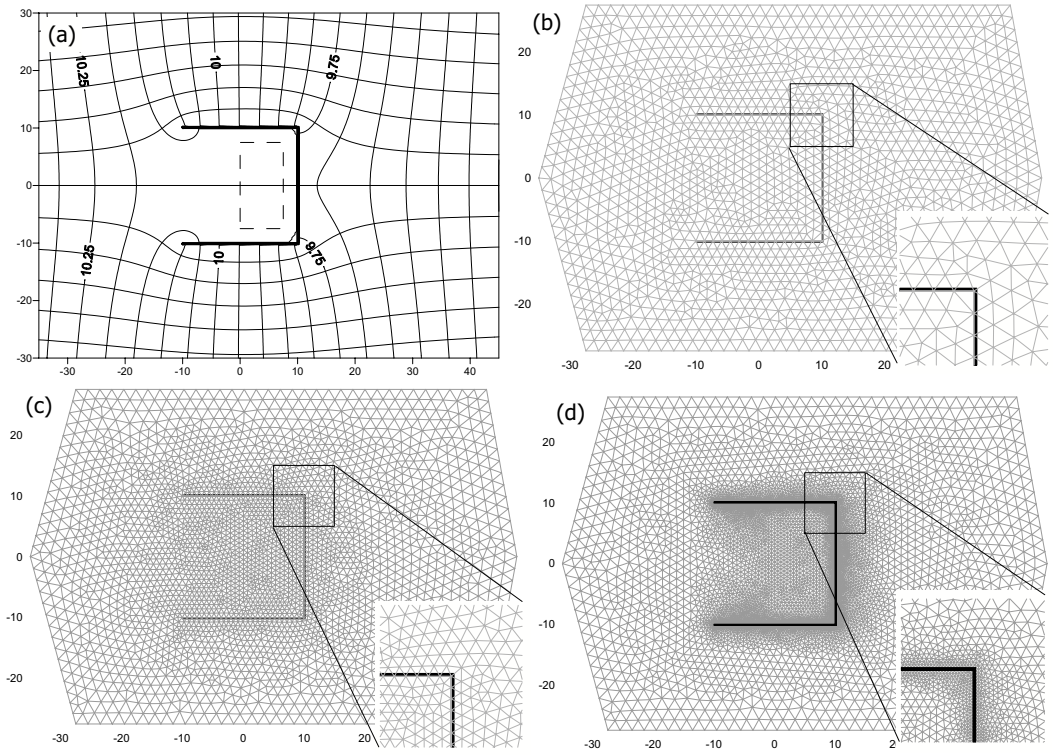

Figure 4.18: Test case setup and mesh configurations for low permeability barrier test case. (a) Head and stream function contours for flow around and through the backward-"C"-shaped low permeability barrier. The 500 mg/L initial source zone is shown with the dashed line. (b) Low-resolution finite element mesh (c) Medium-resolution finite element mesh and (d) High-resolution finite element mesh.

The barrier system was simulated using seven different algorithm/configuration combinations. First, the model was simulated at two different mesh resolutions using the classical (continuous) finite element method of section 3.6 (FECa, FECb) and the discontinuous method of section 3.7 (FEDa, FEDb). The continuous method ignores the gradient of concentration across the wall whereas the discontinuous method explicitly models the sharp change in vertically-averaged concentration across the barrier. These four models all used the "leaky wall" element to represent the barrier in the flow model. Used here as the "true" solution, a high-resolution continuous finite element model (FECc) was used to model transport through the barrier. In this high-resolution model, the barrier was modeled as a polygonal inhomogeneity in the flow model, and both the saturated thickness and the vertically-averaged concentration are continuous across the barrier, circumventing the need for a discontinuous condition. This high resolution model is assumed to provide the most accurate solution, but at a considerable computational cost. The purpose of developing the discontinuous condition was to reduce this computation by modeling transport across

the barrier in an approximate fashion, thus circumventing the need for fine discretization along the barrier.

In addition to the 5 models considered above, the simulation was run twice using the finite difference method on a high-resolution unevenly-spaced 275 x 200 (55000 cells) rectangular grid with a grid spacing of 20 cm in the regions adjacent to and near the barrier. Since the FD discretization constraints do not require any specific relationship between the barrier geometry and the grid, the transport model could be run twice on the same mesh with both the leaky wall representation (FDa) and the inhomogeneity representation (FDb) of the barrier. These two simulations were used to distinguish the effects of the difference in the flow field from the effects of the discontinuous finite element approximation.

The discretization, representational scheme, and computational costs of these seven models are summarized in table 4.7. All simulations were run on a Dell Optiplex GX260 with a pentium 4 processor. Note that the high resolution finite element model was run at a sufficient resolution to capture the concentration gradient across the barrier and is assumed to accurately model transport across the barrier. However, it was significantly more computationally intensive than the low-resolution finite element simulations, thus motivating the use of the discontinuous conditions.

Table 4.7: Low-conductivity barrier model configurations used to test the efficacy of the discontinuous mesh approximation.

Configuration	Resolution	DOF	Barrier Representation	Computational Time
FEDa	Low	1734	Leaky wall	103 sec
FEDb	Med	3100	Leaky wall	281 sec
FECa	Low	1693	Leaky wall	102 sec
FECb	Med	3026	Leaky Wall	268 sec
FECc	High	6988	Inhomogeneity	3264 sec
FDa	High	55000	Leaky wall	391 sec
FDb	High	55000	Inhomogeneity	412 sec

DOF: Transport model degrees of freedom (no. of nodes or cells)

Before assessing the discontinuous and continuous representations of transport through the barrier, it was desirable to first identify the effects of the two different flow discretizations used. In both breakthrough curves and plume results, differences between finite difference models using the different flow representation of the barrier were roughly less than 2% for the concentration value at any point and time. This difference is negligible compared to the differences exhibited between the discontinuous mesh and continuous mesh simulations. This demonstrates that the differences

in results between the finite element simulations may be attributed solely to the discretization and handling of the transport problem.

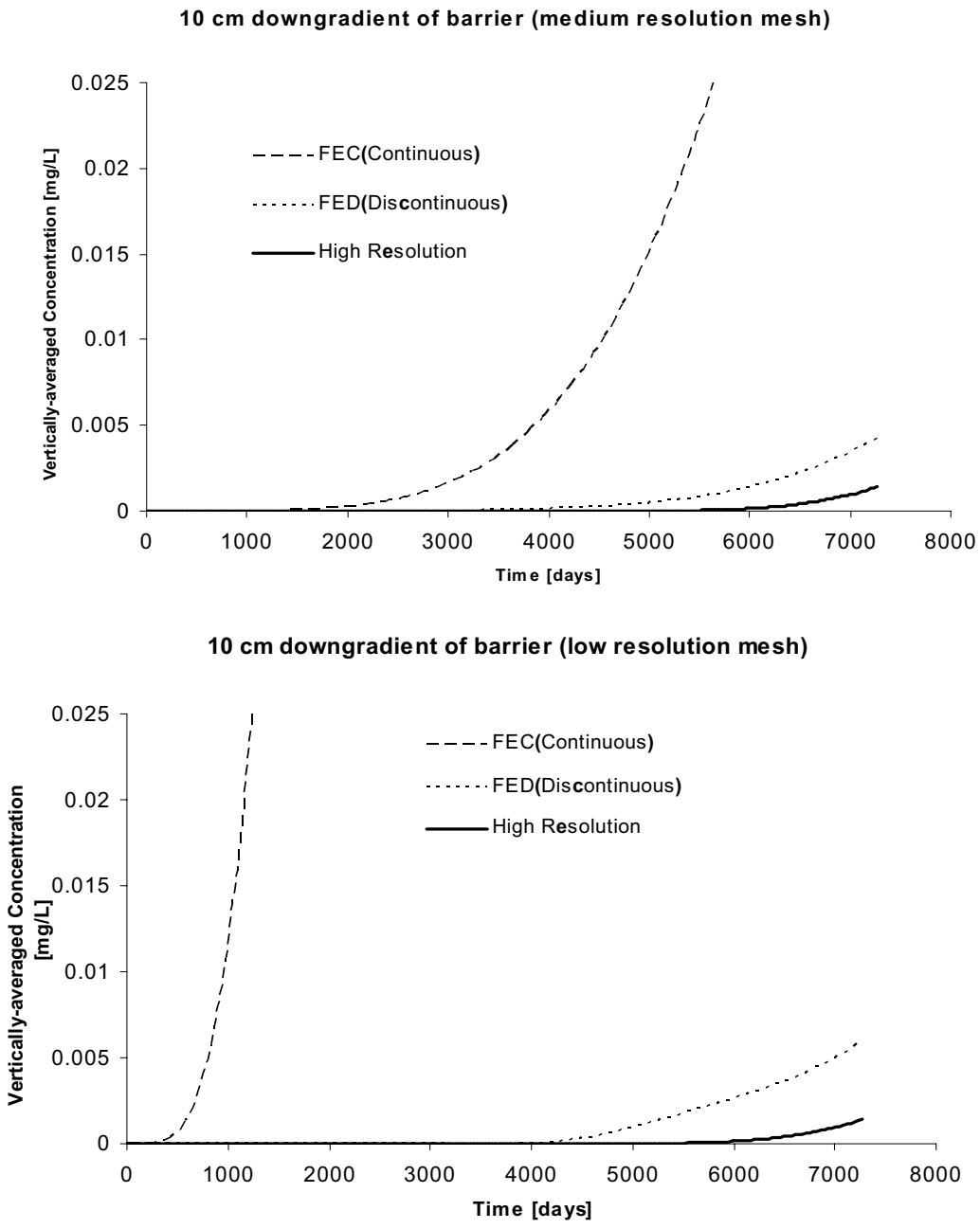

Figure 4.19: Breakthrough curves for discontinuous transport across a low conductivity barrier. The use of a finite element method with discontinuous mesh conditions produces solutions much closer to the high resolution finite difference approach than the continuous (traditional) FE method.

Breakthrough curves along the center axis of the domain at distances of $10cm$ downgradient are shown in figure 4.19. As can be seen from these curves, the approximate discontinuous model

produces results closer to the the high resolution model. The classical low-resolution FE model performs poorly in comparison, especially at the lowest resolution. The accuracy of both continuous and discontinuous models improve with increased mesh resolution, with the discontinuous method consistently closer to the high resolution FE solution. The discontinuous finite element method may be deemed as an appropriate method for approximating this sharp internal model condition, one which, while approximate, requires significantly fewer degrees of freedom than modeling the transport across the boundary explicitly. It is also important to note that a more appropriate estimate of the dispersive flux across the barrier will provide even better results. The dispersive/diffusive flux is overestimated with the discontinuous approximation of equation 3.113, because of the assumption of a linear concentration gradient across the barrier. A more rigorous analysis is needed to develop robust discontinuous flux conditions consistent with the physics of the problem (e.g., a 1D transport model solved across the discontinuity). However, the current approximation is deemed adequate for preliminary testing of system designs, and significantly more appropriate than using a conventional low resolution finite element model. More advanced means of determining the flux term are beyond the scope of this dissertation.

The results of this test demonstrate that for a very challenging application, the AEM-based discontinuous method can provide a decent approximation to the transport phenomenon at a reduced computational cost, and all that is required is the addition of a few more degrees of freedom than the conventional FEM. However, the quality of the approximation depends upon the particulars of the implementation: a high-resolution conventional FEM will often be the better choice for such difficult problems, but a a considerable computational cost. The technique presented here is likely better suited for preliminary hypothesis testing, whereas for policy or design decisions, a high resolution model could be used to obtain more rigorous estimates of breakthrough curves, etc.

4.3.2 Transport Around an Impermeable Wall

The extreme case of transport past an infinitely thin impermeable wall in the subsurface is a challenging test of the ability of a numerical method to simulate the impact of sharp discontinuities in the transport system. To investigate and compare the effectiveness of the finite element and finite difference methods for handling this difficult condition, a simple test case was run. An initial concentration source of 100 mg/L was specified upstream of an infinitely thin impermeable barrier (modeled with the same "leaky wall" element as used above) in uniform flow of 1 m^2/d. The

system configuration and results of both the discontinuous finite element method and standard finite difference method at a time of 600 days is shown in figure 4.20.

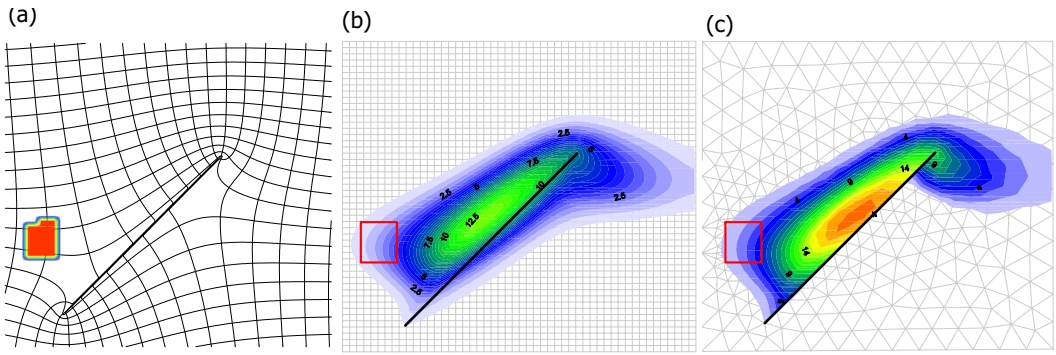

Figure 4.20: Results of finite difference and finite element simulations of transport around an impermeable wall. (a) Model configuration, flow net, and initial source zone (b) Plume after 600 days as modeled with the finite difference method on a 50x50 grid (c) Plume after 600 days as modeled with the discontinuous finite element method.

As apparent from figure 4.20, the finite element method does not allow any solute mass to cross the impermeable barrier, and the concentration is appropriately discontinuous across the boundary. However, the finite difference method has no means of appropriately handling the discontinuous conditions unless the discontinuity is aligned with a cell face. While mass balance, Peclet, and Courant constraints were met for both methods, discretization error still occurs in the finite difference method, because fluxes are averaged over the cell perimiter, and thus cannot simulate a no flow condition across the cell. This simple illustrative test case was not analyzed in a quantitative fashion. Rather, it qualitatively demonstrates (1) the benefits of the geometric flexibility of the finite element method, (2) the consistency of the discontinuous condition, and (3) the potential errors that may arise when discretizing discontinuous AEM flow solutions using finite difference methods.

4.4 Field Scale Reactive Transport Through a PRB

One of the most promising applications of AEM-based transport models is to problems characterized by both regional-scale flow features and highly localized chemical reactions. The design of subsurface remediation systems is one such application. In particular, the permeable reactive barrier (PRB) is an example of a system where both factors are important. PRBs are engineered trenches placed in the path of a groundwater plume, filled with reactive material that sorbs or transforms the contaminants *in situ*. One type of PRB, made of natural zeolite, has been tested at both laboratory and pilot scales (Lee et al. 1998; Moore et al. 2000) for remediation of radioactive Strontium-90 (Sr90). The dominant reaction phenomena within the barrier is competitive ion exchange. These barriers function by providing a porous media surface that has a strong selectivity for Sr90.

The performance of a PRB depends both the flow regime, which may be influenced by regional features, and the biochemistry within the PRB. To date, the design of PRBs has been approached using a decoupled approach in which the barrier is modeled using a simplified batch or one-dimensional model, and the field-scale flow and contaminant behavior outside the barrier is idealized as a boundary condition (e.g., Gavaskar et al. (1998), EPA (2000), Rabideau et al. (2001)). A separate flow model is often used to evaluate hydraulic capture, but the potential coupling between flow and PRB reactions is ignored. There are several reasons why a "whole system" model that simultaneously considers both flow and transport would be desirable: (1) the potentially nonuniform flow regime inside the barrier could be more accurately represented, avoiding the need to select a "representative" velocity for use in a separate model, (2) the temporal and spatially nonuniform nature of the influent contaminant plume could be captured, and (3) a single integrated model for performance assessment would be much simpler to use, visualize, and communicate to stakeholders.

The previous test cases in this dissertation simulated non-reactive transport of a single solute. The following series of reactive test cases, implemented using the finite element method of section 3.6, were developed to simulate field-scale transport through a zeolite PRB. The purposes of these tests were to demonstrate the ability of CARDINAL to effectively simulate complex multi-solute reactive transport using a conventional non-iterative split-operator approach and adaptive spatial enabling of reactions. As discussed below, future work will be required to identify the most efficient

configuration for PRB applications, and to assess the potential for computational artifacts. To the author's knowledge, the test case represents the first effort to simultaneously model a chemically complex PRB within a field-scale flow regime. The results of the following tests are not particular to the use of the analytic element method. Rather, the following computationally challenging simulations motivate the need to further reduce grid and mesh constraints on reactive transport models.

The PRB test case is based loosely on the chemistry of the zeolite treatment wall installed at the West Valley Demonstration site in Western New York. As discussed by Rabideau et al. (2004), performance assessment for this project was conducted using a one-dimensional model based on an idealized flow field and PRB influent concentrations. The PRB was designed to remove Sr90 from groundwater by cation exchange. The complexity of the application arises from the fact naturally occurring cations compete for exchange sites on the zeolite, and that eventually the capacity to remove Sr is exhausted and the media must be replaced. The model proposed by Rabideau et al. (2004) considers 6 aqueous and 6 sorbed species including natural and radioactive Sr. The modeled behavior of the system can be considered in two stages: (1) an initial period, in which the zeolite equilibrates with the mix of dominant cations in the groundwater, which is expressed as an "ion exchange front" that occurs in the breakthrough curve after approximately 50 pore volumes, and (3) an extended period of "active" PRB life in which the most preferred solute (Sr) continues to displace other cations and is essentially absent from the effluent, and (3) a "breakthrough" period, in which the equilibrium with the strongly sorbing Sr is reached and the PRB effluent approaches the pre-barrier conditions for all solutes. Because of the long time required to reach breakthrough (thousands of pore volumes), the test case focuses the initial period in which the first ion exchange front appears.

The configuration of the test case is shown in figure 4.21. A conventional "funnel-and-gate" barrier configuration was used. The 56 meter long impermeable walls (modeled as "leaky wall" analytic elements) channel groundwater through the 2m thick barrier (modeled as a polygonal inhomogeneity in conductivity). The regional uniform flow was specified as 1 m^2/d, with a background hydraulic conductivity of 10 m/d and a barrier conductivity of 12 m/d. The 20 m wide barrier has a porosity, θ, of 0.6 (twice that of the background). The 10 μg/L initial source zone of radioactive strontium 90 was placed 50 m upgradient of the PRB, so that the influx of strontium to the wall would be a gradual pulse of increased Sr90 concentration. The unconfined aquifer has an average

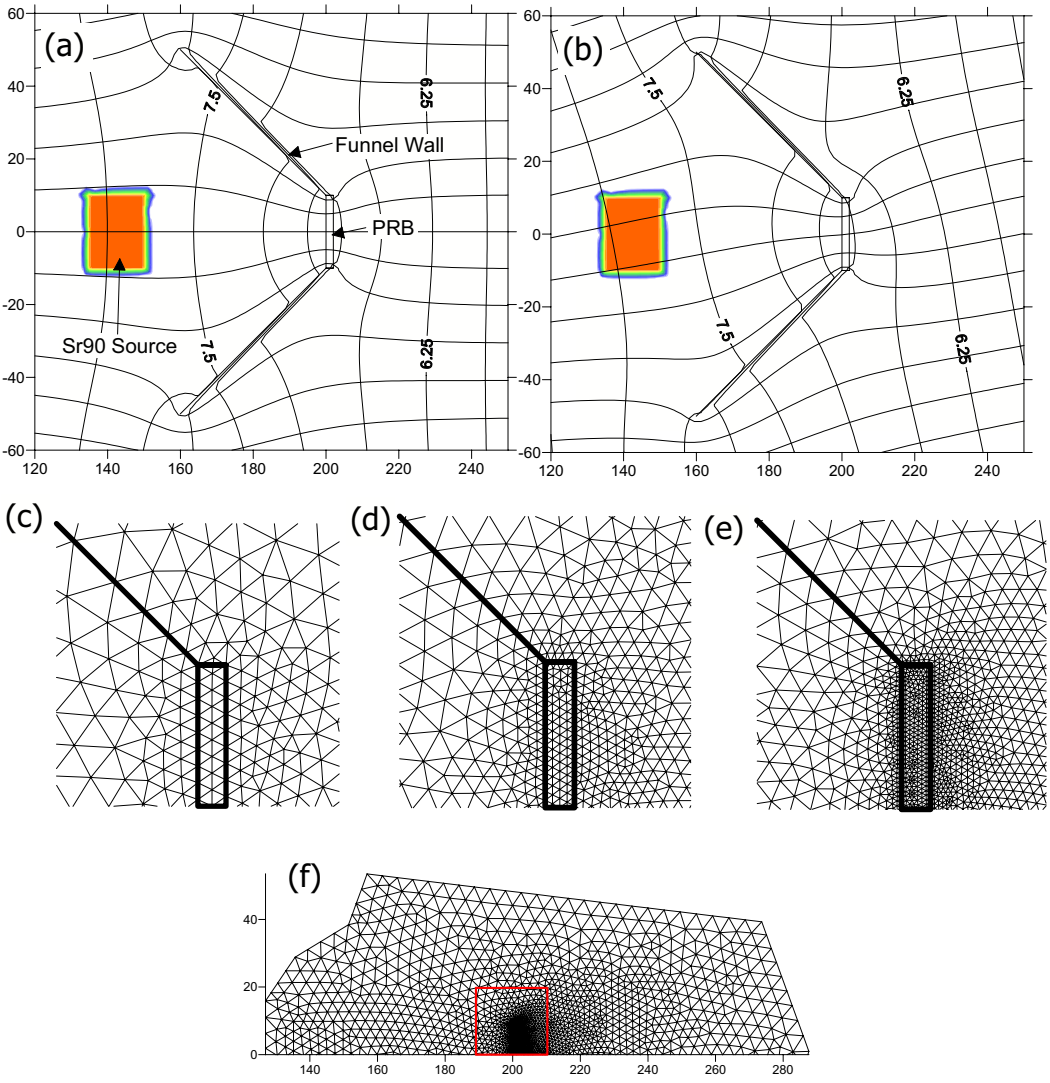

Figure 4.21: Permeable reactive barrier test case configuration. (a) System geometry, head, and stream function contours for flow perpendicular to barrier. (b) Head and stream function contours for angular flow (10 degrees from x-axis) (c, d, and e) Local mesh geometry near funnel gate mouth for mesh 2 (1000 nodes), mesh 4 (3496 nodes), and mesh 7 (3473 nodes), respectively. (f) Top half of system mesh geometry for mesh 7.

saturated thickness of 7 meters, resulting in an average flow velocity of 0.5 m/day in the aquifer, but a flow velocity of roughly 1 m/day through the barrier. Three simulations were run using three different mesh resolutions (shown in figure 4.21c-e). To reduce the computational cost, the cation exchange reaction calculations were only applied at nodes within the PRB, as discussed in section 3.8. It is important to note that the barrier component of the funnel-and-gate system, while difficult to model using a grid-based finite different approach, are easily accommodated using the "leaky wall" line element, an appealing feature of the AEM-based approach

The chemical and hydraulic parameters for the test case are shown in table 4.8. The majority of the reaction parameters were obtained from Rabideau et al. (2004), and the background/initial concentrations of the aqueous cations were set to be within the range of reasonable field values reported by several investigators (e.g., Carlyle et al. (2004)).

Table 4.8: Cation Exchange Test Case Chemical Parameters

	Q_{cx}	ρ_b	μ_a	θ
	[meq/g]	[kg/L]	[meq/L]	[-]
Aquifer	N/A	1.86	N/A	0.3
Zeolite	1.143[a]	0.82[a]	3.504[a]	0.6

			Zeolite Barrier	
Ion	Background C^c	Mol. Wt.	Initial S	$K_{x/Na}$
	[mg/L]	[g/mol]	[mg/kg]	[-];[mmol/L]†
Na^+	68[b]	23	6000[a]	N/A
K^+	3.5[b]	39	25000[a]	28[a]
Mg^{2+}	15[b]	24	120[a]	300[a†]
Ca^{2+}	100[b]	40	4600[a]	350[a†]
Sr^{2+}	0.2[b]	87.6	87.6[a]	4800[a†]
$Sr_{90}{}^{2+}$	0.00[b]	90	0.0[a]	4800[a†]
$Sr_{90}{}^{2+}$(source)	0.01[b]	90	0.0[a]	4800[a†]

[a] - Obtained from Rabideau et al. (2004)
[b] - Set at reasonable field values
[c] - Background concentrations were used for initial concentrations and influx conditions on upgradient system boundaries
† - Divalent selectivity coefficients have native units of mmol/L; Monovalent selectivity coefficients have no units.

Figure 4.22 shows 18 different breakthrough curves for the six different cations simulated in the perpendicular flow test case. These concentration profiles were calculated on three different finite element meshes at a point just downstream of the zeolite barrier, in the center of the funnel and gate system. These results are similar in behavior to those of the 1-dimensional PRB simulations reported by Rabideau et al. (2004), and exhibit the same essential features (i.e., the crossover of Na and Ca concentrations and the relative concentrations of the cations before and after the development of the ion exchange front). This result suggests that the cation exchange reaction formulation (in appendix G) was implemented properly. Additional comparisons with the 1D transport software MOUSER (Rabideau 2003) (not reported here) were used to confirm the accuracy of the reaction module as implemented in CARDINAL. The purpose of this test case is not to verify previous modeling results or compare the model to field data, but rather to investigate the advantages and disadvantages of simulating complex reactive barrier systems using 2D site models.

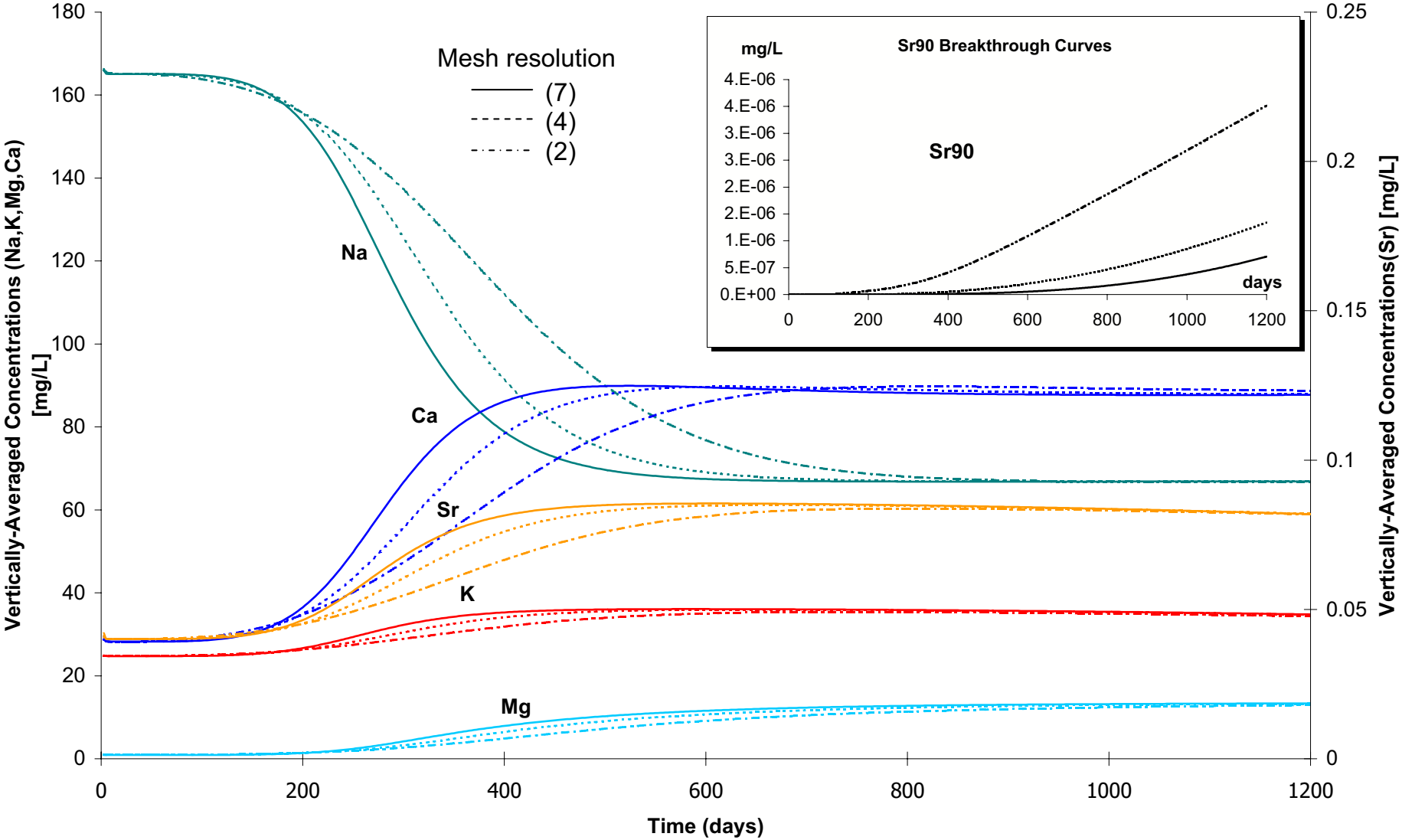

Figure 4.22: Cation breakthrough curves as simulated using multiple mesh resolutions. The (2), (4), and (7) designations refer to the resolution of the finite element mesh used for simulation.

The primary difference between the simulation of Rabideau et al. (2004) and those presented here is that transport upgradient of the barrier was explicitly simulated, rather than specified as a forcing function to a 1-dimensional model. That is, instead of specifying the strontium 90 influx concentrations as constant, the influx conditions to the wall are a function of field scale transport phenomena. The modeled strontium 90 arrives at the wall as a near-Gaussian pulse of contaminant. This distinction accounts for most of the differences in the behavior of the Sr90 breakthrough curves between the 1D models simulated by Rabideau et. al and those depicted here. Additional differences are ascribed to the lack of simulating decay of Sr90 in this test case. Also, the time period of simulation (in terms of pore volumes flushed through the barrier) was significantly shorter because the computational cost of modeling a 20- or 30-year design period were prohibitive. The 3.3 year simulations shown here (using a maximum mesh Courant number of 0.1) ran from 7 hours (the 1000 node mesh) to 76 hours (the 3473 node mesh) on a 1Ghz Pentium 3 processor. Most of this computational cost is due to the simulation of the reaction at many nodes within the barrier (all mesh configurations have relatively dense spacing within the barrier).

As apparent from the figure, the 2D mesh resolution has a minor effect upon the breakthrough curves for the non-radioactive cations, which enter the barrier at a constant concentration equal to the ambient concentration. However, the three breakthrough curves for strontium-90 exhibit more pronounced differences. Since the breakthrough curves just upgradient of the barrier (not shown) exhibit roughly the same degree of difference, it appears that the distinction is primarily a function of the accuracy of the transport simulation upgradient of the PRB. While this result may be particular to the test case shown here, it suggests that a more appealing option for simulating reactive barrier systems is to decouple the problem into a (2D or 3D) single species field scale simulation and one or more (1D) barrier/column scale reactive transport simulations. This has been the standard approach in the literature (Gavaskar et al. 1998; Rabideau et al. 2001). However, the appropriateness of this approach has never been tested against a complete 2D transport model.

The primary result from the test case is that it demonstrates the ability of the AEM-based modeling approach to simulate chemically complex reactive transport. This result is not surprising because the underlying operator splitting methodology has been successfully demonstrated in many published applications. However, the successful implementation for this test case (and others not reported here) lays the groundwork for future expansion to other scenarios of interest. While it is expected that the AEM-based approach will be especially appealing for particular applications

involving large domains and complex chemistry (e.g., regional scale carbon and nutrient cycling), detailed evaluation will be the subject of future work.

Despite the successful PRB simulations, it is clear that additional work is needed to improve the computational performance for these challenging applications. The choice of a sorbing barrier was perhaps the most difficult of candidate applications because of the need to model the full breakthrough curve of the sorbing solute, which would require a simulation period of decades and would be infeasible for the current model configuration. A more promising application would be the popular iron-based PRB in which "steady-state" conditions (with respect to multi-solute decay and production) are reached relatively quickly. The proposed AEM-based approach could potentially expand the range of performance assessment of these systems to include a more accurate consideration of flow field and influent concentration variability. The details of these implementations will be the subject of future work.

Chapter 5

Discussion

The following chapter summarizes the methods and results contained within this dissertation, and discusses the key conclusions of this research.

5.1 Linking AEM and Transport

The primary contribution of this dissertation is the detailed development of approaches and algorithms that enable the use of AEM flow solutions by contaminant transport simulators. A significant byproduct of this work is the implementation of these algorithms within the robust AEM-based software tool, CARDINAL. The new techniques introduced here have been used to link AEM flow solutions to a variety of Eulerian, Lagrangian, and Eulerian-Lagrangian solute transport algorithms, including the finite element method, finite difference method, backwards method of characteristics, and random walk. The implementation of this AEM-based approach to transport modeling illuminates a few important points about the possibilities, advantages, and pitfalls of the AEM/transport model merger.

First, it has been demonstrated that finite difference and finite element flow solutions are not a necessary prerequisite for finite difference or finite element transport simulations. Any shallow aquifer system can be simulated using AEM (as opposed to discrete methods) and used as a basis for 2D reactive transport simulation without loss of model quality. Carefully selected test cases (as described in section 4.1) have demonstrated that transport models using analytic element or finite difference flow solutions can produce results that are, for all practical purposes, equivalent. The benchmark tests furthermore demonstrate that AEM-based algorithms can replicate basic

analytic solutions to simple transport problems, but are plagued by the same numerical issues as conventional transport simulation methods (i.e., numerical dispersion and oscillation).

Second, for many realistic cases, the use of an analytic element flow solution can improve the overall quality of a transport model, without increasing the resolution of the corresponding grid or mesh. This is due to the highly accurate water balance and velocity representation inherent in AEM flow solutions. Methods for preserving the near-perfect water balance during the translation of analytic flow solutions to a discrete (finite difference or finite element) equivalent were developed in sections 3.3.2 and 3.6.3. This water balance is often more precise than that obtained from discrete flow models, and can have a significant impact upon the quality of a transport simulation, as demonstrated with the zeroth-order test case of section 4.1.3. The results of this test case highlighted the danger of using a conservative formulation of the ADRE that can conceal errors associated with an inexact water balance and underlined the need for the intelligent discretization techniques developed in section 3.3.2. The exact water balance of AEM is expected to prove useful for modeling transport in systems difficult to simulate accurately with finite difference flow methods (e.g., systems with very high contrasts in hydraulic conductivity).

In addition to the benefits apparent in using AEM for Eulerian simulation of contaminant transport, particle-based methods (e.g., MOC and the random walk method) can be improved by using the continuous representation of velocities and other parameters. The EPVA random walk method, tested in section 4.2.2, was not demonstrably improved by the use of closed-form solutions for the "drift" term, even though the effective parameter formulation had the appealing property of being entirely grid-independent. The characteristic-based Eulerian-Lagrangian methods fared better. The results from the simple backward method of characteristics tests (section 4.2.4) suggest that the use of continuous velocity information will provide greater accuracy to any EL method without additional discretization. Unfortunately, while the continuous approach provides additional accuracy, existing high-precision tracking algorithms are often computationally inhibitive, and need to be optimized for speed. It is expected that alternative discretization schemes for the velocity field and/or use of a less stringent adaptive Runge-Kutta method could reduce this cost to an acceptable level. Such optimizations of the tracking procedure are reserved for future work, and are discussed briefly below in section 5.8.

Intelligent use of analytic element flow solutions has been shown to improve the quality of contaminant transport simulation algorithms without increasing the number of degrees of freedom in

the model. However, this use requires a corresponding increase in complexity of the transport algorithms. For example, the finite difference method, generally considered to be the simplest of the contaminant transport algorithms, requires unique closed-form integration schemes for translation of analytic element fluxes. Similarly, the finite element method requires higher-order numerical integration methods to properly use AEM velocity and flux information and requires sophisticated unstructured mesh generation algorithms to accommodate AEM geometry. While the use of continuous parameters is appealing, it can introduce significant complexity to the model that, in turn, can introduce additional computational costs that somewhat offset the benefit of using AEM. It is expected that a compromise between discrete and continuous representation will be most beneficial, using more accurate continuous information while intelligently averaging quantities to obtain the speed of discrete parameterization. One potential compromise (for particle tracking) is discussed later in section 5.5.

Importantly, the process of developing AEM-based simulation algorithms provided information about what *not* to do when developing transport simulation algorithms that utilize AEM. Some of these results are obvious (such as the limitations of the Dupuit-Forcheimer assumption), some significantly less so (such as the impediment to solving the EPVA transport formulation using finite element techniques discussed in section 3.5.1). A brief summary of some important "lessons learned" is provided here as a reference for future work:

- Care is needed in handling singularities. In finite element methods, for example, the triangles used for integration must be slightly inset from the element boundaries to avoid evaluating singular parameters. Likewise, in the finite difference method, care must be taken to ensure that grid cell boundaries do not intersect point singularities (wells or the ends of linesinks).

- It is important to understand the effects of discretization across discontinuities in velocity and/or saturated thickness. Multiple techniques were developed in this dissertation (i.e., mesh generation and discontinuous mesh conditions) to avoid the effects of improper discretization. However, for finite difference methods, the results of models with discontinuous parameters must be approached with caution, as many models may provide results that are inconsistent with the (insufficiently resolved) physics of the problem, as shown in section 4.3.2. Simulating the same system using multiple grid orientations and resolutions is recommend to test the sensitivity of the problem to discretization.

- It is important to interpret the results from vertically-averaged simulations in the context of the assumptions required to use this 2-dimensional approximation. Specifically, variation in the vertical distributions of mass can influence the degree of both longitudinal and transverse spreading of a plume.

Significantly, the existence of a coupled AEM flow and vertically-averaged transport simulator has enabled the development of transport models that can use existing AEM flow solutions. This will directly benefit practitioners who have invested time in existing AEM-based modeling projects. It also expands the general applicability of the analytic element method, which may now be used as the basis of water quality investigations.

5.2 Reducing the Size of the Transport Problem

The "size" of the transport problem is defined here as the total number of degrees of freedom calculated during the course of the model ([no. of species/components] x [no. of nodes/cells] x [no. of time steps]). This size is often increased by requiring the use of a single grid or mesh designed to model both flow *and* transport. It was hypothesized that the use of the grid-free analytic element method would reduce the size of any given transport model by (1) affording more flexibility in the discretization process and (2) improving the accuracy of the flow-based transport parameters. Both of these advances were expected to reduce the total number of required nodes or cell in a transport model.

Demonstrating that AEM may be used as a basis for solute transport was the first step towards reducing the size of the transport problem. Use of AEM allows the transport system to be discretized without having to accommodate the grid or mesh structure of a discrete flow model. The flow-based requirements of grid or mesh design when using an analytic element flow solution are minor in comparison: the finite difference grid has no specific requirements and finite element meshes only require consistency along parameter discontinuities (as shown in section 3.6.2). Of course, relevant Peclet, Courant, and adjacency constraints must still be satisfied, but the mesh is essentially independent of the artifacts of flow discretization.

As an example of the benefits of the AEM-based approach, consider the case of transport near a well. Discrete flow models require high resolution near the well because the pumping well induces high pressure gradients. Transport models, on the other hand, benefit from coarser discretization

near the well. The Courant constraint, which determines the simulation time step size, suggests that, to optimize the speed of simulation the grid resolution should be coarser near zones of higher velocity. This is in direct opposition to the needs of the flow model. This distinction is illustrated in figure 5.1, which shows two finite difference grids and two finite element meshes, each designed to either improve the flow model accuracy (b and d) or maximize the speed of the transport calculation (by reducing the number of nodes and increasing the time step of the simulation)(a and c). This incongruence of flow and transport grids, irrelevant in systems modeled with AEM, is amplified when the well is in a low-conductivity zone, and the pumping induced hydraulic gradient is even larger. For AEM-based simulations, only the discretization for the transport model must be considered.

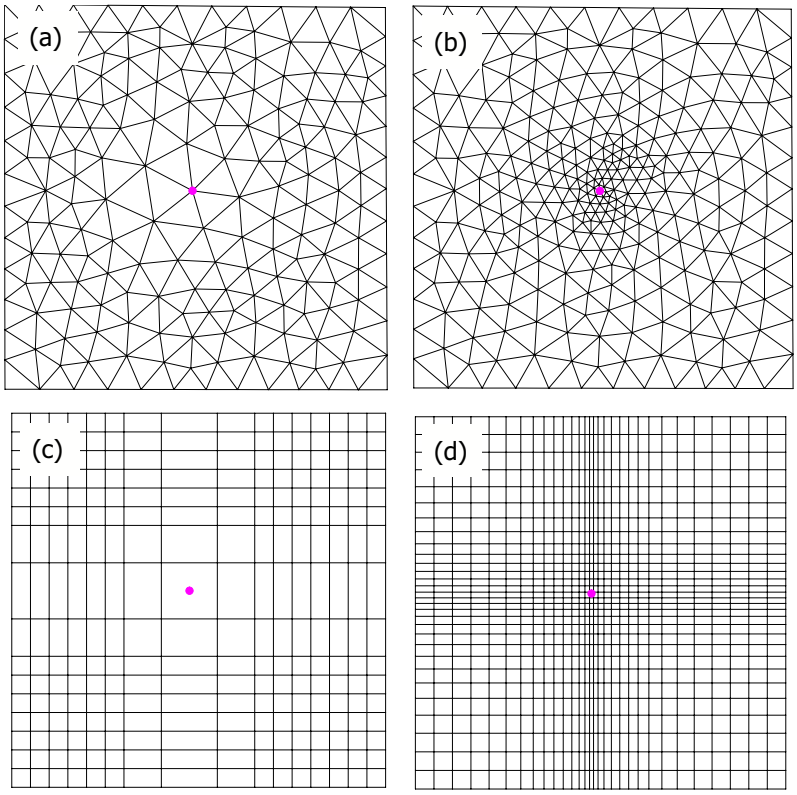

Figure 5.1: Optimal system grid discretization for flow models and for transport models. Finite element mesh (a) and finite difference grid (c) were designed to minimize the required time step size for the model (consequently reducing the number of nodes). Finite element mesh (b) and finite difference grid (d) were designed to accurately model the hydraulic gradient near the well.

Removing the influence of the flow grid on the transport discretization process is a significant contribution. However, perhaps the clearest example of the added flexibility afforded by AEM flow solutions is the significant reduction in the required number of nodes needed to resolve transport

behavior near relatively small or thin hydrogeologic features. The new discontinuous mesh approach of section 3.7, dependant upon the precision and resolution of high-order AEM flow solutions, provided a means of reducing the number of nodes in the system while still providing an adequate (though approximate) solution for solute transport across infinitely thin features.

In addition to this reduction in constraints on grid design, the added accuracy of AEM flow solutions often increases the quality of the transport simulation without adding additional nodes or cells. Thus, for the same level of model error, fewer degrees of freedom are required. This was demonstrated most dramatically with the backwards method of characteristics test of section 4.2.4, but is also apparent from the results of the finite element residual integration test of section 4.2.3. While appealing in theory, the EPVA approach (developed to further reduce discretization error of models) has not yet been coupled to a transport solution method that can fully exploit its advantages. However, it is hoped that later integration with meshless methods or more sophisticated finite element methods may prove successful.

Even with the flexibility in mesh or grid design afforded by the use of AEM flow solutions, the Peclet, Courant, and adjacency constraints imposed by Eulerian methods remain the dominant factor constraining the size of the transport model. The less prohibitive Peclet constraints of Eulerian-Lagrangian methods are appealing, allowing use of coarser discretization and larger time steps. However, the inability of these methods to preserve the global or local mass balance is a drawback. This is especially true with reactive transport, which can be highly sensitive to minor errors in concentration. For similar reasons, fully Lagrangian methods (subject to local conservation problems) are also not appealing for reactive transport simulation in complex flow domains. These methods can be prohibitively expensive when the small time steps required for reactive transport modeling is combined with the large number of particles required to resolve the plume distribution. Use of the analytic element method does not appear to significantly relieve either of these limitations, despite the removal of the tracking errors (Oliveira and Baptista 1998; Ruan and McLaughlin 1999) associated with conventional flow solutions.

The ideal AEM-based reactive transport model would be limited by Courant constraints only, which, in contrast to the Peclet and adjacency constraints, is a limit imposed by the physics of the problem as well as the mathematics. This method would additionally maintain global and local mass balance and incur a minimal degree of numerical dispersion. The only existing method that appears to meet this criteria is the Eulerian-Lagrangian localized adjoint method (ELLAM)

of Celia et al. (1990), which is primarily limited by Courant constraints and adjacency constraints. It is possible that a 2D multigrid ELLAM implementation, integrated with the precise tracking, exact water balance, and flexibility in grid design of AEM, would prove to be the most beneficial approach for reducing the size of the transport problem. These developments will be the subject of future work.

While not related to the use of AEM, the simple techniques for enabling or disabling reaction calculations presented in section 3.8 can also reduce the size of the transport model considerably. This benefit comes not from reducing the number of degrees of freedom in the model, but rather by removing unnecessary calculations from the simulation process.

5.3 Using Continuous Parameters

One of the key goals of this research was to identify, develop, and analyze options for using continuous AEM-based parameters as an input to different transport models. Depending upon the particular numerical method used for transport simulation, the use of continuous parameterization requires intelligent discretization, pathline integration, volume integration, and/or volume-averaging schemes. Each transport simulation method can use continuous parameters in different ways, as summarized in this section.

5.3.1 Finite Difference Methods

Finite difference methods are probably the most limited with regards to their ability to incorporate continuous parameters. The method relies upon a discrete representation of both independent and dependent parameters, with parameters such as saturated thickness and velocity represented by either (1) volume/area-averaged quantities (e.g., concentrations, saturated thicknesses) or (2) transect/line-averaged quantites (e.g., fluxes). While the methods for calculating cell-integrated fluxes described in section 3.3.2 are robust, some interesting artifacts of discretization are still present.

The finite difference discretization process may introduce errors if the velocity is discontinuous within a cell, rather than along a cell boundary. Because of the carefully selected geometry of the test cases in this dissertation, this type of error was only apparent with the impermeable wall test case of section 4.3.2. In that particular case, the discontinuity resulted in non-local propagation of

error (non-physical flux of solute through the impermeable boundary). In the MT3DMS test case of section 4.1.3, cell faces were aligned with discontinuities, and no error was present. Additional testing found that the magnitude of this discretization error depends upon the particulars of the system, and most reasonable systems exhibit local errors only. One such model is illustrated in figure 5.2. A non-representative concentration may be obtained at the center in the highlighted cell in the figure because the mass flux into the cell (in fact limited to the small bottom right corner of the cell) is averaged over the entire cell perimeter. Such errors are mostly local in nature, with a few notable exceptions (e.g., near a thin impermeable feature or a single cell has multiple intersecting discontinuities).

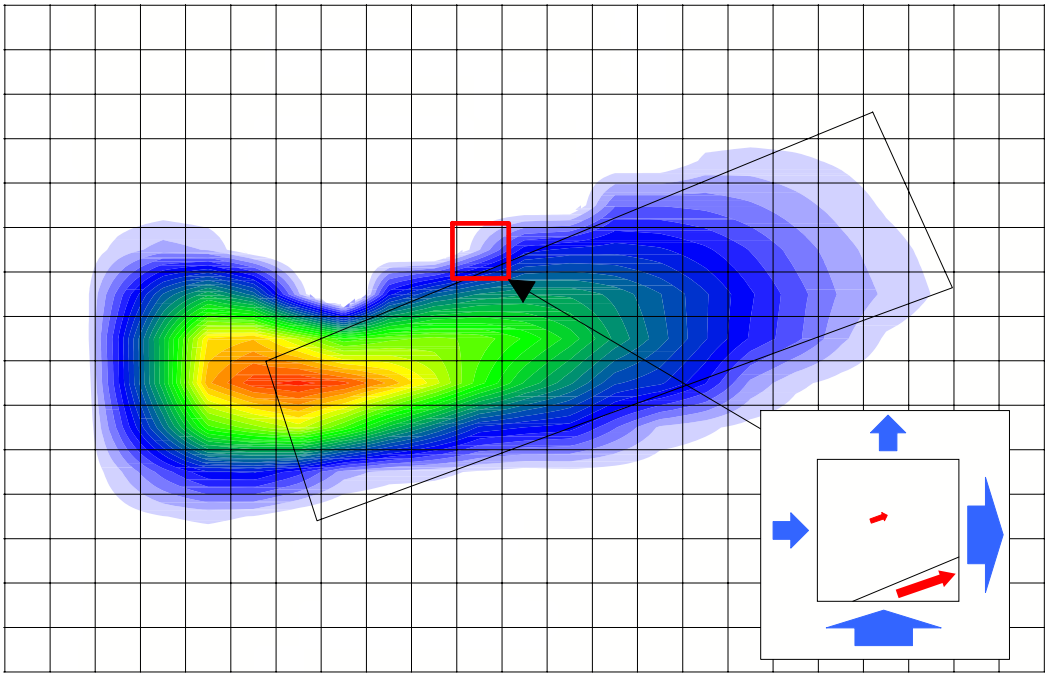

Figure 5.2: A plume modeled using the finite difference method is shown advancing through a highly conductive polygonal inhomogeneity in hydraulic conductivity. The inset depicts the face-averaged fluxes in the highlighted cell, which cannot accurately depict the actual local distribution of flux (higher within the inhomogeneity than outside it). This causes local errors in the concentration distribution.

Though more restricted in their ability to handle certain types of continuous (or sharply discontinuous) parameters, the finite difference method is generally the most robust of the methods implemented in CARDINAL, due to the use of the divergence form of the governing equation. However, this robustness (in terms of mass balance), can obscure local errors near features that are of smaller scale than the grid cells.

5.3.2 Finite Element Methods

The revised Eulerian finite element method developed here incorporates the effects of continuous parameters quite well. The generic formulation of the finite element system of equations is expressed in terms of integrals of continuous functions over the domain. Whereas conventional FE methods (e.g., Istok (1989)) use a piecewise continuous representation of velocity and other parameters, use of AEM flow solutions allows the method to be implemented without deviating from the original continuous formulation of the finite element residual. Only the dependent variable of concentration needs to be discretized. However, it is also apparent (from the results of section 4.2.3) that the errors associated with transforming an AEM solution into finite-element-averaged values are negligible if higher order integration schemes are used to calculate the element velocities. This allows discretized AEM solutions to be exported to alternative finite element software products (e.g., FEFLOW (Diersch 1998b)) with little loss of accuracy.

In addition to accommodating smoothly continuous parameters, the finite element method is able to handle sharp discontinuities in the parameter field if finite element sides are aligned with analytic element boundaries. Unlike with FD methods, when finite element methods are used, the only parameter discretization error accrues from the use of the basis function gradient to calculate the influence of parameter (e.g., velocity) derivatives. The information contained in the spatially continuous parameters is fully preserved.

Additional improvements to the AEM-based finite element method are needed to handle two special artifacts of a continuous AEM representation. First, the integration of singular functions (such as the velocity near a pumping well) using Gaussian quadrature is error-prone. Special quadrature schemes for singular functions on a triangle are available (Akin 1994; Lyness and Cools 1994) and are expected to better maintain mass balance in systems with wells. In addition, to adequately handle the geometry of circular, elliptical, and curvilinear analytic elements, elements with higher-order shape functions are desirable. Various isoparametric 6-node and superparameteric 3-node triangular elements are available to meet this need (Akin 1994). While both revisions will improve the quality of the FEM solutions, preliminary testing indicates that the existing approach is adequate for a wide range of model configurations. These extensions will be considered for future work.

As expected, the flexibility of the finite element method in its ability to conform to the irregular geometry of AEM flow models is a distinct advantage over finite difference methods, and makes

the FE method more appealing for handling general continuous parameterization.

5.3.3 Lagrangian/Eulerian-Lagrangian Methods

It was initially hypothesized that particle-tracking-based Lagrangian and Eulerian-Lagrangian methods would most effectively benefit from a continuous flow solution. With an AEM-based velocity field, particle paths and characteristic paths may be tracked to a high degree of precision (using the adaptive Runge-Kutta method of appendix F). The accuracy of this algorithm is such that tracking errors may be considered negligible. Tracking errors are a significant source of mass balance error in EL methods and mass allocation error in Lagrangian methods (Oliveira and Baptista 1998).

The BMOC test case of section 4.2.4 demonstrated that mass balance error was significantly reduced by the use of continuous parameterization. However, the remaining global and local mass balance errors associated with characteristic methods (independent of the flow solution) are still deemed unsatisfactory for transport in heterogeneous domains. Therefore, while EL methods are improved by the use of AEM flow solutions, AEM-based Eulerian methods are still preferred, if Peclet constraints are not inhibitive.

The fully Lagrangian random walk technique also benefits from continuous representation of the velocity field. As with the BMOC, tracking error due to velocity discretization is removed. The EPVA random walk technique, hoped to remove further spatial discretization error, was not found to be a marked improvement over the standard random walk technique. However, the EPVA test case of section 4.2.2 demonstrates that it is possible to simulate contaminant transport without the use of *any* grid or mesh.

5.3.4 Implications for Other Methods

There are many approaches for simulating reactive transport that were not implemented or tested for this dissertation. However, the development and testing of the new AEM-based methods provide some insight into the applicability of using continuous parameters for other methods, including streamline methods, flux-limiting schemes, ELLAMs, the finite volume method, and meshless methods.

Though not discussed here, a preliminary version of the deterministic streamline method (Thiele 1994; Batycky 1997; Crane and Blunt 1999) was implemented in CARDINAL and found to benefit

from continuous parameterization in a similar way as Lagrangian methods (the streamline geometry is highly accurate). With the streamline method, the one-dimensional advection-dispersion equation is solved along a collection of streamlines using analytic or Eulerian techniques. The solution is often mapped to a 2-dimensional grid for visualization. These 1D solutions will benefit from continuous parameterization in a similar manner as the 2D finite element and finite difference method. It was found that the development of an flexible and rigorous streamline method algorithm required a large amount of bookkeeping. However, there are many potential benefits of such a merger (e.g., ease of parallelization and reduced grid constraints) and future work will extend the existing implementation.

Flux-limiting schemes such as the Total Variation Diminishing (TVD) scheme (Leonard 1988) are an alternative to traditional Eulerian-Lagrangian schemes for circumventing the Peclet constraints of Eulerian methods. Unlike EL methods, they are mass-conservative. However, they have their own time step requirements, which are generally more prohibitive that standard Courant constraints for Eulerian methods. Their implementation within an AEM-based finite difference transport simulator is relatively straightforward, and would have to be based upon the water-balance-preserving discrete flux calculations of section 3.3.2.

The Eulerian-Lagrangian localized adjoint method (ELLAM) uses a grid-based representation of dispersion and a Lagrangian representation of advection. Therefore, both the flux discretization methods of section 3.3.2 and the Runge-Kutta approach for tracking particles will benefit an AEM-based ELLAM.

The finite volume method may be considered a simple subset of finite element methods (Gresho and Sani 1998) with the appealing properties meeting both the global and local mass balance. It would be expected to benefit in a similar manner to the graded finite element method developed here.

Meshless methods for solving PDEs (Belytschko et al. 1996; Šarler 2002) are a relatively new subject of research and have not received much attention in the contaminant transport literature. The accuracy, stability, and conservation properties of the method when applied to advection-dispersion problems remain open research questions. However, the lack of any grid or mesh is appealing, and it is hoped that the method may later be integrated with AEM to obtain entirely grid-free solutions to the effective parameter advection-dispersion equation. It is not clear to what degree these methods can incorporate continuous variation in parameters.

5.4 Multi-scale Transport Modeling

The adjacency constraints of finite element and finite difference methods are rarely confronted as a source of computational inefficiency. They are viewed as a necessary artifact of a discrete representation. However, these constraints increase the cost of multi-scale models by requiring fine discretization not only along small-scale features but also away from such features. One of the most appealing ways to enable the development of multi-scale models is to circumvent these adjacency constraints. The discontinuous mesh method of section 3.7, enabled by the use of an AEM flow solution, was shown to be able to do so (albeit in an approximate fashion) in section 4.3. The use of AEM allows small-scale features in the transport model to be modeled as infinitely thin internal boundary conditions. In the case of the low-permeability barrier condition, this reduces adjacency requirements, encouraging the development of multi-scale transport models. Similar approaches may later be developed to model solute transport in 2-dimensional fracture networks.

5.5 Computational Considerations

The methods and algorithms for solute transport simulation developed within this dissertation may be considered significantly more complicated than those used in standard finite difference or finite element models. Most of this complexity is due to the need to account for the continuous representation of flow parameters. Because the analytic element does not produce results in a discrete format, the solutions (i.e., velocities, saturated thicknesses, etc.) must be either translated to a discrete format or used directly. This processing requires computation unique to the use of AEM. This is in addition to the computational costs of a standard reactive transport model, which are determined by the resolution and sophistication of the transport model (the number of particles, cells, elements, time steps, species, and/or reactions). The relative magnitude of this AEM-based computational overhead depends upon whether Eulerian, Lagrangian, or Eulerian-Lagrangian techniques are used for simulation.

With Eulerian methods, most of the additional sophistication is associated with the discretization of the analytic element flow solution to an equivalent finite difference or finite element representation. For finite difference methods, the complexity lies in the calculation of integrated fluxes across cell boundaries and within the cell. For finite element methods, the complexity is associated with the integration of the continuous residual integrals. In both cases, the computational over-

head associated with using AEM solutions only influences the cost of formulating the coefficient matrices. Because only steady-state flow solutions are considered here, the system of equations needs to be constructed once. Once the system of equations is assembled, the computational cost of AEM-based Eulerian methods is equivalent to that of standard discrete approaches. Facilitated by the use of operator-splitting, revisions to the system of equations (required for multi-species transport or adaptive time stepping) are incorporated "on-the-fly" in CARDINAL. The influence of flow parameters does not have to be recalculated every time a change to the system of equations is made. While the overhead in the construction of the system of equations can be significant (on the order of minutes for high resolution models with hundreds of flow features), the additional computation is negligible for most simulations. This cost is easily leveraged by the ability to develop models with fewer degrees of freedom than required using conventional discrete flow solutions.

Lagrangian and Eulerian-Lagrangian methods, where high-resolution particle tracking is desirable, are significantly more burdened by the overhead of using analytic element flow solutions. There are multiple means of implementing particle-based methods that use AEM flow solutions. One is to use the high-resolution approach of chapter 3.5.4, which tracks particle paths using the adaptive Runge-Kutta method of appendix F. This approach is (by far) the most accurate, as particle trajectories may be tracked to an arbitrary degree of precision, essentially removing the tracking errors discussed by Oliveira and Baptista (1998). However, with the large number of particles required in complex domains, this tracking algorithm can be prohibitive for reactive transport, because the computational cost of hydrodynamic (advective and dispersive) simulation becomes larger than that required for reactive simulation.

There are two means of avoiding the computational cost of tracking: precalculation and optimization. For the backwards method of characteristics, where particles are repeatedly backtracked from the nodes of the domain to compute the advective change in concentration, the "foot" of the characteristic path may be saved, and tracking calculations need only be performed once at the beginning of the simulation. However, with this approach, adaptive time stepping of the transport simulation is no longer an option (without recalculating characteristic paths). Additionally, this precalculation option is specific to the BMOC, and is not applicable to other Lagrangian or Eulerian-Lagrangian methods (e.g., the random walk or standard MOC) where the particle locations are changing during the course of the simulation. An appealing (and method-independent) alternative is to use a surrogate grid or mesh (*independent* of the simulation grid or mesh) on which

discrete velocities (or effective velocities) may be calculated and stored. The saved velocities may be interpolated using semi-analytic methods (e.g., Pollock (1988)), just like with traditional discrete simulators, to obtain approximate particle or characteristic paths. The overhead cost of building the velocity grid is incurred before the transport simulation, and would enable particle-based methods to be used without the prohibitive cost of Runge-Kutta pathline integration. Tracking errors are once again introduced when the velocities are interpolated. However, unlike the grid used in the BMOC test case of section 4.2.4, the grid used to store velocities can be wholly independent of the transport simulation mesh, and a quad-tree representation may be used to maximize accuracy while minimizing both the memory requirements and preprocessing cost. This approach may also be advantageous for other Lagrangian techniques, such as the random walk method.

The computational cost of including reactions in AEM-based transport models is on par with that of discrete methods. Importantly, this is facilitated by the use of operator-splitting. If the globally implicit method were used (i.e., transport and reaction were solved simultaneously), the system of equations would have to be reconstructed for each time step, and the cost of using AEM for any of the methods above would be prohibitive. For similar reasons, this reconstruction cost may also be prohibitive for the later development of transport simulation algorithms based upon transient AEM flow models.

5.6 Software Developments

5.6.1 Products

The backbone of this dissertation is the object-oriented flow and transport libraries, Bluebird and Cardinal, which contain all of the methods and algorithms developed here. To extend the impact of the research and these software products, both libraries (in the form of a single executable) have been released into the public domain (available at http://groundwater.buffalo.edu). The code has been successfully linked to the optimization/parameter estimation software Ostrich (Matott 2003). It has also been integrated into a user interface, Visual Bluebird(Craig and Matott 2004), as briefly discussed below.

5.6.2 Object Orientation

The development of the Bluebird and Cardinal libraries using object-oriented methods proved, on more than one occasion, to facilitate rapid development of algorithms, addition of new features, and revision to existing features. For example, Pollock's method was coded and linked to the backwards method of characteristics in less than two hours, and elliptical analytic elements were added in a similar time frame. While the benefits of object-orientation are difficult to quantify, the author sees no alternative for the type of complex algorithm development undertaken for this dissertation, which generated more than 30,000 lines of code.

5.6.3 User Interface

The development and solutions of the test cases within this dissertation were facilitated by the parallel development of Cardinal and Visual Cardinal (a module of Visual Bluebird). This interface is a significant byproduct of this work, and facilitates the use of the tools developed within this dissertation. A screenshot of Visual Cardinal is shown in figure 5.6.3.

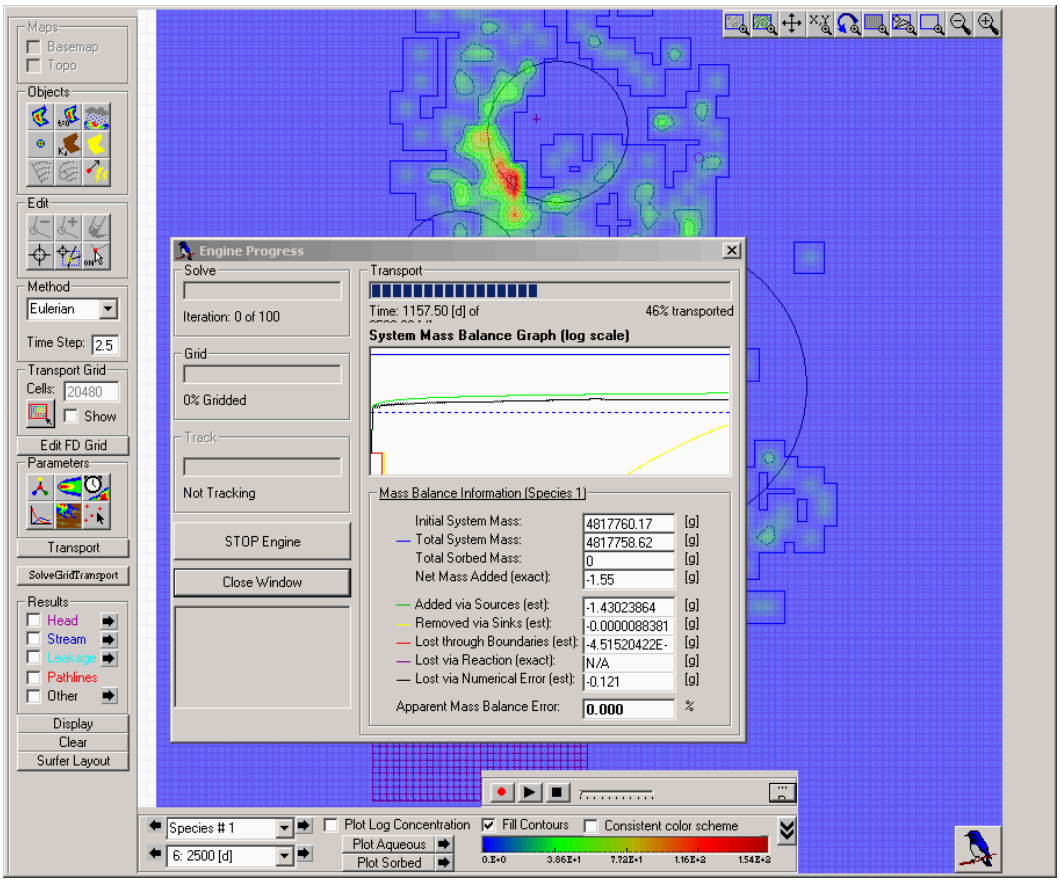

Figure 5.3: VISUAL CARDINAL Screenshot

5.7 Conclusions

The investigations within this dissertation have examined the advantages, disadvantages and challenges of using AEM flow solutions as a basis for contaminant transport simulation. After the preceding analysis of AEM-based transport simulation, the following summary conclusions are offered:

- In most cases, finite element transport simulators should be used for modeling complex reactive systems with the analytic element method. While the computation of hydrodynamic transport is more cumbersome (per degree of freedom) than with finite difference methods, the smaller number of nodes directly reduces the cost of reaction calculation. In addition, the finite element method can consistently fit the geometry of analytic element flow models and account for sharp discontinuities in velocity or saturated thickness. However, the existing finite element implementation, based upon the convective form of the ADRE, may be less robust (in terms of mass balance) than the finite difference method. This limitation may later be circumvented by solving the divergence form of the vertically-averaged advection-dispersion equation. Also, revisions are required to more robustly account for the effects of singularities and curvilinear features.

- The development of accurate *and* fast adaptive tracking algorithms for AEM are a high priority for the development of more computationally efficient AEM-based Eulerian-Lagrangian methods for transport simulation. Until this development occurs, it is recommended that the faster (and mass-conservative) Eulerian methods are used.

- The robust calculation of intercellular fluxes for finite difference transport simulation (section 3.3.2) is *required* for successful results, yet requires very little computation (typically only a little more than one evaluation of the complex potential per cell). Alternative discretization approaches (e.g., low-order numerical flux integration) should be avoided.

- For 2-dimensional transport simulation in systems that exhibit mixed confined/unconfined behavior and are appropriately approximated as shallow (Dupuit-Forcheimer) flow, use of the analytic element method has a distinct advantage. Because AEM can model mixed confined/unconfined systems and conventional 2-dimensional finite difference and finite element methods cannot (they solve the governing equations in terms of head, rather than potential),

AEM-based flow solutions are the only option.

- For systems defined by high contrasts in hydraulic conductivity, the use of the analytic element method offers particular advantages. This is because finite difference methods and finite element methods are susceptible to water balance errors, which can affect the quality of the transport solution. Additionally, the analytic element method is able to simulate flow through systems where hydraulic conductivity varies by orders of magnitude.

- The current state of practice for modeling PRBs is to treat the barrier as a 1D system, with the averaged flow and influent concentrations treated as idealized boundary conditions. The methods implemented in this work allow the inclusion of a PRB in a 2-dimensional model, in a manner in which complex regional flow patterns and complex PRB chemistry can be simultaneously incorporated. Although this approach was successfully demonstrated for a difficult test problem, the resulting computational demand is significant, and without further computational improvements, the applications where this approach is appealing may be limited.

The results of the preceding research have demonstrated that the use of the analytic element method as basis for transport simulations is not only possible, but often beneficial, and for some particular applications (such as simulating transport through low conductivity barriers), advantageous. In most cases, the choice of whether AEM or discrete flow solutions should be used will continue to be dictated by the needs of the particular application. However, the option to model contaminant transport using existing (and future) AEM flow models is now available.

5.8 Future Work

The methods and results presented within this dissertation provided an essential framework for effective coupling of AEM and transport simulators. It is expected that these new and revised methods, all incorporated within a single software code, can all be optimized for improved computational performance and accuracy. In addition, the tools developed here can be used as a basis for future methods development. Future research should address the following:

Methods

- The 3D implementation of the algorithms in this dissertation is likely the most important "next step" in the integration of AEM and contaminant transport simulators, as the vertically-averaged assumption is only valid in a subset of cases. Much of the analysis contained within this dissertation easily extends to three-dimensional transport in 2-dimensional shallow flow systems, and it is likely that the pseudo-3-dimensional discharge approximation of (Strack 1984) will adequately approximate the vertical component of advection in many cases.

- The computational efficiency of the adaptive Runge-Kutta tracking algorithm (used by all particle-based methods in this dissertation) must be significantly improved. Multiple options are available, including the use of complex Taylor series expansions to speed up the evaluation of the velocity term, the use of intelligently discretized quad-tree velocity fields that may be used for Pollock's method (independent of transport system discretization), and/or a more optimized adaptive tracking algorithm that is less computationally expensive.

- Discontinuous finite element methods for the simulation of transport through fractures (represented as line dipoles in the analytic element method) may be an appealing means of modeling fracture transport. Additionally, more sophisticated discontinuous flux conditions (i.e., highly resolved 1-dimensional transport across a barrier) may be desirable.

- One of the more appealing features of the merger of AEM and Eulerian methods is the removal of the constraints associated with the flow grid or mesh. It is desirable to develop automated mesh generation algorithms that develop a mesh based completely upon the Peclet and Courant constraints identified from the AEM flow solution. Ideally, a finite element mesh could be created such that the mesh spacing is maximized everywhere without exceeding the Peclet constraint, thus maximizing the time step determined by courant limitations. Such a mesh generation algorithm would allow users to fully utilize the benefits associated with a continuous AEM flow solution.

- The effects of using operator-splitting to decouple hydrodynamic transport and sorption should be investigated, particularly for finite element methods, which are susceptible to mass balance errors due to the nature of this type of reaction.

- The majority of the transport simulation approaches within this dissertation have used approximate numerical solution techniques. However, it is desirable to combine the accuracy

of analytic flow solutions to the accuracy and simplicity of analytic transport solutions. Coordinate mapping approaches may be later developed to map existing analytic solutions for the transport of contaminants in uniform flow (e.g., those catalogued by Ségol (1994)) to the more complicated flow geometries obtained from AEM.

- While the standard finite element method was shown to be unable to solve the EPVA formulation of the ADRE (section 3.5.1), alternative weak forms may be possible which do not suffer from the limitations of the standard FEM. The mathematics behind such a development are complicated, and were deemed to be beyond the scope of this dissertation. However, future developments may include a more sophisticated finite element method which can utilize the closed-form solutions of section 3.4.

- The currently limited implementation of the deterministic streamline method in CARDINAL needs to be extended and assessed. The parallel nature of the algorithm and the reliance upon accurate calculation of streamlines bodes well for integration with AEM. One appealing application of the streamline method is the simulation of sorbing contaminant in highly heterogenous systems. Such tests could help to develop insight into the the effects of heterogeneity in sorption parameters. Three-dimensional flow solutions, such as those used in the work done by Fiori et al. (2003), could be used in conjunction with 1D analytic solutions for reactive transport along streamlines.

Software

- It is desirable to develop a more complete reaction library that could be used to model a variety of pollutants at the field and local scales. This reaction library would enable the use of CARDINAL to test research hypotheses about new contaminant transport issues, rather than just to be used as a testbed for algorithm development. Reaction modules are under development for simulation of nitrate transport and parent-daughter decay. Others will likely follow.

- Further development of the user interface for CARDINAL and BLUEBIRD, VISUAL BLUEBIRD, is planned for the fall of 2004. The software and interface will be released as public domain software to extend the impact of the work performed here.

Applications

- It is expected that the ability of AEM to model flow phenomenon at regional scales may support the development of regional scale transport models. Regional scale models of non-point source pollution are a likely byproduct of the developments encompassed by this dissertation

- The proposed AEM-based approach could potentially expand the range of performance assessment of iron-based PRB systems to include a more accurate consideration of flow field and influent concentration variability. Iron barriers are not constrained by the long time scales required to model the zeolite barrier in section 4.4. The recent development of elliptical analytic elements (Suribhatla et al. 2004) and their proposed applications to PRBs (Rabideau et al, submitted) enhances the potential value of the AEM-based approach.

Chapter 6

Summary

A suite of vertically-averaged contaminant transport simulation methods that use AEM flow solutions have been successfully developed and implemented in the object-oriented software library CARDINAL. These revised Eulerian, Lagrangian and Eulerian-Lagrangian methods facilitate the development of solute transport models that are (1) less restricted by conventional discretization constraints and (2) often more accurate than models based upon discrete flow solutions. The reduction in grid- and mesh-based constraints can reduce the overall computational cost of complex reactive transport models by allowing such models to be spatially discretized solely with consideration of the transport problem in mind. The improved accuracy of the methods allow for some systems to be modeled with fewer degrees of freedom.

The methods developed to enable the merger of AEM and transport simulation include:

- Techniques for translating AEM solutions so that they may be exported to standard finite difference and finite element simulators
- Techniques for directly using continuous AEM flow solutions to improve the accuracy of the Eulerian finite element method, characteristic methods, and the random walk method
- A new "discontinuous mesh" finite element technique that allows for discontinuities in vertically-averaged concentrations to be simulated without excessive discretization
- Closed-form solutions for continuous AEM-based "effective" parameters for use by modified transport solution techniques
- Simple-to-implement adaptive enabling of reactions

The above methods and algorithms have been verified against analytic and numerical solutions and compared to alternative approaches that use discrete parameterization. It was found that the majority of the methods benefited from continuous representation, and that the use of AEM can facilitate the development of computationally efficient multi-scale reactive transport models. These improvements may later be extended to transport methods that utilize pseudo-3-dimensional, 3-dimensional, and transient analytic element models.

Appendix A

Parameter Derivatives

For the following derivation of spatial derivatives of transport parameters, only x-direction calculations are shown. It is assumed that the functional forms of the porosity, base, and layer thickness spatial distributions are known and once differentiable.

A.1 Saturated Thickness Spatial Derivatives

The saturated thickness, h, can be defined as:

$$h = \zeta\,(\phi - B) + (1 - \zeta)H \tag{A.1}$$

where ζ is equal to 1 if unconfined ($B < \phi < B + H$), zero otherwise. For the unconfined condition, application of Darcy's law gives

$$\frac{\partial h^{-1}}{\partial x} = -\frac{1}{h^2}\frac{\partial h}{\partial x} = \frac{1}{h^3}\frac{Q_x}{k} + \frac{B'_x}{h^2} \tag{A.2}$$

For confined conditions, the saturated thickness is known a priori, and

$$\frac{\partial h^{-1}}{\partial x} = -\frac{1}{h^2}\frac{\partial h}{\partial x} = -\frac{H'_x}{h^2} \tag{A.3}$$

These may be incorporated into a single term, Υ_x $[L^{-1}]$, which represents the relative influence of changes in saturated thickness and porosity.

$$\Upsilon_x = h\frac{\partial h^{-1}}{\partial x} + \theta\frac{\partial \theta^{-1}}{\partial x} = \frac{\zeta}{h^2}\frac{Q_x}{k} - (1 - \zeta)\frac{H'_x}{h} + \frac{B'_x}{h} - \frac{\theta'_x}{\theta} \tag{A.4}$$

$$\Upsilon_y = h\frac{\partial h^{-1}}{\partial y} + \theta\frac{\partial \theta^{-1}}{\partial y} = \frac{\zeta}{h^2}\frac{Q_y}{k} - (1-\zeta)\frac{H'_y}{h} + \frac{B'_y}{h} - \frac{\theta'_y}{\theta} \tag{A.5}$$

A.2 Velocity Spatial Derivatives

The derivative of the x-component of velocity is given as

$$\frac{\partial v_x}{\partial x} = \frac{\partial}{\partial x}\left(\frac{Q_x}{h\theta}\right) \tag{A.6}$$

This may be expanded by applying the chain rule as follows,

$$\frac{\partial v_x}{\partial x} = \frac{1}{h\theta}\frac{\partial Q_x}{\partial x} + \frac{Q_x}{\theta}\frac{\partial h^{-1}}{\partial x} + \frac{Q_x}{h}\frac{\partial \theta^{-1}}{\partial x} \tag{A.7}$$

And may be expressed as a function of the discharge derivative and other known continuous parameters,

$$\frac{\partial v_x}{\partial x} = v_x\left(\frac{\Re(G_x)}{Q_x} + \Upsilon_x\right) \tag{A.8}$$

$$\frac{\partial v_y}{\partial x} = v_y\left(-\frac{\Im(G_x)}{Q_y} + \Upsilon_x\right) \tag{A.9}$$

$$\frac{\partial v_x}{\partial y} = v_x\left(\frac{\Re(G_y)}{Q_x} + \Upsilon_y\right) \tag{A.10}$$

$$\frac{\partial v_y}{\partial y} = v_y\left(-\frac{\Im(G_y)}{Q_y} + \Upsilon_y\right) \tag{A.11}$$

A.3 Velocity Magnitude Spatial Derivatives

The magnitude of velocity is given as follows:

$$|v| = \sqrt{v_x^2 + v_y^2} \tag{A.12}$$

Rewriting,

$$|v| = \left(\frac{Q_x^2}{h^2\theta^2} + \frac{Q_y^2}{h^2\theta^2}\right)^{\frac{1}{2}} = \frac{|W|}{h\theta} \tag{A.13}$$

Taking the derivative and applying the chain rule,

$$\frac{\partial |v|}{\partial x} = \frac{1}{h\theta}\frac{\partial |W|}{\partial x} + \frac{|W|}{\theta}\frac{\partial h^{-1}}{\partial x} + \frac{|W|}{h}\frac{\partial \theta^{-1}}{\partial x} \tag{A.14}$$

Simplifying the second two derivative terms,

$$\frac{\partial|v|}{\partial x} = \frac{1}{h\theta}\frac{\partial|W|}{\partial x} + |v|\Upsilon_x \tag{A.15}$$

The only term in this expansion that is not an explicit function of location is $\partial|W|/\partial x$, in the first term. The term may be written out as follows:

$$\frac{\partial|W|}{\partial x} = \frac{1}{|W|}\left(Q_x\frac{\partial Q_x}{\partial x} + Q_y\frac{\partial Q_y}{\partial x}\right) \tag{A.16}$$

Which may be obtained from the discharge derivative function, G_x,

$$\frac{\partial|W|}{\partial x} = \frac{Q_x\Re(G_x) - Q_y\Im(G_x)}{|W|} = \frac{\Re(\overline{W}G_x)}{|W|} \tag{A.17}$$

where $\overline{W}$ is the complex conjugate of W. Substituting into (A.15),

$$\frac{\partial|v|}{\partial x} = |v|\left(\frac{\Re(\overline{W}G_x)}{|W|^2} + \Upsilon_x\right) \tag{A.18}$$

and, through a similar process,

$$\frac{\partial|v|}{\partial y} = |v|\left(\frac{\Re(\overline{W}G_y)}{|W|^2} + \Upsilon_y\right) \tag{A.19}$$

In the relationship for dispersion coefficients, the derivatives of $|v|^{-1}$ is more important. These may be written as:

$$\frac{\partial|v|^{-1}}{\partial x} = -\frac{1}{|v|}\left(\frac{\Re(\overline{W}G_x)}{|W|^2} + \Upsilon_x\right) \tag{A.20}$$

$$\frac{\partial|v|^{-1}}{\partial y} = -\frac{1}{|v|}\left(\frac{\Re(\overline{W}G_y)}{|W|^2} + \Upsilon_y\right) \tag{A.21}$$

Appendix B

Pseudo-3D Parameter Derivatives

B.1 Vertical Velocity Component

For pseudo-three-dimensional flow in Dupuit-Forcheimer models, a vertical component of the velocity vector may be estimated as (from (Strack 1989)):

$$v_z = \frac{1}{\theta}\left[\frac{|\mathbf{Q}|}{h^2}\frac{\partial h}{\partial s}z' - B - \frac{N}{h}z' + (N_b^+ - N_b^-)\right] \tag{B.1}$$

Where z' is the vertical coordinate measured from the aquifer base (the superscript is used to differentiate it from the complex coordinate, z), ζ is equal to one for unconfined flow, zero otherwise, and N is the net vertical leakage ($N = N_t^+ - N_t^- + N_b^+ - N_b^-$). The coordinate s is along a streamline, with $|\mathbf{Q}|$ being the magnitude of the discharge in the flow direction and $\partial h/\partial s$ being the saturated thickness gradient in the direction of flow. Expanding out $|\mathbf{Q}|$ and $\partial h/\partial s$ for the most general case (with sloping base and thickness (where h is defined as in equation A.1),

$$v_z = \frac{1}{\theta}\left[\begin{array}{r}\zeta\frac{|W|}{h^2}\left(\left(\frac{\partial\phi}{\partial x}\right)^2 + \left(\frac{\partial\phi}{\partial y}\right)^2 - 2\frac{\partial\phi}{\partial x}B'_x - 2\frac{\partial\phi}{\partial y}B'_y + (B'_xB'_y)^2\right)^{\frac{1}{2}}z' + \\ (1-\zeta)\frac{|W|}{h^2}|H'|z' - \frac{N}{h}z' + (N_b^+ - N_b^-)\end{array}\right] \tag{B.2}$$

This expression may be rewritten as

$$v_z = \frac{1}{\theta}\left[\zeta\frac{|W|}{h^2}\left(\frac{|W|^2}{k^2h^2} + 2\frac{Q_x}{kh}B'_x + 2\frac{Q_y}{kh}B'_y + (B'_xB'_y)^2\right)^{\frac{1}{2}}z' + (1-\zeta)\frac{|W|}{h^2}|H'|z' - \frac{N}{h}z' + (N_b^+ - N_b^-)\right] \tag{B.3}$$

To simplify the following analysis, it will be assumed that the base elevation, B, and aquifer thickness, H, are piecewise constant, giving:

$$v_z = \frac{1}{\theta}\left[\zeta\frac{|W|^2}{kh^3}z' - \frac{N}{h}z' + N_b\right] \tag{B.4}$$

Where the total vertical flux *into* the aquifer from the bottom $N_b^+ - N_b^-$ has been expressed as N_b.

B.2 Vertical Velocity Spatial Derivatives

$$\frac{\partial v_z}{\partial x} = \frac{\partial}{\partial x}\left[\zeta\frac{|W|^2}{kh^3\theta}z' - \frac{N}{h\theta}z' + \frac{N_b}{\theta}\right] \tag{B.5}$$

For the multi-quadric area sink (the means of simulating recharge in this dissertation), the spatial distribution of leakage and recharge have the functional form of a multi-quadric radial basis function, i.e.,

$$N(z) = N_{ave} + \sum_n^{N_{AS}} a_n(z - z_n) \tag{B.6}$$

Where N_{AS} is the number of radial basis points z_n, and N_{ave} is the average leakage/recharge in the area-sink. The spatial gradients of this leakage (identical functions are available for representing N_b as well) may be expressed as

$$\frac{\partial N}{\partial x} = \sum_n^{N_{AS}} a_n\frac{x - x_n}{|z - z_n|} \tag{B.7}$$

$$\frac{\partial N}{\partial y} = \sum_n^{N_{AS}} a_n\frac{y - y_n}{|z - z_n|} \tag{B.8}$$

Since these expressions are known as a closed-form function of space, we may write the following expression for the gradient of vertical velocity in the x-direction:

$$\frac{\partial v_z}{\partial x} = \zeta\frac{|W|^2}{kh^2}\left[2\frac{\Re(\bar{W}G_x)}{|W|^3} + 3\Upsilon_x + 2\frac{\theta'_x}{\theta}\right]\frac{z'}{h\theta} - \left(N\Upsilon_x + \frac{\partial N}{\partial x}\right)\frac{z'}{h\theta} + \frac{1}{\theta}\left(\frac{\partial N_b}{\partial x} - \frac{N_b}{\theta}\theta'_x\right) \tag{B.9}$$

For the spatial gradient in the y-direction,

$$\frac{\partial v_z}{\partial y} = \zeta\frac{|W|^2}{kh^2}\left[2\frac{\Re(\bar{W}G_y)}{|W|^3} + 3\Upsilon_y + 2\frac{\theta'_y}{\theta}\right]\frac{z'}{h\theta} - \left(N\Upsilon_y + \frac{\partial N}{\partial y}\right)\frac{z'}{h\theta} + \frac{1}{\theta}\left(\frac{\partial N_b}{\partial y} - \frac{N_b}{\theta}\theta'_y\right) \tag{B.10}$$

For the spatial derivative in the z-direction,

$$\frac{\partial v_z}{\partial z'} = \frac{\partial}{\partial z'}\left[\zeta\frac{|W|^2}{kh^3\theta}z' - \frac{N}{h\theta}z' + \frac{N_b}{\theta}\right] \tag{B.11}$$

$$\frac{\partial v_z}{\partial z'} = \zeta\frac{|W|^2}{kh^3\theta}\left(1 - \frac{\theta'_z}{\theta}\right) - \frac{N}{h\theta} - N_b\frac{\theta'_z}{\theta} \tag{B.12}$$

Notice that, in aquifers without vertical variation in porosity, the velocity varies linearly with respect to z ($\partial v_z/\partial z'$ is not a function of z').

B.3 Velocity Magnitude Spatial Derivatives

Once a third component of the velocity is defined as being non-zero, the magnitude of the velocity vector should technically be redefined, therefore requiring a revised definition of the spatial derivatives of velocity magnitude (i.e., one different from that derived in equations A.12 to A.21). However, for most groundwater flow systems (especially those where the Dupuit-Forcheimer assumption is valid), the vertical velocity is significantly smaller than the horizontal velocities (i.e., $v_z << v_x$ and $v_z << v_y$). Therefore, it is realistic to assume that

$$|v|_{3D} = \sqrt{v_x^2 + v_y^2 + v_z^2} \approx |v|_{2D} = \sqrt{v_x^2 + v_y^2} \tag{B.13}$$

For the same reason, the spatial derivative of the velocity magnitude will be assumed to be zero:

$$\frac{\partial|v|}{\partial z} = \frac{\partial|v|^{-1}}{\partial z} = 0 \tag{B.14}$$

This assumption allows the velocity derivatives and magnitude derivatives to be used for transport in domains with pseudo-3D flow.

Appendix C

Element Discharge Derivatives

C.1 A Well

The discharge function from a well is:

$$W = Q_x - iQ_y = -\frac{Q}{2\pi}\frac{1}{z - z_w} \tag{C.1}$$

where z_w is the location of the well. The discharge derivative is obtained as:

$$G_x = -iG_y = \frac{\partial W}{\partial z} = \frac{Q}{2\pi}\frac{1}{(z - z_w)^2} \tag{C.2}$$

C.2 Laurent Series

The formula for a Laurent series (used in far field expansions and circular elements) is:

$$W = Q_x - iQ_y = -\frac{1}{R}\sum_{n=1}^{N} n a_n Z^{-n-1} \tag{C.3}$$

where $Z = (z - z_c)/R$, z_c is the center of the circle and R is the radius. The derivative with respect to z is :

$$G_x = -iG_y = \frac{\partial W}{\partial z} = \frac{1}{R^2}\sum_{n=2}^{N} n(n-1) a_n Z^{-n-2} \tag{C.4}$$

C.3 Taylor Series

The formula for a Taylor series (used in circular elements) is:

$$W = Q_x - iQ_y = -\frac{1}{R}\sum_{n=1}^{N} n a_n Z^{n-1} \tag{C.5}$$

where $Z = (z - z_c)/R$, z_c is the center of the circle and R is the radius. The derivative with respect to z is :

$$G_x = -iG_y = \frac{\partial W}{\partial z} = \frac{1}{R^2}\sum_{n=2}^{N} n(n-1) a_n Z^{n-2} \tag{C.6}$$

C.4 A High-order Doublet

The discharge function for a high-order doublet (as in Janković, 1997) is:

$$W(Z) = \frac{-2}{z_2 - z_1}\frac{1}{2\pi i}\left(\begin{array}{r} \sum_{n=0}^{N} a_n T_n(Z)\frac{2}{(Z-1)(Z+1)} + \\ \sum_{n=0}^{N-1} d_n T_n(Z) ln\frac{Z-1}{Z+1} + \\ \sum_{n=0}^{N-2} e_n T_n(Z) \end{array}\right) \tag{C.7}$$

where a_n are the N element jump coefficients, identified during solution of the flow model.

$$d_n = \begin{cases} 0 & \text{for n>N-1} \\ d_{n+2} + 2(n+1)a_{n+1} & \text{for n=N-1,N-2,N-3...1} \\ d_2/2 + a_1 & \text{for n=0} \end{cases} \tag{C.8}$$

and

$$e_n = \begin{cases} 0 & \text{for n>N-2} \\ e_{n+2} + 2(n+1)b_{n+1} & \text{for n=N-1,N-2,N-3...1} \\ e_2/2 + b_1 & \text{for n=0} \end{cases} \tag{C.9}$$

where

$$\mathbf{b} = \mathbf{Ba} \tag{C.10}$$

and

$$B_{nm} = \begin{cases} \frac{2}{m} & \text{for n=0 and m odd} \\ \frac{4}{m-n} & \text{for 0<n<m and n+m odd} \\ 0 & \text{otherwise} \end{cases} \tag{C.11}$$

It is important to note that the recursive relationship in (C.8) may be written in matrix form as $\mathbf{Da} = \mathbf{d}$, where the elements of the N x N matrix $\mathbf{D}$ may be expressed as

$$D_{nm} = \begin{cases} 2m & \text{if } m > n \text{ and } m - n \text{ is odd and } n \neq 0 \\ m & \text{if } m - n \text{ is odd and } n = 0 \\ 0 & \text{otherwise} \end{cases} \tag{C.12}$$

The derivative of the function $W(Z)$ with respect to z is

$$G_x(Z) = \frac{2}{(z_2 - z_1)^2} \frac{1}{\pi i} \left[\sum_{n=0}^{N} \begin{pmatrix} a_n \frac{4Z}{(Z-1)^2(Z+1)^2} + \\ d_n \frac{2}{(Z-1)(Z+1)} + \\ g_n ln \frac{Z-1}{Z+1} + h_n \end{pmatrix} T_n(Z) \right] \tag{C.13}$$

where $\mathbf{d} = \mathbf{Da}$, $\mathbf{g} = \mathbf{DDa}$ and $\mathbf{h} = \mathbf{DDBa}$. The formulae for G_x due to a dipole or linesink are similarly derived.

C.5 Elliptical Element

The expression for the discharge function an elliptical element is given by:

$$W(\tau) = \begin{cases} \frac{e^{-i\theta}}{d \sinh \tau} \sum_{n=1}^{N} n a_n \left(e^{-n\tau} - e^{n\tau}\right) & \text{for } \eta <= \eta_0 \\ \frac{e^{-i\theta}}{d \sinh \tau} \sum_{n=1}^{N} n b_n e^{-n\tau} & \text{for } \eta > \eta_0 \end{cases} \tag{C.14}$$

Where $\tau = \eta + i\varphi$ are local element coordinates, as defined by Suribhatla et al. (2004). This

expression may be differentiated with respect to z to obtain the discharge derivative, G_x:

$$G_x(\tau) = \begin{cases} \frac{-e^{-i2\theta}}{(d\sinh\tau)^2} \left[\begin{array}{l} \sum_{n=1}^{N} n a_n \left(\coth\tau + \eta\right) e^{-n\tau} \\ + \sum_{n=1}^{N} n a_n \left(\eta - \coth\tau\right) e^{n\tau} \end{array} \right] & \text{for } \eta <= \eta_0 \\ \frac{-e^{-i2\theta}}{(d\sinh\tau)^2} \left[\sum_{n=1}^{N} n b_n \left(\coth\tau - n\right) e^{-n\tau} \right] & \text{for } \eta > \eta_0 \end{cases} \tag{C.15}$$

Appendix D

Triangular Finite Elements

D.1 Local Coordinate System

The local coordinate system for triangular elements is often expressed in terms of barycentric coordinates.

The local triangular element coordinates ξ_i, ξ_j, and ξ_k are given by the following transformation and shown in figure D.1:

$$\xi_i = \frac{A_i}{A^{(e)}} \tag{D.1}$$

or, equivalently, in a more compact (and complex) form,

$$\xi_i = \frac{\Im\left((z - z_k)(\overline{z_k - z_j})\right)}{\Im\left((z_i - z_k)(\overline{z_k - z_j})\right)} \tag{D.2}$$

where z_i, z_j, and z_k are the nodal coordinates in complex form. Note that at $z = z_i$, the local coordinate ξ_i evaluates to 1. At $z = z_j$ and $z = z_k$, ξ_i evaluates to zero. For standard linear basis (shape) functions, we may easily write our basis functions in terms of local coordinates:

$$N_i^{(e)} = \xi_i \tag{D.3}$$

The derivatives of this basis function are given by the following relationships:

$$\begin{array}{lll} \dfrac{\partial N_i}{\partial x} = \dfrac{y_j - y_k}{2A^{(e)}} & \dfrac{\partial N_j}{\partial x} = \dfrac{y_k - y_i}{2A^{(e)}} & \dfrac{\partial N_k}{\partial x} = \dfrac{y_i - y_j}{2A^{(e)}} \\ \dfrac{\partial N_i}{\partial y} = \dfrac{x_j - x_k}{2A^{(e)}} & \dfrac{\partial N_j}{\partial y} = \dfrac{x_k - x_i}{2A^{(e)}} & \dfrac{\partial N_k}{\partial y} = \dfrac{x_i - x_j}{2A^{(e)}} \end{array} \tag{D.4}$$

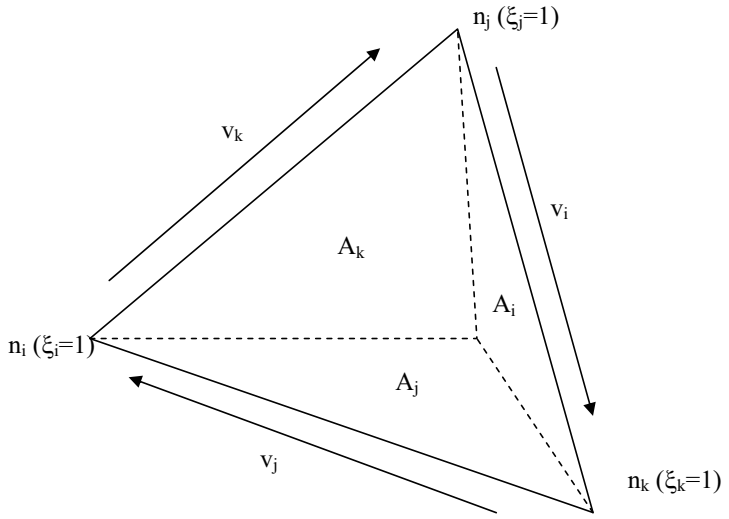

Figure D.1: Local coordinate system for linear triangle elements. The coordinate ξ_i is measured as the ratio of the inner triangle A_i to the total area with the maximum value of 1 at node i and zero along side i

Also useful are expressions for the integral of these basis functions and their derivatives over the element (from Segerlind (1976)):

$$\int_{A^{(e)}} N_i^\alpha N_j^\beta N_k^\gamma dA = \frac{\alpha!\beta!\gamma!}{(\alpha+\beta+\gamma+2)!} 2A^{(e)} \tag{D.5}$$

$$\begin{aligned}
\int_{A^{(e)}} \frac{\partial N_i}{\partial x}\frac{\partial N_j}{\partial x}\frac{\partial N_k}{\partial x} dA &= \frac{b_i b_j b_k}{8A^{(e)2}} \\
\int_{A^{(e)}} \frac{\partial N_i}{\partial x}\frac{\partial N_j}{\partial x}\frac{\partial N_k}{\partial y} dA &= \frac{b_i b_j c_k}{8A^{(e)2}} \\
\int_{A^{(e)}} \frac{\partial N_i}{\partial y}\frac{\partial N_j}{\partial y}\frac{\partial N_k}{\partial y} dA &= \frac{c_i c_j c_k}{8A^{(e)2}} \\
\int_{A^{(e)}} \frac{\partial N_i}{\partial y}\frac{\partial N_j}{\partial y}\frac{\partial N_k}{\partial x} dA &= \frac{c_i c_j b_k}{8A^{(e)2}}
\end{aligned} \tag{D.6}$$

And

$$\begin{aligned}
\int_{A^{(e)}} N_i N_j \frac{\partial N_k}{\partial x} dA &= \frac{b_k\,(1+\delta_{ij})}{24} \\
\int_{A^{(e)}} N_i N_j \frac{\partial N_k}{\partial y} dA &= \frac{c_k\,(1+\delta_{ij})}{24}
\end{aligned} \tag{D.7}$$

where $b_i = 2A^{(e)}\frac{\partial N_i}{\partial x}$ and $c_i = 2A^{(e)}\frac{\partial N_i}{\partial y}$ and

$$\delta_{ij} = \begin{cases} 1 & \text{if i=j} \\ 0 & \text{otherwise} \end{cases} \tag{D.8}$$

The element Jacobian matrix represents the transformation from global to local element coordinates. The Jacobian matrix for a triangular finite element is given by:

$$[J] = \begin{bmatrix} (x_j - x_i) & (x_k - x_i) \\ (y_j - y_i) & (y_k - y_i) \end{bmatrix} \tag{D.9}$$

The inverse Jacobian matrix is given by:

$$\left[J^{-1}\right] = \frac{1}{|J|}\begin{bmatrix} (x_j - x_i) & -(x_k - x_i) \\ -(y_j - y_i) & (y_k - y_i) \end{bmatrix} \tag{D.10}$$

where $|J|$ is the determinant of the Jacobian.

D.2 Upstream Weighting

The upstream weighting functions, $w_i^{(e)}$, for reducing numerical oscillation of the solution are given by Yeh (2000) as:

$$w_i^{(e)} = \xi_i - 3\hat{\alpha}_k\xi_i\xi_j + 3\hat{\alpha}_j\xi_k\xi_i \tag{D.11}$$

The weights $\hat{\alpha}_i$, $\hat{\alpha}_j$, and $\hat{\alpha}_k$ in Eq. D.11 are obtained based upon the velocity tangential to the element sides:

$$\hat{\alpha}_i = \begin{cases} -1 & \text{if } v_t^i < 0 \\ 0 & \text{if } v_t^i = 0 \\ 1 & \text{if } v_t^i > 0 \end{cases} \tag{D.12}$$

Equation D.11 reduces to the standard unweighed linear basis function, $N_i^{(e)}$ when the all weights are set to zero.

D.3 Streamline Upwind Petrov-Galerkin

As an alternative to classic upstream weighting, the streamline upwind Petrov-Galerkin (SUPG) formulation may also be used to weight the upstream nodal concentrations for solution of the advection term of the advection dispersion equation. The element nodal SUPG weighing functions are related to the basis functions by the following relationship (Brooks and Hughes 1982):

$$w_i^{(e)} = N_i^{(e)} + \hat{\tau}^{(e)} \left(v_x^{(e)} \frac{\partial N_i^{(e)}}{\partial x} + v_y^{(e)} \frac{\partial N_i^{(e)}}{\partial y} \right) \tag{D.13}$$

Where the element "stabilization parameter", $\hat{\tau}^{(e)}$, is given as

$$\hat{\tau}^{(e)} = \hat{\alpha} \frac{L^{(e)}}{2|v^{(e)}|} \tag{D.14}$$

The upwind weighting parameter $\hat{\alpha}$ can range between zero and one, and the element effective length, $L^{(e)}$, is often calculated as the square root of the element area.

D.4 Numerical Integration

Any function may be numerically integrated over a unit triangular element using the following approximation:

$$\int_0^1 \int_0^{1-\xi_j} f(\xi_i, \xi_j, \xi_k) d\xi_i d\xi_j = \sum_{i=k}^{M} \omega_k f_k \tag{D.15}$$

where f_i is the value of the function evaluated at integration point i and W_i is the Gaussian Weighting coefficient for that integration point, and M is the number of integration points. Table D.1 shows the locations and weights of the integration points for some lower-order triangular quadrature schemes.

Table D.1: Quadrature points and weights for triangular elements (Adapted from Huyakorn and Pinder (1983))

order (M)	Figure	Error	Points	Coordinates (ξ_i, ξ_j, ξ_k)	Weights ω_i
Linear (1)	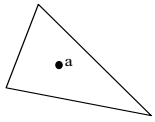	$O(h^2)$	a	$\left(\frac{1}{3}, \frac{1}{3}, \frac{1}{3}\right)$	1
Quadratic (3)	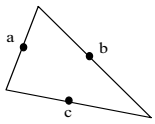	$O(h^3)$	a	$\left(\frac{1}{2}, \frac{1}{2}, 0\right)$	$\frac{1}{3}$
			b	$\left(0, \frac{1}{2}, \frac{1}{2}\right)$	$\frac{1}{3}$
			c	$\left(\frac{1}{2}, 0, \frac{1}{2}\right)$	$\frac{1}{3}$
Quadratic (3)	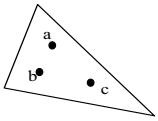	$O(h^3)$	a	$\left(\frac{2}{3}, \frac{1}{6}, \frac{1}{6}\right)$	$\frac{1}{3}$
			b	$\left(\frac{1}{6}, \frac{2}{3}, \frac{1}{6}\right)$	$\frac{1}{3}$
			c	$\left(\frac{1}{6}, \frac{1}{6}, \frac{2}{3}\right)$	$\frac{1}{3}$
Quintic (7)	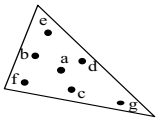	$O(h^6)$	a	$\left(\frac{1}{3}, \frac{1}{3}, \frac{1}{3}\right)$	0.225
			b	$(\alpha_1, \beta_1, \beta_1)$	0.13239415
			c	$(\beta_1, \alpha_1, \beta_1)$	0.13239415
			d	$(\beta_1, \beta_1, \alpha_1)$	0.13239415
			e	$(\alpha_2, \beta_2, \beta_2)$	0.12593918
			f	$(\beta_2, \alpha_2, \beta_2)$	0.12593918
			g	$(\beta_2, \beta_2, \alpha_2)$	0.12593918

where $\alpha_1 = 0.05961587$, $\beta_1 = 0.47014206$, $\alpha_2 = 0.79742699$, and $\beta_2 = 0.10128651$.

Appendix E

Mass Balance Calculations

E.1 Finite Difference Mass Balance

The central-weighted finite difference method for contaminant transport enforces local mass balance within each grid cell, provided the mass balance of water is met. For this reason, it is relatively simple to calculate the mass gained and lost to the system through cell boundaries and through sink/source terms. Many of the same integrated terms used for assembly of the global system of equations (derived in section 3.3.2) are used in CARDINAL for identification of global mass balance.

E.1.1 Total System Mass

The total mass in the finite difference model at a time n may be calculated as

$$M^n = \sum^{NC} \Delta x_i \Delta y_j h_{i,j} \left(\theta_{i,j} C_{ij}^n + (\rho_b)_i S_{ij}^n \right) \tag{E.1}$$

where NC is the number of finite difference cells and S_{ij}^n is the cell-averaged sorbed concentration of the particular species.

E.1.2 Advection through system boundaries

$$\Delta M_{bound}^n = \Delta t^n \sum^{NC_B} C_{ij}^n \sum_{k=1}^{4} \int_{S_k} Q_\eta^- \, dS_k \tag{E.2}$$

where NC_B is the number of cells adjacent to the border, Q_η^- is the normal integrated discharge along any side S_k (of length Δx_i or Δy_i) adjacent to the border, and C_{ij} is the concentration of the cell.

E.1.3 Source Terms

$$\begin{aligned}\Delta M^n_{source} =& \Delta t^n \sum^{NC^+} Q^+_{s(i,j)} c^+_{s(i,j)} + \Delta t^n \sum^{NC} q^+_{s(i,j)} \Delta x_i \Delta y_j + \\ & \Delta t^n \sum^{NC} N^+_{t(i,j)} c^+_{t(i,j)} \Delta x_i \Delta y_j + \Delta t^n \sum^{NC} N^+_{b(i,j)} c^+_{b(i,j)} \Delta x_i \Delta y_j\end{aligned} \tag{E.3}$$

where NC^+ is the number of wet source cells, $Q^+_{s(i,j)}$ is the influx of contaminated water to cell (i,j) with concentration $c^+_{s(i,j)}$, $q^+_{s(i,j)}$ $[M/T]$ is the cell-averaged "dry" specified mass flux per unit area in cell (i,j), NC is the number of finite difference cells, and N^+_t and N^+_b are the vertical influxes with concentrations of c^+_t and c^+_b, respectively. It is important to note that, to maintain mass balance at strong "wet" sources, upstream weighting may not be used at the cell interfaces adjacent to the source.

E.1.4 Sink Terms

$$\Delta M^n_{sink} = -\Delta t^n \left[\sum^{NC^-} \left(Q^-_{s(i,j)} + N^+_{t(i,j)} \Delta x_i \Delta y_j + N^+_{b(i,j)} \Delta x_i \Delta y_j \right) C^n_{ij} \right] \tag{E.4}$$

where NC^- is the number of wet sink cells, $Q^-_{s(i,j)}$ is the outflux of water from cell (i,j), NC is the number of finite difference cells, and N^+_r and N^+_l are the leakage outfluxes through the top and bottom of the layer.

E.1.5 Dirichlet Source/Sink Fluxes

The amount of added mass from dirichlet sources may be identified via a mass balance of each dirichlet cell. The mass added to the domain may be calculated as follows, where NC_d is the number of dirichlet cells, $C^n_{d(i,j)}$ is the specified concentration at time n, and the index i counts through the four cell sides:

$$\begin{aligned}\Delta M^n_{dir} =& \Delta t \sum^{NC_d} \left[h_{(i,j)} \theta_{(i,j)} \Delta x_i \Delta y_j (C^{n+1}_{d(i,j)} - C^n_{d(i,j)}) \right] + \\ & \Delta t \sum^{NC_d} \sum_{i=1}^{4} \left[\frac{\partial}{\partial \eta} \left(-Q_\eta C + h\theta D_\eta \frac{\partial C^n}{\partial \eta} \right) \right]_{n+\Delta t/2}\end{aligned} \tag{E.5}$$

The term in the square brackets is evaluated using the same finite difference approximations described in section 3.3.1.

E.2 Finite Element Mass Balance

E.2.1 Total System Mass

The total mass in the system at time n is given by:

$$M^n = \sum_{e=0}^{NE} \int_{A^{(e)}} \left[h\theta \sum_{i=1}^{3} N_i^{(e)} C_i^n + h\rho_b \sum_{i=1}^{3} N_i^{(e)} S_i^n \right] dA \tag{E.6}$$

E.2.2 Boundary Loss

Boundary losses may be estimated using knowledge of the advective flux along outflow boundaries (dispersive flux is zero along such boundaries).

$$\Delta M^n_{bound} = \int_{\Gamma} Q_\eta C dS \quad \text{if } Q_\eta > 0 \tag{E.7}$$

E.2.3 Source Terms

$$\Delta M^n_{source} = \Delta t^n \sum_{k=0}^{NS^+} Q_k^+ C_s^+ + \Delta t^n \sum_{e=0}^{NE} \int_{A^{(e)}} q_s^+ dA + \Delta t^n \sum_{e=0}^{NE} \int_{A^{(e)}} N_r^+ C_r^+ dA + \Delta t^n \sum_{e=0}^{NE} \int_{A^{(e)}} N_l^+ C_l^+ dA \tag{E.8}$$

E.2.4 Sinks and Sources

Evaluation of sink and source fluxes in the finite element method is straightforward. For a "natural" sink or source associated with a node, Q_i^+ or Q_i^- (identification of these nodal fluxes is shown in section 3.3.2), and specified flux sources q_i^+, the net gain or loss of mass over a time step is given

by:

$$\frac{\partial M}{\partial t}_{source} = \sum_{n=1}^{N} Q_i^+ C_i^s - \sum_{n=1}^{N} Q_i^- C_i + \sum_{n=1}^{N} q_i^+ \tag{E.9}$$

The influence of recharge and leakage is included here within the Q_i^+ and Q_i^- terms.

E.2.5 Dirichlet Source/Sink Fluxes

Unlike with finite difference methods, the approach for identifying the mass added to meet Dirichlet conditions at a finite element node is not clear. However, an a posteriori estimate of the mass added due to a Dirichlet source over a given time step is available. No mention of the following approach was found in the finite element literature, though it is expected that a similar technique must be used in standard finite element transport simulators.

In implicit finite element and finite difference approaches, Dirichlet boundary conditions are met by modifying the global system of equations ($[A]\{C\} = \{B\}$) by modifying the row and column of the left hand equation matrix ($[A]$) associated with the Dirichlet node j and modifying all terms of the right hand vector $\{B\}$. The original system of N equations is given by:

$$\sum_{i=1}^{N} A_{ij} C_j = B_j \quad (j = 1...N) \tag{E.10}$$

The modified system of equations $[A]'\{C\} = \{B\}'$ may be expressed as follows (Akin 1994), where D is the set of all Dirichlet node indices and C_j^* is the specified (Dirichlet) concentration at node j:

$$\begin{gathered} \sum_{\substack{i=1 \\ i \ni D}}^{NN} A_{ij} C_j = B_j - \sum_{\substack{k=1 \\ k \in D}}^{NN} A_{jk} C_k^* \quad (j = 1...NN; j \ni D) \\ C_j = C_j^* \quad (j = 1...NN; j \in D) \end{gathered} \tag{E.11}$$

Recalling that our finite element system of equations is such that external fluxes are applied on the right hand side, we may try to rewrite the revised system of equations, $[A]'\{C\} = \{B\}'$ as equivalent to the original system of equation with only additional flux terms F_j appended to the right hand side, i.e., $[A]\{C\} = \{B\} + \{F\}$.

Each modified equation associated with a non-Dirichlet node j may be re-expressed as follows, by adding the difference between the left hand side of E.10 and the left hand side of E.11a to both

sides of E.10:

$$\sum_{i=1}^{NN} A_{ij}C_j = B_j + \left[\sum_{\substack{k=1 \\ k\in D}}^{NN} A_{kj}C_j - \sum_{\substack{k=1 \\ k\in D}}^{NN} A_{jk}C_k^*\right] \quad (j = 1...NN; j \ni D) \tag{E.12}$$

where the term in square brackets is the flux added to node j from all Dirichlet sources.

Each modified equation associated with a Dirichlet node k may be re-expressed similarly. This is done by adding the difference between the left hand side of E.10 and the left hand side of E.11b to both sides of E.10, then doing the same for the right hand side:

$$\sum_{i=1}^{NN} A_{ij}C_j = B_j + \left[\sum_{i=1}^{NN} A_{ij}C_j + C_j^* - C_j - B_j\right] \quad (j = 1...NN; j \in D) \tag{E.13}$$

where, once again, the flux added to node j is given by the term in square brackets. To compute the mass added to the system from Dirichlet sources over a time step, these terms may be summed:

$$\Delta M_{dir}^n = \Delta t^n \sum_{\substack{j=1 \\ j\ni D}}^{NN} \left[\sum_{\substack{k=1 \\ k\in D}}^{NN} (A_{kj}C_j - A_{jk}C_k^*)\right] + \Delta t^n \sum_{\substack{j=1 \\ j\in D}}^{NN} \left[\sum_{i=1}^{NN} A_{ij}C_j + C_j^* - C_j - B_j\right] \tag{E.14}$$

Multiple tests were run to test the preceding approach, and it was found that using the average concentration over the time step was sufficient for accuracy. As the time step decreased, this *a posteriori* estimate of mass gain improved.

E.3 Characteristic Methods Mass Balance

It has been pointed out in the literature (e.g., Celia et al. (1990)) that characteristic methods do not have a robust means of calculating mass flux from sinks, sources, and boundaries. In the implementation of CARDINAL, the appropriate Eulerian mass balance calculations are applied (as presented above) as an approximation of the distribution of mass influx and outflux.

Appendix F

Adaptive Particle Tracking

The adaptive particle tracking procedure used within this dissertation is based upon a nearly identical approach developed for the AEM flow code SPLIT (Janković 2003). The algorithm uses a basic 4th order Runge-Kutta scheme for integrating the pathline of a particle over a single time step. This time step is adaptive, depending upon the local variation in the velocity (or effective velocity) vector. The adaptive algorithm has been used for tracking in highly heterogeneous domains (Janković et al. 2003) and verified against stream function solutions, exhibiting negligible error, even after thousands of time steps.

A particle, initially located at z_p, is advected over a single time step, Δt, to a new position z_p^* using the local velocity information at four points:

$$z_p^* = z_p + v_t \Delta t \tag{F.1}$$

Where

$$\begin{aligned} v_1 =& v(z_p) \\ v_2 =& v(z_p + \tfrac{1}{2} v_1 \Delta t) \\ v_3 =& v(z_p + \tfrac{1}{2} v_2 \Delta t) \\ v_4 =& v(z_p + v_3 \Delta t) \\ v_t =& \frac{v_1 + 2v_2 + 2v_3 + v_4}{6} \end{aligned} \tag{F.2}$$

The time step is determined based upon the values of these four intermediate velocities (calculated directly from the AEM flow solution). First, the relative change in velocity, Δv, is estimated

as:

$$\Delta v = \frac{||v_1 - v_2|| + ||v_1 - v_3|| + ||v_1 - v_4||}{6|v_t|} \tag{F.3}$$

Where the $||\cdot||$ operator denotes a vector norm defined as the sum of the absolute values of the vector components. Based upon this relative change, the time step is either (1) kept for the next movement (2) increased mildly for the next movement (3) decreased mildly for the next movement or (4) decreased dramatically and the current move is recalculated using equation F.1 with the smaller timestep. The criterion used for determining which option is chosen is presented in equation F.4.

$$\Delta t_{new} = \begin{cases} \frac{1}{2} & \Delta t \quad \text{if } \Delta v > 0.03 \\ \frac{4}{5} & \Delta t \quad \text{if } 0.03 \geq \Delta v > 0.02 \\ & \Delta t \quad \text{if } 0.02 \geq \Delta v > 0.01 \\ \frac{6}{5} & \Delta t \quad \text{if } 0.01 \geq \Delta v \end{cases} \tag{F.4}$$

Appendix G

Cation Exchange Formulation

One of the reactions included in the CARDINAL library (used for the test case of section 4.4) is competitive cation exchange. The implementation is formulated in the same manner that was done in Bandilla (2001) and Rabideau et al. (2004). It is assumed that the anion concentration is known, and the cation exchange capacity, Q_{cx}, is specified. For any set of competing cations with a monovalent reference species (Na^+ in the test case), the conditions for equilibrium with the porous media may be expressed as a set of N_{cat} equations, where N_{cat} is the number of cations in the system. The set of equations is comprised of N_{cat}-1 equilibrium equations and a N_{cat}+1 mass balance equations. For a monovalent cation and monovalent reference species, an equilibrium relationship may be written for each non-reference specie:

$$\gamma_m C_i - \frac{\gamma_m C_{ref} S_i}{S_{ref} K_{i/ref}} = 0 \qquad i\text{=1 to } N_{cat};\ v_i\text{=1};\ i \neq ref \tag{G.1}$$

Where C_{ref} and C_i are the aqueous concentrations of the reference species and the i^{th} cation, respectively. S_{ref} and S_i are the analogous sorbed (exchanged) concentrations, $K_{i/ref}$ is the i^{th} selectivity coefficient with regard to the reference species (based upon the Gaines-Thomas convention), and γ_m is the monovalent activity coefficient, defined below.

For a divalent cation and monovalent reference species, a similar equilibrium relationship may be written:

$$\gamma_d C_i - 2Q_{cx} \frac{\gamma_m^2 C_{ref}^2 S_i}{S_{ref}^2 K_{i/ref}} = 0 \qquad i\text{=1 to } N_{cat};\ v_i\text{=2};\ i \neq ref \tag{G.2}$$

Where γ_d is the divalent activity coefficient. For each cation component, a mass balance expression

(that conserves the total mass of the component) may be written:

$$C_i + S_i \frac{\rho_b}{\theta} - T_i = 0 \qquad i\text{=1 to } N_{cat} \tag{G.3}$$

Where ρ_b [ML^{-3}]is the bulk dry density of the soil. Lastly, a final mass balance relationship may be written specifying that, at all times, the cation exchange capacity is met, and all sites on the porous media surface are populated with cations:

$$\sum_{j=1}^{NC} v_j S_j - Q_{cx} = 0 \tag{G.4}$$

Where v_j is the valence of the j^{th} species. The monovalent and divalent activity coefficients, γ_m and γ_d are given from the Davies equation:

$$\gamma_m = 10^{-\frac{1}{2}\left(\frac{\sqrt{\mu}}{1+\sqrt{\mu}} - 0.2\mu\right)} \tag{G.5}$$

$$\gamma_d = 10^{-2\left(\frac{\sqrt{\mu}}{1+\sqrt{\mu}} - 0.2\mu\right)} \tag{G.6}$$

Where the ionic strength, μ $[mol/L]$ is given as

$$\mu = \sum_{i=1}^{NC} \frac{1}{2} v_i^2 C_i + \mu_a \tag{G.7}$$

Where μ_a is the (assumed known) anionic component of the ionic strength.

The preceding nonlinear system of equations is solved using the Newton method, as described by Bandilla (2001). However, the development of the analytic entries of the Jacobian matrix used to solve this system of equations iteratively has been expanded in CARDINAL for the more general case of any number of monovalent and divalent cations with a monovalent reference species.

Appendix H

Contents of Digital Appendix

- Source code headers for Bluebird
- Source code headers for Cardinal
- Bluebird Developer Manual

References

Ahlstrom, S. W., H. P. Foote, P. C. Arnett, C. R. Cole, and R. J. Serne (1977). Multicomponent mass transport model: Theory and numerical implementation (discrete parcel random walk version). Technical Report Rep. BNWL 2127, Battelle Northwest Laboratory, Richland, WA.

Akin, J. E. (1994). *Finite Elements for Analysis and Design*. Academic Press.

Bandilla, K. (2001). Modeling of Strontium transport in groundwater influenced by competitive ion exchange: Numerical issues. Master's thesis, University at Buffalo.

Baptista, A. M. (1987). *Solution of Advection-Dominated Transport by Eulerian-Lagrangian Methods using the Backwards Method of Characteristics*. Ph. D. thesis, Massachusetts Institute of Technology.

Barry, D. A., K. Bajracharya, M. Crapper, H. Prommer, and C. J. Cunningham (2000). Comparison of split-operator methods for solving coupled chemical non-equilibrium reaction/groundwater transport models. *Mathematics and Computers in Simulation 53*, 113–127.

Barry, D. A., K. Bajracharya, and C. T. Miller (1996). Alternative split-operator approach for solving chemical reaction/groundwater transport models. *Advances in Water Resources 19*, 261–275.

Barry, D. A., C. T. Miller, P. J. Culligan, and K. Bajracharya (1996). Analysis of split operator methods for non-linear and multispecies groundwater chemical transport models. *Mathematics and Computers in Simulation 43*, 331–341.

Batycky, R. (1997). *A Three-dimensional Two-phase Field Scale Streamline Simulator*. Ph. D. thesis, Stanford University.

Bear, J. (1972). *Dynamics of Fluids in Porous Media*. New York: Elsevier.

Bear, J. (1979). *Hydraulics of Groundwater*. New York: McGraw-Hill.

Bellin, A., Y. Rubin, and A. Rinaldo (1994). An Eulerian-Lagrangian approach for modeling of flow and transport in heterogeneous geological formations. *Water Resources Research 30*(11), 2913–2924.

Belytschko, T., Y. Krongauz, D. Organ, M. Fleming, and P. Krysl (1996). Meshless methods: an overview and recent developments. *Computer Methods in Applied Mechanics and Engineering 139*, 3–47.

Bensabat, J., Q. Zhou, and J. Bear (2000). An adaptive pathline-based particle tracking algorithm for the Eulerian-Lagrangian method. *Advances in Water Resources 23*, 383–397.

Bentley, L. R. and G. F. Pinder (1992). Eulerian-Lagrangian solution of the vertically averaged groundwater transport equation. *Water Resources Research 28*, 3011–3020.

Bethke, C. M. (1996). *Geochemical Reaction Modeling: Concepts and Applications*. Oxford Press.

Binning, P. and M. A. Celia (2002). A forward particle tracking Eulerian-Lagrangian Localized Adjoint Method for solution of the contaminant transport equation in three dimensions. *Advances in Water Resources 25*, 145–157.

Booch, G. (1994). *Object-Oriented Analysis and Design with Applications* (Second ed.). Redwood City, CA: Benjamin/Cummings Publishing Co.

Bowyer, A. (1981). Computing dirichlet tessellations. *Computer Journal 24*(2), 162.

Brooks, A. N. and T. J. R. Hughes (1982). Streamline upwind/Petrov-Galerkin formulations for convection dominated flows with particular emphasis on the incompressible Navier-Stokes equations. *Computer Methods in Applied Mechanics and Engineering 32*, 199–259.

Bruch, E. K. (1991). *The Boundary Element Method for Groundwater Flow, Lecture Notes in Engineering*. Berlin: Springer-Verlag.

Carlyle, H. F., J. H. Tellam, and K. E. Parker (2004). The use of laboratory-determined ion exchange parameters in the predictive modelling of field-scale major cation migration in groundwater over a 40-year period. *68*, 55–81.

Celia, M. A., T. F. Russell, I. Herrera, and R. E. Ewing (1990). An Eulerian-Lagrangian Localized Adjoint method for the advection-diffusion equation. *Advances in Water Resources 13*, 187–206.

Charbeneau, R. J. and R. L. Street (1979). Modeling groundwater flow fields containing point singularities: Streamlines, travel times, and breakthrough curves. *Water Resources Research 15*(6).

Chavent, G. and J. Jaffre (1986). *Mathematical models and finite elements for reservoir simulation*. New York: North-Holland.

Chen, Y., L. J. Durlofsky, M. Gerritsen, and X. H. Wen (2003). A coupled local-global upscaling approach for simulating flow in highly heterogeneous formations. *Advances in Water Resources 26*, 1041.

Cheng, R. T., V. Casulli, and S. N. Milford (1984). Eulerian-Lagrangian solution of the convection-dispersion equation in natural coordinates. *Water Resources Research 28*(7), 944–952.

Cirpka, O. A., E. O. Frind, and R. Helmig (1999a). Numerical methods for reactive transport on rectangular and streamline-oriented grids. *Advances in Water Resources 22*(7), 711–728.

Cirpka, O. A., E. O. Frind, and R. Helmig (1999b). Streamline-oriented grid generation for transport modeling in two-dimensional domains including wells. *Advances in Water Resources 22*(7).

Cirpka, O. A. and P. K. Kitanidis (2000). An advective-reactive stream tube approach for the transfer of conservative-tracer data to reactive transport. *Water Resources Research 36*(5).

Cleary, R. W. and M. J. Ungs (1978). Groundwater pollution and hydrology. Technical Report Report 78-WR-15, Department of Civil Engineering, Princeton University.

Cooley, R. L. (1992). *A MODular Finite-Element model (MODFE) for Areal and Axisymmetric Ground-Water-Flow Problems, Part 2: Derivation of Finite-Element Equations and Comparisons with Analytical Solutions*, Chapter A4. Techniques of Water-Resources Investigations, Book 6. U.S. Geological Survey.

Cordes, C. and W. Kinzelbach (1992). Continuous groundwater velocity fields and path lines in linear, bilinear, and trilinear finite elements. *Water Resources Research 28*(11).

Craig, J. R. (2002). Bluebird developers manual. Technical report, Department of Civil, Structural, and Environmental Engineering, University at Buffalo, Buffalo, NY.

Craig, J. R., I. Janković, and R. Barnes (2004). The nested superblock approach for regional scale analytic element models. *Ground Water accepted*.

Craig, J. R. and L. S. Matott (2004). Visual Bluebird users manual: Version 1.8. Technical report, Department of Civil, Structural, and Environmental Engineering, University at Buffalo.

Craig, J. R. and A. Rabideau (2004). Discretization of analytic element flow solutions for transport simulation. In *Computational Methods in Water Resources 2004 International Conference, Jun. 13-17*, Chapel Hill, NC.

Crane, M. J. and M. J. Blunt (1999). Streamline-based simulation of solute transport. *Water Resources Research 35*(10).

Datta-Gupta, A., L. W. Lake, G. A. Pope, K. Sephernoori, and M. J. King (1991). High-resolution monotonic schemes for reservoir fluid flow simulation. *In Situ 15*, 289–317.

Dawson, C., S. Sun, and M. F. Wheeler (2004). Compatible algorithms for coupled flow and transport. *Computer Methods in Applied Mechanics and Engineering 193*, 2565–2580.

Diersch, H. J. G. (1998a). About the differences between the convective and divergence form of the transport equation. Technical report, WASY Inst. for Water Resources and Syst. Research, Berlin.

Diersch, H. J. G. (1998b). *FEflow Reference Manual: Interactive, Graphics-based Finite-Element Simulation System for Modeling Groundwater Flow, Contaminant Mass and Heat Transport Processes*. Berlin: WASY Institute for Water Resources Planning and Systems Research Ltd.

Dupuit, J. (1863). *Etudes Theoriques et Pratiques sur le Mouvement des Eaux dans les Canaux Decouverts et a Travers les Terrains Permeables* (2nd ed.). Paris: Dunod.

Durlofsky, L. J. (1994). Accuracy of mixed and control volume finite element approximations to darcy velocity and related quantities. *Water Resources Research 30*(4).

EPA, U. E. P. A. (2000). *Permeable Reactive Barrier Technologies for Contaminant Remediation*. Washington D.C.: EPA/600/R-98/125, Office of Solid Waste and Emergency Response.

Ewing, R. E. and H. Wang (2001). A summary of numerical methods for time-dependent advection-dominated partial differential equations. *Journal of Computational and Applied Mathematics 128*, 423–445.

Farmer, C. L. (2002). Upscaling: a review. *International Journal of Numerical Methods in Fluids 40*(1).

Farmer, C. L., X. H. Wen, L. J. Durlofsky, and M. G. Edwards (2003). Upscaling of channel systems in two dimensions using flow-based grids. *Transport in Porous Media 51*, 343.

Fiori, A., I. Janković, , and G. Dagan (2003). Flow and transport in highly heterogeneous formations, Part 2. Semi-analytical results for isotropic media. *Water Resources Research 39*(9), 1269. 10.1029/2002WR001719.

Fitts, C. R. (1985). Modeling aquifer inhomogeneities with analytic elements. Master's thesis, Univ. of Minnesota, Minneapolis, MN.

Fitts, C. R. (2002). *Groundwater Science*. San Diego: Academic Press.

Forcheimer, P. (1886). Ueber die ergiebigkeit von brunnen-anlagen und sickerschlitzen. *Z. Architekt. Ing. Ver. Hannover 32*, 539–563.

Frey, W. (1987). Selective refinement: A new strategy for automatic node placement in graded triangular meshes. *International Journal of Numerical Methods in Engineering 24*, 2183–2200.

Frey, W. and D. Field (1991). Mesh relaxation: a new technique for improving triangulations. *International Journal of Numerical Methods in Engineering 31*, 1121–1133.

Frind, E. O. and G. B. Matanga (1985). The dual formulation of flow for contaminant transport modeling 1.Review of theory and accuracy aspects. *Water Resources Research 21*(2).

Gavaskar, A. R., N. Gupta, B. Sass, R. J. Janosy, and D. Sullivan (1998). *Permeable barriers for groundwater remediation*. Battelle Press.

Girinski, N. K. (1946). Complex potential of flow with free surface in a stratum of relatively small thickness and k=f(z) (in russian). *Dokl. Akad. Nauk SSSR 58*(4), 337–338.

Goode, D. (1990). Particle velocity interpolation in block-centered finite difference groundwater flow models. *Water Resources Research 26*(5).

Gray, W. (1982). Derivation of vertically averaged equations describing multiphase flow in porous media. *Water Resources Research 18*(6), 1705–1712.

Gresho, P. M. and R. L. Sani (1998). *Incompressible Flow and the Finite Element Method*. Chichester, UK: John Wiley and Sons.

Haitjema, H. M. (1985). Modeling 3-dimensional flow in confined aquifers by superposition of both two-dimensional and 3-dimensional analytic functions. *Water Resources Research 21*(10), 1557–1566.

Haitjema, H. M. (1987). Comparing a 3-dimensional and a Dupuit-Forcheimer solution for a circular recharge area in a confined aquifer. *Journal of Hydrology 91*(1-2), 83–101.

Haitjema, H. M. (1995). *Analytic Element Modeling of Groundwater Flow*. New York: Academic.

Hálek, V., J. v. (1979). *Developments in Water Science 7: Groundwater Hydraulics*. New York: Elsevier.

Hathorn, W. E. (1996). A second look at the method of random walks. *Stochastic Hydrology and Hydraulics 10*(4), 319–329.

Healy, R. W. and T. F. Russell (1989). Efficient implementation of the modified method of characteristics in finite difference models of solute transport. In *On Solving Ground Water Problems with Models*, Dublin, Ohio. National Water Well Association.

Healy, R. W. and T. F. Russell (1993). A finite-volume Eulerian-Lagrangian localized adjoint method for solution of the advection dispersion equation. *Water Resources Research 29*(7), 2399–2413.

Healy, R. W. and T. F. Russell (1998). Solution of the advective-dispersion equation in two dimensions by a finite-volume Eulerian-Lagrangian localized adjoint method. *Advances in Water Resources 27*, 11–26.

Hills, R. G., K. A. Fisher, M. R. Kirkland, and P. Wierenga (1994). Application of flux-corrected transport to the Las Cruces Trench site. *Water Resources Research 30*(8), 2377–2386.

Hoffman, J. D. (1992). *Numerical Methods for Engineers and Scientists*. New York: McGraw-Hill.

Hunt, B. W. (1978). Dispersive sources in uniform ground water flow. *ASCE Journal of the Hydraulics Division 104*, 75–85.

Huyakorn, P. S. and G. F. Pinder (1983). *Computational Methods in Subsurface Flow*. San Diego: Academic.

Istok, J. (1989). *Groundwater Modeling by the Finite Element Method*. American Geophysical Union, Water Resources Monograph 13.

Janković, I. (1997). *High Order Analytic Elements in Modeling Groundwater Flow*. Ph. D. thesis, University of Minnesota.

Janković, I. (2003, Nov). Split version 2.4 user manual.

Janković, I. and R. Barnes (1999a). High-order line elements in modeling two-dimensional groundwater flow. *Journal of Hydrology 226*(3-4), 211–223.

Janković, I. and R. Barnes (1999b). Three-dimensional flow through large numbers of spheroidal inhomogeneities. *Journal of Hydrology 226*(3-4), 224–233.

Janković, I., A. Fiori, , and G. Dagan (2003). Flow and transport in highly heterogeneous formations, Part 3. Numerical simulations and comparison with theoretical results. *Water Resources Research 39*(9), 1270. 10.1029/2002WR001721.

Kaluarachchi, J. J. and J. Morshed (1995). Critical assessment of the operator-splitting technique in solving the advection-dispersion reaction equation: 1. First order reaction. *Advances in Water Resources 18*, 89–100.

Kinzelbach, W. (1986). *Groundwater Modeling: An Introduction with Sample Programs in Basic*. Amsterdam: Elsevier.

Kinzelbach, W. (1988). *The Random Walk Method in Pollutant Transport Simulation*, pp. 227–246. D. Reidel.

Kinzelbach, W. and G. Uffink (1991). *The Random Walk Method and Extensions in Groundwater Modeling*, pp. 761–787. Norwell,MA: Kluwer Academic.

Kirkner, D. J. and H. Reeves (1988). Multicomponent mass transfer with homogeneous and heterogeneous chemical reactions: Effect of the chemistry on the choice of numerical algorithm. *Water Resources Research 24*(10), 1719–1729.

Knupp, P. M. (2000). Achieving finite element mesh quality via optimization of the Jacobian matrix norm and associated quantities. Part I - a framework for surface mesh optimization. *International Journal of Numerical Methods in Engineering 48*(3), 401–420.

Konikow, L. F. and J. Bredehoeft (1978). *Computer Model of Two-dimensional Solute Transport and Dispersion in Groundwater*. Washington, D.C.: U.S. Government Printing office.

Konikow, L. F., D. J. Goode, and G. Z. Hornberger (1996). A three-dimensional method-of-characteristics solute-transport model (MOC3D). Technical Report Water-Resources Investiga-

tions Report 96-4267, U.S. Geological Survey.

LaBolle, E. M., G. E. Fogg, and A. F. B. Tompson (1996). Random walk simulation of transport in heterogeneous porous media: Local mass-conservation problem and implementation methods. *Water Resources Research 32*(3), 583–593.

Leake, S. A. and D. V. Claar (1999). Procedures and computer programs for telescopic mesh refinement using MODFLOW. Technical Report Open-File Report 99-238, U.S. Geological Survey.

Lee, D. R., D. J. Smith, S. G. Shikaze, R. Jowett, D. S. Hartwig, and C. Milloy (1998). Wall-and-curtain for passive collection/treatment of contaminant plumes. *Proceedings of the First International Conference on Remediation of Contaminant Plumes*. Battelle Press, Columbia, OH.

Leonard, B. P. (1988). Universal Limiter for Transient Interpolation Modeling of the Advective Transport Equations: The ULTIMATE conservative difference scheme. Technical Memorandum 100916 ICOMP-88-11, NASA, Washington, D.C.

Li, S. G. and C. F. Wei (1998). Improved finite analytic methods for heterogeneous transport in multi-dimensions. *Journal of Hydraulic Engineering 124*(4), 358–369.

Liggett, J. and P. Liu (1983). *The Boundary Integral Method for Porous Media Flow*. London: Allen and Unwin.

Lowry, T. and S. Li. (2002). A characteristic-based finite analytic method for solving the two dimensional steady state advection-diffusion equation. *Water Resources Research 38*(7).

Lyness, J. N. and R. Cools (1994). A survey of numerical cubature over triangles. *Proceedings of Symposia in Applied Mathematics 48*, 127–150.

Matott, L. S. (2003). OSTRICH: An optimization software tool: Documentation and users guide. Technical report, Department of Civil, Structural, and Environmental Engineering, University at Buffalo, Buffalo, NY.

McDonald, M. G. and A. W. Harbaugh (1988). Computer model of two-dimensional solute transport and dispersion in ground water. In *Techniques of water resources investigations of the U.S. Geological survey, Book 6*, Chapter A1, pp. 586. San Diego: Academic.

Mehl, S. and M. C. Hill (2002). Development and evaluation of a local grid refinement method for

block-centered finite difference groundwater models using shared nodes. *Advances in Water Resources 25*, 497–511.

Miller, C. and A. Rabideau (1993). Development of split-operator Petrov Galerkin methods to simulate transport and diffusion problems. *Water Resources Research 29*(7), 2227–2240.

Moore, H. R., R. E. Steiner, E. Fallon, C. L. Repp, M. R. Hemann, and A. J. Rabideau (2000). Permeable treatment wall pilot project at the West Valley demonstration project. In *Proceedings of Waste Management 2000*, February 27-March 2, Tuscon, AZ.

Mosé, R., P. Siegel, P. Ackerer, and G. Chavent (1994). Application of the mixed hybrid finite element approximation in a groundwater flow model: Luxury or necessity? *Water Resources Research 30*(11), 3001–3012.

NRC, N. R. C. (2000). *Investigating Groundwater Systems on Regional and National Scales*. Washington D.C.: National Academy Press.

Oliveira, A. and A. M. Baptista (1998). On the role of tracking on Eulerian-Lagrangian solutions of the transport equation. *Advances in Water Resources 21*, 539–554.

Parkhurst, D. L. and C. A. J. Appelo (1999). User's guide to PHREEQC (version 2)- a computer program for speciation, batch-reaction, one-dimensional transport, and inverse geochemical calculations. Technical Report Water Resources Investigations Report 99-4259, USGS.

Peaceman, D. W. (1977). *Fundamentals of Numerical Reservoir Simulation*. Amsterdam: Elsevier.

Pokrajac, D. and R. Lazic (2002). An efficient algorithm for high accuracy particle tracking in finite elements. *Advances in Water Resources 25*(4), 353–369.

Pollock, D. (1988). Semi-analytical computation of path lines for finite-difference models. *Ground Water 26*(6).

Polubarinova-Kochina, P. Y. (1952). *Theory of Groundwater Movement (in Russian)*. Moscow: Gostekhizdat.

Press, W. H., S. A. Teukolsky, W. T. Vetterling, and B. P. Flannery (2002). *Numerical Recipes in C++: The Art of Scientific Computing* (2nd ed.). Cambridge, UK: Cambridge University Press.

Prickett, T. A., T. G. Naymik, and C. G. Longquist (1981). A "random-walk" solute transport model for selected groundwater quality evaluations. Technical Report Bulletin 65, Illinois State Water Survey, Champaign IL.

Quarteroni, A. and A. Valli (1999). *Domain Decomposition Methods for Partial Differential Equations*. Oxford: Oxford Science Publications.

Rabideau, A. J. (2003). MOUSER version 1 user's manual. Technical report, Department of Civil, Structural, and Environmental Engineering, University at Buffalo, Buffalo, NY.

Rabideau, A. J., J. E. V. Benschoten, K. Bandilla, and A. Patel (2004). Performance assessment of a zeolite treatment wall for removing Sr-90 from groundwater. *submitted to Environmental Science and Technology*.

Rabideau, A. J., J. E. V. Benschoten, A. Khandelwal, A. Patel, and C. L. Repp (2001). *Physical/Chemical Subsurface Remediation*, Chapter Sorbing vertical barriers. Kluwer Publishers.

Rebay, S. (1993). Efficient unstructured mesh generation by means of Delunay triangulation and Bowyer-Watson algorithm. *Journal of Computational Physics 105*, 125–138.

Ruan, F. and D. McLaughlin (1999). An investigation of Eulerian-Lagrangian methods for solving heterogeneous advection-dominated transport problems. *Water Resources Research 35*(8), 23592373.

Rubin, J. (1983). Transport of solutes in porous media: Relation between mathematical nature of problem formulation and chemical nature of reactions. *Water Resources Research 19*(5).

Rumbaugh, J. O. (1993). Combining analytic element and finite element techniques for contaminant transport analyses. In *the Proceedings of the 1993 Groundwater Modeling Conference*, Golden, Colorado, pp. 77–86.

Saaltink, M. W., J. Carrera, and S. Olivella (2004). Mass balance errors when solving the convective form of the transport equation in transient flow problems. *Water Resources Research 40*. doi:10.1029/2003WR002866.

Santare, M. H. and J. Lambros (2000). Use of graded finite elements to model the behavior of nonhomogeneous materials. *Journal of Applied Mechanics 67*(4), 819–822.

Schafer-Perini, A. L. and J. L. Wilson (1991). Efficient and accurate front tracking for two-dimensional groundwater flow models. *Water Resources Research 27*(7), 1471.

Scientific Software Group (2003). Wintran user's manual.

Segerlind, L. J. (1976). *Applied Finite Element Analysis*. New York: John Wiley.

Ségol, G. (1994). *Classic Groundwater Simulations*. Englewood Cliffs, NJ: PTR Prentice Hall.

Shewchuk, J. R. (2002). What is a good linear element? Interpolation, conditioning, and quality measures. In *Eleventh International Meshing Roundtable (Ithaca, New York)*, Sandia National Laboratories.

Steefel, C. I. and K. T. B. MacQuarrie (1996). Approaches to modeling of reactive transport in porous media. In E. O. P.C. Lichtner, C.I. Steefel (Ed.), *Reviews in Mineralogy vol. 34: Reactive Transport in Porous Media*. Mineralogical Society of America.

Strack, O. D. L. (1981a). Flow in aquifers with clay laminae: 1. The comprehensive potential. *Water Resources Research 17*(4), 985–992.

Strack, O. D. L. (1981b). Flow in aquifers with clay laminae: 2. Exact solutions. *Water Resources Research 17*(4), 993–1004.

Strack, O. D. L. (1984). 3-dimensional streamlines in Dupuit-Forcheimer models. *Water Resources Research 20*(7), 812–822.

Strack, O. D. L. (1989). *Groundwater Mechanics*. New York: Prentice-Hall.

Strack, O. D. L. (1999). Principles of the analytic element method. *Journal of Hydrology 226*(3-4), 128–138.

Strack, O. D. L. (2003). Theory and applications of the analytic element method. *Reviews of Geophysics 41*(2), 1000. 10.1029/2002RG000111.

Strack, O. D. L. and R. Barnes (2001). Object-oriented design for AEM groundwater modeling.

Strack, O. D. L. and H. M. Haitjema (1981a). Modeling double aquifer flow using a comprehensive potential and distributed singularities: 1. Solution for homogeneous permeability. *Water Resources Research 17*(5), 1535–1549.

Strack, O. D. L. and H. M. Haitjema (1981b). Modeling double aquifer flow using a comprehensive potential and distributed singularities: 2. Solution for inhomogeneous permeabilities. *Water Resources Research 17*(5), 1551–1560.

Strack, O. D. L. and I. Janković (1999). A multi-quadric area-sink for analytic element modeling of groundwater flow. *Journal of Hydrology 226*(3-4), 188–196.

Strack, O. D. L., I. Janković, and R. Barnes (1999). The superblock approach for the analytic element method. *Journal of Hydrology 226*(3-4), 179–187.

Sun, N. (1999). A finite cell method for stimulating the mass transport process in porous media. *Water Resources Research 35*(12), 3649–3662.

Sun, N., C. Zheng, and D. Tian (1994). Efficient local refinement schemes for finite difference groundwater simulation models. In *Proc. 2nd Int. Conf. Groundwater Ecology*, Atlanta, GA, pp. 177–186.

Sun, Y., J. N. Peterson, T. P. Clement, and R. S. Skeen (1999). Development of analytical solutions for multispecies transport with serial and parallel reactions. *Water Resources Research 35*(1), 185–190.

Suribhatla, R., M. Bakker, K. Bandilla, and I. Janković (2004). Steady two-dimensional groundwater flow through many elliptical inhomogeneities. *Water Resources Research 40*. doi:10.1029/2003WR002718.

Székely, F. (1999). Windowed spatial zooming in finite-difference ground water flow models. *Ground Water 37*(6), 718–721.

Thiele, M. R. (1994). *Modeling Multiphase Flow in Heterogeneous Media using Streamtubes*. Ph. D. thesis, Stanford Univ., CA.

Tompson, A. F. B. and D. E. Dougherty (1988). *On the Use of Particle Tracking Methods for Solute Transport in Porous Media*. Boston, MA: VII International Conf. Computational Methods in Water Resources.

Uffink, G. (1985). A random walk method for the simulation of macrodispersion in a stratified aquifer. *IAHS Pub. 146*, 103–114.

Valocchi, A. J. and M. Malmstead (1992). Accuracy of operator-splitting for advection-dispersion-reaction problems. *Water Resources Research 28*, 1471–1476.

Valocchi, A. J. and A. M. Quinodez (1989). Application of the random walk method to simulate the transport of kinetically adsorbing solutes. *Groundwater Contamination* (IAHS Pub. 185), 35–42.

Verrujit, A. (1970). *Theory of Groundwater Flow*. London: Macmillan.

Voss, C. I. (1984). *SUTRA-A Finite Element Simulation Model for Saturated-Unsaturated-Fluid-Density-Dependent Ground Water Flow with Energy Transport or Chemical Reactive Single-Species Solute Transport*. U.S. Geological Survey Water Resources Investigation Report 84-4369.

Šarler, B. (2002). Towards a mesh-free computation of transport phenomena. *Engineering Analysis with Boundary Elements 26*, 731738.

Wang, H. and M. P. Anderson (1982). *Introduction to Groundwater Modeling*. San Francisco: Freeman.

Watson, D. F. (1981). Computing the n-dimensional delaunay tessellation with application to voronoi polytopes. *Computer Journal 24*(2), 167–172.

Weber, W. J., P. M. McGinley, , and L. E. Katz. Review paper, Sorption phenomena in subsurface systems: Concepts, models, and effects on contaminant fate and transport.

Yeh, G. T. (1981). On the computation of Darcian velocity and mass balance in finite element modeling of groundwater flow. *Water Resources Research 15*(5).

Yeh, G. T. (2000). *Computational Subsurface Hydrology: Reactions, Transport, and Fate*. Norwell, MA: Kluwer Academic.

Yeh, G. T., J. R. Chang, and T. E. Short (1992). An exact peak capturing and oscillation-free scheme to solve advection-dispersion transport problems. *Water Resources Research 28*(11), 2937–2951.

Yeh, G. T. and V. Tripathi (1989). A critical evaluation of recent developments in hydrogeochemical transport models of reactive multichemical components. *Water Resources Research 25*(1), 93–108.

Zhang, Z., Y. Xue, and J. Wu (1994). Cubic spline technique to calculate nodal Darcian velocities in aquifers. *Water Resources Research 30*(4).

Zheng, C. (1990). MT3D: A modular three-dimensional transport model for simulation of advection, dispersion and chemical reactions of contaminants in groundwater systems. Technical report, Ada, OK.

Zheng, C. (1993). Extension of the method of characteristics for simulation of solute transport in three dimensions. *Ground Water 31*(3), 456–465.

Zheng, C. (1994). Analysis of particle tracking errors associated with spatial discretization. *Ground Water 32*(5).

Zheng, C. and G. Bennett (2002). *Applied Contaminant Transport Modeling: Theory and Practice*. New York: Van Nostrand.

Zheng, C. and P. Wang (1999). *MT3DMS: A Modular Three-Dimensional Multispecies Transport Model for Simulation of Advection, Dispersion and Chemical Reactions of Contaminants in Groundwater Systems; Documentation and User's Guide, Contract Report SERDP-99-1*. Vicksburg, MS: U.S. Army Engineer Research and Development Center.